RL-TR-95-23
Final Technical Report
February 1995

AMBIGUITY FUNCTION ANALYSIS FOR BISTATIC RADAR

Syracuse University

Pramod K. Varshney, Donald D. Weiner, Harry Schwarzlander,
Mohamed Slamani, and Tzeto Tsao

APPROVED FOR PUBLIC RELEASE; DISTRIBUTION UNLIMITED.

Rome Laboratory
Air Force Materiel Command
Griffiss Air Force Base, New York

This report has been reviewed by the Rome Laboratory Public Affairs Office (PA) and is releasable to the National Technical Information Service (NTIS). At NTIS it will be releasable to the general public, including foreign nations.

RL-TR-95-23 has been reviewed and is approved for publication.

APPROVED: Stanley E. Borek

STANLEY E. BOREK
Project Engineer

FOR THE COMMANDER: Donald W. Hanson

DONALD W. HANSON
Director of Surveillance & Photonics

If your address has changed or if you wish to be removed from the Rome Laboratory mailing list, or if the addressee is no longer employed by your organization, please notify RL (OCSM) Griffiss AFB NY 13441. This will assist us in maintaining a current mailing list.

Do not return copies of this report unless contractual obligations or notices on a specific document require that it be returned.

REPORT DOCUMENTATION PAGE

Form Approved
OMB No. 0704-0188

1. AGENCY USE ONLY (Leave Blank)	2. REPORT DATE	3. REPORT TYPE AND DATES COVERED
	February 1995	Final Oct 90 - Sep 94

4. TITLE AND SUBTITLE
AMBIGUITY FUNCTION ANALYSIS FOR BISTATIC RADAR

5. FUNDING NUMBERS
C - F30602-90-C-0056
PE - 63741D
PR - 3640
TA - 04
WU - 12

6. AUTHOR(S)
Pramod K. Varshney, Donald D. Weiner, Harry Schwarzlander, Mohamed Slamani, and Tzeto Tsao

7. PERFORMING ORGANIZATION NAME(S) AND ADDRESS(ES)
Syracuse University
Office of Sponsored Programs
113 Bowne Hall
Syracuse NY 13244-1200

8. PERFORMING ORGANIZATION REPORT NUMBER
N/A

9. SPONSORING/MONITORING AGENCY NAME(S) AND ADDRESS(ES)
Rome Laboratory (OCTM)
26 Electronic Pky
Griffiss AFB NY 13441-4514

10. SPONSORING/MONITORING AGENCY REPORT NUMBER
RL-TR-95-23

11. SUPPLEMENTARY NOTES
Rome Laboratory Project Engineer: Stanley E. Borek/OCTM/(315) 330-4434

12a. DISTRIBUTION/AVAILABILITY STATEMENT
Approved for public release; distribution unlimited.

12b. DISTRIBUTION CODE

13. ABSTRACT (Maximum 200 words)
The ambiguity function and its plot provide a qualitative assessment of the suitability of different radar signalling waveforms. The concept of the ambiguity function for bistatic radar is investigated in this report. The manner in which the bistatic geometry affects the ambiguity function is derived. A number of illustrative examples are provided to show the effects. The concept of the ambiguity function based on sampled signals is investigated. Expressions for both continuous time-continuous frequency and discrete time-discrete frequency ambiguity functions are derived and relationships between them are established. Sampling rates to avoid aliasing are also determined. A signal model for non-cooperative bistatic radar is presented.

14. SUBJECT TERMS
Ambiguity function-monostatic radar, Ambiguity function-bistatic radar, Continuous time-continuous frequency ambiguity (see reverse)

15. NUMBER OF PAGES
198

16. PRICE CODE

17. SECURITY CLASSIFICATION OF REPORT	18. SECURITY CLASSIFICATION OF THIS PAGE	19. SECURITY CLASSIFICATION OF ABSTRACT	20. LIMITATION OF ABSTRACT
UNCLASSIFIED	UNCLASSIFIED	UNCLASSIFIED	UL

14. (Cont'd)

function, Discrete time-discrete frequency ambiguity function, Non-cooperative bistatic radar, Properties of the correlation function, Time and frequency extent of the correlation function

CONTENTS

1 INTRODUCTION

The target resolution, parameter estimation and clutter rejection capabilities of a radar are determined by the ambiguity function associated with the transmitted waveform [1-3]. The ambiguity function and its plot provide a qualitative assessment of the suitability of different waveforms in meeting system requirements. Theory and application of the ambiguity function to monostatic radars in a Gaussian noise environment is fairly well understood [4]. A monostatic radar refers to a radar system where the transmitter and the receiver are located at the same site. Over the past several years there has been quite a bit of interest in the area of bistatic and multistatic radars. This is primarily due to survivability considerations. In these systems, the transmitters and the receivers are located at different sites in a variety of configurations. The concept and application of ambiguity function for bistatic radars has not been examined in detail. One of the main objectives of this study was to investigate the concept of ambiguity function in the context of bistatic radars. Before discussing the bistatic radar, it is useful to review the manner in which the ambiguity function arises in a monostatic radar. In Chapter 2, we present the derivation of ambiguity function from the basic principles of detection and estimation theory. In Chapters 3 and 4, we present the formulation of ambiguity function for bistatic radars. In Chapter 3, we describe the North-referenced coordinate system for the representation of bistatic geometries. Procedures for transformation from the Global Earth-centered coordinate system and the local north-east-down coordinate system to the North-referenced coordinate system are also given. This will enable the use of our methodology even when the measurements are obtained in these other coordinate

systems. In Chapter 4, we discuss in detail the effect of bistatic geometry on ambiguity function analysis. Two examples are provided to illustrate the nature of ambiguity function for a variety of system configurations. These examples consider a Gaussian pulse and a waveform consisting of three rectangular pulses.

Most of the development of ambiguity function is based on the processing of continuous waveforms at the receiver. However, modern radars employ digital signal processing techniques in that the received signals are sampled prior to signal processing. It is, therefore, imperative that the ambiguity function in terms of discrete-time signals be analyzed in detail. In Chapters 5-8, we examine a number of issues related to the ambiguity function based on sampled signals. In Chapters 5 and 6 we derive expressions for the continuous-time continuous-frequency ambiguity function based on sampled signals. In Chapter 7, the relationship between the discrete-time discrete-frequency and continuous-time continuous-frequency ambiguity functions is established. Sampling rates required to avoid aliasing are also determined. In Chapter 8, the reconstruction of the conventional ambiguity function from the discrete-time discrete-frequency ambiguity function is discussed.

One of the important problems in the operation of a bistatic radar is that of synchronization, i.e., the availability of the transmitted waveform replica at the receiver. In the cooperative mode of operation, this availability is assumed. In Chapter 4, ambiguity function analysis for a cooperative bistatic radar was carried out. When the bistatic radar operates in a noncooperative mode, uncertainties exist in the reference signal available at the receiver. In Chapter 9, this problem is briefly considered and a signal model that includes these uncertainties is suggested. In Chapter 10, a summary of the major contributions of this investigation is provided.

2 AMBIGUITY FUNCTION FOR MONOSTATIC RADARS

This chapter is devoted to the study and derivation of ambiguity functions for monostatic radars. It is shown that the notion of ambiguity function comes up naturally when dealing with the detection and parameter estimation problems. It is typically derived assuming a slowly fluctuating point target. The model associated with such a target is developed next.

2.1 Slowly fluctuating point target model

In the propagation direction of an electromagnetic pulse, assume a target has scatterers distributed over the range interval (R_1, R_2), as shown in Fig. 2-1. Let t_i denote the time instant at which the leading edge of the pulse reaches range R_i where $i = 1,2$. We assume the time origin to correspond to the instant at which the leading edge of the pulse appears at the transmitting antenna. If T denotes the time duration of the transmitted pulse, we say that the target can be modeled as a point target provided

$$t_2 - t_1 << T. \tag{2.1}$$

Assume the transmitted pulse contains n complete cycles of carrier. (Here, "transmitted pulse" refers to a single finite-duration radar waveform which may actually be composed of a number of simple subpulses.) It follows that the carrier frequency is related to the pulse width by

$$f_c = \frac{n}{T}. \tag{2.2}$$

Since

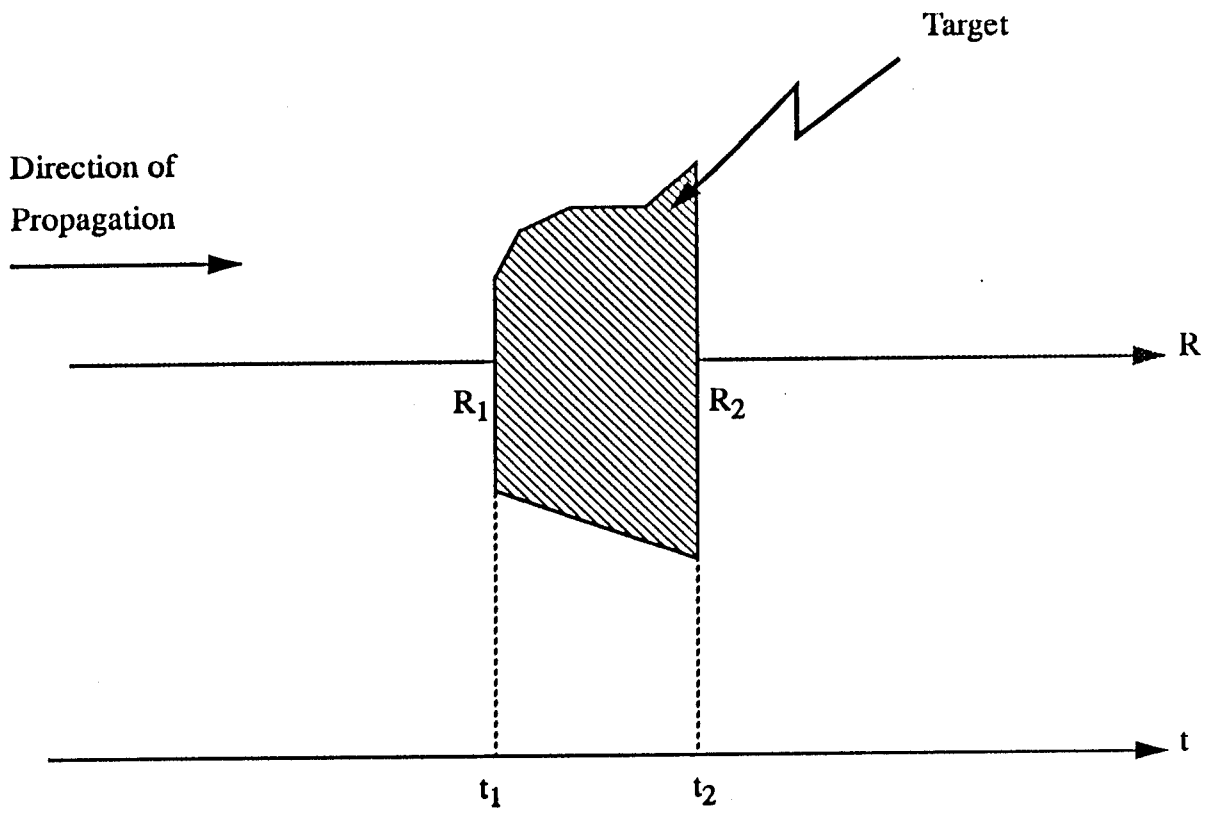

Fig. 2-1 Illustration of target that extends in range from R_1 to R_2.

$$\lambda f_c = c, \tag{2.3}$$

where λ and c are the wavelength and the velocity of propagation, respectively, of the transmitted pulse, it follows that

$$T = \frac{n}{f_c} = \frac{n\lambda}{c} . \tag{2.4}$$

At time t, assume that the leading edge of the transmitted pulse arrives at range R. Since

$$R = ct, \tag{2.5}$$

the time difference (t_2-t_1) can be expressed as

$$t_2-t_1 = \frac{R_2-R_1}{c} . \tag{2.6}$$

Thus, the inequality used to define a point target becomes

$$\frac{R_2-R_1}{c} << \frac{n\lambda}{c}. \tag{2.7}$$

We conclude that a target can be modeled as a point target, that is, the return pulse shape closely approximates the transmitted pulse, provided

$$R_2-R_1 << n\lambda. \tag{2.8}$$

It should be noted that, if the transmitted pulse consists of a sequence of several subpulses, n still refers to the number of carrier cycles in one pulse. For convenience, some people use the more restrictive condition

$$R_2 - R_1 << \lambda \tag{2.9}$$

in order to define a point target.

To examine the significance of the term "slowly fluctuating", assume that the transmitted pulse is given by

$$\begin{aligned} s_T(t) &= \sqrt{2}\,\sqrt{E_t}\,A(t)\cos[\omega_c t + \phi(t)] \\ &= \sqrt{2}\,\mathrm{Re}\left\{\sqrt{E_t}\,A(t)e^{j\phi(t)}e^{j\omega_c t}\right\} \\ &= \sqrt{2}\,\mathrm{Re}\left\{\sqrt{E_t}\,\tilde{f}(t)e^{j\omega_c t}\right\} \end{aligned} \tag{2.10}$$

where Re {•} denotes the real part operation,

$$\omega_c = 2\pi f_c, \tag{2.11}$$

and

$$\tilde{f}(t) = A(t)e^{j\phi(t)} \tag{2.12}$$

is the complex envelope of the transmitted pulse. Let the complex envelope be normalized such that

$$\int_{-\infty}^{\infty} |\tilde{f}(t)|^2\,dt = 1. \tag{2.13}$$

Then the energy of the transmitted signal is equal to E_t.

For a monostatic radar, assume that a point target is located at range R_a with radial velocity v_a. The geometry is indicated in Fig. 2-2. Let the point target consist of a rough surface with K scatterers. The received waveform due to the reflection from the i^{th} scatterer is

$$s_i(t) = \sqrt{2}\,\mathrm{Re}\left\{\sqrt{E_t}\,g_i e^{j\theta_i}\,\tilde{f}(t-\tau_a)e^{j\omega_{D_a}(t-\tau_a)}e^{j\omega_c(t-\tau_a)}\right\} \tag{2.14}$$

where g_i and θ_i denote the attenuation and phase shift, respectively, incurred in the reflection process, $\tau_a = 2R_a/c$ denotes the round-trip time delay and

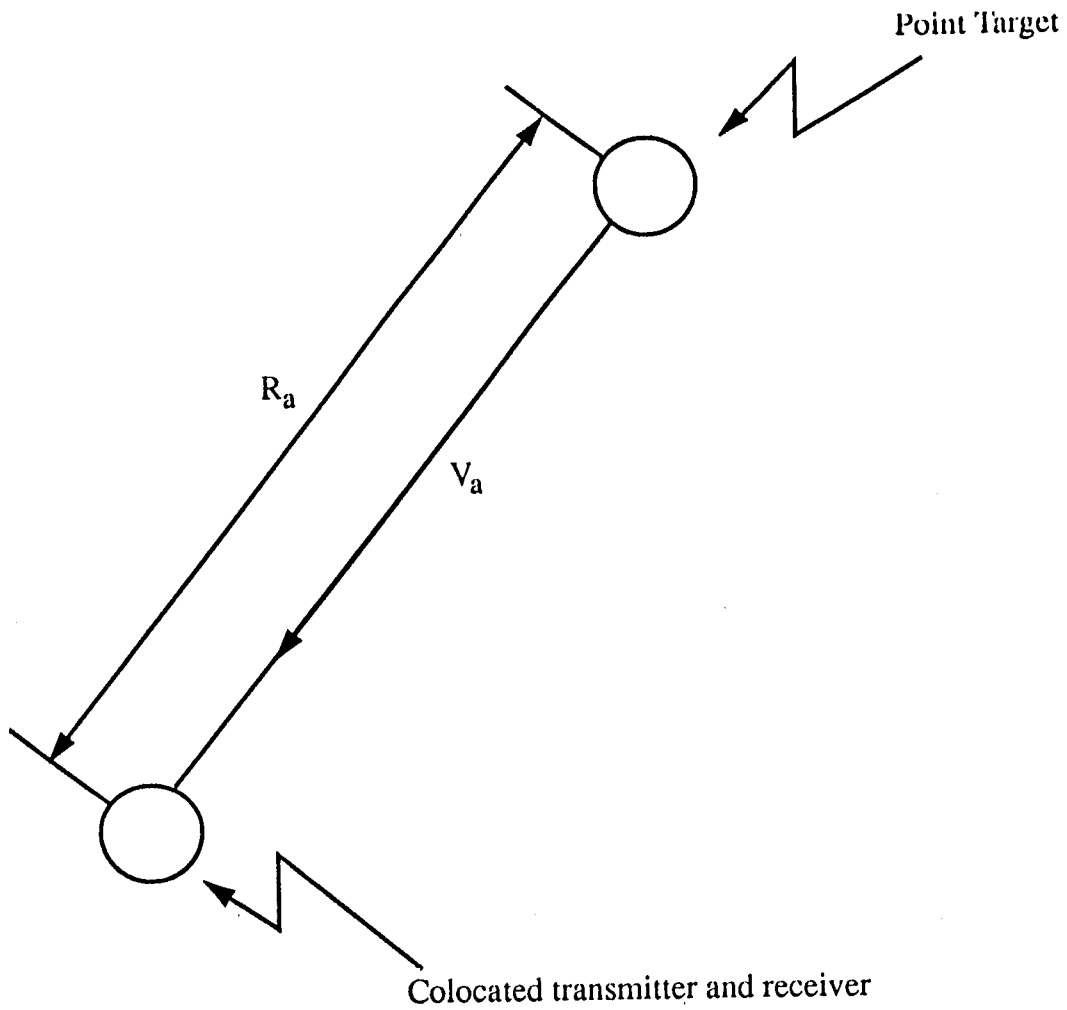

Fig. 2-2 Geometry for a monostatic radar.

$$\omega_{D_a} = \left(\frac{2v_a}{c}\right)\omega_c \tag{2.15}$$

is the shift in the carrier frequency due to the radial velocity of the target. ω_{Da} is called the Doppler shift. Summing the returns from the K scatterers, the total received waveform is

$$\begin{aligned} s_R(t) &= \sum_{i=1}^{K} s_i(t) \\ &= \sqrt{2}\ \mathrm{Re}\left\{\sqrt{E_t}\left[\sum_{i=1}^{K} g_i\, e^{j\theta_i}\right]\tilde{f}\,(t-\tau_a)\, e^{j\omega_{D_a}(t-\tau_a)} e^{j\omega_c(t-\tau_a)}\right\} \\ &= \sqrt{2}\ \mathrm{Re}\left\{\sqrt{E_t}\,\tilde{b}\,\tilde{f}\,(t-\tau_a) e^{j\omega_{D_a}(t-\tau_a)} e^{j\omega_c(t-\tau_a)}\right\} \end{aligned} \tag{2.16}$$

where the operations of summation and real part have been interchanged and

$$\tilde{b} = \sum_{i=1}^{K} g_i\, e^{j\theta_i} = \sum_{i=1}^{k} \tilde{g}_i. \tag{2.17}$$

Assuming that the complex random numbers $\tilde{g}_i$ are statistically independent and that K is sufficiently large, we can use a central limit theorem argument to conclude that

$$\tilde{b} = b_I + jb_Q = |\tilde{b}|e^{j\theta_b} \tag{2.18}$$

is a zero-mean complex Gaussian random variable. It follows that

$$|\tilde{b}| = \sqrt{b_I^2 + b_Q^2} \tag{2.19}$$

is a Rayleigh distributed random variable and

$$\theta_b = \tan^{-1}\frac{b_Q}{b_I} \tag{2.20}$$

is a uniformly distributed random variable. Absorbing the constant factors

$$e^{-j\omega_{D_a}\tau_a} \text{ and } e^{-j\omega_c\tau_a} \tag{2.21}$$

into the phase component of $\tilde{b}$, the total received signal becomes

$$s_R(t) = \sqrt{2}\ \mathrm{Re}\left\{\sqrt{E_t}\ \tilde{b}\ \tilde{f}(t-\tau_a)e^{j\omega_{D_a}t}\ e^{j\omega_c t}\right\} \quad . \tag{2.22}$$

The point target is defined to be slowly fluctuating if $\tilde{b}$ can be assumed to be constant while the target is illuminated by the transmitted pulse of duration T.

Having defined what is meant by a slowly fluctuating point target, we now show how the ambiguity function arises in the radar detection problem.

2.2 The Radar Detection Problem

Let $\tilde{f}(t)$ denote the complex envelope of the transmitted radar pulse. Assume that $\tilde{f}(t)$ is zero outside the interval $0 \le t \le T$. Given the complex envelope of the received waveform over the interval $\tau_H \le t \le \tau_H + T$, we are interested in determining whether a slowly fluctuating point target, at range R with radial velocity v, is located at the point

$$\left(\tau_H = \frac{2R}{c}\ ,\ \omega_{D_H} = \frac{2v}{c}\ \omega_c\right) \tag{2.23}$$

in the delay - Doppler plane. In the absence of a target, the complex envelope of the received waveform is assumed to be

$$\tilde{r}(t) = \tilde{n}(t),\ \tau_H \le t \le \tau_H + T \tag{2.24}$$

where $\tilde{n}(t)$ denotes the complex envelope of a Gaussian white noise process. On the other hand, if a slowly fluctuating point target is located at the point (τ_H, ω_{D_H}) in the

delay - Doppler plane, the complex envelope of the received waveform is

$$\tilde{r}(t) = \sqrt{E_t}\,\tilde{b}\,\tilde{f}(t-\tau_H)e^{j\omega_{D_H}t} + \tilde{n}(t),\ \tau_H \le t \le \tau_H + T\ . \tag{2.25}$$

Hence, given the two hypotheses

$$\begin{aligned} H_0 &: \tilde{r}(t) = \tilde{n}(t) \\ H_1 &: \tilde{r}(t) = \sqrt{E_t}\,\tilde{b}\,\tilde{f}(t-\tau_H)e^{j\omega_{D_H}t} + \tilde{n}(t), \qquad \tau_H \le t \le \tau_H + T \end{aligned} \tag{2.26}$$

we wish to determine the Neyman-Pearson receiver, i.e., the receiver that maximizes the detection probability for a specified false alarm probability, for detecting a slowly fluctuating point target at the hypothesized point (τ_H, ω_D) in the delay-Doppler plane.

For this purpose, it is convenient to expand $\tilde{r}(t)$ in a Karhunen-Loeve expansion as given by

$$\tilde{r}(t) = \sum_{i=1}^{\infty} \tilde{r}_i\,\tilde{\phi}_i(t), \qquad \tau_H \le t \le \tau_H + T. \tag{2.27}$$

Because $\tilde{b}$ is a complex Gaussian random variable and $\tilde{n}(t)$ is a white complex Gaussian random process, the coefficients

$$\tilde{r}_i = \int_{\tau_H}^{\tau_H+T} \tilde{r}(t)\,\tilde{\phi}_i^*(t)\,dt, \tag{2.28}$$

are statistically independent complex Gaussian random variables. In addition, since the noise is white, the basis functions $\tilde{\phi}_i(t)$ can be chosen from any set which is complete and orthonormal over the interval $\tau_H \le t \le \tau_H + T$. For convenience, let the first basis function be

$$\tilde{\phi}_1(t) = \tilde{f}(t-\tau_H)e^{j\omega_{D_H}t} . \tag{2.29}$$

The first coefficient in the expansion of $\tilde{r}(t)$ is then

$$\tilde{r}_1 = \int_{\tau_H}^{\tau_H+T} \tilde{r}(t)\, \tilde{f}^*(t-\tau_H)e^{-j\omega_{D_H}t}\, dt = \begin{cases} \tilde{n}_1 & : H_0 \\ \sqrt{E_t}\,\tilde{b} + \tilde{n}_1 & : H_1 \end{cases} \tag{2.30}$$

where

$$\tilde{n}_1 = \int_{\tau_H}^{\tau_H+T} \tilde{n}(t)\tilde{f}^*(t-\tau_H)e^{-j\omega_{D_H}t}dt \tag{2.31}$$

is the first coefficient in the Karhunen-Loeve expansion of the complex white noise process. Let

$$E\,[|\tilde{n}_1|^2] = N_0 \quad \text{and } E[|\tilde{b}|^2] = 2\sigma_b^2. \tag{2.32}$$

It follows that the conditional probability density functions of $\tilde{r}_1$ are given by

$$p_{\tilde{r}_1|H_0}(\tilde{R}_1|H_0) = \frac{1}{\pi N_0} \exp\left\{-\frac{|\tilde{R}_1|^2}{N_0}\right\} \tag{2.33}$$

and

$$p_{\tilde{r}_1|H_1}(\tilde{R}_1|H_1) = \frac{1}{\pi(2\sigma_b^2E_t+N_0)} \exp\left\{-\frac{|\tilde{R}_1|^2}{2\sigma_b^2E_t+N_0}\right\} . \tag{2.34}$$

2.3 Derivation Based on Sufficient Statistics

The remaining orthonormal functions in the basis set can be selected in any convenient manner. For i > 1, the ith coefficient in the Karhunen-Loeve expansion of $\tilde{r}(t)$

is

$$\tilde{r}_i = \begin{cases} \tilde{n}_i & :H_0 \\ \tilde{n}_i & :H_1 \end{cases}, \quad i>1 \tag{2.35}$$

where $\tilde{n}_i$ is the ith coefficient in the Karhunen-Loeve expansion of $\tilde{n}(t)$. Since $\tilde{n}(t)$ is a complex Gaussian white noise process, $\tilde{n}_i$ for $i > 1$ is statistically independent of $\tilde{n}_1$. Also, by assumption, $\tilde{n}_i$ is statistically independent of $\tilde{b}$. Thus, $\tilde{r}_i$ for $i > 1$ contains no information either about the target return or the noise coefficient $\tilde{n}_1$. It follows that $\tilde{r}_1$ is a sufficient statistic. The log likelihood ratio is given by

$$\ln\left[\frac{p_{\tilde{r}_1|H_1}(\tilde{R}_1|H_1)}{p_{\tilde{r}_1|H_0}(\tilde{R}_1|H_0)}\right] = \ln\left[\frac{N_0}{2\sigma_b^2E_t+N_0}\right] + \frac{2\sigma_b^2E_t}{N_0(2\sigma_b^2E_t+N_0)}|\tilde{R}_1|^2 . \tag{2.36}$$

Because the constants can be combined with the threshold, the Neyman-Pearson receiver performs the likelihood ratio test

$$|\tilde{R}_1|^2 \underset{H_0}{\overset{H_1}{\gtrless}} \gamma \tag{2.37}$$

where the threshold γ is selected so as to achieve a specified false alarm probability.

The above test maximizes the detection probability under a false alarm probability constraint assuming that a slowly fluctuating point target, if present, is located at the point (τ_H, ω_{D_H}) in the delay - Doppler plane. However, the target may actually be located at the point (τ_a , ω_{D_a}). The complex envelope of the received waveform is then

$$\tilde{r}(t) = \sqrt{E_t}\,\tilde{b}\,\tilde{f}(t-\tau_a)e^{j\omega_{D_a}t} + \tilde{n}(t). \tag{2.38}$$

Hence,

$$\begin{aligned}\tilde{r}_1 &= \int_{\tau_H}^{\tau_H+T}\tilde{r}(t)\tilde{f}^*(t-\tau_H)e^{-j\omega_{D_H}t}\,dt \\ &= \sqrt{E_t}\,\tilde{b}\int_{\tau_H}^{\tau_H+T}\tilde{f}(t-\tau_a)\tilde{f}^*(t-\tau_H)e^{j(\omega_{D_a}-\omega_{D_H})t}dt \\ &\quad + \int_{\tau_H}^{\tau_H+T}\tilde{n}(t)\tilde{f}^*(t-\tau_H)e^{-j\omega_{D_H}t}dt\end{aligned} \tag{2.39}$$

It follows that

$$\begin{aligned}|\tilde{r}_1|^2 = E_t|\tilde{b}|^2\left|\int_{\tau_H}^{\tau_H+T}\tilde{f}(t-\tau_a)\tilde{f}^*(t-\tau_H)e^{j(\omega_{D_a}-\omega_{D_H})t}dt\right|^2 \\ + \text{terms involving } \tilde{n}(t).\end{aligned} \tag{2.40}$$

Ignoring the noise terms and the multiplicative factor $E_t|\tilde{b}|^2$, the ambiguity function is defined to be

$$\theta(\tau_H,\tau_a,\omega_{D_H},\omega_{D_a}) = \left|\int_{\tau_H}^{\tau_H+T}\tilde{f}(t-\tau_a)\tilde{f}^*(t-\tau_H)e^{j(\omega_{D_a}-\omega_{D_H})t}dt\right|^2. \tag{2.41}$$

Because $\tilde{f}(t-\tau_H)$ is zero outside the interval $\tau_H \le t \le \tau_H + T$, the range of integration may be extended from $-\infty$ to $+\infty$. Hence, the ambiguity function is commonly expressed as

$$\theta(\tau_H,\tau_a,\omega_{D_H},\omega_{D_a}) = \left|\int_{-\infty}^{\infty}\tilde{f}(t-\tau_a)\tilde{f}^*(t-\tau_H)e^{j(\omega_{D_a}-\omega_{D_H})t}dt\right|^2. \tag{2.42}$$

It is convenient to express the ambiguity function in terms of the differences

$$\tau' = \tau_a - \tau_H \text{ and } \omega_D' = (\omega_{D_a} - \omega_{D_H}). \tag{2.43}$$

This results in

$$\theta(\tau_H, \tau_a, \omega_{D_H}, \omega_{D_a}) = \left| \int_{-\infty}^{\infty} \tilde{f}(t-\tau_H-\tau')\tilde{f}^*(t-\tau_H) e^{j\omega_D'(t-\tau_H+\tau_H)} dt \right|^2. \tag{2.44}$$

Moving the factor

$$e^{j(\omega'_D)\tau_H} \tag{2.45}$$

outside of the integral and noting that

$$\left| e^{j(\omega'_D)\tau_H} \right|^2 = 1, \tag{2.46}$$

we have

$$\theta(\tau_H, \tau_a, \omega_{D_H}, \omega_{D_a}) = \left| \int_{-\infty}^{\infty} \tilde{f}(t-\tau_H-\tau')\tilde{f}^*(t-\tau_H) e^{j\omega'_D (t-\tau_H)} dt \right|^2 \tag{2.47}$$

A shift of the time origin results if $t-\tau_H$ is replaced by t. This gives

$$\begin{aligned} \theta(\tau_H, \tau_a, \omega_{D_H}, \omega_{D_a}) &= \theta(\tau', \omega_D') \\ &= \left| \int_{-\infty}^{\infty} \tilde{f}(t-\tau')\tilde{f}^*(t) e^{j\omega_D' t} dt \right|^2. \end{aligned} \tag{2.48}$$

A symmetrical form of the ambiguity function is obtained by a further shift of the time origin. Replacing t by $t + \tau'/2$ gives

$$\theta(\tau', \omega_D') = \left| \int_{-\infty}^{\infty} f(t-\frac{\tau'}{2})\tilde{f}^*(t+\frac{\tau'}{2})\, e^{j\omega_D'(t+\frac{\tau'}{2})} dt \right|^2. \tag{2.49}$$

Moving the factor $e^{j\omega'_D\tau'/2}$ outside of the integral and noting that

$$|e^{j\omega_D' \frac{\tau'}{2}}|^2 = 1, \tag{2.50}$$

the symmetrical form of the ambiguity function reduces to

$$\theta(\tau',\omega_D') = |\int_{-\infty}^{\infty} f(t-\frac{\tau'}{2})\tilde{f}^*(t+\frac{\tau'}{2})e^{j\omega_D' t}dt|^2. \tag{2.51}$$

The effect of changing over to variables τ' and ω_D' is to shift the target to the origin of the τ',ω_D' plane. In other words, when $\tau' = \omega_D' = 0$, then

$$\tau_H = \tau_a \text{ and } \omega_{D_H} = \omega_{D_a} \quad . \tag{2.52}$$

Clearly, to minimize the likelihood that a target will be detected at the point $\tau_H,\omega_{D_H})$ when it is actually located at the point (τ_a, ω_{Da}), it is desirable that $\theta(\tau', \omega'_D)$ be an impulse located at the origin. This ideal ambiguity function cannot be achieved in practice.

2.4 Alternative Derivation

It is instructive to rederive the ambiguity function by an alternative approach to the detection problem. In the previous development, use was made of the fact that the first coefficient in the Karhunen-Loeve expansion of the complex envelope of the received signal is a sufficient statistic. Even so, the solution could have proceeded by considering all of the coefficients in the expansion

$$\tilde{r}(t) = \sum_{i=1}^{\infty} \tilde{r}_i \, \tilde{\phi}_i(t), \; \tau_H \le t \le \tau_H + T. \tag{2.53}$$

This latter approach is discussed next.

As before, the two hypotheses are assumed to be

$$H_0 : \tilde{r}(t) = \tilde{n}(t)$$
$$H_1 : \tilde{r}(t) = \tilde{s}(t) + \tilde{n}(t) \quad , \tau_H \le t \le \tau_H + T \tag{2.54}$$

where

$$\tilde{s}(t) = \sqrt{E_T}\, \tilde{b}\, \tilde{f}(t-\tau_H) e^{j\omega_{D_H} t} \quad . \tag{2.55}$$

Recalling that $E[\,|b|^2\,] = 2\sigma_b^2$, the covariance function of $\tilde{s}(t)$ is given by

$$\tilde{K}_{\tilde{s}}(t,u) = E[\tilde{s}(t)\tilde{s}^*(u)] = \bar{E}_t\, \tilde{f}(t-\tau_H)\tilde{f}^*(u-\tau_H) e^{j\omega_{D_H}(t-u)} \tag{2.56}$$

where

$$\bar{E}_t = 2\sigma_b^2 E_t \, . \tag{2.57}$$

The complex envelope of the Gaussian white noise process is assumed to be statistically independent of $\tilde{s}(t)$ with covariance function

$$\tilde{K}_{\tilde{n}}(t,u) = E[\tilde{n}(t)\tilde{n}^*(u)] = N_o \delta(t-u). \tag{2.58}$$

Keeping all of the terms in the Karhunen-Loeve expansion of $\tilde{r}(t)$, the sufficient statistic for the Neyman-Pearson receiver is given by [4]

$$\ell = \frac{1}{N_0} \int_{\tau_H}^{\tau_H+T} \int \tilde{r}^*(t)\tilde{h}(t,u)\tilde{r}(u)\,dt\,du \tag{2.59}$$

where $\tilde{h}(t,u)$ is the solution to the integral equation

$$N_0\tilde{h}(t,u) + \int_{\tau_H}^{\tau_H+T} \tilde{h}(t,z)\tilde{K}_{\tilde{s}}(z,u)\,dz = \tilde{K}_{\tilde{s}}(t,u), \quad \tau_H \le t,u \le \tau_H+T. \tag{2.60}$$

Substituting for the signal covariance function, the integral equation becomes

$$N_0\tilde{h}(t,u) + \int_{\tau_H}^{\tau_H+T} \tilde{h}(t,z)\,\bar{E}_r\tilde{f}(z-\tau_H)\tilde{f}^*(u-\tau_H)e^{j\omega_{D_H}(z-u)}dz \qquad (2.61)$$
$$= \bar{E}_r\tilde{f}(t-\tau_H)\tilde{f}^*(u-\tau_H)e^{j\omega_{D_H}(t-u)}, \qquad \tau_H \le t,u \le \tau_H+T.$$

By inspection, the solution is seen to be

$$\tilde{h}(t,u) = \frac{\bar{E}_r}{\bar{E}_r+N_0}\,\tilde{f}(t-\tau_H)\,\tilde{f}^*(u-\tau_H)e^{j\omega_{D_H}(t-u)} \qquad (2.62)$$

where use is made of the fact that $\tilde{f}(t)$ is normalized to have unit energy such that

$$\int_{\tau_H}^{\tau_H+T} |\tilde{f}(z-\tau_H)|^2\,dz = 1. \qquad (2.63)$$

Substitution of the expression for $\tilde{h}(t,u)$ into the sufficient statistic results in

$$\ell = \frac{1}{N_0}\int_{\tau_H}^{\tau_H+T}\int \tilde{r}^*(t)\,\frac{\bar{E}_r}{\bar{E}_r+N_0}\,\tilde{f}(t-\tau_H)\,\tilde{f}^*(u-\tau_H)e^{j\omega_{D_H}(t-u)}\tilde{r}(u)dtdu$$
$$= \frac{\bar{E}_r}{N_0(\bar{E}_r+N_0)}\left|\int_{\tau_H}^{\tau_H+T}\tilde{r}(t)\tilde{f}^*(t-\tau_H)e^{-j\omega_{D_H}t}dt\right|^2 \qquad (2.64)$$
$$= \frac{\bar{E}_r}{N_0(\bar{E}_r+N_0)}\,|\tilde{r}_1|^2$$

where $\tilde{r}_1$ is the first coefficient in the Karhunen-Loeve expansion of $\tilde{r}(t)$ as defined previously. Because the multiplicative constant can be combined with the threshold, the above result is consistent with the likelihood ratio test derived in the previous approach. The second approach was discussed because it proves to be more useful

when considering sampled data.

2.5 The Parameter Estimation Problem

The ambiguity function is also related to the parameter estimation problem for a slowly fluctuating point target where the complex envelope of the received signal is assumed to be of the form

$$\tilde{r}(t) = \sqrt{E_t}\, \tilde{b}\, \tilde{f}(t-\tau_H)\, e^{j\omega_{D_H} t} + \tilde{n}(t), \quad \tau_H \le t \le \tau_H + T \tag{2.65}$$

and τ_H and ω_{D_H} are unknown nonrandom parameters that we wish to estimate.

Because the unknown parameters are nonrandom, we use a maximum likelihood estimation procedure. The maximum likelihood estimates are those values of τ_H and ω_{D_H} for which the likelihood function is a maximum. The derivation of the likelihood function is similar to that of the likelihood ratio. The first step is to make a Karhunen-Loeve expansion for $\tilde{r}(t)$ assuming τ_H and ω_{D_H} are known. This means that we must choose basis functions that are conditionally dependent on τ_H and ω_{D_H}. We write

$$\tilde{r}(t) = \sum_{i=1}^{\infty} \tilde{r}_i(\tau_H, \omega_{D_H})\, \tilde{\phi}_i(t:\tau_H, \omega_{D_H}), \quad \tau_H \le t \le \tau_H + T \tag{2.66}$$

where

$$\tilde{r}_i(\tau_H, \omega_{D_H}) = \int_{\tau_H}^{\tau_H+T} \tilde{r}(t)\tilde{\phi}_i^*(t:\tau_H, \omega_{D_H})\, dt \quad . \tag{2.67}$$

For convenience, let the first basis function be

$$\tilde{\phi}_1(t:\tau_H,\omega_{D_H}) = \tilde{f}(t-\tau_H)e^{j\omega_{D_H}t} . \tag{2.68}$$

The first coefficient in the expansion of $\tilde{r}(t)$ is then

$$\tilde{r}_1(\tau_H,\omega_{D_H}) = \sqrt{E_T}\,\tilde{b} + \tilde{n}_1(\tau_H,\omega_{D_H}) \tag{2.69}$$

where

$$\tilde{n}_1(\tau_H,\omega_{D_H}) = \int_{\tau_H}^{\tau_H+T} \tilde{n}(t)\,\tilde{f}^*(t-\tau_H)e^{-j\omega_{D_H}t}dt \tag{2.70}$$

is the first coefficient in the Karhunen-Loeve expansion of the complex white noise process assuming τ_H and ω_{D_H} are given. Because $\tilde{b}$ is a complex Gaussian random variable and $\tilde{n}(t)$ is a complex Gaussian random process, the coefficients $\tilde{r}_i$ are statistically independent complex Gaussian random variables. As before, let

$$E[|\tilde{n}_1|^2] = N_o \text{ and } E[|\tilde{b}|^2] = 2\sigma_b^2. \tag{2.71}$$

The conditional probability density function of

$$\tilde{r}_1(\tau_H,\omega_{D_H}) \tag{2.72}$$

is then given by

$$p_{\tilde{r}_1(\tau_H,\omega_{D_H})|\tau_H,\omega_{D_H}}(\tilde{R}_1(\tau_H,\omega_{D_H})|\tau_H,\omega_{D_H}) = \frac{1}{\pi(2\sigma_b^2E_t+N_0)}\, e^{-\frac{|\tilde{R}_1(\tau_H,\omega_{D_H})|^2}{2\sigma_b^2E_t+N_0}} . \tag{2.73}$$

The remaining orthonormal functions in the basis set can be selected in any convenient manner. For $i > 1$, the ith coefficient in the Karhunen-Loeve expansion of $\tilde{r}(t)$

is

$$\tilde{r}_i(\tau_H,\omega_{D_H}) = \tilde{n}_i(\tau_H,\omega_{D_H}),\ i > 1 \tag{2.74}$$

where $\tilde{n}_i(\tau_H,\omega_{D_H})$ is the ith coefficient in the Karhunen-Loeve expansion of $\tilde{n}(t)$ assuming τ_H and ω_{D_H} are known. Because the coefficients $\tilde{n}_i(\tau_H,\omega_{D_H})$, for $i > 1$, depend only on the noise and are statistically independent of $\tilde{n}_1(\tau_H,\omega_{D_H})$, they contain no useful information for estimating τ_H and ω_{D_H}. We conclude that $\tilde{r}_1(\tau_H,\omega_{D_H})$ is a sufficient statistic. Since the conditional probability density function

$$p_{\tilde{r}_1(\tau_H,\omega_{D_H})|\tau_H,\omega_{D_H}}(\tilde{R}_1(\tau_H,\omega_{D_H})|\tau_H,\omega_{D_H}) \tag{2.75}$$

is maximized by maximimizing the exponent, it follows that the maximum likelihood estimates of τ_H and ω_{D_H} are those values of τ_H and ω_{D_H} for which

$$|\tilde{R}_1(\tau_H,\omega_{D_H})|^2 = \left|\int_{\tau_H}^{\tau_H+T} \tilde{r}(t)\ \tilde{f}^*(t-\tau_H)e^{-j\omega_{D_H}t}dt\right|^2 \tag{2.76}$$

is a maximum.

As in the detection problem, the ambiguity function is defined by ignoring those terms in $|\tilde{R}_1(\tau_H,\omega_{D_H})|^2$ that involve $\tilde{n}(t)$. If the actual values of delay and Doppler frequency are τ_a and ω_{D_a}, the ambiguity function is found to be

$$\theta(\tau_H,\tau_a,\omega_{D_H},\omega_{D_a}) = \left|\int_{-\infty}^{\infty} \tilde{f}(t-\tau_a)\tilde{f}^*(t-\tau_H)e^{j(\omega_{D_a}-\omega_{D_H})t}dt\right|^2 \tag{2.77}$$

which is identical to that obtained in the detection problem. Thus, introducing the

change of variables

$$\tau' = \tau_a - \tau_H \text{ and } \omega'_D = (\omega_{D_a} - \omega_{D_H}), \tag{2.78}$$

the ambiguity function can again be written in the symmetrical form

$$\theta(\tau', \omega'_D) = \left| \int_{-\infty}^{\infty} f(t - \frac{\tau'}{2})\, \tilde{f}^*(t + \frac{\tau'}{2})\, e^{j\omega'_D t} dt \right|^2. \tag{2.79}$$

Clearly, to minimize the maximum likelihood estimation errors, it is desirable that $\theta(\tau', \omega'_D)$ be an impulse located at the origin. As pointed out previously, this ideal ambiguity function cannot be achieved in practice.

As opposed to simply defining the ambiguity function, as is done in most references, we have shown that the ambiguity function arises naturally in both the detection and parameter estimation problems. In both applications, it is desirable to choose a waveform for $\tilde{f}(t)$ such that the shape of the ambiguity function in its symmetrical form approximates an impulse located at the origin. Examples and properties of the ambiguity function are well documented and are not repeated here.

3 COORDINATE SYSTEMS

Much of the radar systems analysis employs the Global, Earth-centered coordinate system using the earth as the reference. This three-dimensional coordinate system was also employed in the previous Rome Laboratory efforts on bistatic radar. However, this coordinate system is quite cumbersome and unnecessarily complex for expressing the bistatic configuration. Jackson [5] presented the North-referenced coordinate system to describe the bistatic radar geometry. It is a two-dimensional system and is fairly convenient to use. Willis [6] further elaborated on this system and has employed it extensively to analyze the bistatic radar system and to obtain many useful results. For this reason, we also employ the North-referenced coordinate system for the ambiguity function analysis for the bistatic radar. In this section, both of these coordinate systems are introduced. The procedure for transformation from the Global, Earth-centered coordinate system to the North-referenced coordinate system is derived. This will enable the use of our results if the measurements are provided in the Global, Earth-centered coordinate system.

Another common measurement practice is to use a local coordinate system. An example of such a coordinate system is the north-east-down coordinate system. We present this coordinate system and the procedure for converting the measurements provided in this system to the North-referenced system. If any other coordinate systems are employed for measurements, appropriate coordinate conversion procedures can be developed so that our results can be used.

3.1 North-referenced Coordinate System

This is a two-dimensional coordinate system confined to the bistatic plane

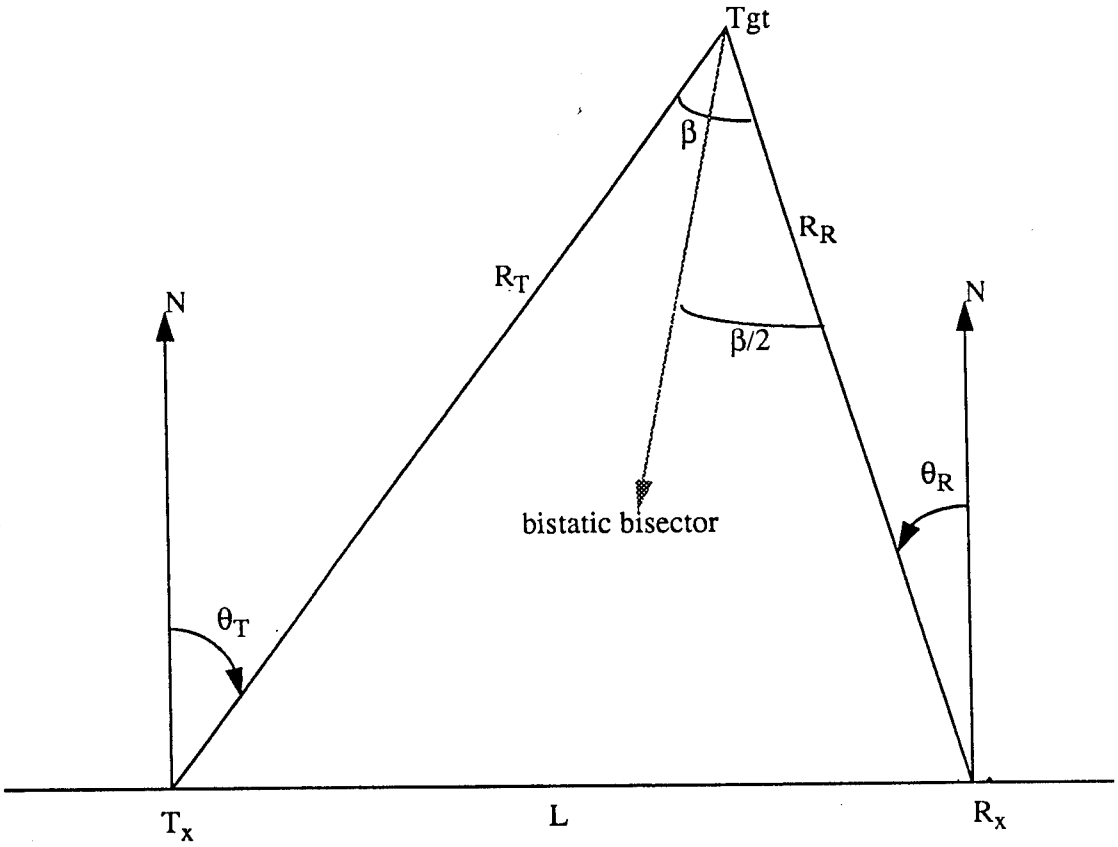

Tx - Transmitter
Rx - Receiver
Tgt - Target
N - North of North-referenced Coordinate System

θ_T = transmitter's look angle
θ_R = receiver's look angle
$\beta = \theta_T - \theta_R$
L = baseline range
R_T = transmitter to target range
R_R = receiver to target range
$R = R_T + R_R$

Fig. 3-1: North-referenced Coordinate System

formed by the transmitter T_x, the receiver R_x and the target Tgt. Figure 3-1 shows the coordinate system and its parameters. This coordinate system is represented as in maps with a north-up orientation. The distance between the transmitter and the receiver is the baseline range, or simply baseline and is denoted by L. The receiver is at the eastern end and the transmitter is at the western end of the baseline. The triangle formed by the transmitter, the receiver and the target is called the bistatic triangle. Transmitter's look angle θ_T and receiver's look angle θ_R are measured from the north of the coordinate system, positive clockwise. Also, the angles θ_T and θ_R are restricted to the interval $[-\frac{\pi}{2}, \frac{3\pi}{2}]$. The bistatic angle β is the angle between the transmitter and the receiver in the bistatic triangle with the target as the vertex. It is given by $\beta = \theta_T - \theta_R$. Using the definition and the restriction on the values θ_T and θ_R, the bistatic angle is positive and in the interval $[0, \pi]$ when the target is to the north of the baseline, and is negative and in the interval $[-\pi, 0]$ when the target is to the south of the baseline. The line that bisects the bistatic angle is called the bistatic bisector. The region to the north of the baseline is called the northern hemisphere, and likewise, the southern hemisphere is the region to the south of the baseline. In general, bistatic radar operation and performance in the northern and southern hemispheres are equivalent for symmetric geometries. The range from the transmitter to the target is denoted by R_T. The range from the receiver to the target is denoted by R_R. For a bistatic radar, the target range is measured in terms of the total range, or range sum, given by $R = R_T + R_R$. Note that in bistatic radar a constant range contour can be described by an ellipse. This is defined as the locus of points for which $R_T + R_R$ is constant. For a monostatic radar, the constant range contour reduces

to a circle because in this case, $R_T = R_R$. An example of constant range or constant delay contours is shown in Fig. 3-2. Also, constant signal-to-noise ratio contours can be described in terms of ovals of Cassini. These ovals are the loci of points for which the product $R_T R_R$ is constant. Typical ovals of Cassini are shown in Fig. 3-3. Again, for a monostatic radar, the constant SNR contour reduces to a circle. Note that in bistatic radars, these ovals of Cassini define three distinct operating regions: (I) receiver-centered region, the small oval around the receiver as given in Fig. 3-3; (II) transmitter-centered region, the small oval arround the transmitter; and (III) receiver/transmitter-centered region, called the cosite region, any of the regions surrounding both the transmitter and the receiver. As given in [6], the receiver centered region can be used for applications such as passive situation awareness where one is interested in the detection of a target around a passive receiver. The transmitter-centered region can be used with a non-cooperative transmitter. The cosite region can be used for medium range air defense and satellite or missile tracking.

The bistatic radar geometry can be defined in terms of four parameters, namely, θ_T, θ_R, L and R. However, it is sufficient to know any three of these, and the fourth one can be obtained from the knowledge about the other three. Also, R_T and R_R can be determined. In the following, relations among the parameters are developed. Three cases are considered.

Case I: θ_R, R and L are specified.

In this case, we assume that the total range R, baseline L and the receiver's look angle, or the angle of arrival of the target return, θ_R, are available. Applying the law of cosines to the bistatic triangle, we have

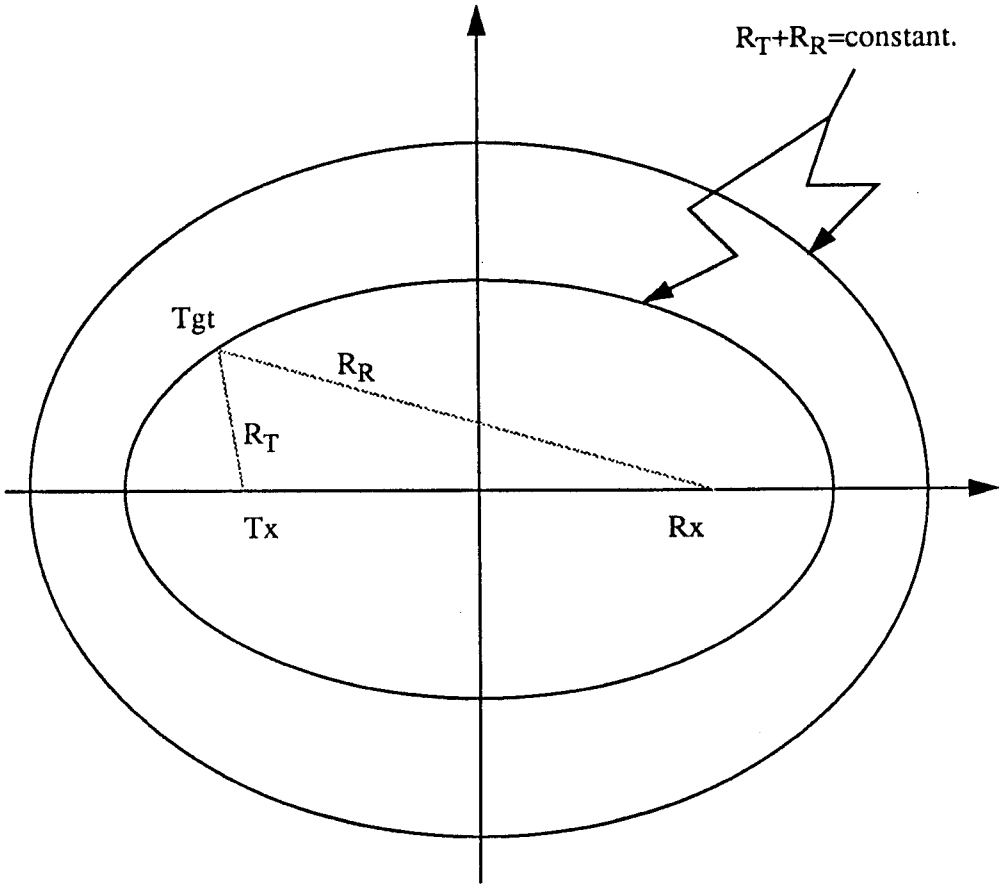

Fig. 3-2: Concentric Ellipses (Constant Range Contours)

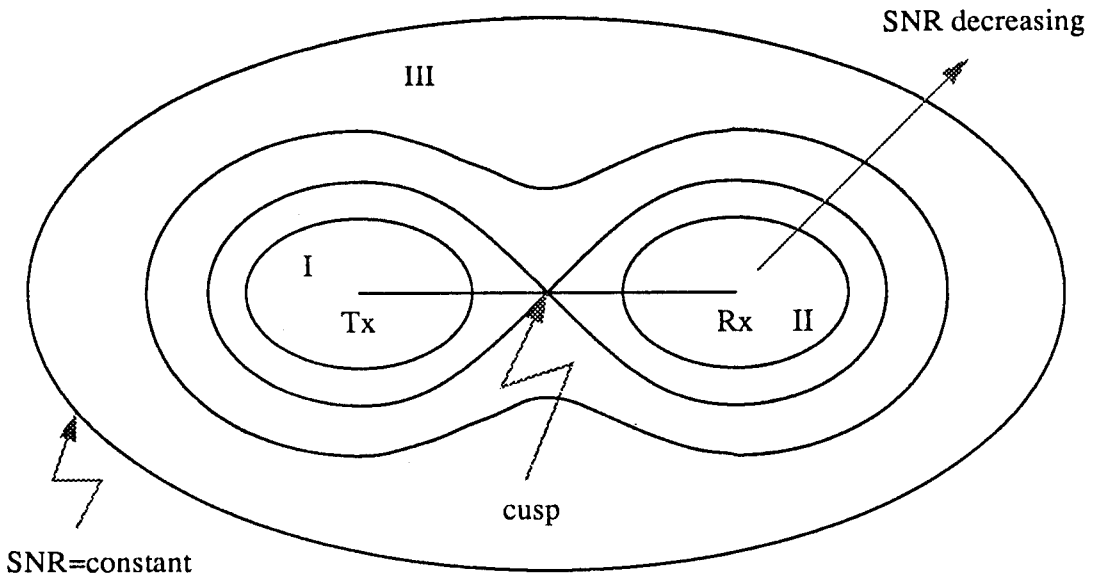

operating regions: I transmitter-centered region
II receiver-centered region
III cosite region

Fig. 3-3: Contours of Constant Signal-to-Noise Ratios (Ovals of Cassini)

$$R_T^2 = R_R^2 + L^2 - 2R_R L \cos(90^0 + \theta_R) \tag{3.1}$$

By definition, $R_T = R - R_R$. Then,

$$R_T^2 = (R - R_R)^2 = R^2 - 2RR_R + R_R^2 \tag{3.2}$$

Combining (3.1) and (3.2), we have

$$R^2 - 2RR_R + R_R^2 = R_R^2 + L^2 - 2R_R L \cos(90^0+\theta_R) \tag{3.3}$$

Rearranging terms of the two sides of (3.3), we obtain

$$R_R = \frac{R^2-L^2}{2(R+L\sin\theta_R)} \tag{3.4}$$

From (3.1),

$$R_T = [R_R^2 + L^2 + 2R_R L\sin\theta_R]^{1/2} \tag{3.5}$$

Using (3.4), we may obtain another expression for R_T

$$R_T = R - R_R = \frac{R^2+L^2+2RL\sin\theta_R}{2(R+L\sin\theta_R)} \tag{3.6}$$

Now, the distance between the target and both the transmitter and the receiver have been obtained.

Again, using the law of cosines, it can be written that

$$\begin{aligned} R_R^2 &= R_T^2 + L^2 - 2R_T L \cos(90^0 - \theta_T) \\ &= (R - R_R)^2 + L^2 - 2(R - R_R)L\sin\theta_T \\ &= R^2 - 2RR_R + R_R^2 + L^2 - 2(R - R_R)L\sin\theta_T \end{aligned} \tag{3.7}$$

Rearranging the two sides of (3.7), we have

$$\sin\theta_T = \frac{R^2+L^2-2RR_R}{2(R-R_R)L} \tag{3.8}$$

Substituting (3.4) into (3.8), we have

$$\theta_T = \begin{cases} \sin^{-1}\dfrac{(R^2+L^2)\sin\theta_R+2RL}{(R^2+L^2)+2RL\sin\theta_R}, & -\frac{\pi}{2} \le \theta_R < \frac{\pi}{2} \quad (3.9a) \\ \pi-\sin^{-1}\dfrac{(R^2+L^2)\sin\theta_R+2RL}{(R^2+L^2)+2RL\sin\theta_R}, & \frac{\pi}{2} \le \theta_R < \frac{3\pi}{2} \quad (3.9b) \end{cases}$$

where $-\frac{\pi}{2} \le \sin^{-1}(\cdot) < \frac{\pi}{2}$. Note that (3.9a) represents the case when the target is in the northern hemisphere, i.e., $-\frac{\pi}{2} \le \theta_R < \frac{\pi}{2}$. The operation $\sin^{-1}(\cdot)$ yields θ_T which is also in the northern hemisphere. However, when the target is in the southern hemisphere, i.e., $\frac{\pi}{2} \le \theta_R < \frac{3\pi}{2}$, θ_T is defined as in (3.9b) so that the resulting θ_T also corresponds to the southern hemisphere.

Thus, using (3.4), (3.6) and (3.9), the bistatic triangle is specified and the target's position is determined with the measurements of θ_R, R and L.

Case II: θ_T, R and L are specified

In this case, the total range R, baseline L and the transmitter's look angle θ_T are assumed to be given. Applying the law of cosines to the bistatic triangle, we have

$$R_R^2 = R_T^2 + L^2 - 2R_TL\cos(90^0 - \theta_T) \tag{3.10}$$

By definition $R_R = R - R_T$. Then

$$R_R^2 = (R - R_T)^2 = R^2 - 2RR_T + R_T^2 \tag{3.11}$$

Combining (3.10) and (3.11),

$$R^2 - 2RR_T + R_T^2 = R_T^2 + L^2 - 2R_T L \cos(90^0 - \theta_T) \tag{3.12}$$

Rearranging terms of the two sides of (3.12), we obtain

$$R_T = \frac{R^2 - L^2}{2(R - L\sin\theta_T)} \tag{3.13}$$

From (3.10),

$$R_R = [R_T^2 + L^2 - 2R_T L\sin\theta_T]^{1/2} \tag{3.14}$$

Alternatively, using (3.13), we may obtain another expression for R_R,

$$R_R = R - R_T = \frac{R^2 + L^2 - 2RL\sin\theta_T}{2(R - L\sin\theta_T)} \tag{3.15}$$

Thus, the distances between the target and both the transmitter and the receiver have been obtained.

Next, using the law of cosines, it is also found that

$$\begin{aligned} R_T^2 &= R_R^2 + L^2 - 2R_R L \cos(90^0 + \theta_R) \\ &= (R - R_T)^2 + L^2 - 2(R - R_T)L \cos(90^0 + \theta_R) \\ &= R^2 - 2RR_T + R_T^2 + L^2 + 2(R - R_T) L\sin\theta_R \end{aligned} \tag{3.16}$$

Rearranging the two sides of (3.16), we have

$$\sin\theta_R = \frac{2RR_T - R^2 - L^2}{2(R - R_T)L} \tag{3.17}$$

Substituting (3.13) into (3.17), we have

$$\theta_R = \begin{cases} \sin^{-1}\dfrac{(R^2+L^2)\sin\theta_T - 2RL}{R^2+L^2-2RL\sin\theta_T}, & -\dfrac{\pi}{2} \le \theta_T < \dfrac{\pi}{2} \quad (3.18a) \\ \pi - \sin^{-1}\dfrac{(R^2+L^2)\sin\theta_T - 2RL}{R^2+L^2-2RL\sin\theta_T}, & \dfrac{\pi}{2} \le \theta_T < \dfrac{3\pi}{2} \quad (3.18b) \end{cases}$$

As before, the cases of northern and southern hemispheres are treated separately in (3.18a) and (3.18b) respectively.

Hence, using (3.13), (3.15) and (3.18), the bistatic triangle is specified and target's position is determined with the measurements θ_T, R and L.

Case III: θ_R, θ_T and R are specified.

In this case, the angle measurements θ_R and θ_T, and the range measurement R are assumed to be available. Consider Fig. 3-4. It is found that, in the bistatic triangle,

$$R_T \cos\theta_T = R_R \cos\theta_R \quad (3.19)$$

Substituting $R_T = R - R_R$ into (3.19),

$$(R - R_R)\cos\theta_T = R_R \cos\theta_R \quad (3.20)$$

Rearranging the two sides of (3.20), we have

$$R_R = \frac{R\cos\theta_T}{\cos\theta_R + \cos\theta_T} \quad (3.21)$$

and

$$R_T = R - R_R = \frac{R\cos\theta_R}{\cos\theta_R + \cos\theta_T} \quad (3.22)$$

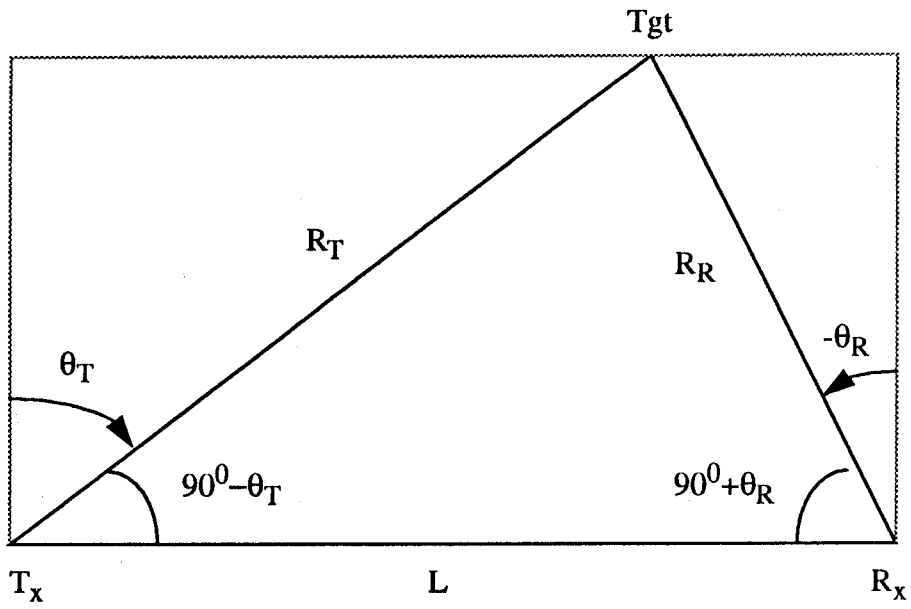

Fig. 3-4: Bistatic triangle and associated parameters

In the bistatic triangle, it is also true that

$$L = R_T \sin \theta_T - R_R \sin \theta_R \tag{3.23}$$

Substituting (3.21) and (3.22) for R_R and R_T, respectively, into (3.23), we have

$$L = \frac{R\sin(\theta_T - \theta_R)}{\cos \theta_T + \cos\theta_R} \tag{3.24}$$

Now, with (3.21), (3.22) and (3.24), and the given angle measurements, the bistatic triangle is totally specified.

3.2 Global, Earth-centered Coordinate System (DOD World Geodetic System)

This is a three-dimensional, right-handed rectangular coordinate system, with its origin set at the center of the earth, as shown in Figure 3-5. The z-axis points to the true north of the earth, and the x-y plane contains the equator. The x-axis passes through the zero (Greenwich) meridian. Position of an object is often provided in this coordinate system. Sometimes it is more convenient to specify the position of an object in terms of its geographic coordinates, i.e., the position is given in terms of its latitude λ, longitude L and height h above the mean sea level. These can be converted to the Global, Earth-centered coordinate system as follows:

$$X = (R_e + h) \cos \lambda \cos L$$

$$Y = (R_e + h) \cos \lambda \sin L$$

$$Z = (R_e + h) \sin \lambda$$

where R_e is the radius of the earth.

As indicated earlier, the North-referenced coordinate system is a convenient representation for the bistatic geometry and has been employed in this work. Next, we focus on the conversion of data presented in the Global, Earth-centered coordinate

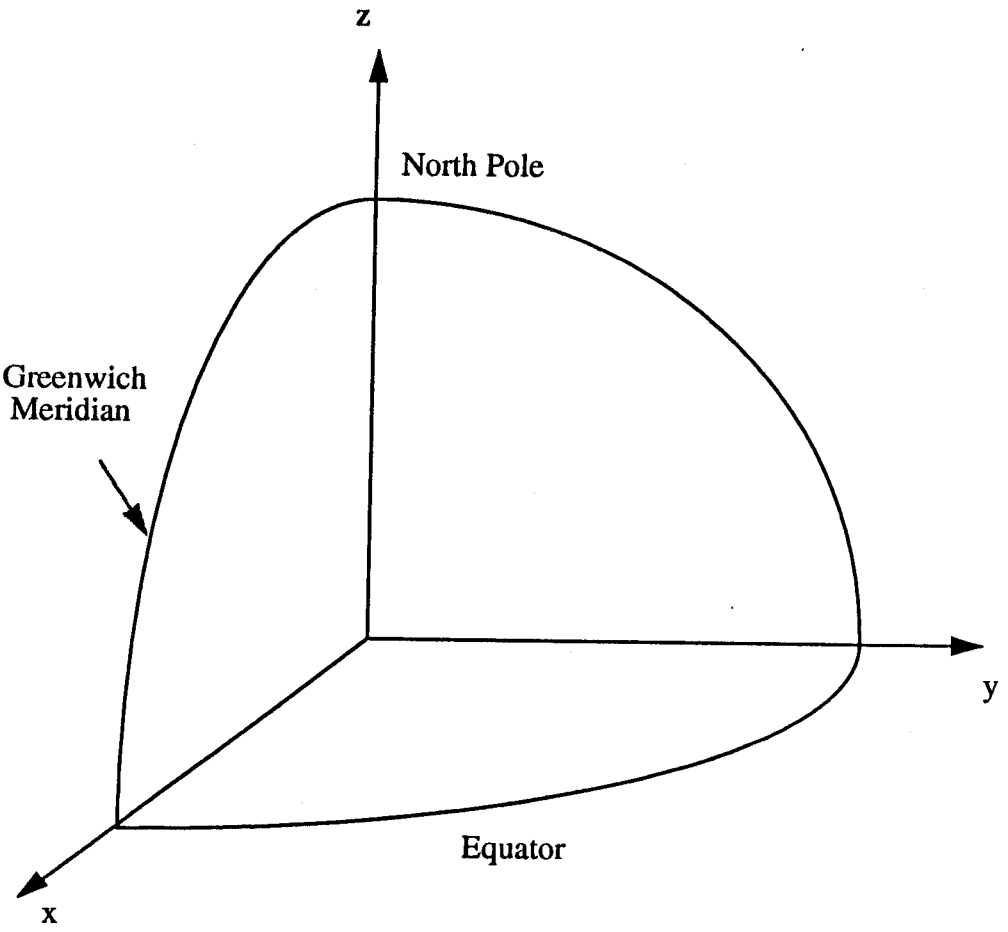

Fig. 3-5: Global, Earth-centered Coordinate System

system to the North-referenced coordinate system.

The measurements of the total range and baseline are readily available, and are independent of the coordinate system in use. Therefore, their conversion need not be considered here. On the other hand, the angles θ_T and θ_R in the bistatic plane are not available as direct radar measurements, when Global, Earth-centered coordinate system is used. The calculations of θ_T and θ_R, using the data given in the Global, Earth-centered coordinate system, are straightforward. Let us consider the system shown in Fig. 3-6. Using the position vectors of the transmitter $\vec{P}_T = (X_T, Y_T, Z_T)^T$, the receiver $\vec{P}_R = (X_R, Y_R, Z_R)^T$, and the target $\vec{P}_{Tgt} = (X_{Tgt}, Y_{Tgt}, Z_{Tgt})^T$, the following vectors can be formed:

$$\vec{L}_{TT} = \vec{P}_T - \vec{P}_{Tgt} = (X_T - X_{Tgt}, Y_T - Y_{Tgt}, Z_T - Z_{Tgt})^T \tag{3.25}$$

$$\vec{L}_{RT} = \vec{P}_R - \vec{P}_{Tgt} = (X_R - X_{Tgt}, Y_R - Y_{Tgt}, Z_R - Z_{Tgt})^T \tag{3.26}$$

and

$$\vec{L}_B = \vec{P}_T - \vec{P}_R = (X_T - X_R, Y_T - Y_R, Z_T - Z_R)^T \tag{3.27}$$

Then, from the definition of the inner product, the angle between $\vec{L}_{TT}$ and $\vec{L}_B$ is given by

$$\alpha = \cos^{-1} \frac{\vec{L}_{TT} \cdot \vec{L}_B}{|\vec{L}_{TT}| \cdot |\vec{L}_B|} \tag{3.28}$$

and the angle between $\vec{L}_{RT}$ and $(-\vec{L}_B)$ is given by

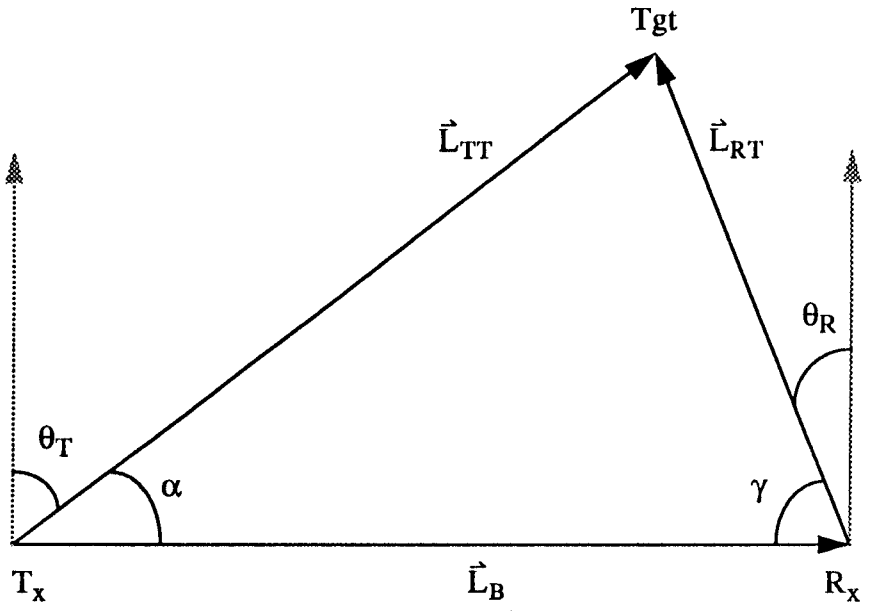

Fig. 3-6 : Geometry for the conversion of the Global, earth-centered coordinate system to the North-referenced coordinate system

$$\gamma = \cos^{-1}\frac{\vec{L}_{RT} \cdot (-\vec{L}_B)}{|\vec{L}_{RT}| \cdot |\vec{L}_B|} \tag{3.29}$$

where $\vec{A} \cdot \vec{B}$ is the inner product of vectors $\vec{A}$ and $\vec{B}$ and $|\vec{A}|$ is the magnitude of the vector $\vec{A}$. Since, $0 \le \cos^{-1}(\cdot) < \pi$, the angles θ_T and θ_R, in the bistatic plane, can be obtained as

$$\theta_T = \begin{cases} \frac{\pi}{2} - \alpha, & \text{when target is in the northern hemisphere} \\ \frac{\pi}{2} + \alpha, & \text{when target is in the southern hemisphere} \end{cases} \tag{3.30}$$

$$\theta_R = \begin{cases} \frac{\pi}{2} - \gamma, & \text{when target is in the northern hemisphere} \\ \frac{\pi}{2} + \gamma, & \text{when target is in the southern hemisphere} \end{cases} \tag{3.31}$$

Using the above procedure, measurements given in the Global earth-centered coordinate system can be converted to the North-referenced system.

3.3 Local Vertical Coordinate System

Another typical situation encountered in practice is that the measurements are taken in a local vertical coordinate system centered at the receiver site. This local coordinate system is usually specified with the receiver's local vertical as the z-axis, and the local horizontal as the x-y plane, in which the x-axis points in a convenient direction, such as towards the North pole and the y-axis points towards east. This configuration is known as the north-east-down coordinate system. In this setup, the target angle of arrival is measured in terms of the azimuth angle A_R, positive

clockwise from the x-axis, and the elevation angle E_R, measured from the receiver's nadir. Note that the measurements of the total range and the baseline are independent of the coordinate system in use. Therefore, their conversion need not be considered. In the following, we consider the derivation of θ_R. The angle θ_T can be obtained using the formula given in Section 3.1. Assume that the receiver has an estimate of the transmitter's angular position A_{RT} and E_{RT}. Also assume that the target and transmitter are both above the local horizontal, i.e., the x-y plane. Other situations will be considered later. Consider the geometry shown in Figure 3-7 (case I). Note that Tgt, K and M form a plane parallel to the local horizontal where K and M denote the intersections of this plane with the z-axis and the baseline respectively. Using the cosine law in the triangle Tgt K M, we have

$$\overline{Tgt\ M}^{\,2} = \overline{Tgt\ K}^{\,2} + \overline{KM}^{\,2} - 2\ \overline{Tgt\ K}\ \overline{KM}\cos(A_R - A_{RT}) \tag{3.32}$$

Next consider the bistatic plane, i.e., the plane formed by T_x, Tgt and R_x. Using the cosine law for the triangle with vertices M, Tgt and R_x in the bistatic plane, we have

$$\begin{aligned} \overline{TgtM}^{\,2} &= \overline{TgtR_x}^{\,2} + \overline{R_xM}^{\,2} - 2\ \overline{TgtR_x}\ \overline{R_xM}\cos(90^0+\theta_R) \\ &= \overline{TgtR_x}^{\,2} + \overline{R_xM}^{\,2} + 2\ \overline{TgtR_x}\ \overline{R_xM}\sin\theta_R \end{aligned} \tag{3.33}$$

But

$$\overline{TgtK} = \overline{TgtR_x}\cos(E_R - 90^0) = \overline{TgtR_x}\sin E_R \tag{3.34}$$

$$\overline{R_xK} = \overline{TgtR_x}\sin(E_R - 90^0) = \overline{R_xM}\sin(E_{RT} - 90^0) \tag{3.35}$$

and

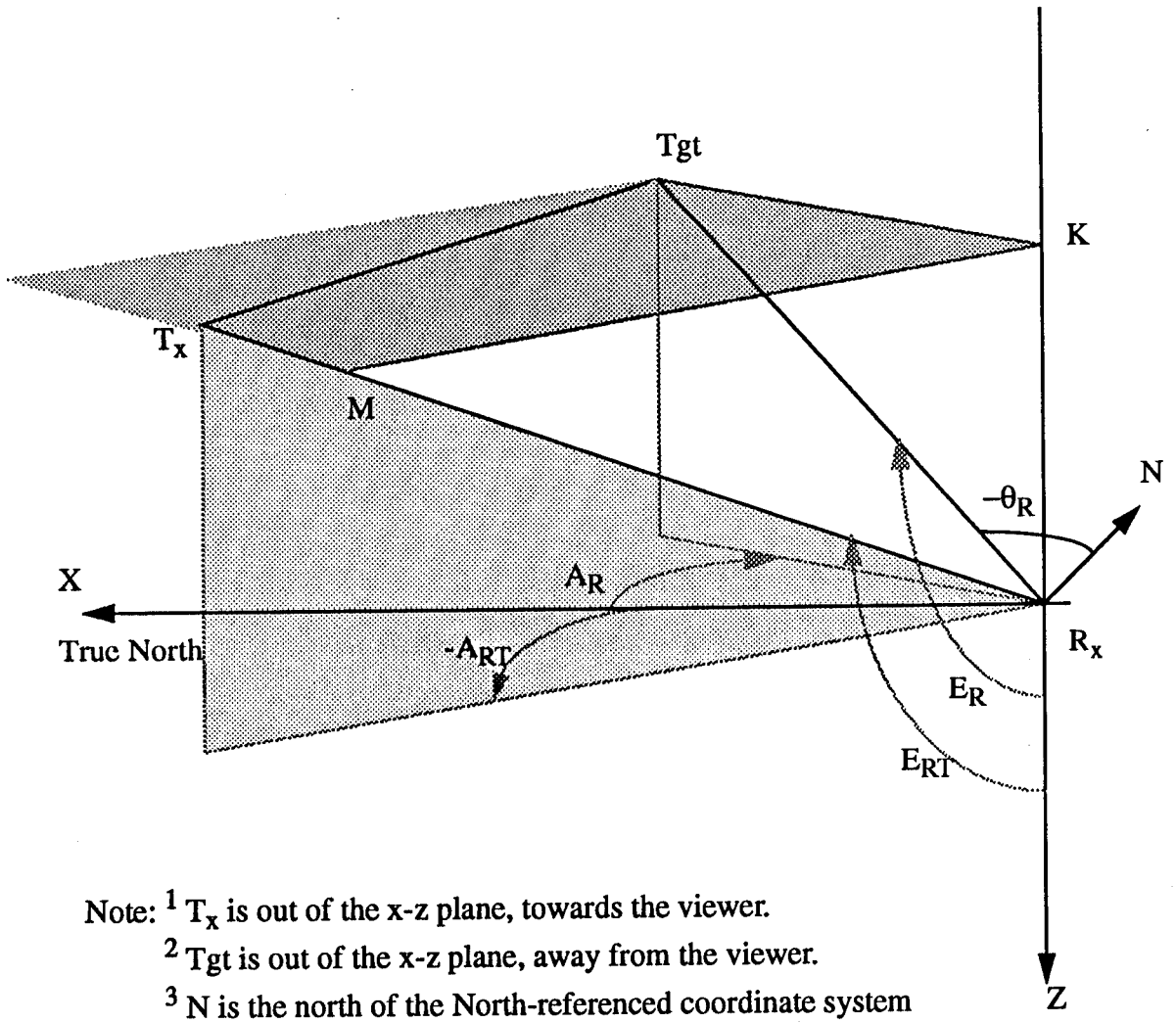

Note: [1] T_x is out of the x-z plane, towards the viewer.

[2] Tgt is out of the x-z plane, away from the viewer.

[3] N is the north of the North-referenced coordinate system

Fig. 3-7: Geometry for the conversion of the local vertical coordinate system to the North-referenced coordinate system for case I

$$\overline{KM} = \overline{R_x M}\cos(E_{RT}-90^0) = \overline{R_x M}\sin E_{RT} \tag{3.36}$$

From (3.35),

$$\begin{aligned}\overline{R_x M} &= \overline{TgtR_x}\sin(E_R-90^0)[\sin(E_{RT}-90^0)]^{-1} \\ &= \overline{TgtR_x}\left(\frac{\cos E_R}{\cos E_{RT}}\right)\end{aligned} \tag{3.37}$$

Substituting (3.37) into (3.36), we have

$$\overline{KM} = \overline{TgtR_x}\left(\frac{\cos E_R}{\cos E_{RT}}\right)\sin E_{RT} \tag{3.38}$$

Substituting (3.34) and (3.38) into (3.32), we have

$$\begin{aligned}\overline{TgtM}^{\,2} = \overline{TgtR_x}^{\,2}\sin^2 E_R + \overline{TgtR_x}^{\,2}\left(\frac{\cos E_R}{\cos E_{RT}}\right)^2\sin^2 E_{RT} \\ - 2\,\overline{TgtR_x}^{\,2}\sin E_R\left(\frac{\cos E_R}{\cos E_{RT}}\right)\sin E_{RT}\cos(A_R-A_{RT})\end{aligned} \tag{3.39}$$

Substituting (3.37) into (3.33), we have

$$\overline{TgtM}^{\,2} = \overline{TgtR_x}^{\,2} + \overline{TgtR_x}^{\,2}\left(\frac{\cos E_R}{\cos E_{RT}}\right)^2 + 2\,\overline{TgtR_x}^{\,2}\left(\frac{\cos E_R}{\cos E_{RT}}\right)\sin\theta_R \tag{3.40}$$

Equating the right-hand sides of (3.39) and (3.40), and then dividing by $\overline{TgtR_x}^{\,2}$, we have

$$\sin^2 E_R + \left(\frac{\cos E_R}{\cos E_{RT}}\right)^2 \sin^2 E_{RT} - 2\sin E_R \left(\frac{\cos E_R}{\cos E_{RT}}\right) \sin E_{RT} \cos(A_R - A_{RT}) = 1 + \left(\frac{\cos E_R}{\cos E_{RT}}\right)^2 + 2\left(\frac{\cos E_R}{\cos E_{RT}}\right) \sin\theta_R \quad (3.41)$$

Rearranging the two sides of (3.41), we arrive at

$$-\sin\theta_R = \left[\cos(A_R - A_{RT})\sin E_R \sin E_{RT} + \cos E_R \cos E_{RT}\right] \quad (3.42)$$

Note that, when $A_R - A_{RT} > 0$, the target is in the northern hemisphere; and when $A_R - A_{RT} < 0$, the target is in the southern hemisphere. Thus,

$$\theta_R = \begin{cases} -\sin^{-1}[\cos(A_R - A_{RT})\sin E_R \sin E_{RT} + \cos E_R \cos E_{RT}], \text{ when } A_R - A_{RT} > 0 & (3.43a) \\ \pi + \sin^{-1}[\cos(A_R - A_{RT})\sin E_R \sin E_{RT} + \cos E_R \cos E_{RT}], \text{ when } A_R - A_{RT} < 0 & (3.43b) \end{cases}$$

Next consider the case where, as shown in Fig. 3-8, both the target and the transmitter are below the local horizontal, i.e., below the x-y plane (case II). Compared with the prior situation, it is obvious that the derivation of θ_R can be carried out using the same procedure. In fact, the only modifications needed are the substitutions of $\pi - E_R$ and $\pi - E_{RT}$ for E_R and E_{RT}, respectively, in equations (3.34), (3.35) and (3.36). Thus, the result of (3.42) still holds true in this case. Finally, consider the case when the target and the transmitter are on different sides of the local horizontal of the receiver (case III). Without loss of generality, we assume that the target is above the plane and the transmitter is below it, as shown in Fig. 3-9. Note that point T is the mirror image of the transmitter T_x, with respect to the x-y plane. Also, Tgt, K and M form a plane parallel to the x-y plane. The point S is the intersection of the

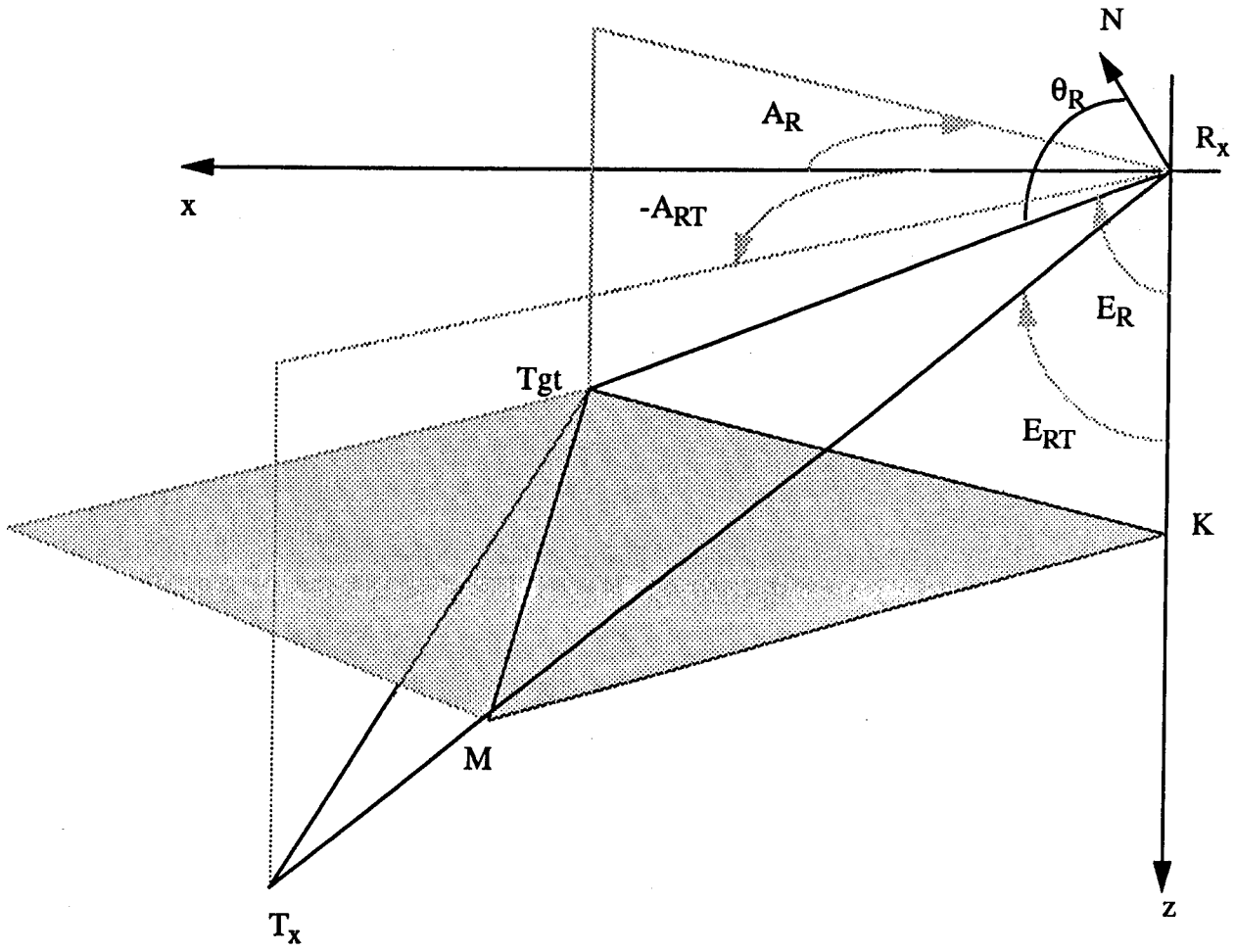

Note: [1] T_x is out of the x-z plane, towards the viewer.

[2] Tgt is out of the x-z plane, away from the viewer.

[3] N is the north of the North-referenced coordinate system

Fig. 3-8 : Geometry for the conversion of the local vertical coordinate system to the North-referenced coordinate system for case II

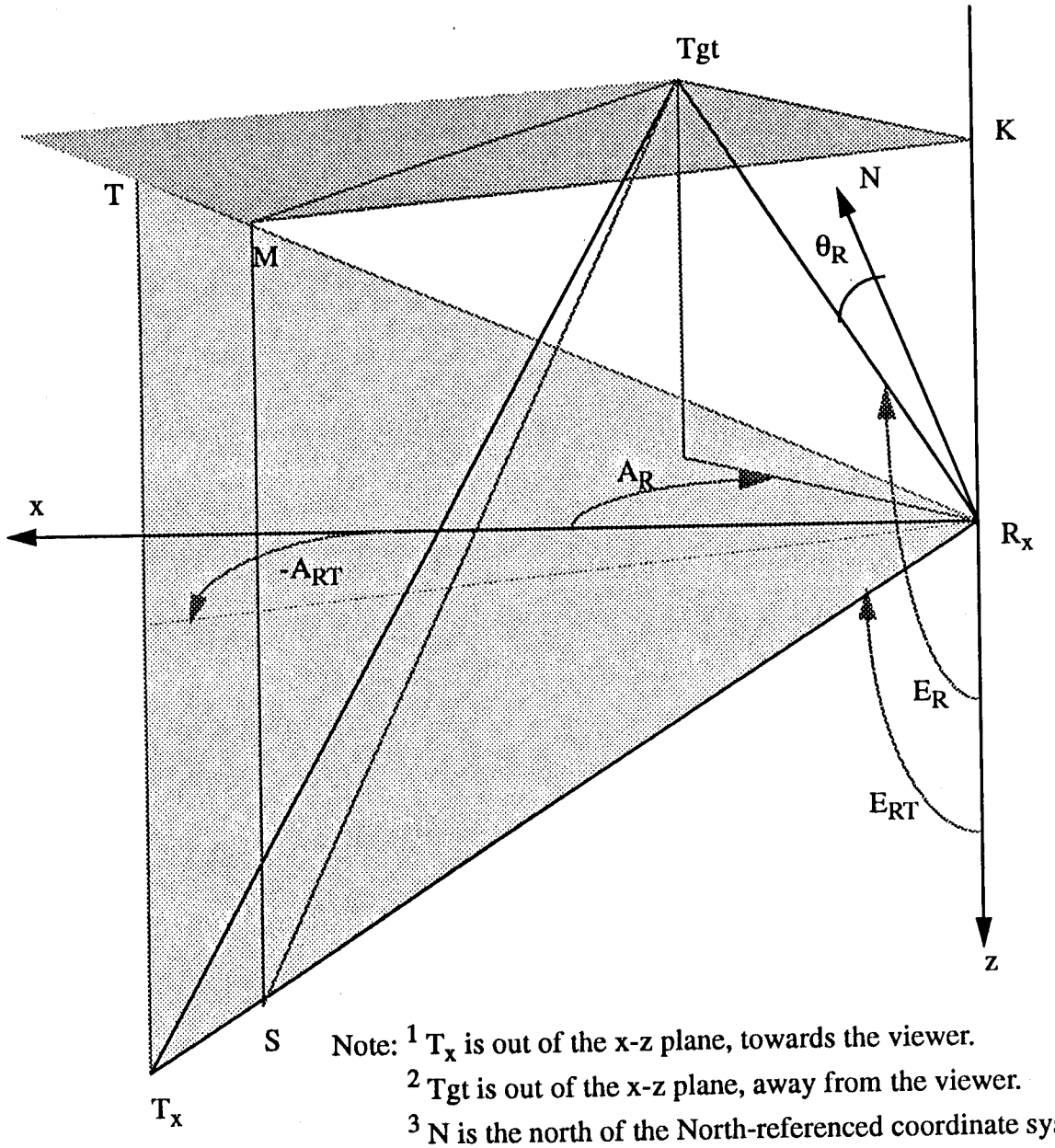

Note: [1] T_x is out of the x-z plane, towards the viewer.
[2] Tgt is out of the x-z plane, away from the viewer.
[3] N is the north of the North-referenced coordinate system

Fig. 3-9 : Geometry for the conversion of the local vertical coordinate system to the North-referenced coordinate system for case III

line $\overline{R_xT_x}$ and the line normal to the x-y plane and passing through M. Note that $\overline{TgtM} \perp \overline{MS}$, and $\overline{R_xM} = \overline{R_xS}$. Also, in the triangle formed by M, S and R_x, it is found that

$$\begin{aligned}\overline{MS}^2 &= \overline{R_xM}^2 + \overline{R_xS}^2 - 2\,\overline{R_xM}\,\overline{R_xS}\cos[2(90^0-E_{RT})] = 2\,\overline{R_xM}^2(1-\cos 2(90^0-E_{RT})) \\ &= 2\,\overline{R_xM}^2(1-(\cos^2(90^0-E_{RT}) - \sin^2(90^0-E_{RT}))) = 2\,\overline{R_xM}^2(1-\sin^2E_{RT} + \cos^2E_{RT}) \\ &= 4\,\overline{R_xM}^2\cos^2E_{RT}\end{aligned} \tag{3.44}$$

where we have used the fact that the x-y plane bisects the angle $\angle TR_xT_x$, and the lower half of this angle is equal to 90^0-E_{RT}. However, in the triangle formed by M, S and Tgt, we have

$$\begin{aligned}\overline{TgtS}^2 &= \overline{TgtM}^2 + \overline{MS^2} \\ &= \overline{TgtM}^2 + 4\,\overline{R_xM}^2\cos^2 E_{RT}\end{aligned} \tag{3.45}$$

where (3.44) has been used. In the triangle formed by Tgt, S and R_x, using the cosine law, we have

$$\begin{aligned}\overline{TgtS}^2 &= \overline{TgtR_x}^2 + \overline{R_xS}^2 - 2\,\overline{TgtR_x}\,\overline{R_xS}\cos(90^0+\theta_R) \\ &= \overline{TgtR_x}^2 + \overline{R_xM}^2 + 2\,\overline{TgtR_x}\,\overline{R_xM}\sin\theta_R\end{aligned} \tag{3.46}$$

where $\overline{R_xS} = \overline{R_xM}$ has been invoked. Combining (3.45) and (3.46), and rearranging terms, we have

$$\overline{TgtM}^2 = \overline{TgtR_x}^2 + \overline{R_xM}^2 - 4\,\overline{R_xM}^2\cos^2E_{RT} + 2\,\overline{TgtR_x}\,\overline{R_xM}\sin\theta_R \tag{3.47}$$

Also, in the triangle formed by Tgt, K and M, using the law of cosines,

$$\overline{TgtM}^{\,2} = \overline{TgtK}^{\,2} + \overline{KM}^{\,2} - 2\,\overline{TgtK}\;\overline{KM}\cos(A_R - A_{RT}) \tag{3.48}$$

From the triangle formed by Tgt, K and R_x, we have

$$\overline{TgtK} = \overline{TgtR_x}\cos(E_R - 90^0) = \overline{TgtR_x}\sin E_R \tag{3.49}$$

$$\overline{R_xK} = \overline{TgtR_x}\sin(E_R - 90^0) = \overline{R_xM}\sin(90^0 - E_{RT}) \tag{3.50}$$

and

$$\overline{KM} = \overline{R_xM}\cos(90^0 - E_{RT}) = \overline{R_xM}\sin E_{RT} \tag{3.51}$$

where, in (3.50) and (3.51), we have again used the fact that the x-y plane bisects the angle $\angle TR_xT_x$. From (3.50),

$$\overline{R_xM} = \overline{TgtR_x}\sin(E_R - 90^0)\left[\sin(90^0 - E_{RT})\right]^{-1} = \overline{TgtR_x}\left(-\frac{\cos E_R}{\cos E_{RT}}\right) \tag{3.52}$$

Substituting (3.52) into (3.51), we have

$$\overline{KM} = \overline{TgtR_x}\left(-\frac{\cos E_R}{\cos E_{RT}}\right)\sin E_{RT} \tag{3.53}$$

Substituting (3.49) and (3.53) into (3.48), we obtain

$$\begin{aligned}\overline{TgtM}^{\,2} = {} & \overline{TgtR_x}^{\,2}\sin^2 E_R + \overline{TgtR_x}^{\,2}\left(\frac{\cos E_R}{\cos E_{RT}}\right)^2\sin^2 E_{RT} \\ & + 2\,\overline{TgtR_x}^{\,2}\sin E_R\left(\frac{\cos E_R}{\cos E_{RT}}\right)\sin E_{RT}\cos(A_R - A_{RT})\end{aligned} \tag{3.54}$$

Substituting (3.52) into (3.47), we have

$$\overline{TgtM}^{\,2} = \overline{TgtR_x}^{\,2} + \overline{TgtR_x}^{\,2}\left(\frac{\cos E_R}{\cos E_{RT}}\right)^2 - 4\,\overline{TgtR_x}^{\,2}\left(\frac{\cos E_R}{\cos E_{RT}}\right)^2 \cos^2 E_{RT} - \overline{TgtR_x}^{\,2}\left(\frac{\cos E_R}{\cos E_{RT}}\right)\sin\theta_R \tag{3.55}$$

Equating the right hand sides of (3.54) and (3.55), and dividing the result by $\overline{TgtR_x}^{\,2}$, we have

$$\sin^2 E_R + \left(\frac{\cos E_R}{\cos E_{RT}}\right)\sin^2 E_{RT} + 2\sin E_R\left(\frac{\cos E_R}{\cos E_{RT}}\right)\sin E_{RT}\cos(A_R - A_{RT}) = 1 + \left(\frac{\cos E_R}{\cos E_{RT}}\right)^2 - 4\cos^2 E_R - \left(\frac{\cos E_R}{\cos E_{RT}}\right)\sin\theta_R \tag{3.56}$$

After rearranging terms in (3.56), we again arrive at the same result as (3.42). Also, the analysis for the case, in which the target is below the local horizontal of the receiver, while the transmitter is above, it takes exactly the same steps as before, and results in the same equation as (3.42). Therefore, it is concluded that (3.43) properly describes the general situation. Then, with the expression (3.43) and using the procedures developed in Section 3.1, θ_T can be obtained.

3.4 Discussion

In this chapter, we have described the two-dimensional North-referenced coordinate system. It adequately describes the bistatic geometry. Due to its convenience, we have used it in our analysis. We also described two other widely used coordinate systems and provided transformation procedures for conversion to the north-referenced coordinate system. It should be noted that conversion from the north-referenced coordinate system to other higher dimensional systems is not possible.

4 ANALYSIS OF AMBIGUITY FUNCTION FOR BISTATIC RADAR

This chapter investigates the concept of ambiguity function for a bistatic radar. First, we consider the return signal from a moving target for a bistatic radar and derive expressions for target position and its velocity. This problem has been studied extensively for a monostatic radar [2] but no results for the bistatic case are available and are developed here. Next, bistatic geometry factors are included in the evaluation of the ambiguity function. It is shown that plotting the ambiguity function on the delay-Doppler plane is no longer appropriate. Suitable arguments for the ambiguity function are determined. Examples are given to illustrate the concepts developed in this chapter.

4.1 Measurements on A Moving Target

Consider the bistatic geometry consisting of the transmitter T_x, the receiver R_x and the target Tgt as shown in Fig. 4-1. Assume that a signal is transmitted by T_x at time t=0. It reaches the target at $t=\tau_1$ and the reflected signal is received by R_x at $t=\tau_a$. Then the total time delay $\tau(t)$, i.e., the total travel time from T_x to R_x, is given by

$$\tau(t)\big|_{t=\tau_a} = \tau_a \tag{4.1}$$

The time delay $\tau(t)$ is a function of the bistatic geometry, i.e., the relative positions of T_x, Tgt and R_x. The same value of $\tau(t)$ is attained for targets lying on the same constant range contours. Therefore, we may express

$$\tau(\tau_a) = \frac{1}{c}R(\tau_1) = \frac{1}{c}[R_T(\tau_1)+R_R(\tau_1)] \tag{4.2}$$

where c is the wave propagation speed, $R(\cdot)$ is the total range, $R_T(\cdot)$ and $R_R(\cdot)$ are the range components corresponding to the transmitter and receiver respectively. Note

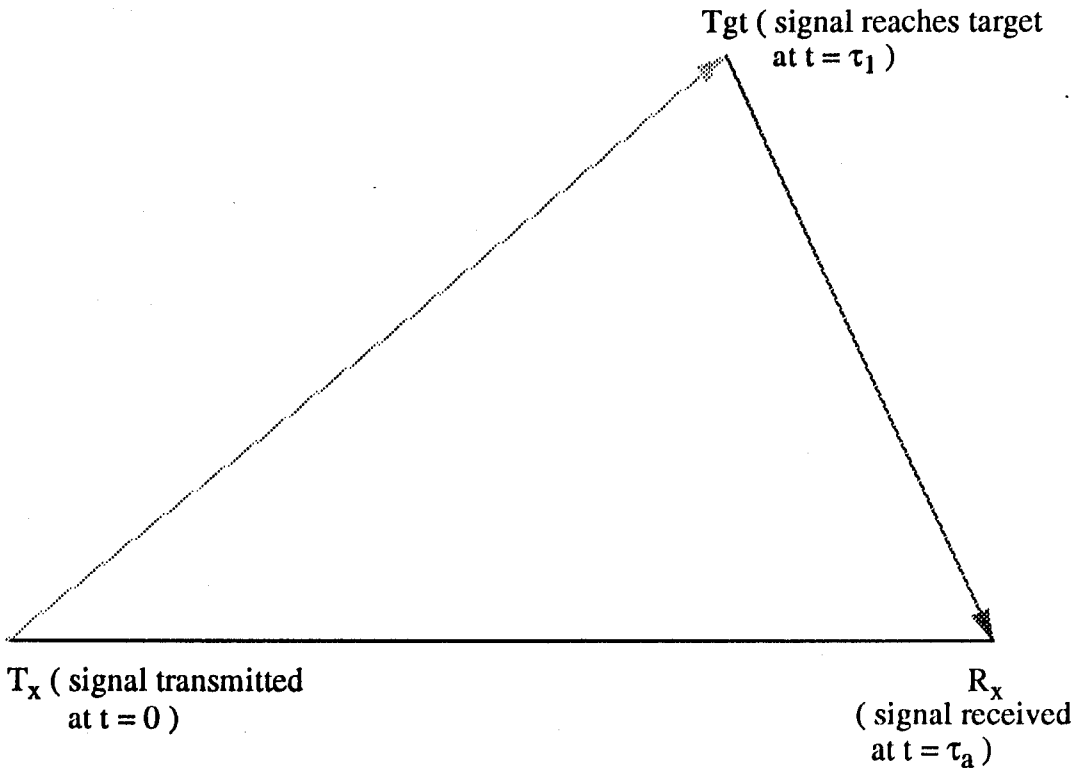

$\overline{T_xTgt}$ = (speed of light)$\times\tau_1$

$\overline{TgtR_x}$ = (speed of light)$\times$(τ_a-τ_1)

total time delay (total travel time of the signal) = τ_a

Fig. 4-1: Timing relationships in bistatic radar geometry

that (4.2) indicates that the total time delay at $t=\tau_a$ depends on the target's position at $t=\tau_1$.

The time delay $\tau_R(t)$, corresponding to the travel time from the target to the receiver, is given by

$$\tau_R(\tau_a) = \tau_a - \tau_1 \tag{4.3}$$

But, it can also be written as

$$\tau_R(\tau_a) = \frac{1}{c} R_R(\tau_1) \tag{4.4}$$

Thus, using (4.3), we have

$$\tau_R(\tau_a) = \frac{1}{c} R_R(\tau_a - \tau_R(\tau_a)) \tag{4.5}$$

Similarly using (4.2),

$$\tau(\tau_a) = \frac{1}{c} R(\tau_a - \tau_R(\tau_a)) \tag{4.6}$$

Using Taylor series expansion to expand $\tau(t)$ around τ_a we can write

$$\tau(t) = \tau(\tau_a) + \frac{(t-\tau_a)}{1} \frac{d}{dt} \tau(\tau_a) + \frac{(t-\tau_a)^2}{2!} \frac{d^2}{dt^2} \tau(\tau_a) + \cdots \tag{4.7}$$

Let us next consider the first two derivatives of $\tau(t)$ in the above expansion. From (4.6),

$$\frac{d}{dt}\tau(\tau_a) = \frac{1}{c}\frac{d}{dt}R(t-\tau_R(t))\Big|_{t=\tau_a}$$

$$= \frac{1}{c}\dot{R}(t-\tau_R(t))[1-\dot{\tau}_R(t)]\Big|_{t=\tau_a} \tag{4.8}$$

$$\frac{d^2}{dt^2}\tau(\tau_a) = \frac{d}{dt}[\frac{d}{dt}\tau(t)]\Big|_{t=\tau_a} = \frac{1}{c}\frac{d}{dt}[\dot{R}(t-\tau_R(t))(1-\dot{\tau}_R(t))]\Big|_{t=\tau_a}$$

$$= \frac{1}{c}[\ddot{R}(t-\tau_R(t))[1-\dot{\tau}_R(t)]^2-\dot{R}(t-\tau_R(t))\ddot{\tau}_R(t)]\Big|_{t=\tau_a} \tag{4.9}$$

where (4.8) has been used in deriving (4.9). From (4.5)

$$\frac{d}{dt}\tau_R(\tau_a) = \frac{1}{c}\frac{d}{dt}R_R(t-\tau_R(t))\Big|_{t=\tau_a}$$

$$= \frac{1}{c}\dot{R}_R(t-\tau_R(t))[1-\dot{\tau}_R(t)]\Big|_{t=\tau_a} \tag{4.10}$$

Rearranging (4.10), we have

$$\frac{d}{dt}\tau_R(\tau_a) = \frac{1}{c}\dot{R}_R(t-\tau_R(t))\ [1+\frac{1}{c}\dot{R}_R(t-\tau_R(t))]^{-1}\Big|_{t=\tau_a} \tag{4.11}$$

Also, using (4.10) and (4.11)

$$\frac{d^2}{dt^2}\tau_R(\tau_a) = \frac{d}{dt}[\frac{d}{dt}\tau_R(t)]\Big|_{t=\tau_a}$$

$$= \frac{1}{c}\ddot{R}_R(t-\tau_R(t))\ [1-\dot{\tau}_R(t)]^2 - \frac{1}{c}\dot{R}_R(t-\tau_R(t))\ddot{\tau}_R(t)\Big|_{t=\tau_a}$$

$$= \frac{1}{c}\ddot{R}_R(t-\tau_R(t))\ [1+\frac{1}{c}\dot{R}_R(t-\tau_R(t))]^{-2}-\frac{1}{c}\dot{R}_R(t-\tau_R(t))\ddot{\tau}_R(t)\Big|_{t=\tau_a} \tag{4.12}$$

Thus, rearranging (4.12)

$$\frac{d^2}{dt^2}\tau_R(\tau_a) = \frac{1}{c}\ddot{R}_R(t-\tau_R(t))\ [1+\frac{1}{c}\dot{R}_R(t-\tau_R(t))]^{-3}|_{t=\tau_a} \tag{4.13}$$

Using (4.11) and (4.13), we can rewrite (4.8) and (4.9) as

$$\frac{d}{dt}\tau(\tau_a) = \frac{1}{c}\dot{R}(t-\tau_R(t))\ [1+\frac{1}{c}\dot{R}_R(t-\tau_R(t))]^{-1}|_{t=\tau_a} \tag{4.14}$$

and

$$\begin{aligned}
\frac{d^2}{dt^2}\tau(\tau_a) &= \frac{1}{c}\ddot{R}(t-\tau_R(t))\ [1+\frac{1}{c}\dot{R}_R(t-\tau_R(t))]^{-2}-\frac{1}{c}\dot{R}(t-\tau_R(t))\ [\frac{1}{c}\ddot{R}_R(t-\tau_R(t))]\ [1+\frac{1}{c}\dot{R}_R(t-\tau_R(t))\\
&= \frac{1}{c}[\ddot{R}(t-\tau_R(t))(1+\frac{1}{c}\dot{R}_R(t-\tau_R(t)))\\
&\quad -\dot{R}(t-\tau_R(t))(\frac{1}{c}\ddot{R}_R(t-\tau_R(t)))]\ [1+\frac{1}{c}\dot{R}_R(t-\tau_R(t))]^{-3}|_{t=\tau_a}\\
&= \frac{1}{c}[(\ddot{R}_T(t-\tau_R(t))+\ddot{R}_R(t-\tau_R(t)))(1+\frac{1}{c}\dot{R}_R(t-\tau_R(t)))\\
&\quad -(\dot{R}_T(t-\tau_r(t))+\dot{R}_R(t-\tau_R(t)))(\frac{1}{c}\ddot{R}_R(t-\tau_R(t)))]\ [1+\frac{1}{c}\dot{R}_R(t-\tau_R(t))]^{-3}|_{t=\tau_a}\\
&= \frac{1}{c}[\ddot{R}_T(t-\tau_R(t))+\ddot{R}_R(t-\tau_R(t))+\frac{1}{c}\ddot{R}_T(t-\tau_R(t))\dot{R}_R(t-\tau_R(t))+\frac{1}{c}\ddot{R}_R(t-\tau_R(t))\dot{R}_R(t-\tau_R(t))\\
&\quad -\frac{1}{c}\ddot{R}_R(t-\tau_R(t))\dot{R}_T(t-\tau_R(t))-\frac{1}{c}\ddot{R}_R(t-\tau_R(t))\dot{R}_R(t-\tau_R(t))]\ [1+\frac{1}{c}\dot{R}_R(t-\tau_R(t))]^{-3}|_{t=\tau_a}\\
&= \frac{1}{c}[(1+\frac{1}{c}\dot{R}_R(t-\tau_R(t)))\ddot{R}_T(t-\tau_R(t))\\
&\quad +(1-\frac{1}{c}\dot{R}_T(t-\tau_R(t)))\ddot{R}_R(t-\tau_R(t))]\ [1+\frac{1}{c}\dot{R}_R(t-\tau_R(t))]^{-3}|_{t=\tau_a}
\end{aligned} \tag{4.15}$$

where, in deriving (4.15), we have used the relationships

$\dot{R}(t) = \dot{R}_T(t)+\dot{R}_R(t)$ and $\ddot{R}(t) = \ddot{R}_T(t)+\ddot{R}_R(t)$.

As a check, if we set $R_T(t) = R_R(t) = \frac{1}{2}R(t)$ and $\tau_R(t) = \frac{1}{2}\tau(t)$, equations (4.6),

(4.14) and (4.15) reduce to the well known results for the monostatic case [2]. Specifically, (4.6) can be written as

$$\begin{aligned}\tau(\tau_a) &= \frac{1}{c}R(\tau_a - \tau_R(\tau_a)) \\ &= \frac{2}{c}R_R(\tau_a - \frac{1}{2}\tau(\tau_a)) \\ &= \frac{2}{c}R_R(\tau_a - \frac{1}{2}\tau_a) \\ &= \frac{2}{c}R_R(\frac{\tau_a}{2})\end{aligned} \tag{4.16}$$

where (4.1) has been used, i.e., $\tau(\tau_a) = \tau_a$. Also, (4.14) can be written as

$$\begin{aligned}\frac{d}{dt}\tau(\tau_a)|_{t=\tau_a} &= \frac{1}{c}\dot{R}(\tau_a - \tau_R(\tau_a))[1 + \frac{1}{c}\dot{R}_R(\tau_a - \tau_R(\tau_a))]^{-1} \\ &= \frac{2}{c}\dot{R}_R(\tau_a - \frac{1}{2}\tau(\tau_a))\ [1 + \frac{1}{c}\dot{R}_R(\tau_a - \frac{1}{2}\tau(\tau_a))]^{-1} \\ &= \frac{2}{c}\dot{R}_R(\frac{\tau_a}{2})\ [1 + \frac{1}{c}\dot{R}_R(\frac{\tau_a}{2})]^{-1}\end{aligned} \tag{4.17}$$

and (4.15) can be written as

$$\frac{d^2}{dt^2}\tau(\tau_a) = \frac{1}{c}\left[\left(1+\frac{1}{c}\dot{R}_R(\tau_a-\tau_R(\tau_a))\right)\ddot{R}_T(\tau_a-\tau_R(\tau_a)) + \left(1-\frac{1}{c}\dot{R}_R(\tau_a-\tau_R(\tau_a))\right)\ddot{R}_R(\tau_a-\tau_R(\tau_a))\right]$$

$$\cdot\left[1+\frac{1}{c}\dot{R}_R(\tau_a-\tau_R(\tau_a))\right]^{-3}$$

$$= \frac{1}{c}\left[\left(1+\frac{1}{c}\dot{R}_R(\tau_a-\frac{1}{2}\tau(\tau_a))\right)\ddot{R}_R(\tau_a-\frac{1}{2}\tau(\tau_a)) + \left(1-\frac{1}{c}\dot{R}_R(\tau_a-\frac{1}{2}\tau(\tau_a))\right)\ddot{R}_R(\tau_a-\frac{1}{2}\tau(\tau_a))\right]$$

$$\cdot\left[1+\frac{1}{c}\dot{R}_R(\tau_a-\frac{1}{2}\tau(\tau_a))\right]^{-3}$$

$$= \frac{2}{c}\ddot{R}_R(\frac{1}{2}\tau_a)\left[1+\frac{1}{c}\dot{R}_R(\frac{\tau_a}{2})\right]^{-3} \tag{4.18}$$

For targets of practical interest, $\dot{R}_T(t)/c$ and $\dot{R}_R(t)/c$ are very small. Consequently, (4.14) and (4.15) reduce to

$$\frac{d}{dt}\tau(\tau_a) \approx \frac{1}{c}\dot{R}(t-\tau_R(t))\Big|_{t=\tau_a} \tag{4.19}$$

and

$$\frac{d^2}{dt^2}\tau(\tau_a) \approx \frac{1}{c}\ddot{R}(t-\tau_R(t))\Big|_{t=\tau_a} \tag{4.20}$$

Substituting the expressions for the derivatives in the series expansion (4.7), we have

$$\tau(t) = \tau(\tau_a) + (\tau-\tau_a)\frac{d}{dt}\tau(\tau_a) + \frac{(t-\tau_a)^2}{2}\frac{d^2}{dt^2}\tau(\tau_a) + \cdots$$

$$\approx \tau_a + (t-\tau_a)\left[\frac{1}{c}\dot{R}(\tau_a-\tau_R(\tau_a))\right] + \frac{(t-\tau_a)^2}{2}\left[\frac{1}{c}\ddot{R}(\tau_a-\tau_R(\tau_a))\right] + \cdots \tag{4.21}$$

In the analysis to follow, we will assume that the total range is a relatively smooth function of time, over the coherent processing period, such that the second

and higher order derivatives can be dropped, i.e., $\dot{R}(\tau_a-\tau_R(\tau_a))$, $\ddot{R}(\tau_a-\tau_R(\tau_a))$, ... are negligible. Note that this assumption may not hold true for a maneuvering target. It will further be assumed that the transmitted radar signal is narrowband, so that the complex envelope of the signal is insensitive to the target's motion. That is,

$$\tilde{f}(t-[\tau_a+\frac{1}{c}(t-\tau_a)\dot{R}(\tau_a-\tau_R(\tau_a))]) \approx \tilde{f}(t-\tau_a) \tag{4.22}$$

where $\tilde{f}(t)$ is the complex envelope of the transmitted signal. In short, we have assumed that the range rates of the second and higher orders are negligible, and the effect of the first order range rate, upon the complex envelope, can be ignored. The validity of these assumptions has been generally accepted for monostatic radars [2]. Yet, little consideration has been given to the bistatic case. From the analysis in the following subsection, it is found that, for the same target motion relative to the ground, the resulting range rates are smaller in the bistatic radar than in the monostatic case. Therefore, in this work these assumptions are employed for the ambiguity function analysis of bistatic radar. However, a detailed study of this issue, i.e., the conditions under which these assumptions are valid, is desirable and may be carried out in the next phase of this effort.

With the aforementioned simplifications, the return signal can be modeled as

$$\begin{aligned}\tilde{r}(t) &= \tilde{b}\sqrt{E_t}\tilde{f}(t-\tau(t))\, e^{j\omega_0(t-\tau(t))}+\tilde{n}(t) \\ &= \tilde{b}\sqrt{E_t}\tilde{f}(t-\tau_a)\, e^{j[\omega_0-\frac{\omega_0}{c}\dot{R}(\tau_a-\tau_R(\tau_a))](t-\tau_a)}+\tilde{n}(t), \qquad 0\le t\le T\end{aligned} \tag{4.23}$$

where $\tilde{b}$ is given by the reflectivity of the target, E_t is the energy of the transmitted

signal, ω_0 is the carrier's angular frequency, T is the duration of the signal, and $\tilde{n}(t)$ is the complex envelope of the additive noise.

Note that the term τ_a in (4.23) is given by the total range, and the term $\frac{\omega_0}{c}\dot{R}(\tau_a - \tau_R(\tau_a))$ represents the Doppler shift. Then, the delay τ_a and the Doppler shift $\frac{\omega_0}{c}\dot{R}(\tau_a - \tau_R(\tau_a))$ can be extracted by using a matched filter and a square-law envelope detector, as described in Chapter 2.

In the following, we will examine the manner in which the measurements of range and range rate are related to target location and its velocity. That is, for a hypothesized target location and its velocity, the resulting total time delay and Doppler shift will be derived.

4.1.1 Range and Target Location

In bistatic radars, the target location may be specified either with respect to the receiver, or the transmitter. That is, in the North-referenced coordinate system, the range R_R and the angle θ_R, or the range R_T and the angle θ_T, are given to specify the target location. Given the baseline, the calculation of the resulting total range from a given target location is then straightforward.

In the case where target location is given in terms of R_R and θ_R, recall equation (3.1),

$$R = R_R + \sqrt{R_R^2 + L^2 + 2R_R L \sin\theta_R}$$

Thus, with the additional knowledge of the baseline, the total range is determined. To emphasize the functional relationship between the total range and the parameters

R_R, L and θ_R, we define the function

$$D_R = D(R_R, L, \theta_R) \triangleq \frac{1}{c}[R_R + \sqrt{R_R^2 + L^2 + 2R_R L \sin\theta_R}] \tag{4.24}$$

Note that D_R is the total time delay given as a function of R_R, L and θ_R. In the case where the target location is given in terms of R_T and θ_T, from (3.11), we have

$$R = R_T + \sqrt{R_T^2 + L^2 - 2R_T L \sin\theta_T} \tag{4.25}$$

We may define the total time delay D_T as a function of R_T, L and θ_T in a similar manner, i.e.,

$$D_T = D(R_T, L, -\theta_T) = \frac{1}{c}[R_T + \sqrt{R_T^2 + L^2 - 2R_T L \sin\theta_T}] \tag{4.26}$$

Now, the total time delay, or equivalently the total range, can be found using the function D. In other words, when bistatic geometry is given in terms of R_R, L and θ_R, or in terms of R_T, L and θ_T, the resulting total time delay is given by D_R, or D_T, respectively.

4.1.2 Range Rate and Target Velocity

As derived earlier, the Doppler shift is given by $\omega_D = \frac{\omega_0}{c}\dot{R}(\tau_a - \tau_R(\tau_a))$.

Since the time argument in the measurements is not of concern in this analysis, it will not be expressed explicitly in the following derivation. We will first consider the generalized case where T_x, R_x and Tgt are all moving, as shown in Fig. 4-2, and then focus on the effects of target motion alone. Note that the angle ϕ_T is the angle between the transmitter's velocity vector V_T and the north of the North-referenced coordinate system, while the angle ϕ_R is the angle between the receiver's velocity

vector V_R and the north. Both ϕ_T and ϕ_R are measured in the same convention as θ_T and θ_R, i.e., they are positive clockwise. The angle ϕ is the angle between the target velocity vector V and the bistatic bisector, positive clockwise from the bisector. By definition, it can be written that

$$\frac{d}{dt}R = \frac{d}{dt}R_T + \frac{d}{dt}R_R \tag{4.27}$$

From Fig. 4-2, it is easy to see that

$$\frac{d}{dt}R_T = -V\cos\left(\phi - \frac{|\beta|}{2}\right) - V_T\cos(\phi_T - \theta_T) \tag{4.28}$$

Note that the first term on the right hand side of (4.28) is the velocity projection of V along the line connecting Tgt and T_X, and the second term the projection of V_T along the same line. Also, we find that

$$\frac{d}{dt}R_R = -V\cos\left(\phi + \frac{|\beta|}{2}\right) - V_R\cos(\phi_R - \theta_R) \tag{4.29}$$

Here, in (4.29), the first term on the right hand side represents the velocity component of V along the line connecting Tgt and R_X, and the second term the component of V_R along the same line. The appearances of the absolute sign in (4.28) and (4.29) are due to the way β is defined. Recall that $\beta = \theta_T - \theta_R$. Then, $0 \le \beta < \pi$ when the target is in the northern hemisphere, and $-\pi < \beta < 0$ when the target is in the southern hemisphere.

Thus, substituting (4.28) and (4.29) into (4.27), we have

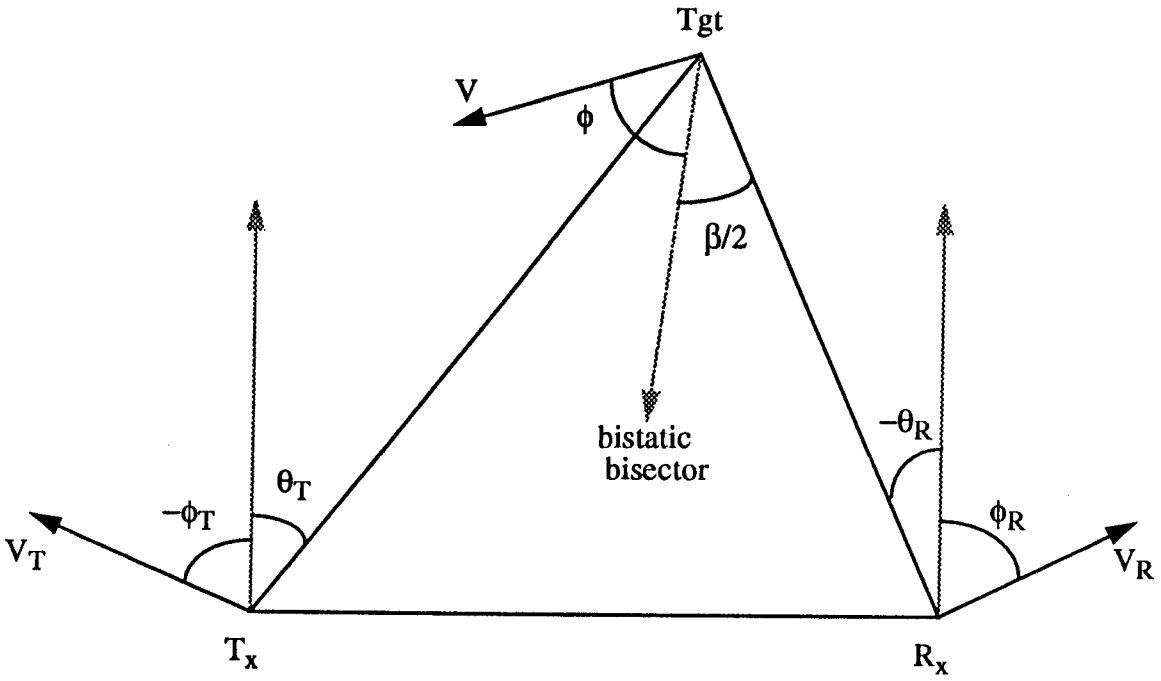

Fig. 4-2 : Velocity relationships in bistatic radar geometry

$$\frac{d}{dt}R = -V[\cos(\phi - \frac{|\beta|}{2}) + \cos(\phi + \frac{|\beta|}{2})] - V_T \cos(\phi_T - \theta_T) - V_R \cos(\phi_R - \theta_R)$$

$$= -V[\cos\phi\cos\frac{\beta}{2} + \sin\phi\sin\frac{|\beta|}{2} + \cos\phi\cos\frac{\beta}{2} - \sin\phi\sin\frac{|\beta|}{2}]$$

$$- V_T\cos(\phi_T - \theta_T) - V_R\cos(\phi_R - \theta_R)$$

$$= -2V\cos\phi\cos\frac{\beta}{2} - V_T\cos(\phi_T - \theta_T) - V_R\cos(\phi_R - \theta_R) \qquad (4.30)$$

The last two terms on the right hand side of (4.30) are due to transmitter and receiver motion. In this project, we assumed that these two quantities are known, i.e., transmitter and receiver are operating in a cooperative mode and the Doppler due to their motion can be subtracted from the measured Doppler. Equivalently, it was assumed that both the transmitter and the receiver are stationary in the following analysis. Now, the remaining term is the one due to target motion. This term indicates that the resulting Doppler shift is determined by the projection of the target velocity along the bistatic bisector. Note that the Doppler shift depends on the target location in the bistatic geometry and it appears in (4.30) via the term $\cos\frac{\beta}{2}$. Also, due to the multiplication factor, $\cos\frac{\beta}{2}$, the Doppler shift due to the target motion for the bistatic radar is always smaller than or equal to $|2V\cos\phi|$, the corresponding Doppler shift for the monostatic case.

Next, we derive an expression for $\cos\frac{\beta}{2}$ in terms of the bistatic geometry parameters L, R_R, and θ_R. From trigonometry

$$\cos\frac{\beta}{2} = \sqrt{\frac{1+\cos\beta}{2}} \tag{4.31}$$

From the law of cosines,

$$L^2 = R_T^2 + R_R^2 - 2R_T R_R \cos\beta \tag{4.32}$$

Rearranging the two sides of (4.32), we have

$$\cos\beta = \frac{R_T^2+R_R^2-L^2}{2R_T R_R} \tag{4.33}$$

Substituting $R_T = \sqrt{R_R^2+L^2+2R_R L\sin\theta_R}$ into (4.33), we have

$$\cos\beta = \frac{2R_R^2+2R_R L\sin\theta_R}{2R_R\sqrt{R_R^2+L^2+2R_R L\sin\theta_R}} = \frac{R_R+L\sin\theta_R}{\sqrt{R_R^2+L^2+2R_R\,L\sin\theta_R}} \tag{4.34}$$

Then, substituting (4.34) into (4.31), we have

$$2V\cos\phi\cos\frac{\beta}{2} = 2V\cos\phi\sqrt{\frac{1}{2}+\frac{R_R+L\sin\theta_R}{2\sqrt{R_R^2+L^2+2R_R L\sin\theta_R}}} \tag{4.35}$$

Again, to emphasize the functional relationship between the resulting range rate and the location parameters for the bistatic geometry, we define the function

$$W_R = W(V\cos\phi, R_R, L, \theta_R) \triangleq \frac{\omega_0}{c}\left[\,2\,V\cos\phi\sqrt{\frac{1}{2}+\frac{R_R+L\sin\theta_R}{2\sqrt{R_R^2+L^2+2R_R L\sin\theta_R}}}\,\right] \tag{4.36}$$

That is, the Doppler shift is expressed as a function of V cos ϕ, R_R, L and θ_R.

Alternatively, substituting $R_R = \sqrt{R_T^2+L^2-2R_T L\sin\theta_T}$ into (4.33), we have

$$\cos\beta = \frac{2R_T^2 - 2R_T L\sin\theta_T}{2R_T\sqrt{R_T^2+L^2-2R_T L\sin\theta_T}} = \frac{R_T - L\sin\theta_T}{\sqrt{R_T^2+L^2-2R_T L\sin\theta_T}} \tag{4.37}$$

Then, substituting (4.37) into (4.31), we have

$$2V\cos\phi\cos\frac{\beta}{2} = 2V\cos\phi\sqrt{\frac{1}{2}+\frac{R_T - L\sin\theta_T}{2\sqrt{R_T^2+L^2-2R_T L\sin\theta_T}}} \tag{4.38}$$

We may define the Doppler shift W_T as a function of $V\cos\phi$, R_T, L and θ_T, as follows

$$\begin{aligned} W_T &= W(V\cos\phi, R_T, L, -\theta_T) \\ &= \frac{\omega_0}{c}[2V\cos\phi\sqrt{\frac{1}{2}+\frac{R_T - L\sin\theta_T}{2\sqrt{R_T^2+L^2-2R_T L\sin\theta_T}}}\,] \end{aligned} \tag{4.39}$$

Thus, with (4.36) or (4.39), the resulting Doppler shift is described in terms of the target location for the bistatic geometry.

In the analysis thus far, we have derived the target return model for bistatic radars. The geometry factors in the measurements have also been examined by relating the measurements with locations. In the following, we will consider the consequences on the representation of ambiguity function for bistatic radars.

4.2 Ambiguity Function Plots for Bistatic Configuration

In radar systems, waveforms are selected based upon their ability to satisfy the requirements for detection, measurement accuracy, resolution, ambiguity and clutter rejection. Ambiguity function plots are examined for a qualitative determination of the suitability of different waveforms in meeting the above system requirements [1]. In practice, ambiguity function is plotted as a function of delay and Doppler derived from the return signal. In monostatic radars, the use of delay and Doppler as the

arguments of the ambiguity function are adequate because of their linear relationship with the desired quantities, i.e., target range and the range rate. In particular, the delay is equal to two times the range divided by the speed of light and Doppler is equal to two times the range rate divided by the wavelength. Therefore, the pair delay and Doppler or the pair range and range rate may be used in an interchangeable manner as the arguments of the ambiguity function. Note that once the target range and range rate are known, its position and its relative (radial) velocity with respect to the monostatic radar are known completely.

For a bistatic radar, the above observations are no longer valid due to the geometry of the bistatic configuration. The transmitter and the receiver are not at the same site and, therefore, the relative position and the relative velocity of the target needs to be determined with respect to either the transmitter or the receiver or some other suitable reference point. In addition, the effect of the transmitter and the receiver not being at the same site should be taken into account while computing the ambiguity function. In Section 4.1, two functions $D_T(\cdot)$ and $W_T(\cdot)$ with respect to the transmitter and functions $D_R(\cdot)$ and $W_R(\cdot)$ with respect to the receiver were defined. Here, we focus our attention on the evaluation of the ambiguity function with respect to the receiver. Similar results can be obtained with respect to the transmitter or any other reference point.

In the bistatic configuration, the baseline L is assumed to be given. When we evaluate the ambiguity function with respect to the receiver, the receiver's look angle θ_R can also be assumed known. The actual position of the target can be determined from the knowledge about the distance between the target and the receiver, i.e., the range R_{Ra}. The total time delay based on these system parameters and the bistatic

geometry can be expressed as

$$D_{R_a} = \frac{1}{c}[R_{R_a} + \sqrt{R_{R_a}^2 + L^2 + 2R_{R_a} L \sin\theta_R}]$$

Also, the Doppler shift due to target motion which takes into account the bistatic geometry can be expressed as

$$W_{R_a} = \frac{\omega_0}{c}[2V_a \cos\phi \sqrt{\frac{1}{2} + \frac{R_{R_a} + L \sin\theta_R}{2\sqrt{R_{R_a}^2 + L^2 + 2R_{R_a} L \sin\theta_R}}}]$$

where V_a is the target's actual velocity along the bistatic bisector. As in the monostatic case, the ambiguity function for the bistatic radar can be expressed as a function of the delay and Doppler, i.e., as $\theta(D_{R_H}, D_{R_a}, W_{R_H}, W_{R_a})$. As discussed before, the delay and Doppler terms include the effects of bistatic geometry. Note that the subscript "H" denotes the delay and Doppler bin that is under investigation. The peak of the ambiguity function occurs at the point where $D_{R_H}=D_{R_a}$ and $W_{R_H}=W_{R_a}$.

While the ambiguity function expressed in terms of D_R and W_R provides some information, its utility is limited. This is because in most applications, resolution in terms of the position and velocity of the target is desired. Due to the nonlinear relationship between the pair delay D_R and Doppler W_R and the pair R_R and V, one cannot immediately observe the behavior of the waveforms as a function of R_R and V. This is especially inconvenient due to the fact that the primary purpose of the ambiguity function is to provide a visual representation of waveform behavior as a function of position and velocity. Therefore, we suggest the use of R_R and V as the arguments of the ambiguity function. This will enable one to examine the suitability

of different waveforms in a convenient manner. In the following, we present two examples where we consider a Gaussian pulse and a pulse train consisting of three rectangular pulses. Ambiguity function plots as a function of R_R and V for a variety of bistatic configurations are given. These exhibit the effects of geometry on the ambiguity function. In these figures, Rr represents R_R, and both R_{ra} and R_{Ra} represent R_{R_a}.

Example 1: Simple Gaussian Pulse

We first consider a transmitted waveform whose complex envelope is a simple Gaussian pulse. Let

$$\tilde{f}(t) = \left(\frac{1}{\pi T^2}\right)^{\frac{1}{4}} e^{-\frac{t^2}{2T^2}} \quad ; \qquad -\infty \le t \le \infty \tag{4.40}$$

Note that $\tilde{f}(t)$ has unit energy since

$$|\tilde{f}(t)|^2 = \left(\frac{1}{\pi T^2}\right)^{\frac{1}{2}} e^{-\frac{t^2}{T^2}} \tag{4.41}$$

is a zero mean Gaussian function with variance $\frac{T^2}{2}$. The target return can be written as

$$\tilde{f}(t-\tau_a)\, e^{j\omega_{D_a}(t-\tau_a)} = \left(\frac{1}{\pi T^2}\right)^{\frac{1}{4}} e^{\frac{-(t-\tau_a)^2}{2T^2}}\, e^{j\omega_{D_a}(t-\tau_a)} \tag{4.42}$$

The time-frequency autocorrelation function, as defined in Chapter 2, is given by

$$\phi(\tau_H,\tau_a,\omega_{D_H},\omega_{D_a}) = \int_{-\infty}^{\infty} \tilde{f}(t-\tau_a)\, e^{j\omega_{D_a}(t-\tau_a)}\, \tilde{f}^*(t-\tau_H)\, e^{-j\omega_{D_H}(t-\tau_H)} dt \qquad (4.43)$$

Let $z=t-\frac{\tau_H+\tau_a}{2}$. Then,

$$\phi(\tau_H,\tau_a,\omega_{D_H},\omega_{D_a}) = \int_{-\infty}^{\infty} \tilde{f}(z+\tfrac{\tau_H-\tau_a}{2})\, \tilde{f}^*(z-\tfrac{\tau_H-\tau_a}{2})\, e^{j\omega_{D_a}(z+\frac{\tau_H-\tau_a}{2})}\, e^{-j\omega_{D_H}(z-\frac{\tau_H-\tau_a}{2})} dz$$

$$= e^{j(\omega_{D_H}+\omega_{D_a})(\frac{\tau_H-\tau_a}{2})} \int_{-\infty}^{\infty} \tilde{f}(z+\tfrac{\tau_H-\tau_a}{2})\, \tilde{f}^*(z-\tfrac{\tau_H-\tau_a}{2})\, e^{j(\omega_{D_H}-\omega_{D_a})z} dz \qquad (4.44)$$

Substituting (4.40) into (4.44), we have

$$\phi(\tau_H,\tau_a,\omega_{D_H},\omega_{D_a}) = e^{j(\omega_{D_H}+\omega_{D_a})(\frac{\tau_H-\tau_a}{2})} \int_{-\infty}^{\infty} (\frac{1}{\pi T^2})^{\frac{1}{2}}\, e^{(z+\frac{\tau_H-\tau_a}{2})^2/2T^2}\, e^{(z-\frac{\tau_H-\tau_a}{2})^2/2T^2}$$

$$\cdot\, e^{-j(\omega_{D_H}-\omega_{D_a})z} dz \qquad (4.45)$$

Completing the square in the exponent in the integral, and simplifying, we have

$$\phi(\tau_H,\tau_a,\omega_{D_H},\omega_{D_a}) = e^{j(\omega_{D_H}+\omega_{D_a})(\frac{\tau_H-\tau_a}{2})} \int_{-\infty}^{\infty} (\frac{1}{\pi T^2})^{\frac{1}{2}}\, e^{-\frac{1}{T^2}(z-j\frac{(\omega_{D_H}-\omega_{D_a})T^2}{2})^2}$$

$$\cdot\, e^{-\frac{1}{T^2}[\frac{(\tau_H-\tau_a)^2}{4}+\frac{(\omega_{D_H}-\omega_{D_a})^2T^4}{4}]} dz$$

$$= e^{j(\omega_{D_H}+\omega_{D_a})(\frac{\tau_H-\tau_a}{2})}\, e^{-\frac{(\tau_H-\tau_a)^2}{4T^2}-\frac{(\omega_{D_H}-\omega_{D_a})^2T^2}{4}} \qquad (4.46)$$

where the identity

$$\left(\frac{1}{\pi T^2}\right)^{\frac{1}{2}} \int_{-\infty}^{\infty} e^{-\frac{1}{T^2}\left(z-j\frac{(\omega_{D_H}-\omega_{D_a})T^2}{2}\right)^2} dz=1$$

has been used. Then, by definition, the ambiguity function is given by

$$\theta(\tau_H,\tau_a,\omega_{D_H},\omega_{D_a}) = |\phi(\tau_H,\tau_a,\omega_{D_H},\omega_{D_a})|^2$$

$$= e^{-\frac{(\tau_H-\tau_a)^2}{2T^2} - \frac{(\omega_{D_H}-\omega_{D_a})^2T^2}{2}} \qquad (4.47)$$

Figure 4-3 is the plot of the ambiguity function in the delay-Doppler plane given by (4.47) with parameters $T=1.2\times10^{-4}$ sec, $\tau_a=4\times10^{-4}$ sec and $\omega_{D_a}=1200$ rad/sec.. For the monostatic case, the ambiguity function is commonly plotted in this manner. For the bistatic case, if the bistatic geometry is ignored and the ambiguity function is plotted in terms of total delay τ_H and Doppler ω_{DH}, the resulting ambiguity function will be the same as shown in Fig. 4-3. Also given in Fig. 4-3 is the equal-height contour plot, where the magnitude, as a fraction of the peak value, is shown alongside the contour.

As discussed before, for monostatic radars, the ambiguity function given in (4.47) can also be expressed in terms of the range and radial velocity as

$$\theta\ (\tau_H,\tau_a,\omega_{D_H},\omega_{D_a}) = \theta\ \left(\frac{2R_{M_H}}{c}, \frac{2R_{M_a}}{c}, \frac{2\omega_0 V_{M_H}}{c}, \frac{2\omega_0 V_{M_a}}{c}\right) \qquad (4.48)$$

where R_M is the one-way range and V_M is the radial velocity of the target. For comparison, Fig. 4-4 is the plot of (4.48) by setting the carrier frequency $\omega_0 = 3\times10^8$ rad/sec, the actual distance $R_{M_a} = \frac{c\tau_a}{2} = 6\times10^4$ m, and the actual radial velocity $V_{M_a} = \frac{c\omega_{D_a}}{2\omega_0} = 600$ m/sec. Note that, except for constant scaling factors, Fig. 4-3

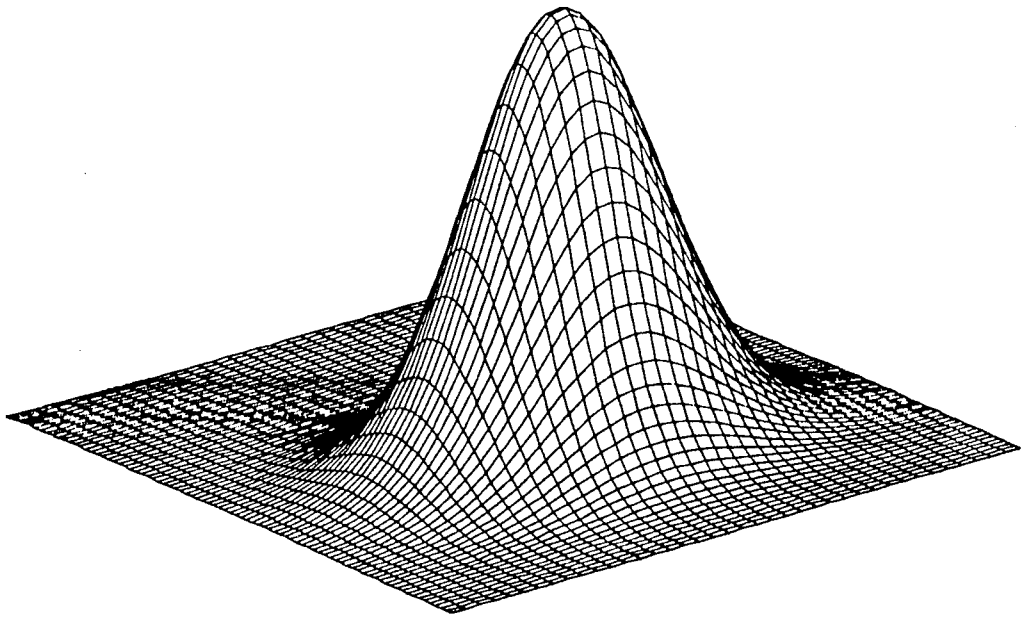

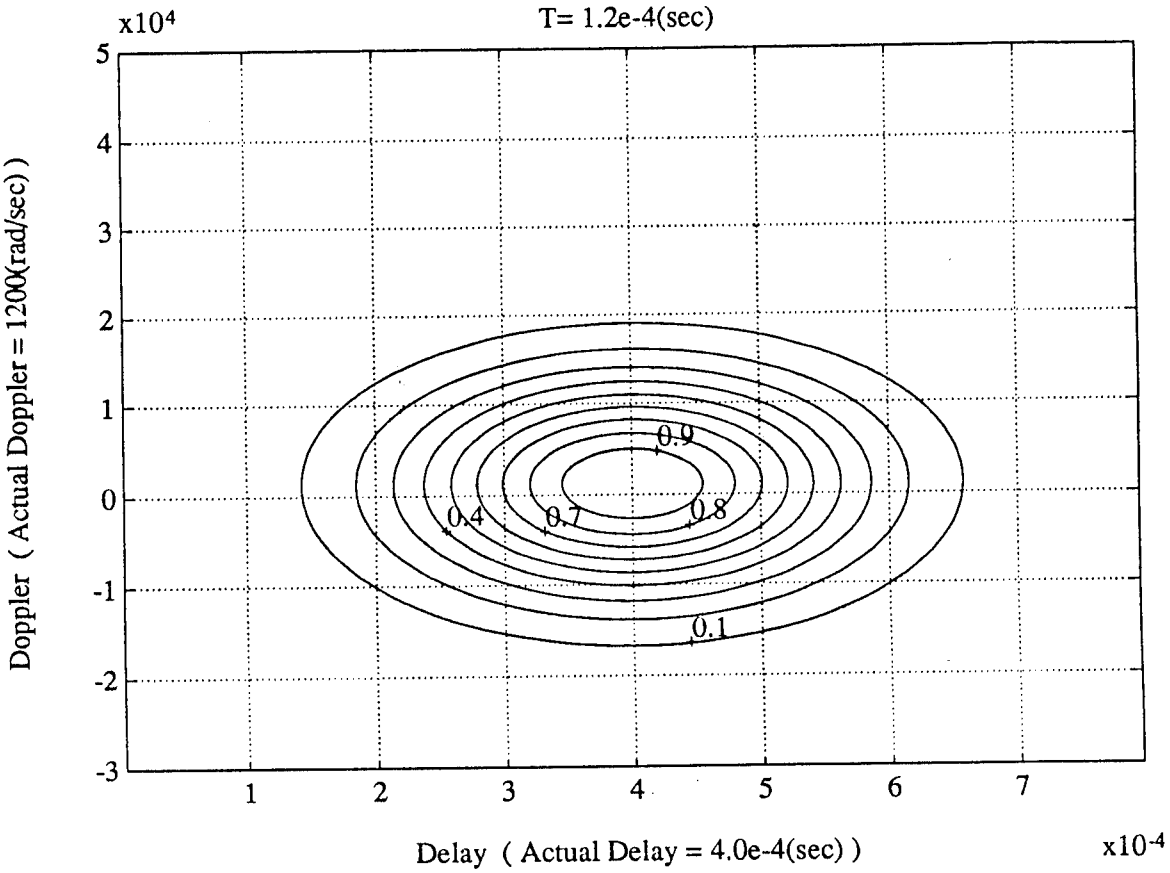

Fig. 4-3 : Ambiguity function for monostatic radar in the delay-Doppler plane for the Gaussian pulse

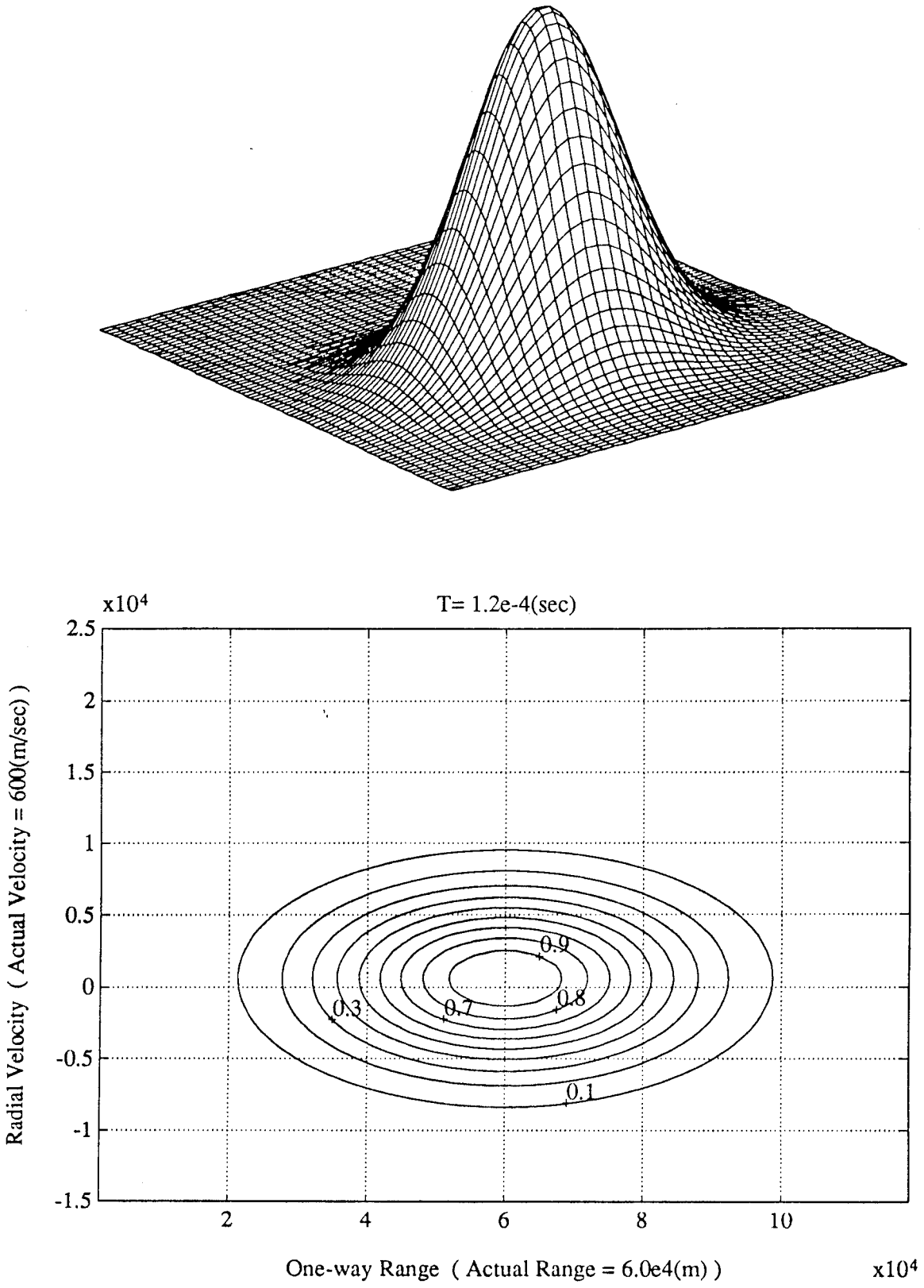

Fig. 4-4 : Ambiguity function for monostatic radar in the range-velocity plane for the Gaussian pulse

and Fig. 4-4 have the same shape. This was expected due to the aforementioned linear relationships.

However, as proposed earlier, ambiguity function for a bistatic radar with respect to the receiver needs to be written as $\theta(D_{R_H}, D_{R_s}, W_{R_H}, W_{R_s})$, so that the transmitted waveform's response to the target can be directly related to target's position and its velocity. In Figures 4-5 to 4-11, we give the plots of $\theta(D_{R_H}, D_{R_s}, W_{R_H}, W_{R_s})$ for various values of receiver look angles. For these results, it has been assumed that $R_{R_s} = 6\text{x}10^4$ m and $L = 10^5$ m. Also, the actual velocity component along the bistatic bisector, V_H, is set at 600 m/sec. With these specifications, the target locations considered represent an operating region close to the receiver. From the resulting ambiguity diagrams, it is obvious that the effects of geometry factors are more prominent as the target approaches the baseline. Moreover, when the target is on the baseline, the resulting delay is $\frac{L}{c}$ and the Doppler is zero, regardless of the position on the baseline and the velocity of the target. Therefore, the ambiguity function diagram of equal height in the region $0 \le R_{R_H} \le 1$ and $-\infty < V_H < \infty$ is obtained, when the receiver look angle is equal to $-\frac{\pi}{2}$. Next, we consider the target at a distance larger than the baseline, by changing L to $5\text{x}10^4$ m. That is, the region being considered encompasses both the transmitter and the receiver, i.e., the cosite region. Figures 4-12 to 4-18 are the plots of the corresponding ambiguity function $\theta(D_{R_H}, D_{R_s}, W_{R_H}, W_{R_s})$, for various values of receiver

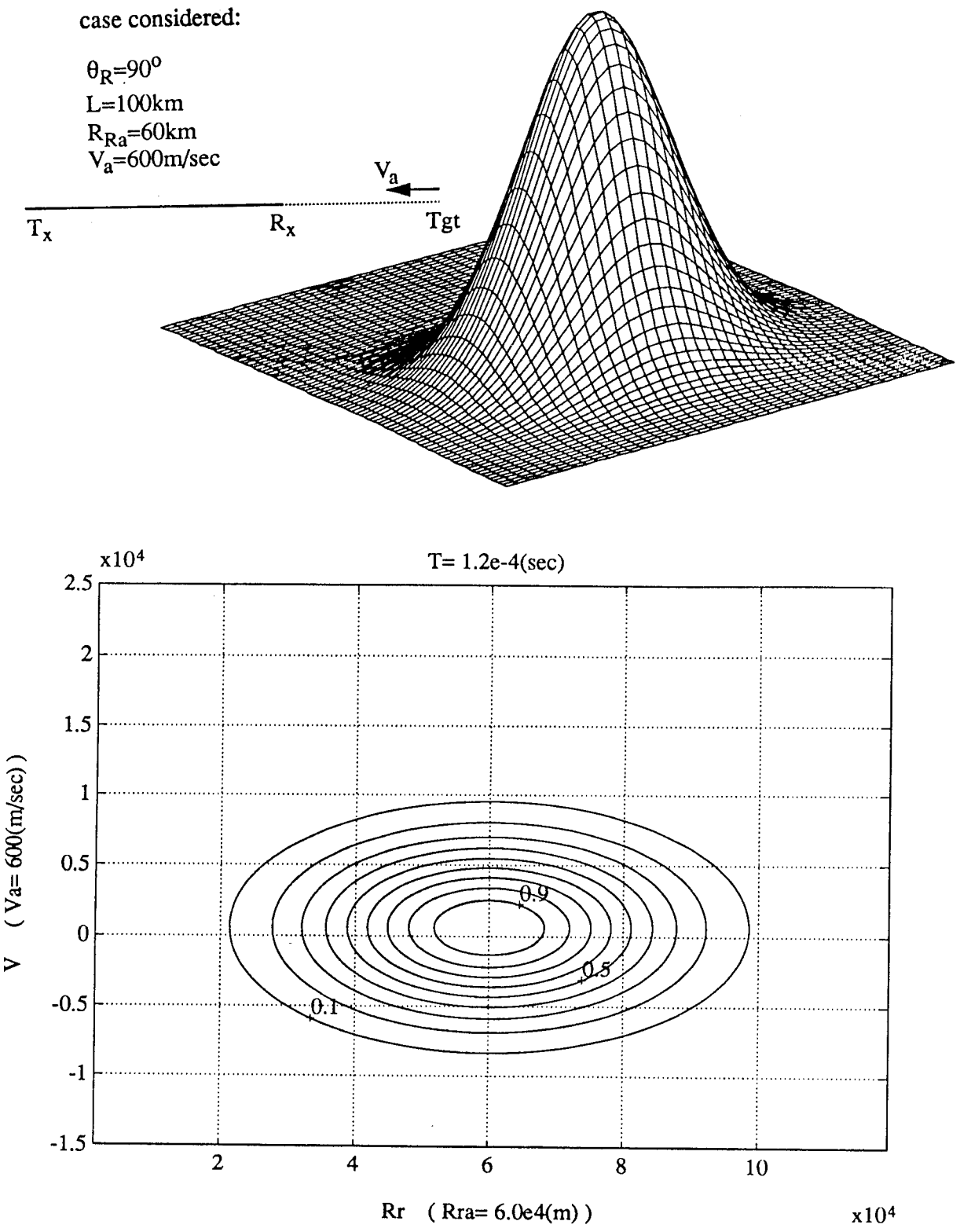

Fig. 4-5: Bistatic ambiguity function for the Gaussian pulse for the case considered

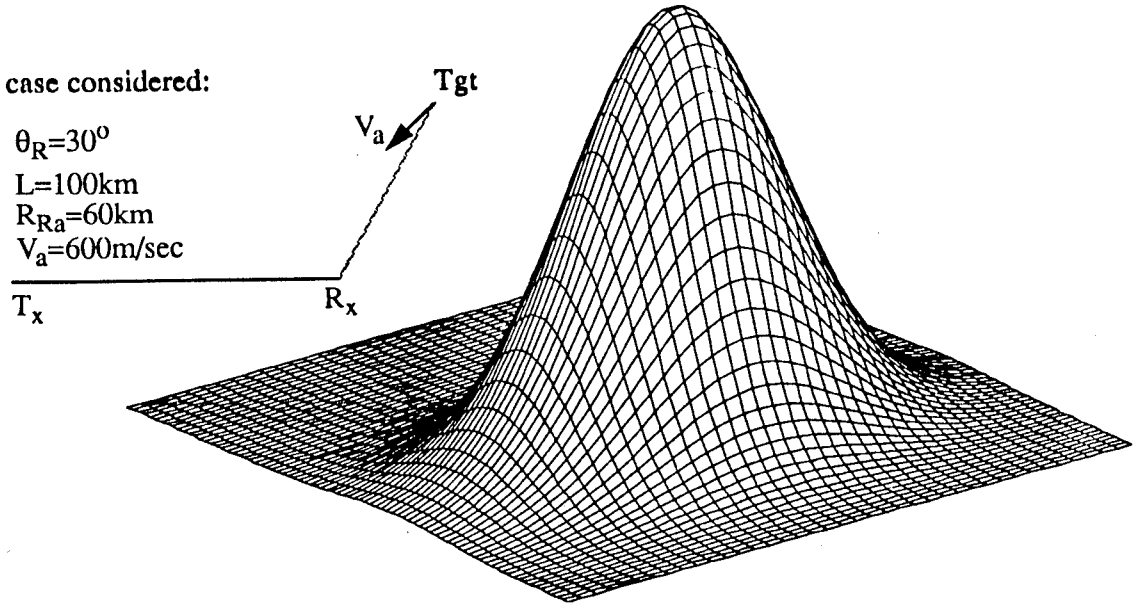

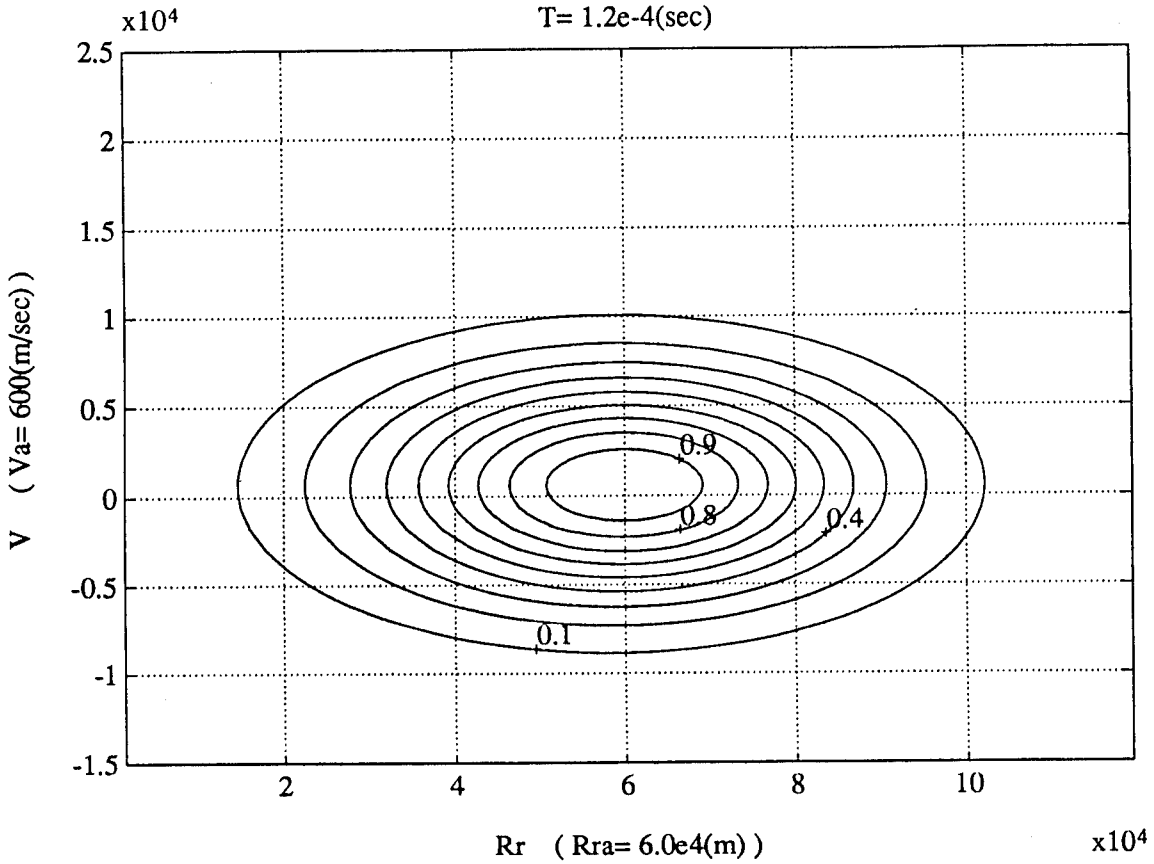

Fig. 4-6: **Bistatic ambiguity function for the Gaussian pulse for the case considered**

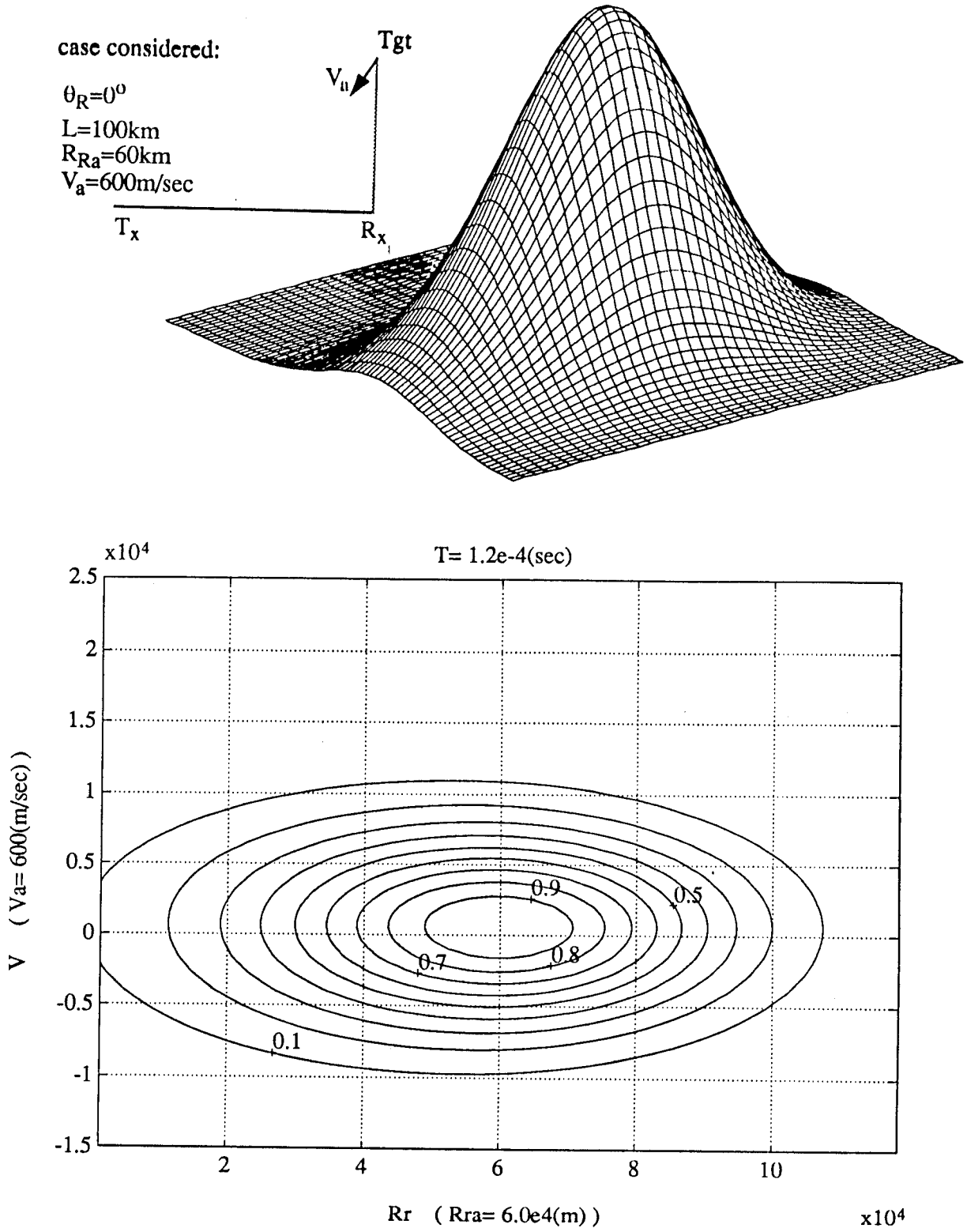

Fig. 4-7: **Bistatic ambiguity function for the Gaussian pulse for the case considered**

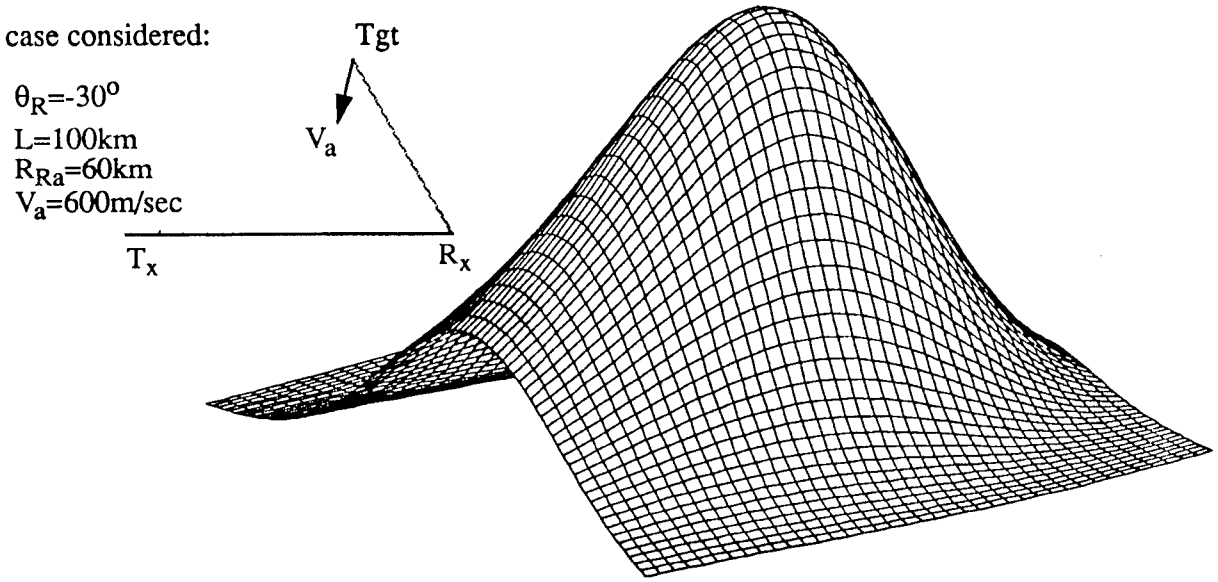

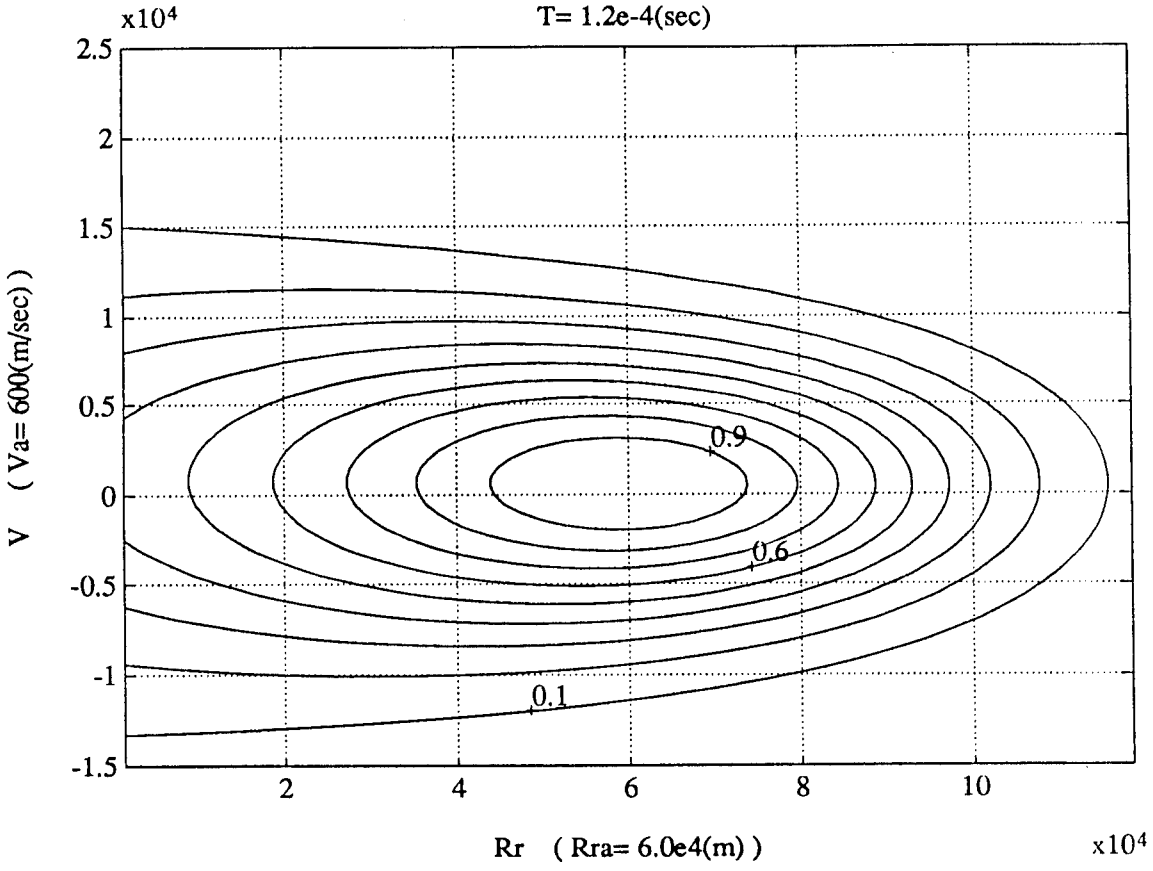

Fig. 4-8: **Bistatic ambiguity function for the Gaussian pulse for the case considered**

case considered:

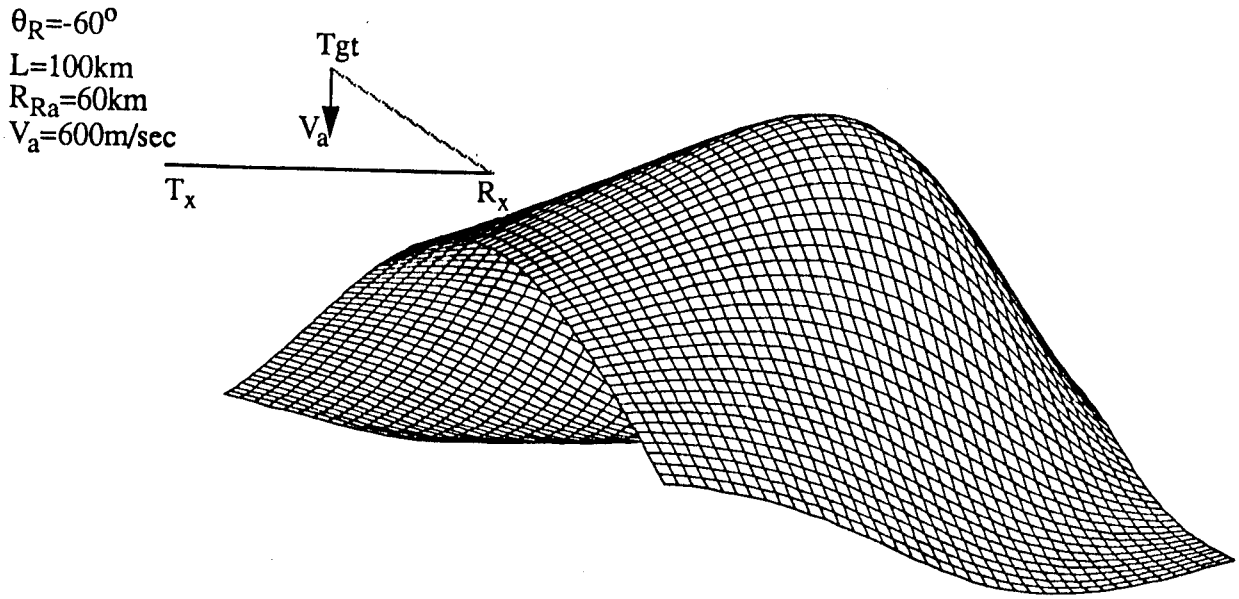

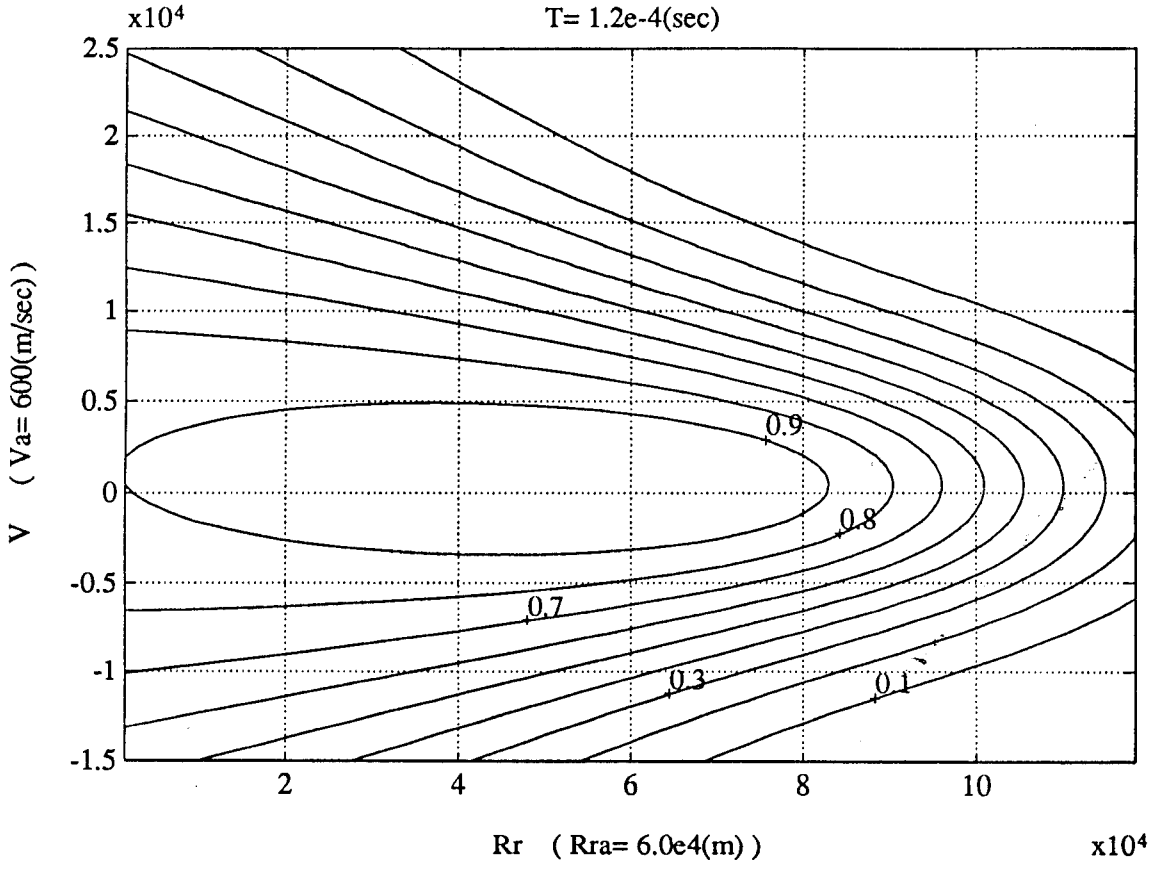

Fig. 4-9: **Bistatic ambiguity function for the Gaussian pulse for the case considered**

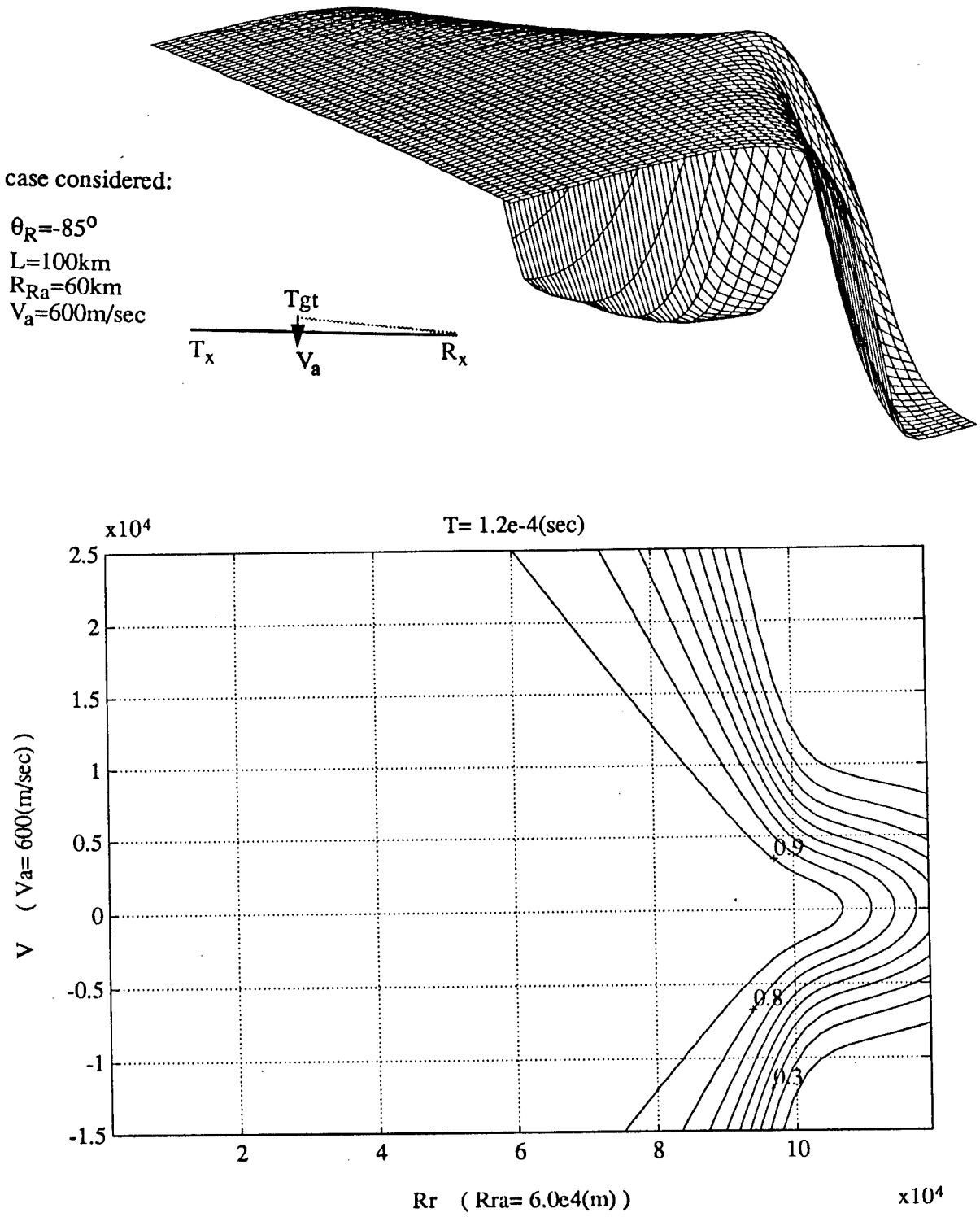

Fig. 4-10: **Bistatic ambiguity function for the Gaussian pulse for the case considered**

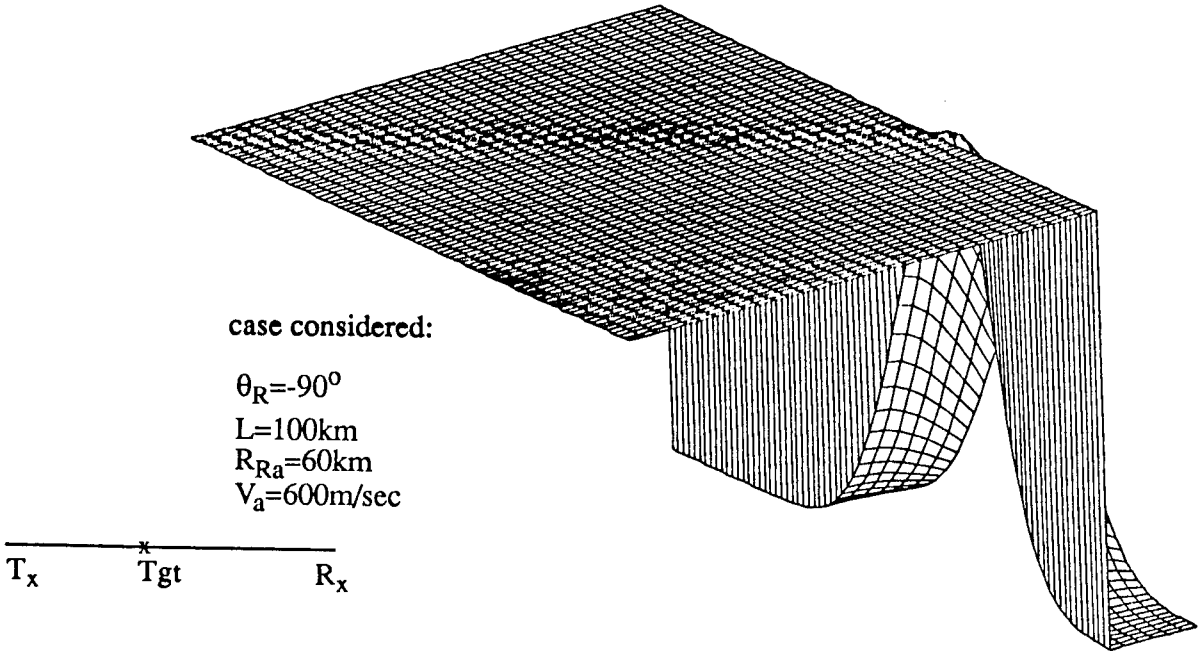

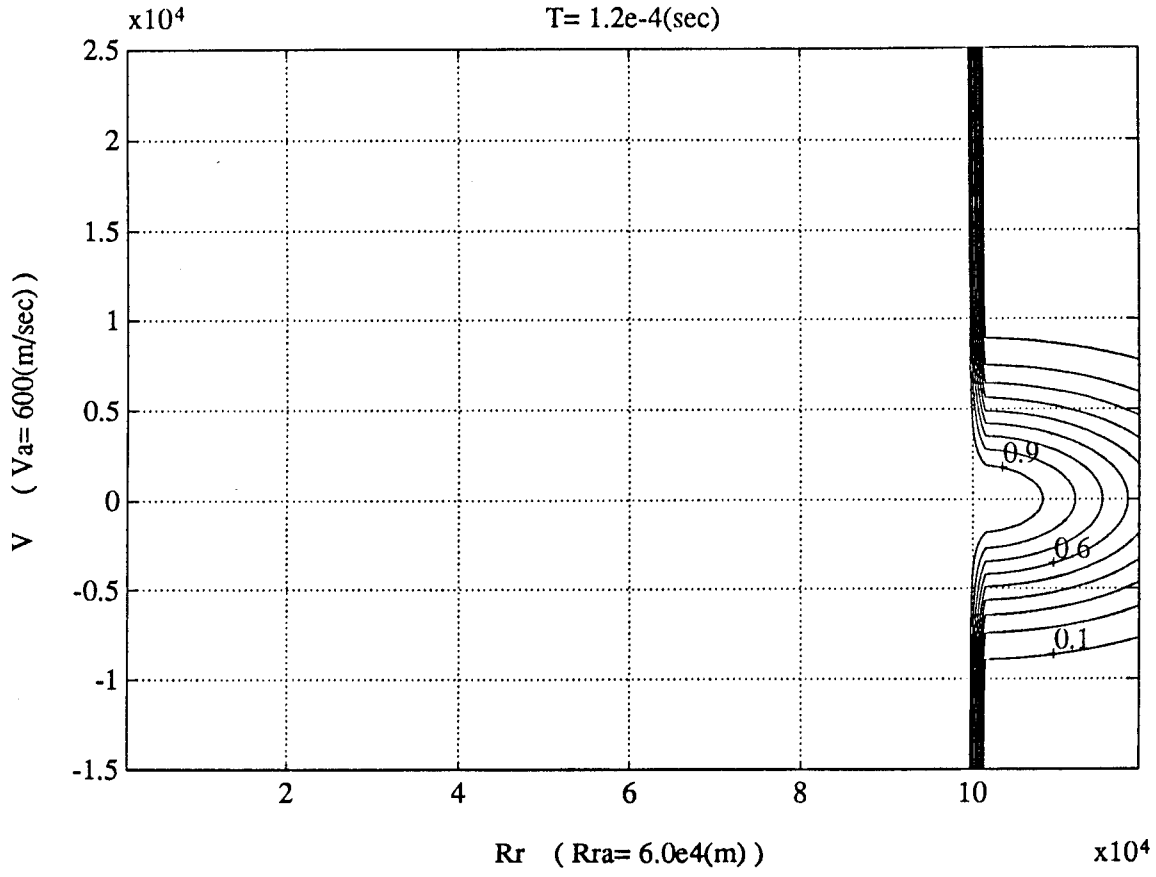

Fig. 4-11: **Bistatic ambiguity function for the Gaussian pulse for the case considered**

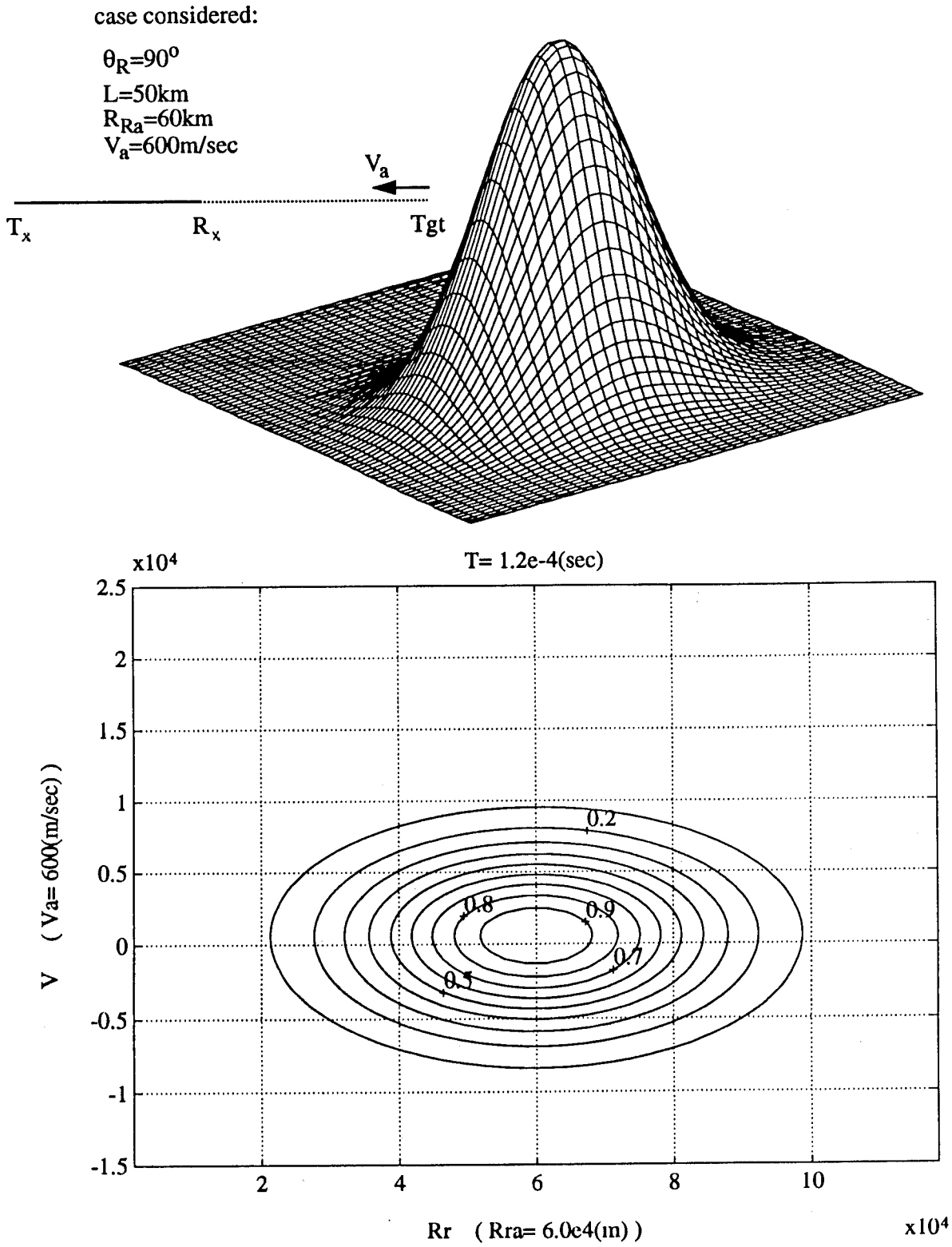

Fig. 4-12: **Bistatic ambiguity function for the Gaussian pulse for the case considered**

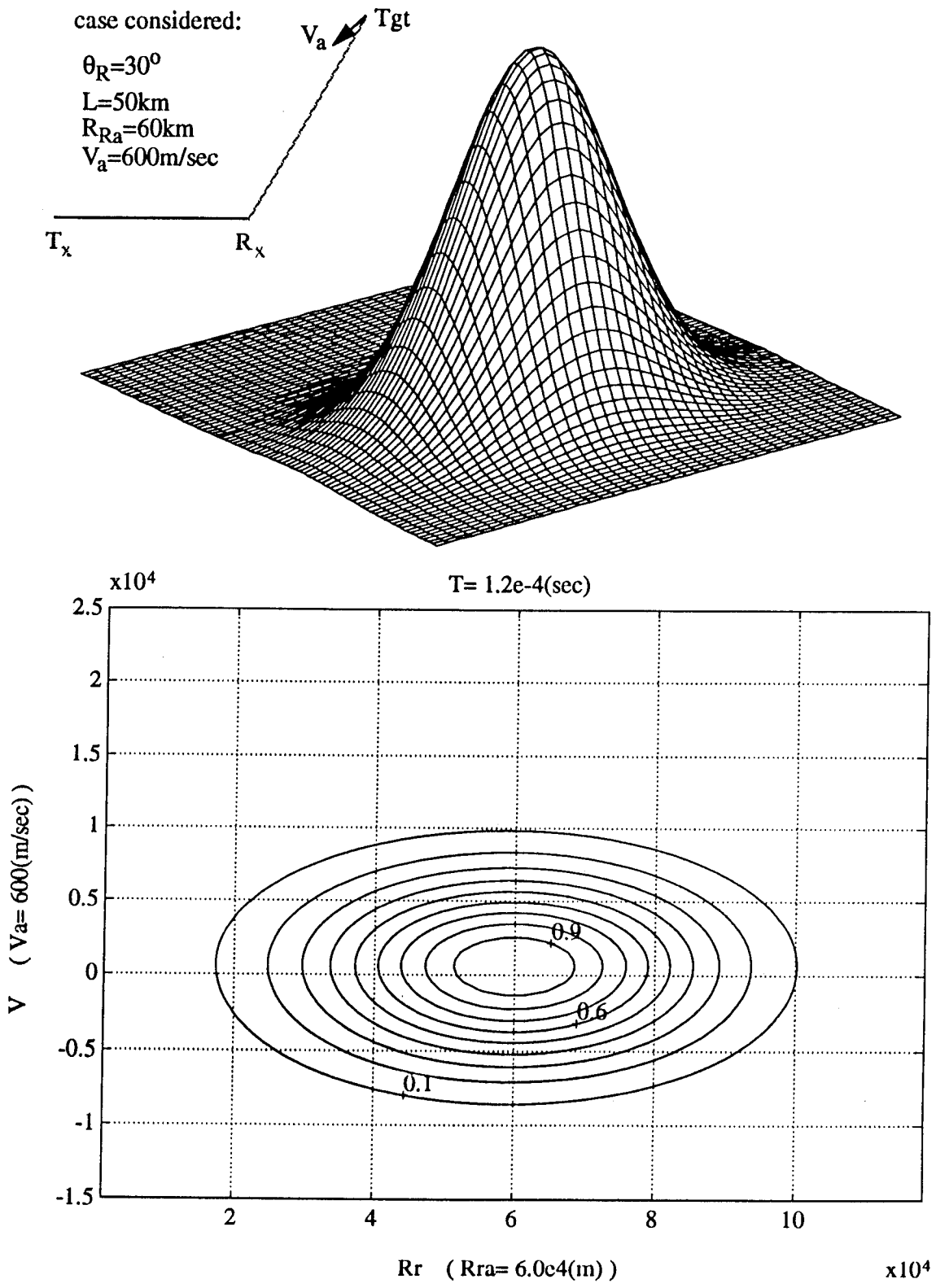

Fig. 4-13: Bistatic ambiguity function for the Gaussian pulse for the case considered

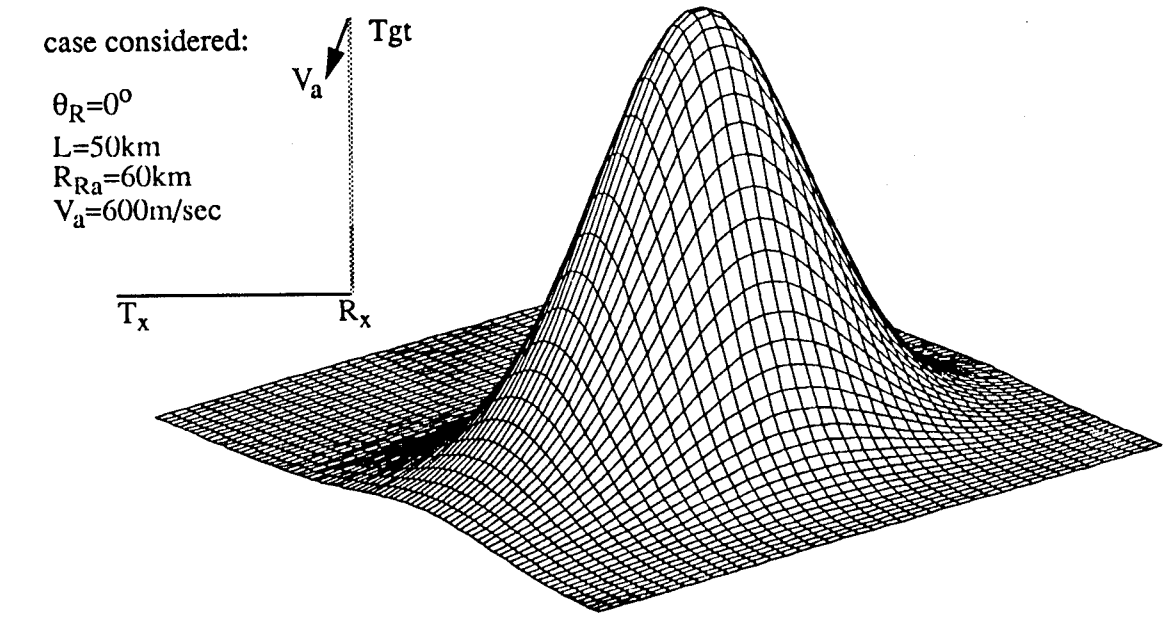

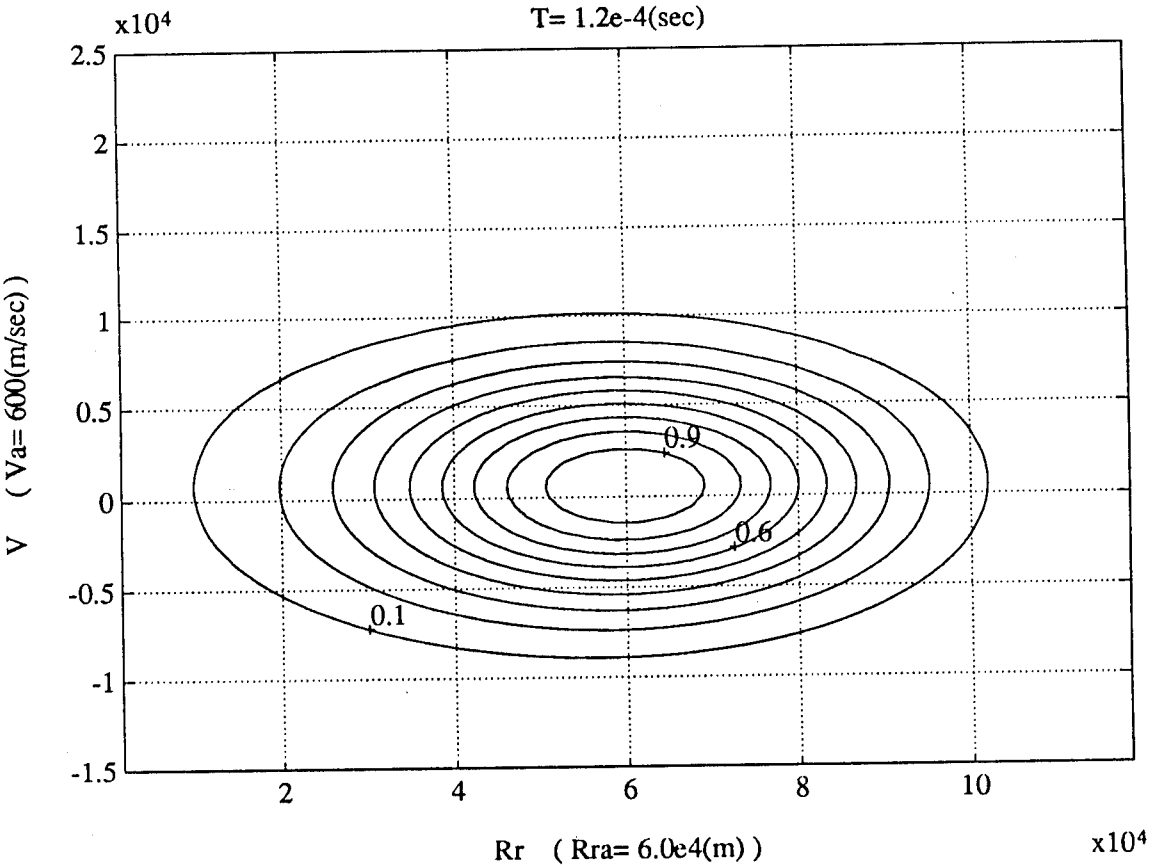

Fig. 4-14: **Bistatic ambiguity function for the Gaussian pulse for the case considered**

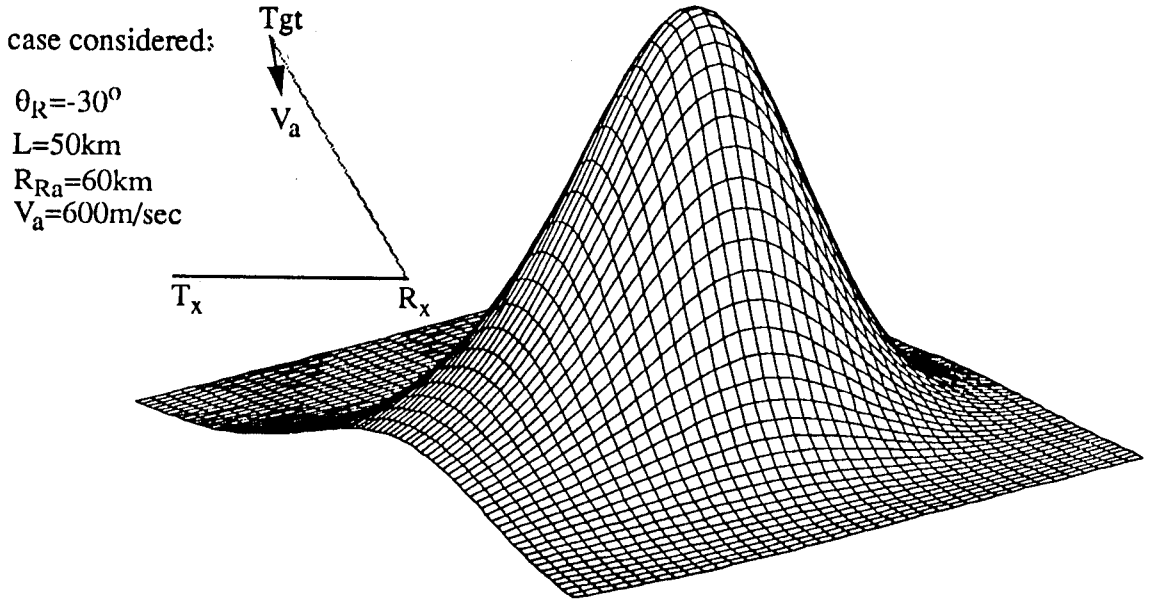

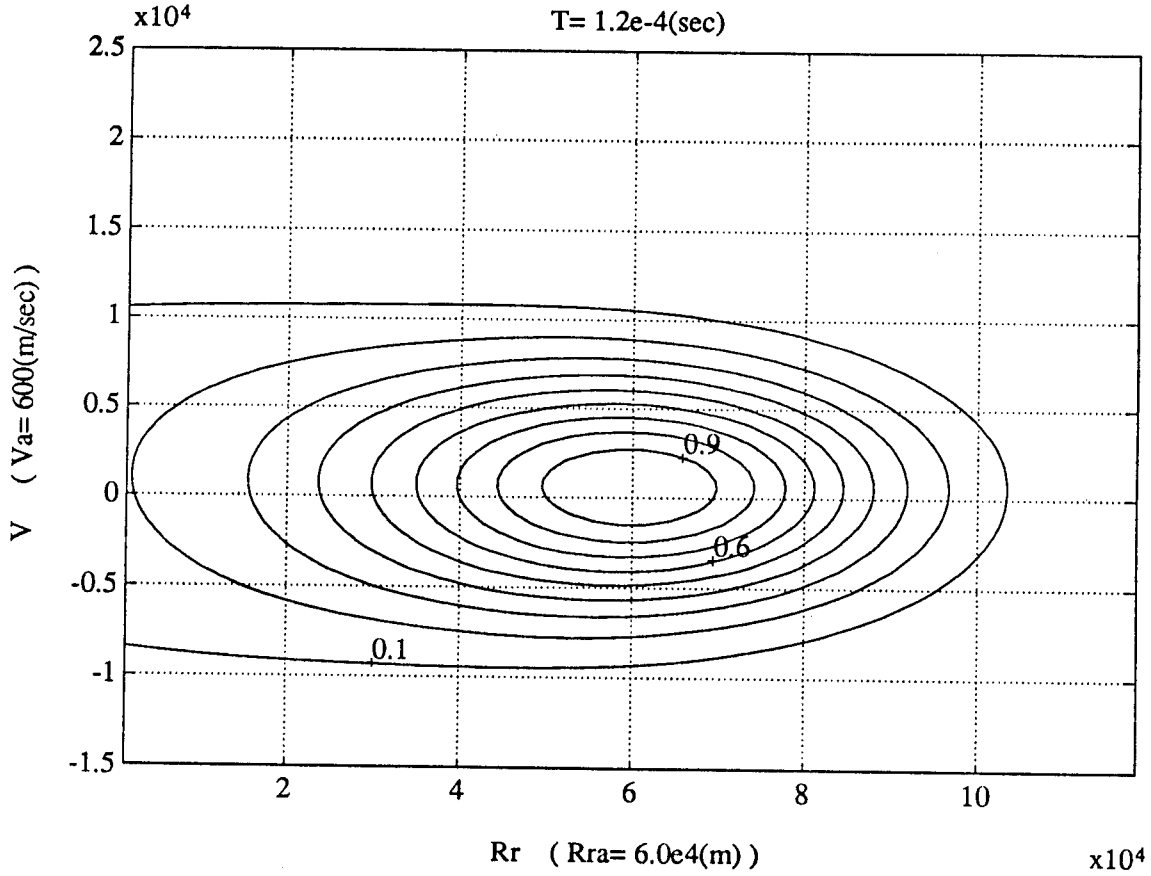

Fig. 4-15: **Bistatic ambiguity function for the Gaussian pulse for the case considered**

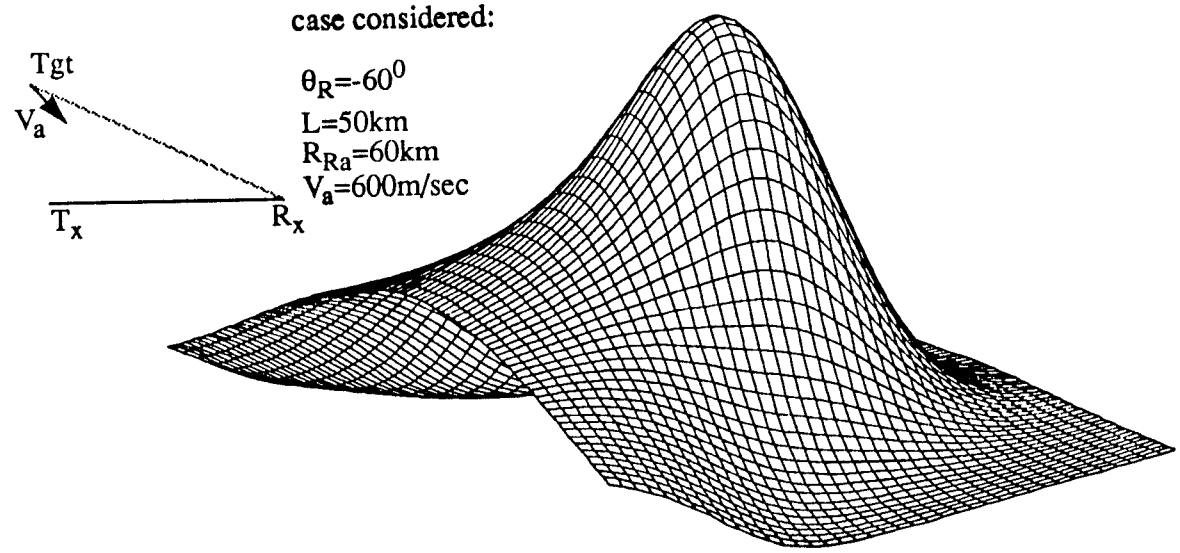

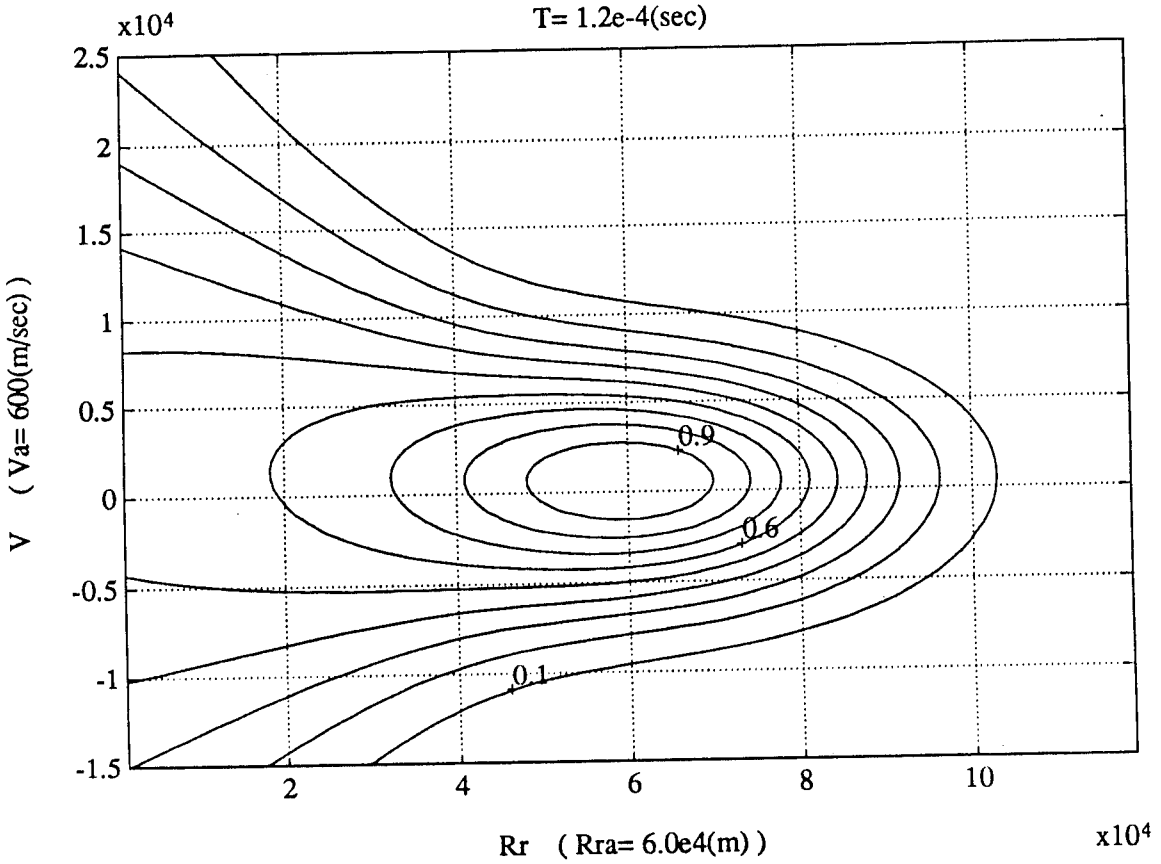

Fig. 4-16: Bistatic ambiguity function for the Gaussian pulse for the case considered

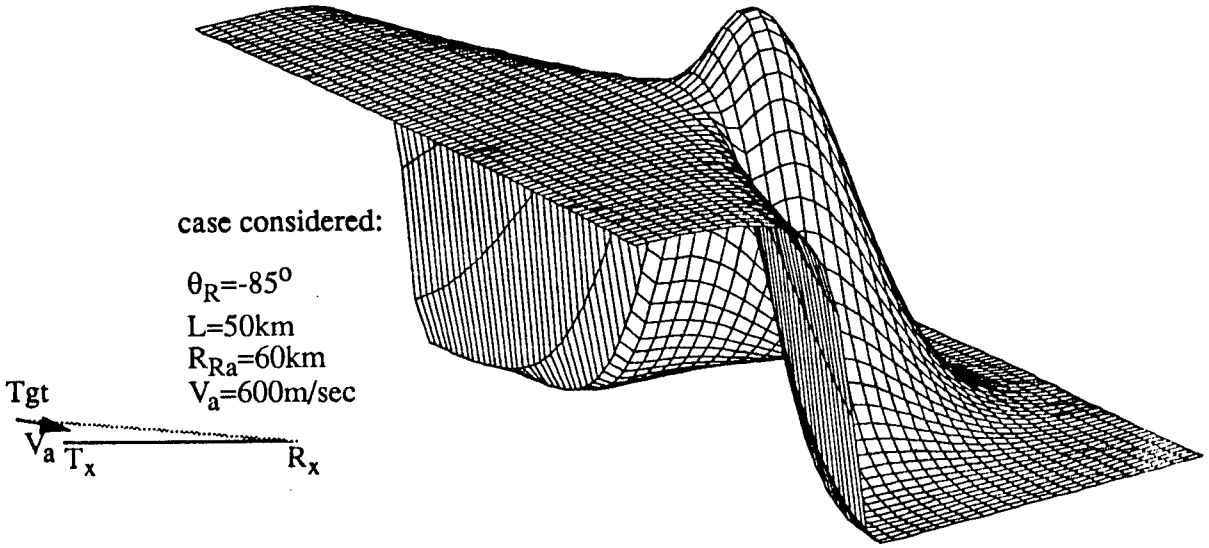

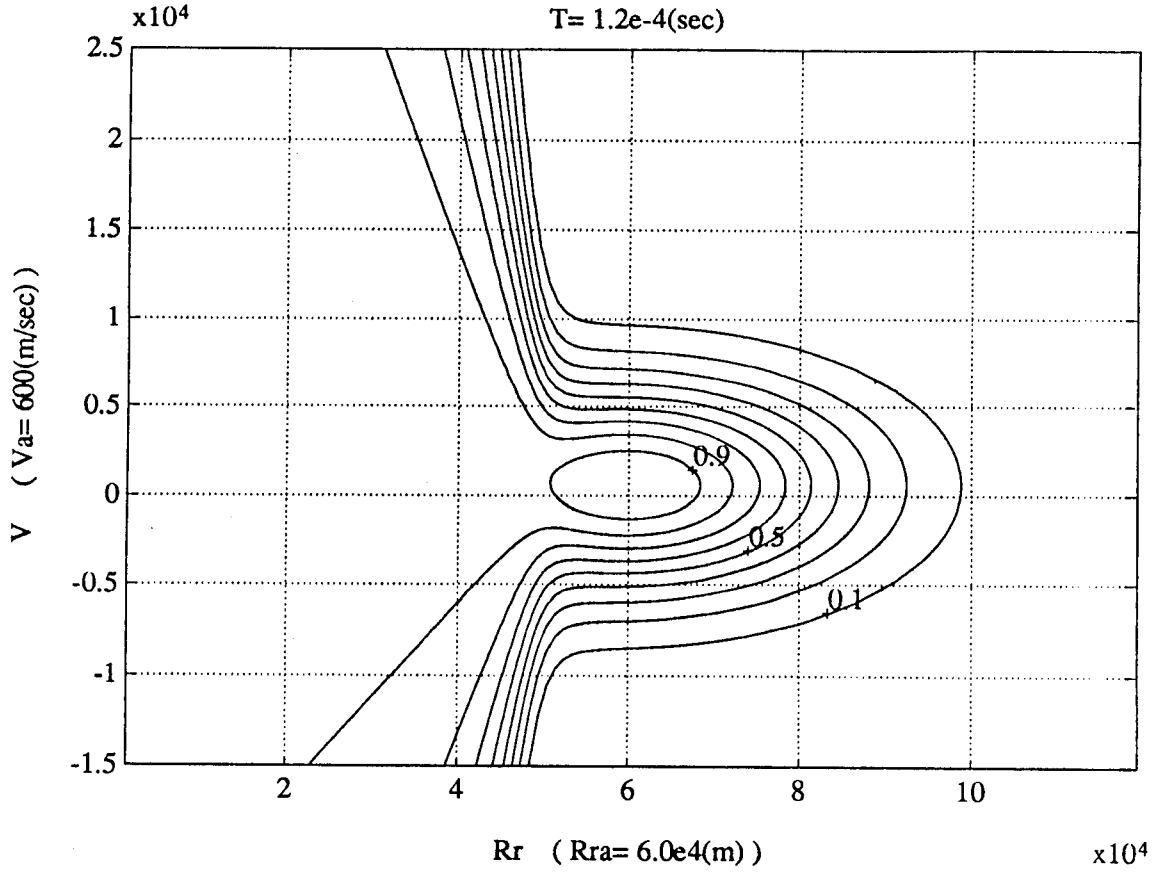

Fig. 4-17: **Bistatic ambiguity function for the Gaussian pulse for the case considered**

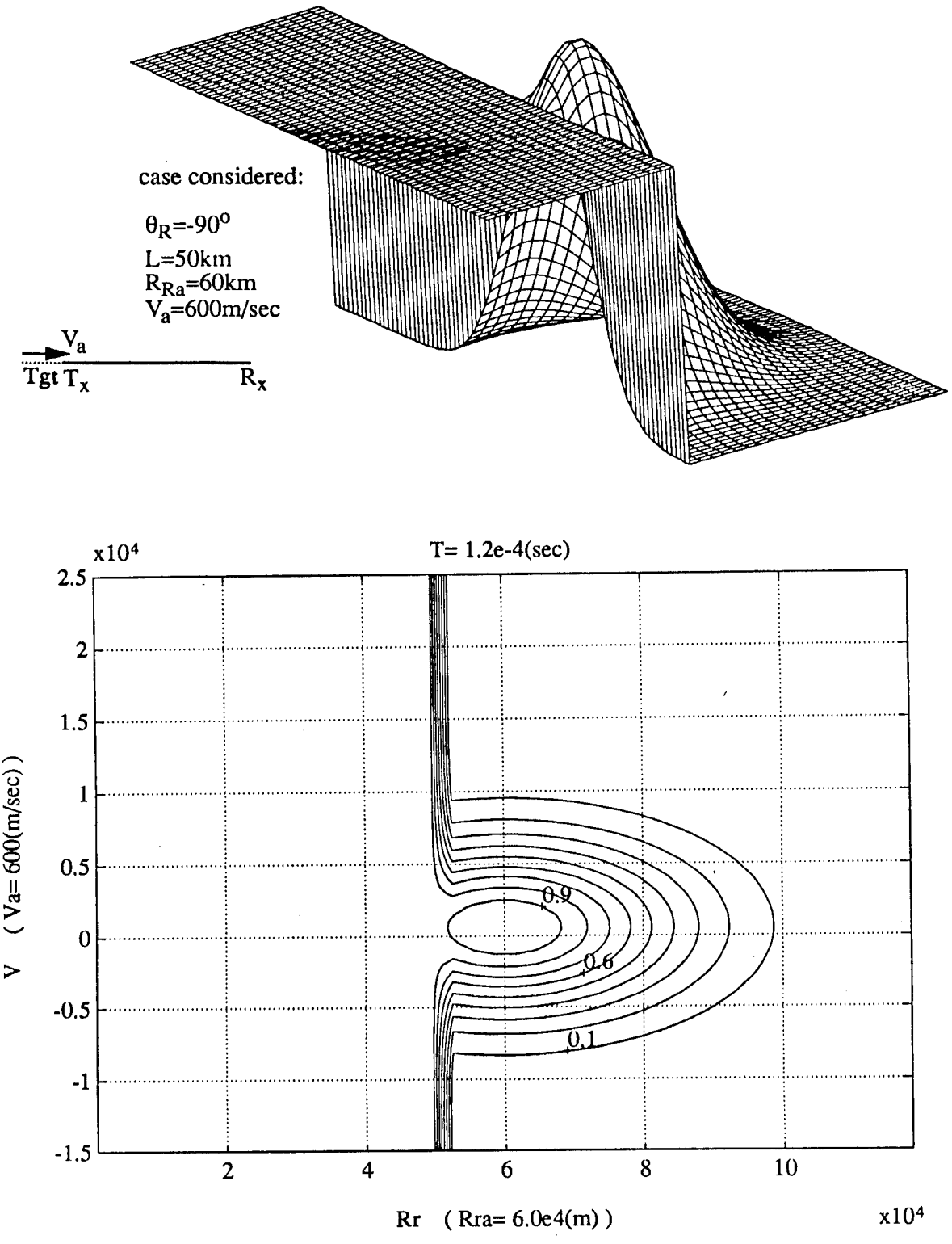

Fig. 4-18: Bistatic ambiguity function for the Gaussian pulse for the case considered

look angles. When this case is compared to the previous one (with larger baseline) the degree of resolution lost due to geometry factors is less. For example, compare Figures 4-10 and 4-17 for θ_R=-85^0 where we observe this effect quite clearly. This phenomenon is due to the fact that in the latter case the total range $R=R_T+R_R$ is much larger than the baseline L. As R increases with respect to L, the degree of resolution lost due to geometry factors will continue to diminish and the bistatic system will behave more and more like a monostatic system. In fact, in the limit as $L\rightarrow 0$, the bistatic system becomes a monostatic system.

Example 2: Three Rectangular Pulses

Here, we first consider a sequence of (2n+1) rectangular pulses having a constant repetition rate of $1/T_p$ with a subpulse duration of T and then specialize the result to the case of three pulses. The duration of the pulse train is $T_d = 2nT_p+T$. In many practical situations, $T<<T_p$ where T_p is not necessarily a multiple of T. Also note that duty cycle $T/T_p < 50\%$ is the only case of interest. Let the complex envelope of a subpulse be denoted by

$$\tilde{u}(t) = \begin{cases} \frac{1}{\sqrt{T}} & ; -\frac{T}{2} \le t \le \frac{T}{2} \\ 0 & ;\text{elsewhere} \end{cases} \qquad (4.49)$$

The complex envelope of the pulse train can be written as

$$\tilde{f}(t) = \frac{1}{\sqrt{2n+1}} \sum_{k=-n}^{n} \tilde{u}(t-kT_p) \qquad (4.50)$$

where $\tilde{f}(t)$ has been normalized to contain unit energy. Assume that the target does not fluctuate in the period T_d during which it is illuminated by the signal.

We first evaluate $\phi(\tau_H, \tau_a, \omega_{D_H}, \omega_{D_a})$ for $|\tau_H-\tau_a| < T$. From (4.44), we have

$$\phi(\tau_H,\tau_a,\omega_{D_H},\omega_{D_a}) = e^{j(\omega_{D_H}+\omega_{D_a})(\frac{\tau_H-\tau_a}{2})} \int_{-\infty}^{\infty} \tilde{f}(t+\frac{\tau_H-\tau_a}{2})\, \tilde{f}^*(t-\frac{\tau_H-\tau_a}{2})\, e^{-j(\omega_{D_H}-\omega_{D_a})t} dt$$

$$= \frac{1}{2n+1} \sum_{k=-n}^{n} e^{j(\omega_{D_H}+\omega_{D_a})(\frac{\tau_H-\tau_a}{2})} \int_{kT_p-\frac{1}{2}(T-|\tau_H-\tau_a|)}^{kT_p+\frac{1}{2}(T-|\tau_H-\tau_a|)} \tilde{u}(t-kT_p+\frac{|\tau_H-\tau_a|}{2})$$

$$\cdot\, \tilde{u}^*(t-kT_p-\frac{|\tau_H-\tau_a|}{2})\, e^{-j(\omega_{D_H}-\omega_{D_a})t} dt \qquad (4.51)$$

Let $z = t-kT_p$. Then,

$$\phi(\tau_H,\tau_a,\omega_{D_H},\omega_{D_a}) = \frac{1}{2n+1} e^{j(\omega_{D_H}+\omega_{D_a})(\frac{\tau_H-\tau_a}{2})} \sum_{k=-n}^{n} e^{-j(\omega_{D_H}-\omega_{D_a})kT_p}$$

$$\cdot \int_{-\frac{1}{2}(T-|\tau_H-\tau_a|)}^{\frac{1}{2}(T-|\tau_H-\tau_a|)} \tilde{u}(z+\frac{|\tau_H-\tau_a|}{2})\, \tilde{u}^*(z-\frac{|\tau_H-\tau_a|}{2})\, e^{-j(\omega_{D_H}-\omega_{D_a})z}\, dz$$

$$= \frac{1}{2n+1} e^{j(\omega_{D_H}+\omega_{D_a})(\frac{\tau_H-\tau_a}{2})} \sum_{k=-n}^{n} e^{-j(\omega_{D_H}-\omega_{D_a})kT_p} \frac{2\sin\left((\frac{\omega_{D_H}-\omega_{D_a}}{2})(T-|\tau_H-\tau_a|)\right)}{(\omega_{D_H}-\omega_{D_a})T}$$

$$= \frac{1}{2n+1} e^{j(\omega_{D_H}+\omega_{D_a})(\frac{\tau_H-\tau_a}{2})} \frac{\sin\left((\frac{\omega_{D_H}-\omega_{D_a}}{2})(n+\frac{1}{2})T_p\right)}{\sin\left((\omega_{D_H}-\omega_{D_a})\frac{T_p}{2}\right)} \frac{2\sin\left((\frac{\omega_{D_H}-\omega_{D_a}}{2})(T-|\tau_H-\tau_a|)\right)}{(\omega_{D_H}-\omega_{D_a})T} \qquad (4.52)$$

Now consider the case $\tau_H-\tau_a > T$. Note that there is no overlap of $\tilde{f}(t+\frac{|\tau_H-\tau_a|}{2})$ and $\tilde{f}^*(t-\frac{|\tau_H-\tau_a|}{2})$ in (4.51), until $\tau_H-\tau_a = T_p - T$. When $\tau_H-\tau_a = T_p - T$, the term $\tilde{f}(t-\frac{|\tau_H-\tau_a|}{2})$ is displaced to the left by $\frac{T_p-T}{2}$ and the term $\tilde{f}(t+\frac{|\tau_H-\tau_a|}{2})$ to the right by $\frac{T_p-T}{2}$. Then one less pulse is included in the overlap, as illustrated in Fig. 4-19. We thus conclude, for

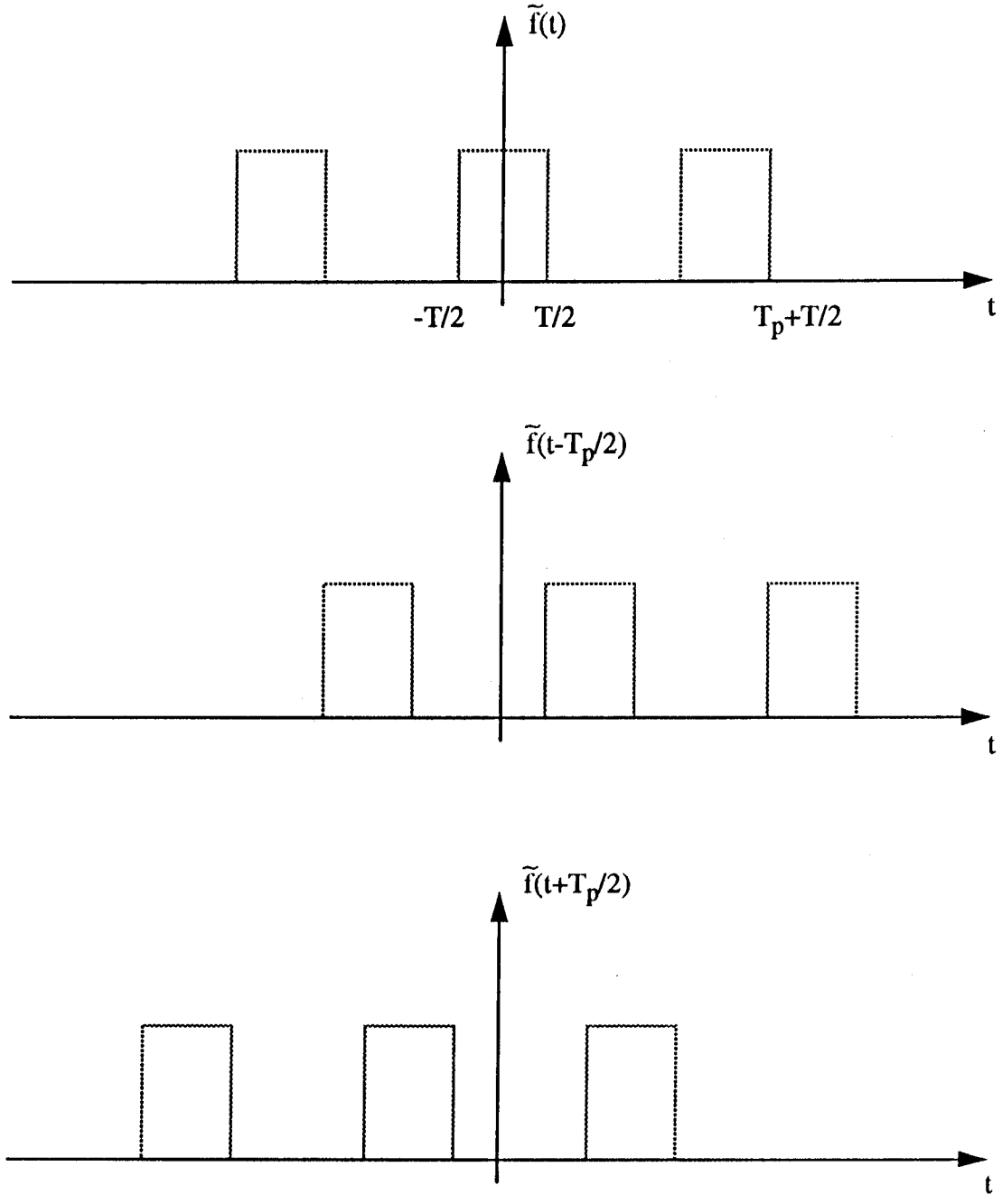

Fig. 4-19 : Computation of ambiguity function for the three rectangular pulses waveform

$|\tau_H-\tau_a-T_p| \le T,$

$$\phi(\tau_H,\tau_a,\omega_{D_H},\omega_{D_a}) = \frac{1}{2n+1}\, e^{j(\omega_{D_H}+\omega_{D_a})(\frac{\tau_H-\tau_a}{2})} \sum_{k=-n+1}^{n} e^{-j(\omega_{D_H}-\omega_{D_a})kT_p} \cdot$$

$$\int_{kT_p-\frac{1}{2}(T-|\tau_H-\tau_a-T_p|)}^{kT_p+\frac{1}{2}(T-|\tau_H-\tau_a-T_p|)} \tilde{u}(t-kT_p+\frac{|\tau_H-\tau_a-T_p|}{2})\, \tilde{u}^*(t-kT_p-\frac{|\tau_H-\tau_a-T_p|}{2})\, e^{-j(\omega_{D_H}-\omega_{D_a})t}\, dt$$

$$= \frac{1}{2n+1}\, e^{j(\omega_{D_H}+\omega_{D_a})(\frac{\tau_H-\tau_a}{2})} \sum_{k=-n+1}^{n} e^{j(\omega_{D_H}-\omega_{D_a})kT_p} \frac{2\sin\left((\frac{\omega_{D_H}-\omega_{D_a}}{2})(T-|\tau_H-\tau_a-T_p|)\right)}{(\omega_{D_H}-\omega_{D_a})T}$$

$$= \frac{1}{2n+1}\, e^{j(\omega_{D_H}+\omega_{D_a})(\frac{\tau_H-\tau_a}{2})} \frac{2\sin\left((\frac{\omega_{D_H}-\omega_{D_a}}{2})(T-|\tau_H-\tau_a-T_p|)\right)}{(\omega_{D_H}-\omega_{D_a})T} \frac{\sin\left((\omega_{D_H}-\omega_{D_a})nT_p\right)}{\sin\left((\omega_{D_H}-\omega_{D_a})\frac{T_p}{2}\right)} \qquad (4.53)$$

Carrying on in this manner, there are (2n+1) expressions similar to the ones given in (4.52) and (4.53). Thus the general expression for the time-frequency autocorrelation function is

$$\phi(\tau_H,\tau_a,\omega_{D_H},\omega_{D_a}) = \frac{1}{2n+1}\, e^{j(\omega_{D_H}+\omega_{D_a})(\frac{\tau_H-\tau_a}{2})} \sum_{k=-n}^{n} \frac{2\sin\left((\frac{\omega_{D_H}-\omega_{D_a}}{2})(T-|\tau_H-\tau_a-kT_p|)\right)}{(\omega_{D_H}-\omega_{D_a})T}$$

$$\cdot \text{rect}\,(\frac{\tau_H-\tau_a-kT_p}{2T}) \cdot \frac{\sin\left((\omega_{D_H}-\omega_{D_a})(2n+1-|k|)\frac{T_p}{2}\right)}{\sin\left((\omega_{D_H}-\omega_{D_a})\frac{T_p}{2}\right)} \qquad (4.54)$$

Finally, the ambiguity function is given by the magnitude square of (4.54). That is,

$$\theta(\tau_H,\tau_a,\omega_{D_H},\omega_{D_a}) = |\phi(\tau_H,\tau_a,\omega_{D_H},\omega_{D_a})|^2$$

$$= \left|\frac{1}{2n+1}\, e^{j(\omega_{D_H}+\omega_{D_a})(\frac{\tau_H-\tau_a}{2})} \sum_{k=-n}^{n} \frac{2\sin\left((\frac{\omega_{D_H}-\omega_{D_a}}{2})(T-|\tau_H-\tau_a-kT_p|)\right)}{(\omega_{D_H}-\omega_{D_a})T}\right.$$

$$\left. \cdot\, \mathrm{rect}(\frac{\tau_H-\tau_a-kT_p}{2T})\, \frac{\sin\left((\omega_{D_H}-\omega_{D_a})(2n+1-|k|)\frac{T_p}{2}\right)}{\sin\left((\omega_{D_H}-\omega_{D_a})\frac{T_p}{2}\right)}\right|^2$$

$$= \sum_{k=-n}^{n} \left|\frac{1}{2n+1}\, \frac{2\sin\left((\frac{\omega_{D_H}-\omega_{D_a}}{2})(T-|\tau_H-\tau_a-kT_p|)\right)}{(\omega_{D_H}-\omega_{D_a})T}\right.$$

$$\left. \cdot\, \frac{\sin\left((\omega_{D_H}-\omega_{D_a})(2n+1-|k|)\frac{T_p}{2}\right)}{\sin\left((\omega_{D_H}-\omega_{D_a})\frac{T_p}{2}\right)}\right|^2 \mathrm{rect}(\frac{\tau_H-\tau_a-kT_p}{2T}) \qquad (4.55)$$

where we have assumed $T < \frac{1}{2} T_p$. In Figure 4-20, we give the plot of (4.55) assuming the carrier frequency $\omega_0 = 3\text{x}10^8$ rad/sec, the number of pulses transmitted $N = 2n+1 = 3$, the subpulse duration $T = 4\text{x}10^{-5}$ sec, and the period $T_p = 10^{-4}$ sec. Also, it is assumed that the actual delay $\tau_a = 4\text{x}10^{-4}$ sec, and the actual Doppler $\omega_{D_a} = 1200$ rad/sec.

For monostatic radars, Figure 4-21 shows the result of (4.55) plotted on the R_{M_H}-V_{M_H} plane, i.e., it is plotted with the hypothesized one-way range and the radial velocity as variables. Note that, here, $R_{M_a} = \frac{c\tau_a}{2} = 6\text{x}10^4$ m and $V_{M_a} = \frac{c\omega_{D_a}}{2\omega_0} = 600$ m/sec..

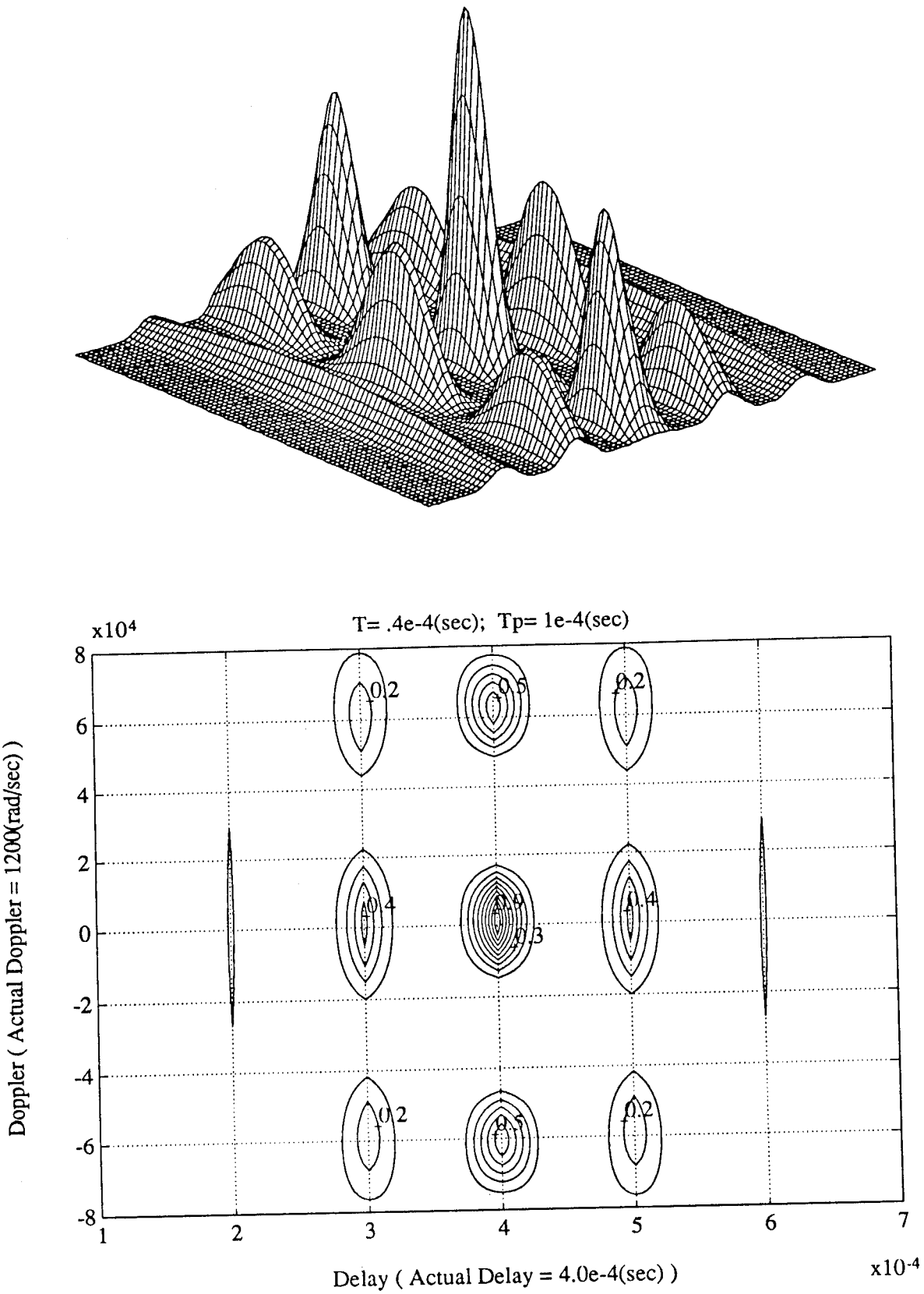

Fig. 4-20 : Ambiguity function for monostatic radar in the delay-Doppler plane for the three rectangular pulses waveform

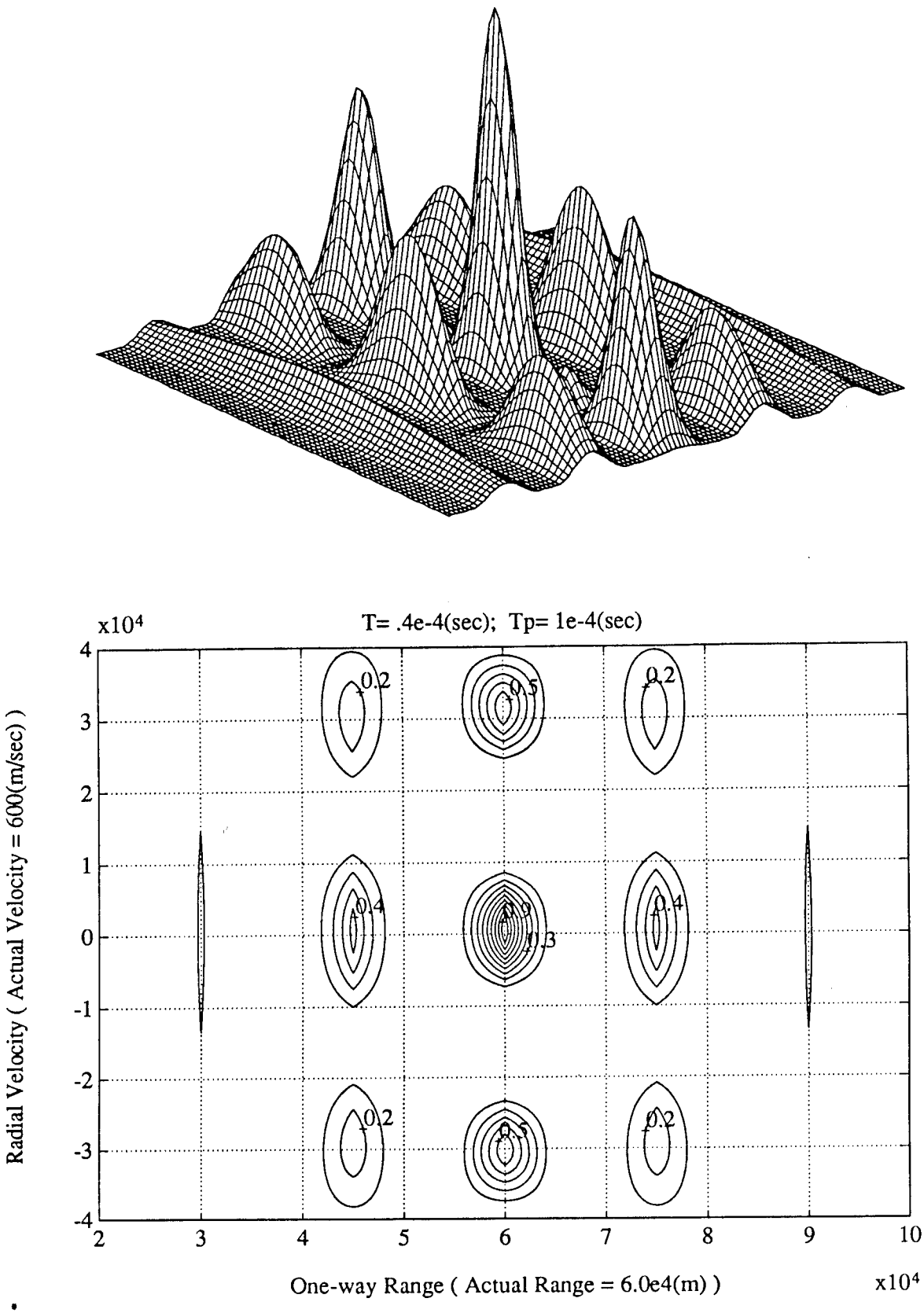

Fig. 4-21 : Ambiguity function for monostatic radar in the range-velocity plane for the three rectangular pulses waveform

Again, as before, the ambiguity function for the bistatic case will be the same as shown in Fig. 4-20 if bistatic geometry is ignored. On the other hand, when this three rectangular pulse train is employed in a bistatic radar, the resulting ambiguity function with respect to the receiver can be examined by writing (4.55) in the form of $\theta(D_{R_H}, D_{R_a}, W_{R_H}, W_{R_a})$. The results are plotted in Figures 4-22 to 4-26 assuming that $R_{R_a} = 6\text{x}10^4\text{m}$, $V_a = 600$ m/sec and $L = 10^5$ m, for various values of receiver look angles. In order to compare the ambiguity function for the above receiver-centered region with the cosite region, we change the value of L to $5\text{x}10^4$ m. The results are plotted in Figures 4-27 to 4-31, for various values of receiver look angles. Now, it is again seen that the geometry factors have more profound effects in the receiver-centered region than in the cosite region. Moreover, within the same operating region, the effects of geometry factors are more prominent when the target is closer to the baseline.

4.3 Discussion

In the previous section, it has been indicated that the ambiguity function for a bistatic radar needs to be plotted with respect to an appropriate point. For example, the reference point can be the transmitter site, the receiver site or some other point of interest. In the examples, we focussed on ambiguity function plots with respect to the receiver only. Similar results can be obtained in other cases. Two examples were considered which demonstrated the fact that bistatic geometry plays an important role in ambiguity function analysis. It was observed that, in the regions close to the receiver, geometry factors have a more pronounced effect on the resolution capabilities of the transmitted waveform than in the cosite region. In fact, resolution

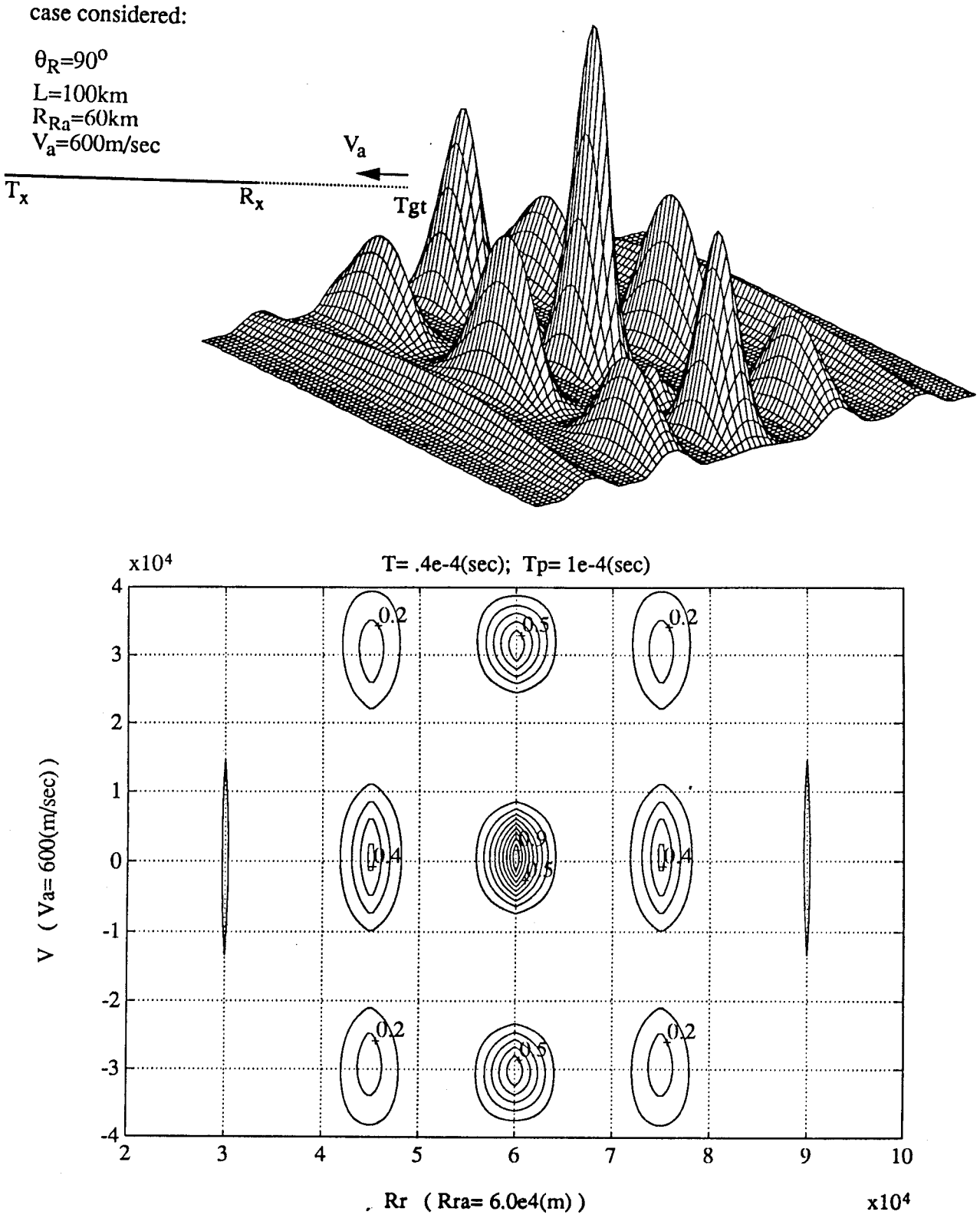

Fig. 4-22: **Bistatic ambiguity function for the three rectangular pulses waveform for the case considered**

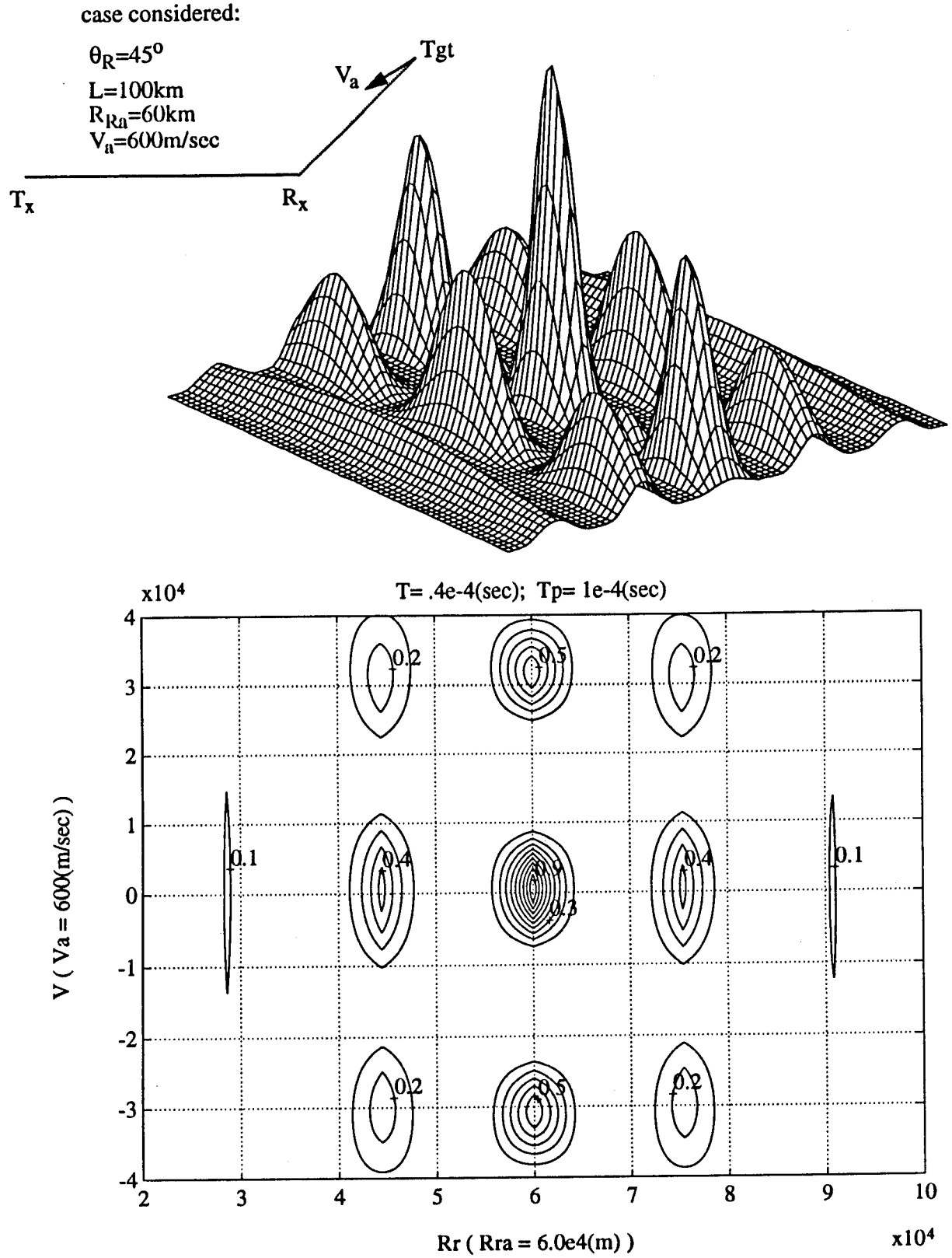

Fig. 4-23: **Bistatic ambiguity function for the three rectangular pulses waveform for the case considered**

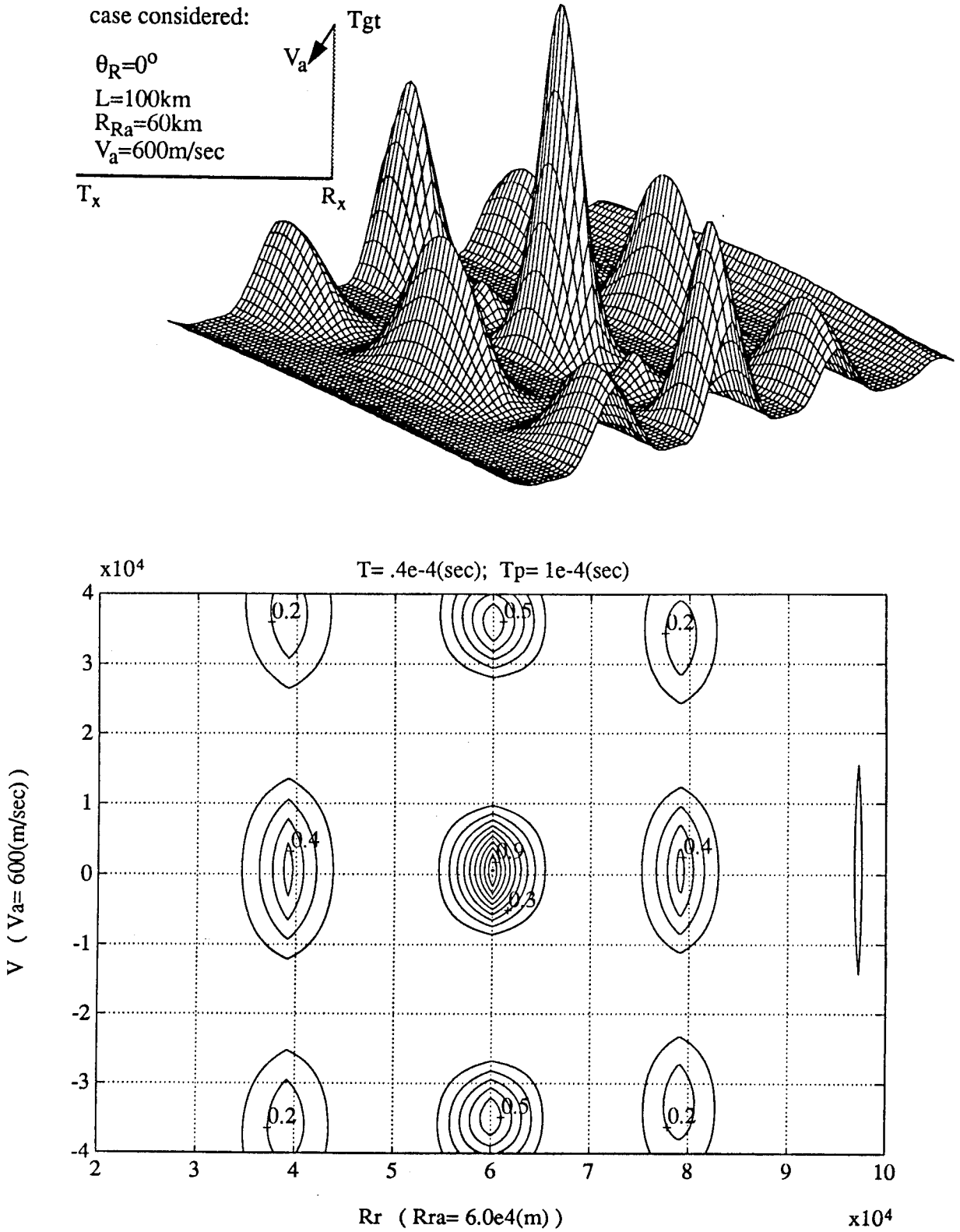

Fig. 4-24: **Bistatic ambiguity function for the three rectangular pulses waveform for the case considered**

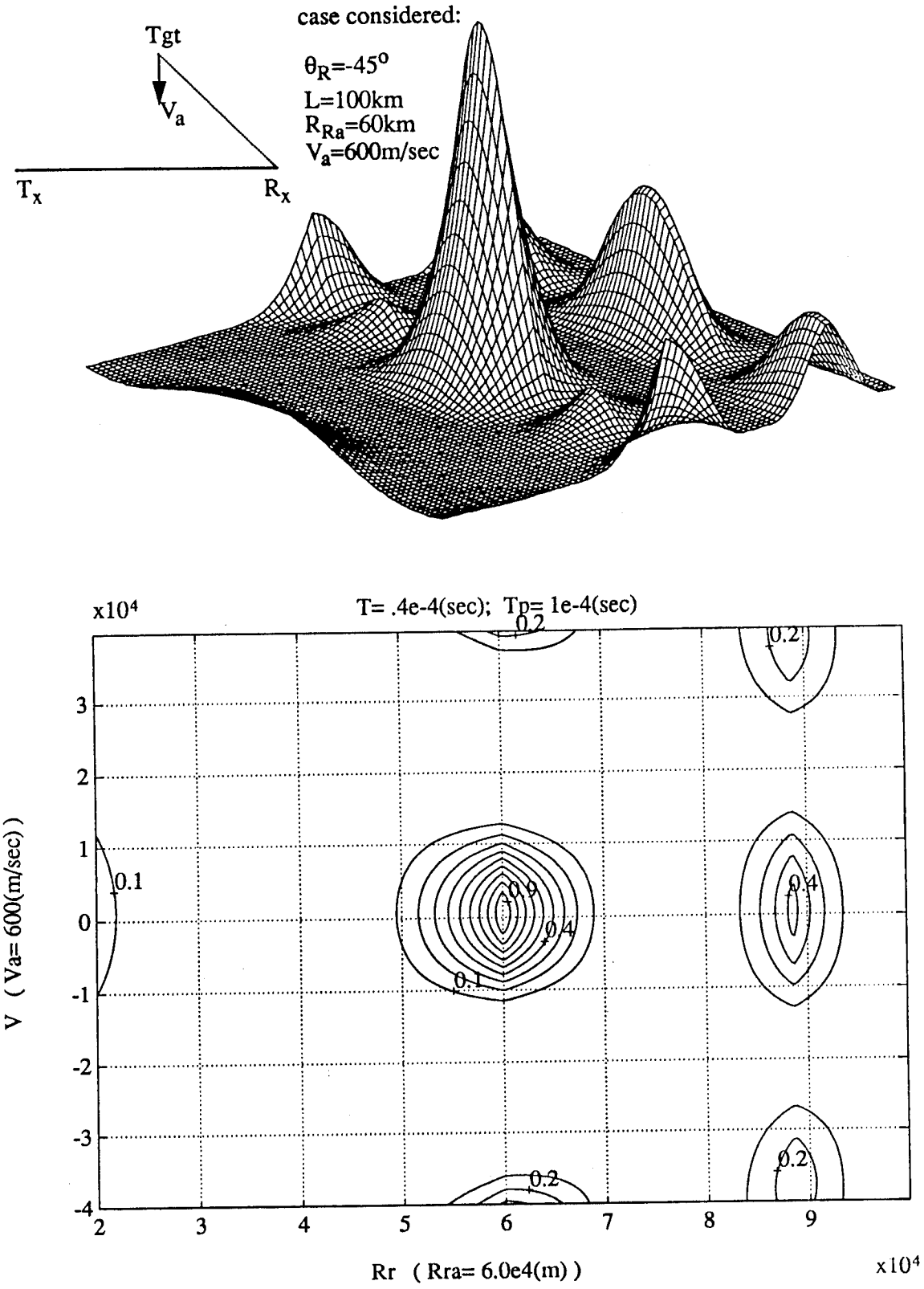

Fig. 4-25: **Bistatic ambiguity function for the three rectangular pulses waveform for the case considered**

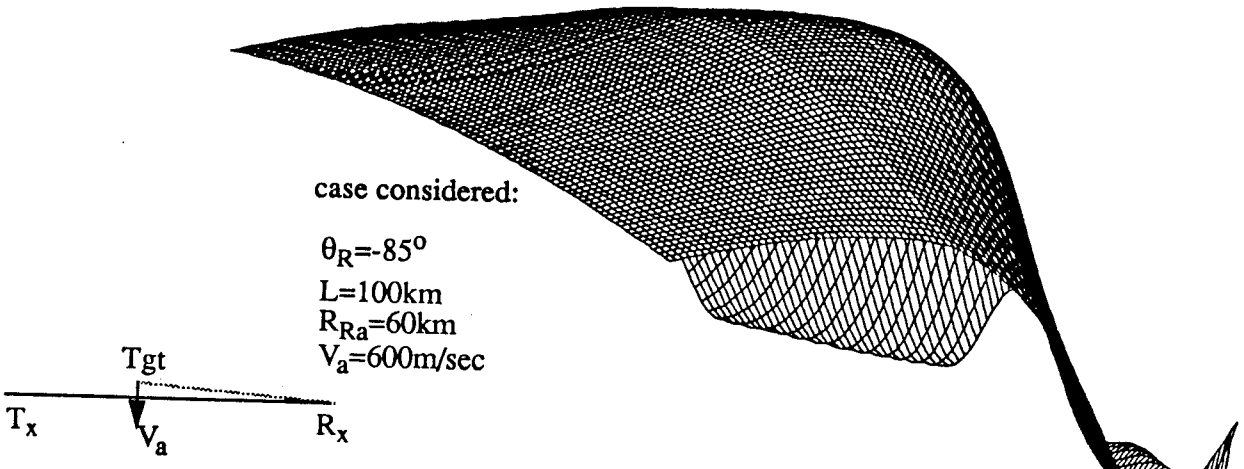

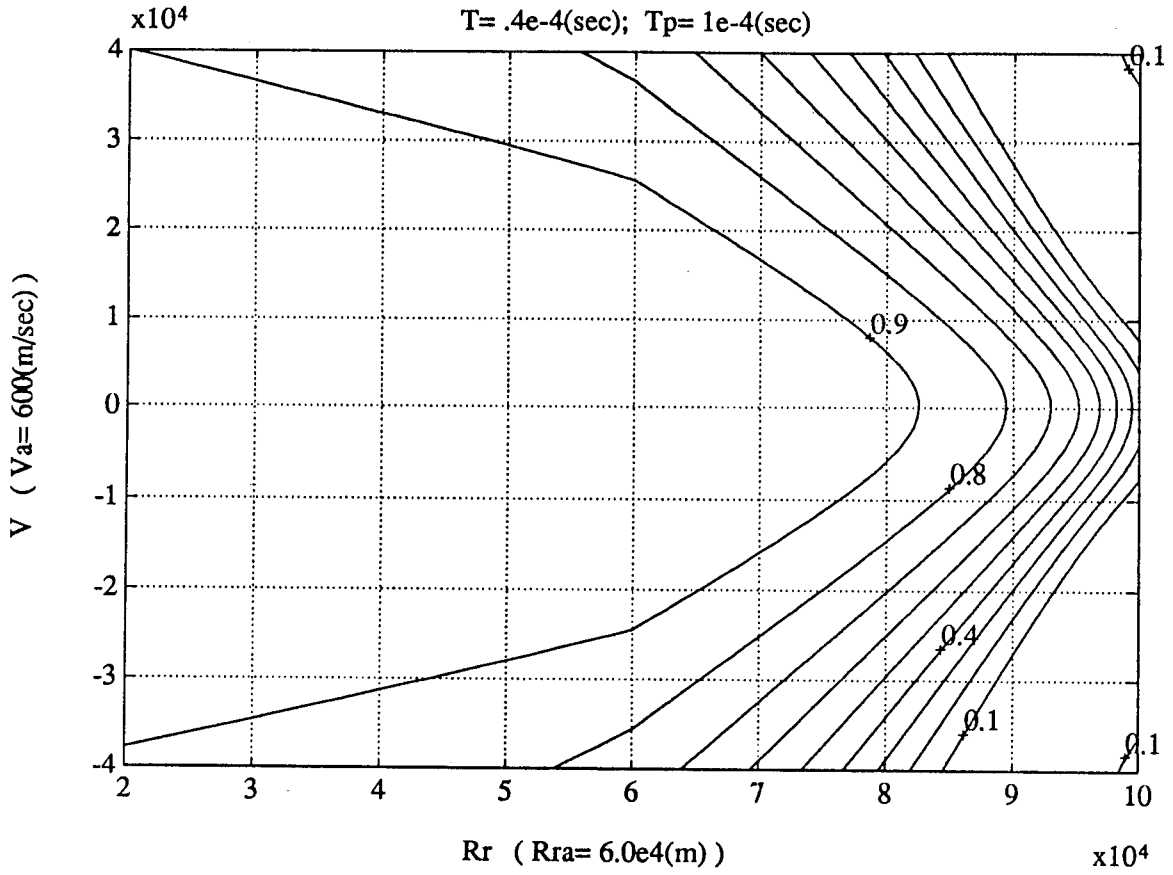

Fig. 4-26: **Bistatic ambiguity function for the three rectangular pulses waveform for the case considered**

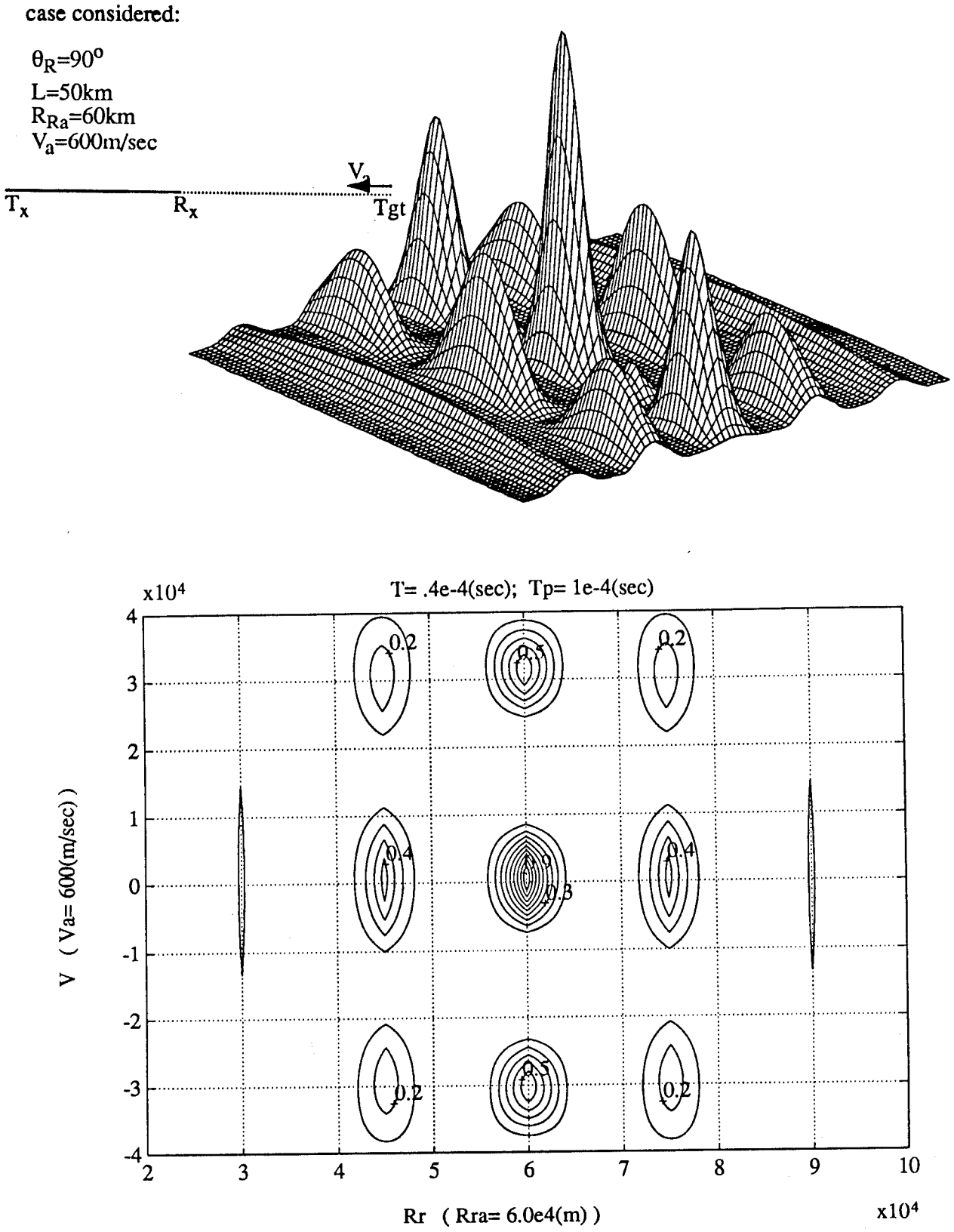

Fig. 4-27: **Bistatic ambiguity function for the three rectangular pulses waveform for the case considered**

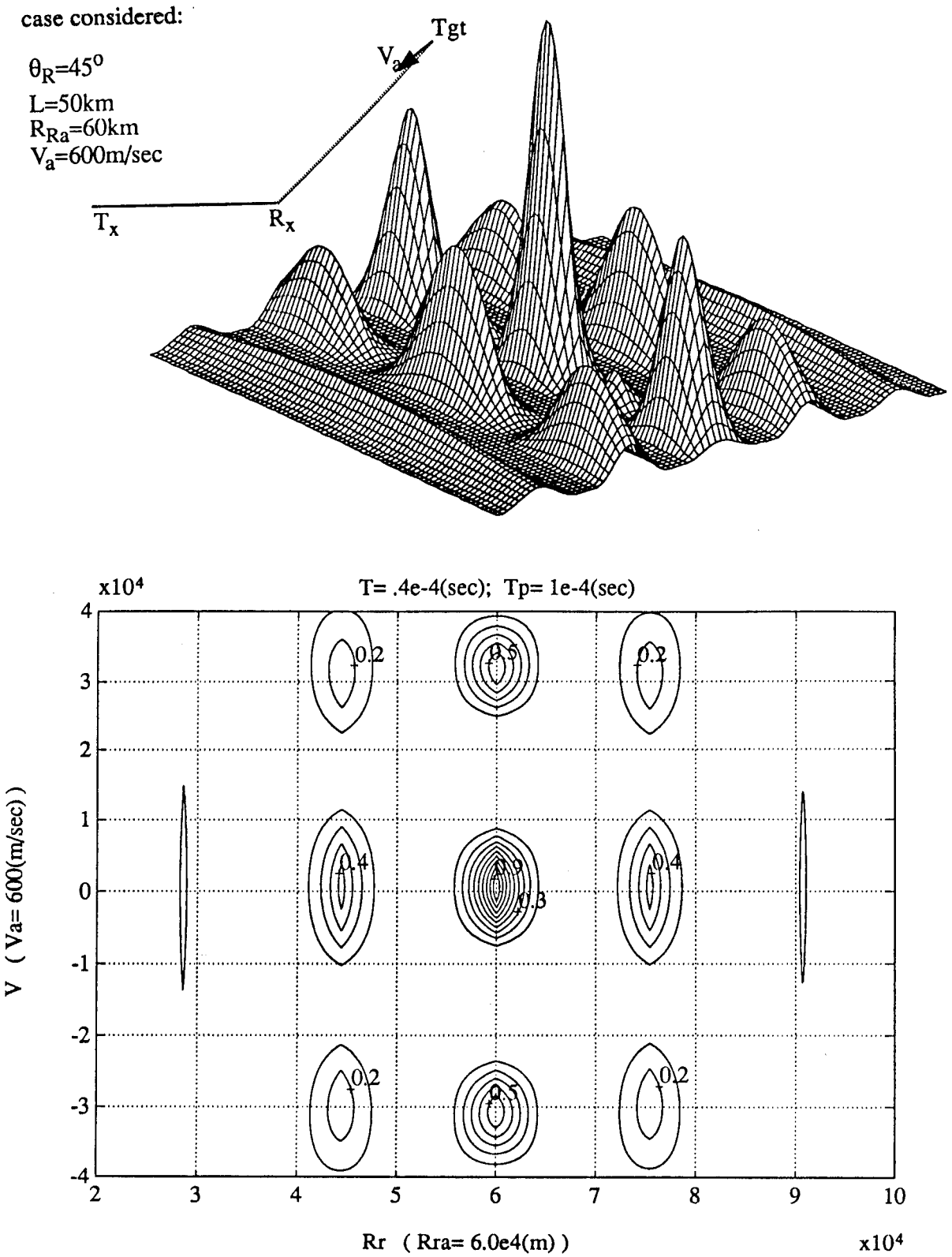

Fig. 4-28: **Bistatic ambiguity function for the three rectangular pulses waveform for the case considered**

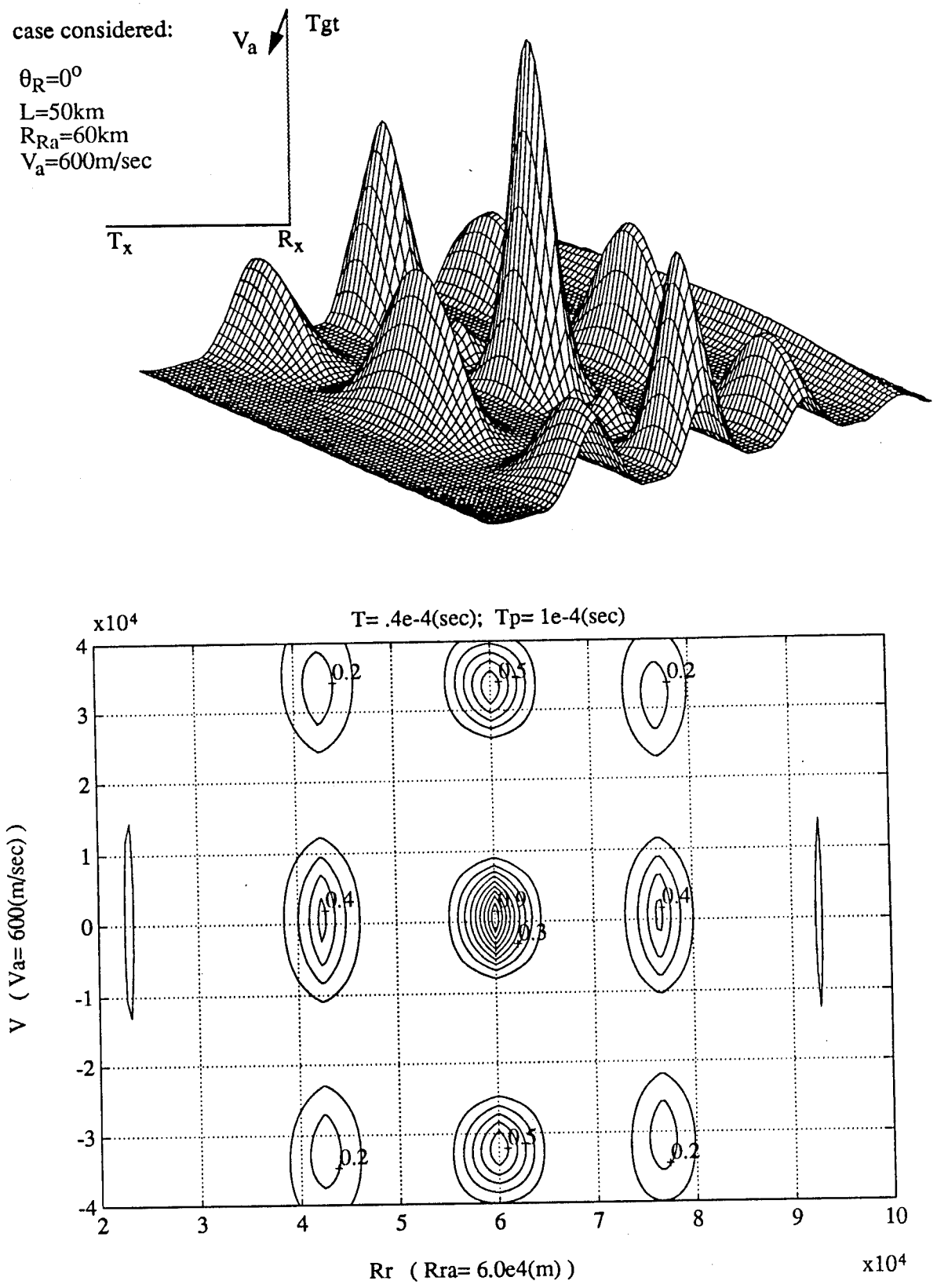

Fig. 4-29: **Bistatic ambiguity function for the three rectangular pulses waveform for the case considered**

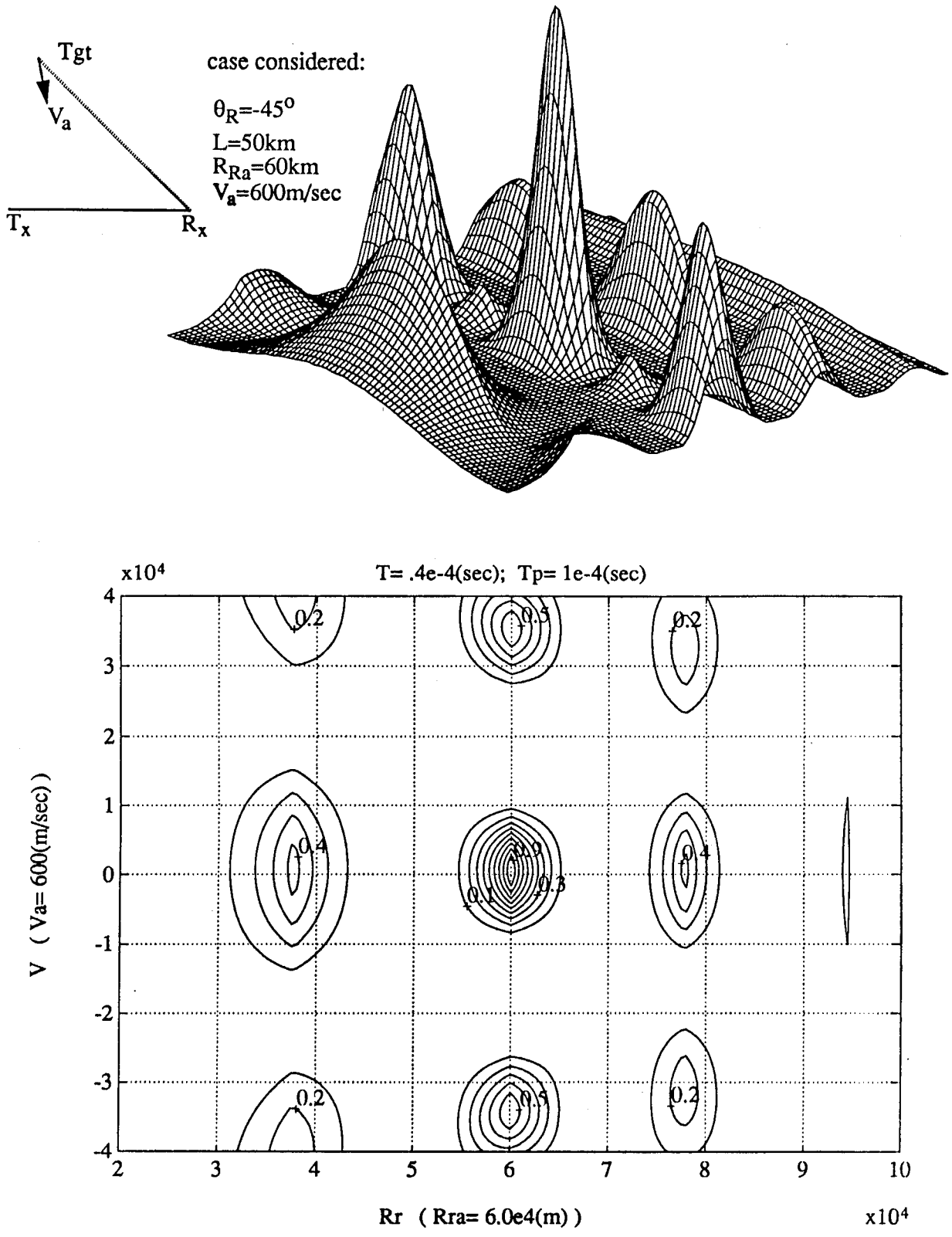

Fig. 4-30: **Bistatic ambiguity function for the three rectangular pulses waveform for the case considered**

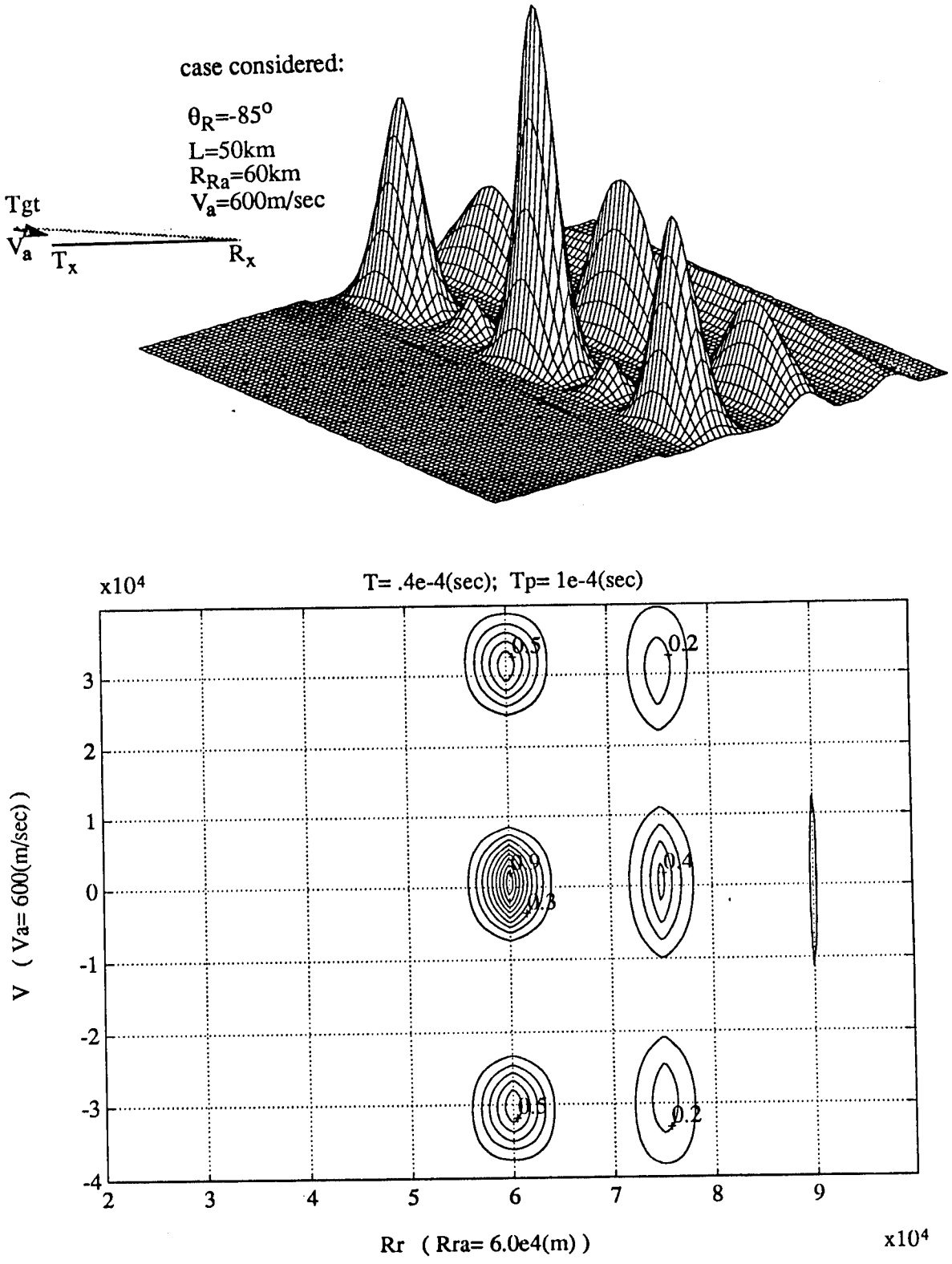

Fig. 4-31: Bistatic ambiguity function for the three rectangular pulses waveform for the case considered

is totally lost if the target is on the baseline. Note that these effects cannot be observed if the ambiguity function is plotted using delay and Doppler as arguments in a conventional manner disregarding the geometry. Note further that even for a simple three rectangular pulse waveform, the bistatic geometry significantly affects the ambiguity function and the associated parameter estimates. This effect will be even more pronounced with more complex waveforms based on PN sequences. The methodology presented here must be used to assess the capabilities of transmitted waveforms for bistatic radar scenarios.

5 CONTINUOUS-TIME CONTINUOUS-FREQUENCY AMBIGUITY FUNCTION OF A SAMPLED SIGNAL

In our work thus far, we have assumed that continuous signals are processed at the receiver input. In practice, however, most modern radars sample the signal after it has been frequency translated to baseband. This sampled discrete-time signal is processed using digital signal processing techniques. Next we consider ambiguity function analysis based on the sampled signal. First we consider the case where τ_H, τ_a, ω_{D_H} and ω_{Da} are allowed to assume all possible values. In this case, the ambiguity function is a continuous function of time and frequency even though the received signal has been sampled.

5.1 Likelihood Ratio Test for a Discrete Signal

We return to the detection problem as discussed earlier, but assume that the complex envelope of the received pulse, $\tilde{r}(t)$, is represented by N complex samples $\tilde{r}_0, \tilde{r}_1,..., \tilde{r}_{N-1}$. The detection problem is now characterized by the two hypotheses

$$\begin{aligned} H_1&: \tilde{r}_k=\tilde{s}_k+\tilde{n}_k \\ H_0&: \tilde{r}_k=\tilde{n}_k \qquad\qquad k=0,1,...N-1 \end{aligned} \tag{5.1}$$

where $\tilde{s}_0, \tilde{s}_1,..., \tilde{s}_{N-1}$ are samples of the received signal complex envelope $\tilde{s}(t)= \sqrt{E_t}\, \tilde{b}\, \tilde{f}(t-\tau_a)e^{j\omega_{Da}t}$ at times $t = \tau_H + k\frac{T}{N}$, and $\tilde{n}_0, \tilde{n}_1,..., \tilde{n}_{N-1}$ represent samples of the complex envelope of the Gaussian white noise process $\tilde{n}(t)$. As before, assume that $\tilde{b}$ remains fixed over the duration of the signal pulse and is statistically independent of the noise samples. Let $\tilde{r}$ be the (column) vector whose elements are

$\tilde{r}_k$, k=0, 1,...,N-1. We introduce the notation

$$\tilde{m}_0 = E[\tilde{r}|H_0] \quad \text{and} \quad \tilde{m}_1 = E[\tilde{r}|H_1] \tag{5.2}$$

for the conditional mean vectors of $\tilde{r}$ under hypotheses H_0 and H_1, respectively. Also, we denote the covariance matrices under H_0 and H_1 by

$$\mathbf{K}_i = E[(\tilde{r}-\tilde{m}_i)(\tilde{r}-\tilde{m}_i)^H|H_i] \qquad i=0,1, \tag{5.3}$$

where the superscript H denotes the conjugate transpose (Hermitian). We may then write the conditional probability densities of $\tilde{r}$ under H_i, i=0,1, as

$$P_{\tilde{r}|H_i}(\tilde{\mathbf{R}}|H_i) = \frac{1}{\pi^N|\mathbf{K}_i|} \exp\{-(\tilde{\mathbf{R}}^H-\tilde{m}_i^H)\mathbf{K}_i^{-1}(\tilde{\mathbf{R}}-\tilde{m}_i)\} \qquad i = 0,1. \tag{5.4}$$

Here, $|\mathbf{K}_i|$ denotes the determinant of $\mathbf{K}_i$. The likelihood ratio test is given by

$$\Lambda(\mathbf{R}) \triangleq \frac{P_{\tilde{r}|H_1}(\tilde{\mathbf{R}}|H_1)}{P_{\tilde{r}|H_0}(\tilde{\mathbf{R}}|H_0)}$$

$$= \frac{|\mathbf{K}_0|\, e^{-(\tilde{\mathbf{R}}^H-\tilde{m}_1^H)\mathbf{K}_1^{-1}(\tilde{\mathbf{R}}-\tilde{m}_1)}}{|\mathbf{K}_1|\, e^{-(\tilde{\mathbf{R}}^H-\tilde{m}_0^H)\mathbf{K}_0^{-1}(\tilde{\mathbf{R}}-\tilde{m}_0)}} \underset{H_0}{\overset{H_1}{\gtrless}} \eta.$$

Taking logarithms, we obtain

$$(\tilde{\mathbf{R}}^H-\tilde{m}_0^H)\mathbf{K}_0^{-1}(\tilde{\mathbf{R}}-\tilde{m}_0) - (\tilde{\mathbf{R}}^H-\tilde{m}_1^H)\mathbf{K}_1^{-1}(\tilde{\mathbf{R}}-\tilde{m}_1)$$

$$\underset{H_0}{\overset{H_1}{\gtrless}} \ln\eta + \ln|\mathbf{K}_1| - \ln|\mathbf{K}_0| \triangleq \gamma. \tag{5.5}$$

5.1.1 Zero-mean Case

Let the mean vectors on the two hypotheses be equal to zero. Then

$$\tilde{\mathbf{m}}_0 = \tilde{\mathbf{m}}_1 = \mathbf{0}.$$

The likelihood ratio test reduces to

$$\tilde{\mathbf{R}}^H \left\{ \mathbf{K}_0^{-1} - \mathbf{K}_1^{-1} \right\} \tilde{\mathbf{R}} \underset{H_0}{\overset{H_1}{\gtrless}} \gamma \ . \tag{5.6}$$

Denote the inverse of the covariance matrix $\mathbf{K}_i$, i=0,1, by $\mathbf{Q}_i$,

$$\mathbf{Q}_i = \mathbf{K}_i^{-1} \qquad i=0,1. \tag{5.7}$$

The likelihood ratio test can then be written as

$$\tilde{\mathbf{R}}^H (\mathbf{Q}_0 - \mathbf{Q}_1) \tilde{\mathbf{R}} \underset{H_0}{\overset{H_1}{\gtrless}} \gamma. \tag{5.8}$$

5.1.2 Zero-mean Vectors and White Noise Case

In addition to the mean vectors being equal to zero on the two hypotheses, let the noise be white with power N_0. Then

$$E[\tilde{\mathbf{n}}\ \tilde{\mathbf{n}}^H] = N_0\ \mathbf{I}$$

where I represents the identity matrix. Let $\mathbf{K}_s$ denote the covariance matrix of the signal,

$$E[\tilde{\mathbf{s}}\ \tilde{\mathbf{s}}^H] = \mathbf{K}_s \ .$$

It follows that

$$\mathbf{K}_0 = E[\tilde{\mathbf{r}}\ \tilde{\mathbf{r}}^H|H_0] = E[\tilde{\mathbf{n}}\ \tilde{\mathbf{n}}^H] = N_0\ \mathbf{I} \tag{5.9}$$

and

$$\mathbf{K}_1 = E[\tilde{\mathbf{r}}\ \tilde{\mathbf{r}}^H|H_1] = E[(\tilde{\mathbf{s}} + \tilde{\mathbf{n}})(\tilde{\mathbf{s}} + \tilde{\mathbf{n}})^H]$$

$$= E[\tilde{\mathbf{s}}\ \tilde{\mathbf{s}}^H] + E[\tilde{\mathbf{n}}\ \tilde{\mathbf{n}}^H] = \mathbf{K}_s + N_0\ \mathbf{I}.$$

The latter result uses the fact that the signal and noise are uncorrelated and both have zero mean. The elements of the vectors $\tilde{\mathbf{s}}$ and $\tilde{\mathbf{n}}$ are $\tilde{s}_k$, $\tilde{n}_k$, k=0, 1..., N-1, respectively.

Consider again the inverse relationship between $\mathbf{Q}_1$ and $\mathbf{K}_1$,

$$\mathbf{Q}_1\ \mathbf{K}_1 = \mathbf{I}.$$

It was shown above that

$$\mathbf{K}_1 = \mathbf{K}_s + N_0\ \mathbf{I}.$$

Now express $\mathbf{Q}_1$ as

$$\mathbf{Q}_1 = \frac{1}{N_0}[\mathbf{I} - \mathbf{H}_1] \tag{5.10}$$

where $\mathbf{H}_1$ is an N x N matrix. Substituting for $\mathbf{K}_1$ and $\mathbf{Q}_1$ in the first equation yields

$$\frac{1}{N_0}[\mathbf{I} - \mathbf{H}_1] \cdot [\mathbf{K}_s + N_0\ \mathbf{I}] = \mathbf{I}$$

which simplifies to

$$\mathbf{K}_s = N_0\ \mathbf{H}_1 + \mathbf{H}_1\ \mathbf{K}_s. \tag{5.11}$$

We notice that this equation is the discrete-time analog to the integral equation obtained in Sec. 2.4 for the continuous case. Since

$$\mathbf{Q}_0 = \mathbf{K}_0^{-1} = [N_0\, \mathbf{I}]^{-1} = \frac{1}{N_0}\, \mathbf{I},$$

we have

$$\mathbf{Q}_1 = \mathbf{Q}_0 - \frac{1}{N_0}\, \mathbf{H}_1$$

or we can write

$$\mathbf{Q}_0 - \mathbf{Q}_1 = \frac{1}{N_0}\, \mathbf{H}_1.$$

The likelihood ratio test can, therefore, be expressed also in terms of the matrix $\mathbf{H}_1$:

$$\ell_R = \frac{1}{N_0} \tilde{\mathbf{R}}^H \mathbf{H}_1 \tilde{\mathbf{R}} \underset{H_0}{\overset{H_1}{\gtrless}} \gamma\ . \tag{5.12}$$

5.1.3 Comparison with an Estimation Problem

Consider the minimum-mean-square-error (MMSE) estimation problem shown in Fig. 5.1; $\tilde{\mathbf{s}}_{MMSE} = \mathbf{H}_1\, \tilde{\mathbf{r}}$ denotes the minimum mean square estimate of $\tilde{\mathbf{s}}$ and $\tilde{\mathbf{r}} = \tilde{\mathbf{s}} + \tilde{\mathbf{n}}$. By definition, $\tilde{\mathbf{s}}_{MMSE} - \tilde{\mathbf{s}}$ and $\tilde{\mathbf{r}}$ must be orthogonal:

$$\begin{aligned} &E[(\tilde{\mathbf{s}}_{MMSE} - \tilde{\mathbf{s}}).\tilde{\mathbf{r}}^H] \\ &= E[(\mathbf{H}_1\tilde{\mathbf{s}} + \mathbf{H}_1\tilde{\mathbf{n}} - \tilde{\mathbf{s}})(\tilde{\mathbf{s}} + \tilde{\mathbf{n}})^H] = 0. \end{aligned} \tag{5.13}$$

Assuming the signal and noise vectors to be uncorrelated and zero mean, we get

$$\mathbf{H}_1\, \mathbf{K}_s + \mathbf{H}_1\, N_0\, \mathbf{I} - \mathbf{K}_s = 0$$

or

$$\mathbf{K}_s = N_0\, \mathbf{H}_1 + \mathbf{H}_1\, \mathbf{K}_s. \tag{5.14}$$

This last equation is the same as the one found previously. We conclude that $\mathbf{H}_1$

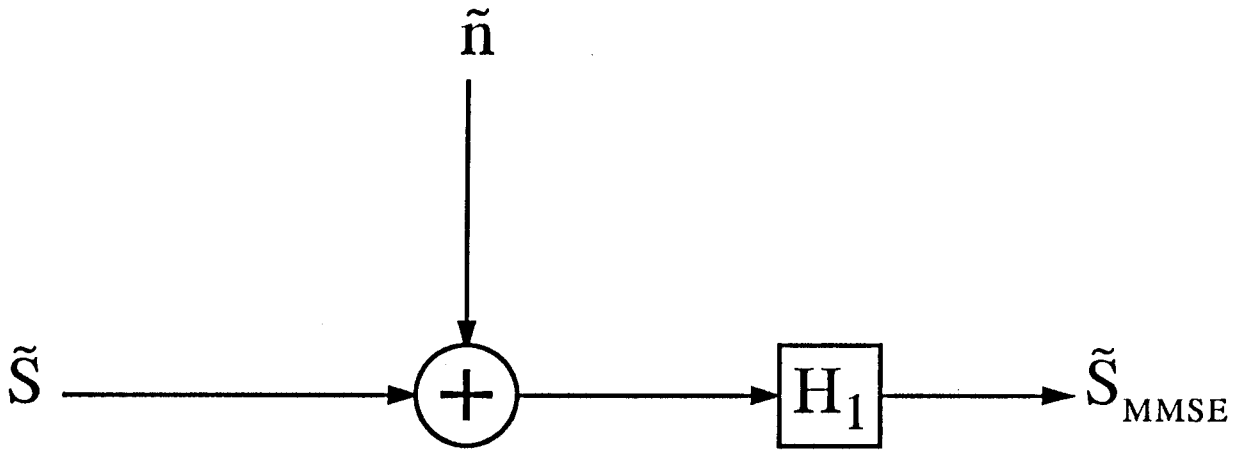

Fig. 5.1 MMSE estimation problem

characterizes the filter which generates the minimum mean square estimate of $\tilde{s}$ from $\tilde{r}$.

5.2 Ambiguity Function for the Discrete Signal

For the slowly fluctuating point target case, let the elements of the signal vector $\tilde{s}$ at the receiver, assuming reference time delay τ_H and reference Doppler frequency ω_{D_H}, be given by

$$\tilde{s}_k = \tilde{b}\sqrt{E_t}\,\tilde{f}(kT_s)e^{j\omega_{D_H}kT_s} \qquad k=0,1,\ldots,N-1 \tag{5.15}$$

where T_s is the sampling period. Now define the N×1 column vector $\tilde{\Psi}$ with elements

$$\tilde{\Psi}_k = \tilde{f}(kT_s)\,e^{j\omega_{D_H}kT_s} \qquad k=0,1,\ldots,N-1 \tag{5.16}$$

so that

$$\tilde{s} = \tilde{b}\sqrt{E_t}\tilde{\Psi}$$

and

$$\begin{aligned} K_s = E[\tilde{s}\,\tilde{s}^H] &= E\{|\tilde{b}|^2\}\,E_t\tilde{\Psi}\tilde{\Psi}^H \\ &= 2\,\sigma_b^2\,E_t\,\tilde{\Psi}\,\tilde{\Psi}^H \\ &= \bar{E}_r\,\tilde{\Psi}\,\tilde{\Psi}^H, \end{aligned}$$

where $\bar{E}_r$ denotes average energy

$$\bar{E}_r = 2\sigma_b^2 E_t.$$

We now introduce the matrix $\mathbf{H}_1$ from Sec. 5.1.2 and assume $\mathbf{H}_1$ to be of the form

$$\mathbf{H}_1 = c\tilde{\Psi}\ \tilde{\Psi}^H$$

where c is a constant. We are interested in finding c so that $\mathbf{H}_1$ is the solution of the matrix equation derived in Sec. 5.1.2,

$$\mathbf{K}_s = N_0\ \mathbf{H}_1 + \mathbf{H}_1\ \mathbf{K}_s,$$

which is the discrete form of the integral equation in Sec. 2.4. Substituting for $\mathbf{K}_s$ and $\mathbf{H}_1$ from above gives

$$\bar{E}_r\ \tilde{\Psi}\ \tilde{\Psi}^H = N_0\ c\ \tilde{\Psi}\ \tilde{\Psi}^H + c\ \bar{E}_r\ \tilde{\Psi}\ \tilde{\Psi}^H\ \tilde{\Psi}\ \tilde{\Psi}^H. \qquad (5.17)$$

Notice that $\tilde{\Psi}^H\ \tilde{\Psi}$ is a scalar and represents the energy of the vector $\tilde{\Psi}$. Assume this energy to be normalized to unity:

$$\tilde{\Psi}^H\tilde{\Psi} = 1. \qquad (5.18)$$

We have then

$$\bar{E}_r\ \tilde{\Psi}\ \tilde{\Psi}^H = N_0\ c\ \tilde{\Psi}\ \tilde{\Psi}^H + c\ \bar{E}_r\ \tilde{\Psi}\ \tilde{\Psi}^H,$$

or

$$\bar{E}_r = N_0\ c + c\ \bar{E}_r,$$

giving

$$c = \frac{\bar{E}_r}{N_0+\bar{E}_r} .$$

Therefore, the assumed form for $\mathbf{H}_1$ is correct and $\mathbf{H}_1$ is given by

$$\mathbf{H}_1 = \frac{\bar{E}_r}{N_0+\bar{E}_r} \; \tilde{\Psi} \; \tilde{\Psi}^H. \tag{5.19}$$

The likelihood ratio can then be rewritten as follows:

$$\begin{aligned} \ell_r &= \frac{1}{N_0} \tilde{\mathbf{R}}^H \mathbf{H}_1 \tilde{\mathbf{R}} \\ &= \frac{1}{N_0} \frac{\bar{E}_r}{N_0 + \bar{E}_r} \tilde{\mathbf{R}}^H \tilde{\Psi} \tilde{\Psi}^H \tilde{\mathbf{R}} \\ &= \frac{1}{N_0} \frac{\bar{E}_r}{N_0 + \bar{E}_r} |\tilde{\Psi}^H \tilde{\mathbf{R}}|^2 \\ &= \frac{1}{N_0} \frac{\bar{E}_r}{N_0 + \bar{E}_r} \Big| \sum_{k=-\infty}^{\infty} \tilde{R}_k \tilde{f}^*(kT_s) e^{-j\omega_{D_H} kT_s} \Big|^2. \end{aligned} \tag{5.20}$$

The received vector $\tilde{\mathbf{R}}$ can be written as the sum of the incoming actual signal vector $\tilde{\mathbf{s}}_a$ and the noise vector $\tilde{\mathbf{n}}$:

$$\tilde{\mathbf{R}} = \tilde{\mathbf{s}}_a + \tilde{\mathbf{n}} \tag{5.21}$$

The samples which constitute $\tilde{\mathbf{s}}_a$ assume a reference delay τ_H. Thus, the elements of $\tilde{\mathbf{s}}_a$ are

$$\tilde{s}_{ak} = \tilde{b}\ \tilde{f}(kT_s - \tau')e^{j\omega_{D_a}kT_s} \qquad k=0,1,\ldots,\ N-1 \tag{5.22}$$

where τ' is the delay discrepancy $\tau_a - \tau_H$.

For the parameter estimation problem, the likelihood function is the same as the likelihood ratio. At first we assume $\tilde{b}$ given, so the likelihood function is

$$\ell_R(\tilde{\mathbf{R}}|\tilde{b}) = \frac{1}{N_0}\frac{\bar{E}_r}{N_0+\bar{E}_r}\Big|\sum_{k=-\infty}^{+\infty}\tilde{R}_k\,\tilde{f}^*(kT_s)e^{-j\omega_{D_H}kT_s}\Big|^2$$

$$= \frac{1}{N_0}\frac{\bar{E}_r}{N_0+\bar{E}_r}\Big|\sum_{k=-\infty}^{+\infty}(\tilde{b}\,\tilde{f}(kT_s-\tau')e^{j\omega_{D_a}kT_s}+\tilde{n}_k)\,\tilde{f}^*(kT_s)e^{-j\omega_{D_H}kT_s}\Big|^2$$

$$= \frac{1}{N_0}\frac{\bar{E}_r}{N_0+\bar{E}_r}\Big|\sum_{k=-\infty}^{\infty}(\tilde{b}\,\tilde{f}(kT_s-\tau')\,e^{j\omega'_D kT_s} + \tilde{n}_k e^{-j\omega_{D_H}kT_s})\,\tilde{f}^*(kT_s)\Big|^2 \tag{5.23}$$

Here, ω'_D is the Doppler shift discrepancy $\omega_{D_a} - \omega_{D_H}$.

Averaging over the distribution of $\tilde{b}$ yields the likelihood function as a function of only the parameters τ' and ω'_D:

$$\ell_R = \int_{-\infty}^{+\infty}\ell_R(\tilde{\mathbf{R}}|\tilde{b})f_{\tilde{b}}(\tilde{b})d\tilde{b} \tag{5.24}$$

where $f_{\tilde{b}}(\tilde{b})$ is the density function for $\tilde{b}$. We can write

$$\ell_R = \frac{1}{N_0}\frac{\bar{E}_r}{N_0+\bar{E}_r}\int_{-\infty}^{+\infty}\Big|\sum_{k=-\infty}^{+\infty}\tilde{b}\,\tilde{f}(kT_s-\tau')e^{j\omega'_D kT_s}\,\tilde{f}^*(kT_s)\Big|^2 f_{\tilde{b}}(\tilde{b})\,d\tilde{b}$$

+ (noise x noise term) + (noise x signal terms)

$$= \frac{2\sigma_b^2 \bar{E}_r}{N_0(N_0+\bar{E}_r)} \left| \sum_{k=-\infty}^{+\infty} \tilde{f}(kT_s-\tau')\tilde{f}^*(kT_s)e^{j\omega_D' kT_s} \right|^2$$

+ other terms involving $\tilde{n}_k$. (5.25)

The point in the τ', ω_D' plane for which ℓ_R is maximum represents the maximum likelihood estimate of the pair (τ', ω_D') for a given pair of values (τ_H, ω_{D_H}).

The continuous time, continuous frequency ambiguity function of the discrete signal is proportional to the noiseless part of the likelihood function ℓ_R and is given by

$$\Theta_d(\tau',\omega_D') = \left| \sum_{k=-\infty}^{+\infty} \tilde{f}(kT_s-\tau')\tilde{f}^*(kT_s)e^{j\omega_D' kT_s} \right|^2. \quad (5.26)$$

5.3 Relationships Between the Continuous Ambiguity Function of the Discrete Signal and the Continuous Ambiguity Function of the Continuous Signal

We compare now the AF (ambiguity function) of the discrete signal, obtained in the preceeding Section, Eq. (5.26), with the AF of the continuous signal as presented in Sec. 2.3., Eq. (2.48)

$$\Theta(\tau',\omega_D') = \left| \int_{-\infty}^{+\infty} \tilde{f}(t-\tau')\tilde{f}^*(t)e^{j\omega_D' t}\, dt \right|^2. \quad (5.27)$$

Let $\phi_d(\tau', \omega_D')$ denote the time-frequency correlation of the discrete signal,

$$\phi_d(\tau',\omega_D') = \sum_{k=-\infty}^{+\infty} \tilde{f}(kT_s-\tau')\tilde{f}^*(kT_s)e^{j(\omega_D')kT_s} \quad (5.28)$$

so that

$$\Theta_d(\tau',\omega_D') = |\phi_d(\tau',\omega_D')|^2 . \tag{5.29}$$

Similarly, let $\phi(\tau',\omega_D')$ be the time-frequency correlation of the continuous signal $\tilde{f}$,

$$\phi(\tau',\omega_D') = \int_{-\infty}^{+\infty} \tilde{f}(t-\tau')\tilde{f}^*(t)e^{j\omega_D' t}\, dt$$

so that

$$\Theta(\tau',\omega_D') = |\phi(\tau',\omega_D')|^2.$$

We can express $\phi_d(\tau',\omega_D')$ as follows:

$$\phi_d(\tau',\omega_D') = \sum_{k=-\infty}^{+\infty} \int_{-\infty}^{+\infty} \tilde{f}(t-\tau')\tilde{f}^*(t)e^{j(\omega_D')t}\, \delta(t-kT_s)dt$$

$$= \int_{-\infty}^{+\infty} \tilde{f}(t-\tau')\tilde{f}^*(t)e^{j\omega_D' t} \sum_{k=-\infty}^{+\infty} \delta(t-kT_s)\, dt.$$

Using Poisson's sum formula, the sum of impulses can be written as [7]

$$\sum_{k=-\infty}^{+\infty} \delta(t-kT_s) = \frac{1}{T_s} \sum_{p=-\infty}^{+\infty} e^{-j2\pi \frac{p}{T_s} t}. \tag{5.30}$$

This results in

$$\begin{aligned} \phi_d(\tau',\omega_D') &= \frac{1}{T_s} \sum_{p=-\infty}^{+\infty} \int_{-\infty}^{+\infty} \tilde{f}(t-\tau')\tilde{f}^*(t)e^{+j\omega_D' t - j\frac{2\pi p}{T_s} t}\, dt \\ &= \frac{1}{T_s} \sum_{p=-\infty}^{+\infty} \phi(\tau',\omega_D' - \frac{2\pi p}{T_s}). \end{aligned} \tag{5.31}$$

Finally,

$$\Theta_d(\tau',\omega_D') = |\phi_d(\tau',\omega_D')|^2 = |\frac{1}{T_s}\sum_{p=-\infty}^{+\infty}\phi(\tau',\omega_D'-\frac{2\pi p}{T_s})|^2$$

$$= \frac{1}{T_s^2}\sum_{p=-\infty}^{+\infty}\sum_{k=-\infty}^{+\infty}\phi(\tau',\omega_D'-\frac{2\pi p}{T_s})\phi^*(\tau',\omega_D'-\frac{2\pi k}{T_s})$$

$$= \frac{1}{T_s^2}\sum_{p=-\infty}^{+\infty}\Theta(\tau',\omega_D'-\frac{2\pi p}{T_s})$$

$$+ \frac{1}{T_s^2}\sum_{p=-\infty}^{+\infty}\sum_{\substack{k=-\infty \\ k\neq p}}^{+\infty}\phi(\tau',\omega_D'-\frac{2\pi p}{T_s})\phi^*(\tau',\omega_D'-\frac{2\pi k}{T_s}) . \qquad (5.32)$$

The above relationship shows that the AF of the discrete signal consists of the AF of the continuous signal repeated in frequency every $\frac{1}{T_s}$ Hertz, and some other terms due to the overlapping of $\phi(\tau',\omega_D'-\frac{2\pi p}{T_s})$ and $\phi^*(\tau',\omega_D'-\frac{2\pi k}{T_s})$, $k\neq p$. When T_s is chosen properly so that aliasing due to overlapping does not occur, the above result reduces to

$$\Theta_d(\tau',\omega_D') \approx \frac{1}{T_s^2}\sum_{p=-\infty}^{+\infty}\Theta(\tau',\omega_D'-\frac{2\pi p}{T_s}). \qquad (5.33)$$

Thus, we have the relationship between the AF of the discrete signal and the continuous signal.

6 DISCRETE-TIME DISCRETE-FREQUENCY AMBIGUITY FUNCTION OF A TIME SAMPLED SIGNAL

In this chapter we seek an expression for the discrete-time discrete-frequency ambiguity function of a sampled signal. We begin by considering a signal that is sampled both in time and frequency.

6.1 Expression for a Signal Sampled in Both Time and Frequency

Consider a signal $\tilde{s}(t)$ that is nonzero only on the interval $[0,T_f]$. A signal $\tilde{s}_e(t)$ that is time limited to interval $[0,T_d]$ can be obtained from $\tilde{s}(t)$ in the following manner:

$$\tilde{s}_e(t) = \begin{cases} \tilde{s}(t) & 0 \le t \le T_d \\ 0 & \text{elsewhere} \end{cases} \tag{6.1}$$

where $T_d \le T_f$. We can write $\tilde{s}_e(t)$ as

$$\tilde{s}_e(t) = \tilde{s}(t).w_d(t) \tag{6.2}$$

where

$$w_d(t) = \begin{cases} 1 & 0 \le t \le T_d \\ 0 & \text{elsewhere.} \end{cases} \tag{6.3}$$

A periodic version of $\tilde{s}_e(t)$ is now created by replicating $\tilde{s}_e(t)$ every $1/\lambda$ seconds where the spacing between the replications is required to be greater than or equal to T_d. This can be done by convolving $\tilde{s}_e(t)$ with a periodic impulse train, as shown below,

$$\tilde{s}_p(t) = \tilde{s}_e(t) * \sum_{m=-\infty}^{+\infty} \delta(t-\tfrac{m}{\lambda}). \tag{6.4}$$

Notice that

$$\tilde{s}_e(t) = \begin{cases} \tilde{s}_p(t) & 0 \le t \le T_d \\ 0 & \text{elsewhere.} \end{cases} \tag{6.5}$$

$\tilde{s}_e(t)$ is now sampled every T seconds to obtain $\hat{\tilde{s}}_e(t)$. Formally, this can be expressed as

$$\begin{aligned} \hat{\tilde{s}}_e(t) &= \tilde{s}_e(t) \sum_{k=-\infty}^{+\infty} \delta(t-kT) \\ &= \sum_{k=-\infty}^{+\infty} \tilde{s}_e(kT)\, \delta(t-kT). \end{aligned} \tag{6.6}$$

Assume $T_d = (N-1)T$. Note that $\tilde{s}_e(kT)$ is zero for $k < 0$ and $k > N-1$. A periodic version of $\hat{\tilde{s}}_e(t)$ is obtained by replicating $\hat{\tilde{s}}_e(t)$ every $\frac{1}{\lambda}$ seconds. This results in

$$\begin{aligned} \hat{\tilde{s}}_p(t) &= \hat{\tilde{s}}_e(t) * \sum_{m=-\infty}^{+\infty} \delta(t-\tfrac{m}{\lambda}) \\ &= \sum_{m=-\infty}^{+\infty} \hat{\tilde{s}}_e(t-\tfrac{m}{\lambda}) \\ &= \sum_{m=-\infty}^{+\infty} \sum_{k=0}^{N-1} \tilde{s}_e(kT)\, \delta(t-kT-\tfrac{m}{\lambda}). \end{aligned} \tag{6.7}$$

Note that $\hat{\tilde{s}}_p(t)$ is discrete in time. Because it is also periodic in time, its Fourier

transform is discrete in frequency. It is in this sense that $\hat{\tilde{s}}_p(t)$ represents a signal which is sampled in both time and frequency. Observe that the m=0 term in the expression for $\hat{\tilde{s}}_p(t)$ is equal to $\hat{\tilde{s}}_e(t)$. Since $\tilde{s}_e(t)$ is equal to $\tilde{s}_p(t)$ for $t \in [0, (N-1)T]$, $\hat{\tilde{s}}_p(t)$ can also be written as

$$\hat{\tilde{s}}_p(t) = \sum_{m=-\infty}^{+\infty} \sum_{k=0}^{N-1} \tilde{s}_p(kT)\, \delta(t-kT-\tfrac{m}{\lambda}). \tag{6.8}$$

The signals arising in the transformation from $\tilde{s}(t)$ to $\hat{\tilde{s}}_p(t)$ are illustrated in Fig. 6.1.

Assume that the spectrum of $\tilde{s}_e(t)$ is approximately bandlimited to the interval [-B,B], as shown in Fig. 6.2. Therefore, to prevent aliasing in frequency, the sampling interval T should be chosen such that

$$\frac{1}{T} \geq 2B \tag{6.9}$$

(i.e. the sampling rate should be greater than or equal to the Nyquist rate). In order to avoid aliasing in time, the sampling rate in frequency should be chosen such that

$$\frac{1}{\lambda} \geq T_d + \epsilon \tag{6.10}$$

where ϵ is a small non-negative constant added to prevent aliasing of the end points. Since $T_d = (N-1)T$, note that

$$\frac{1}{\lambda} \geq (N-1)T+\epsilon \tag{6.11}$$

or equivalently

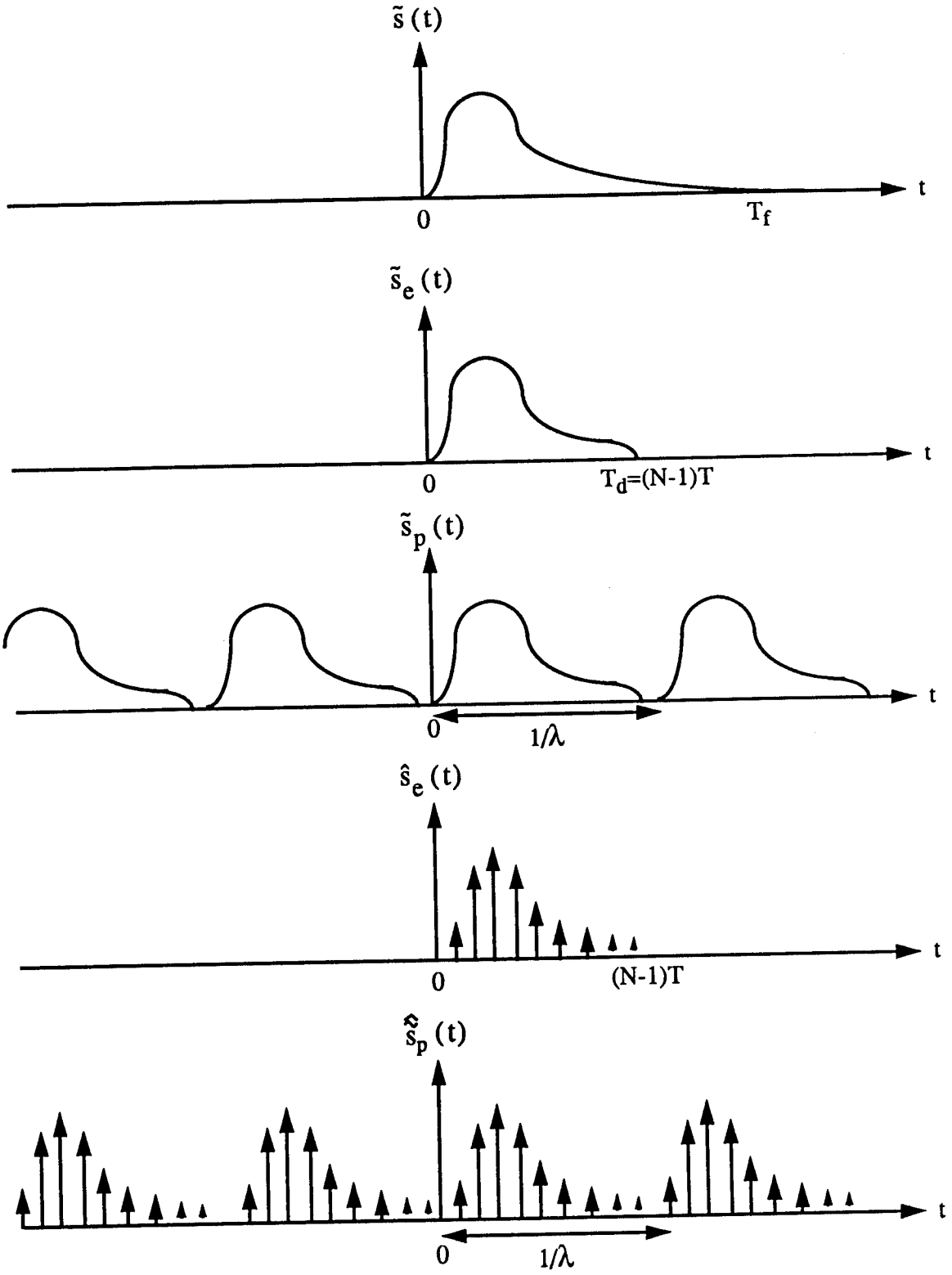

Figure 6.1 - Illustration of signals arising in the transformation from $\tilde{s}(t)$ to $\hat{\tilde{s}}_p(t)$.

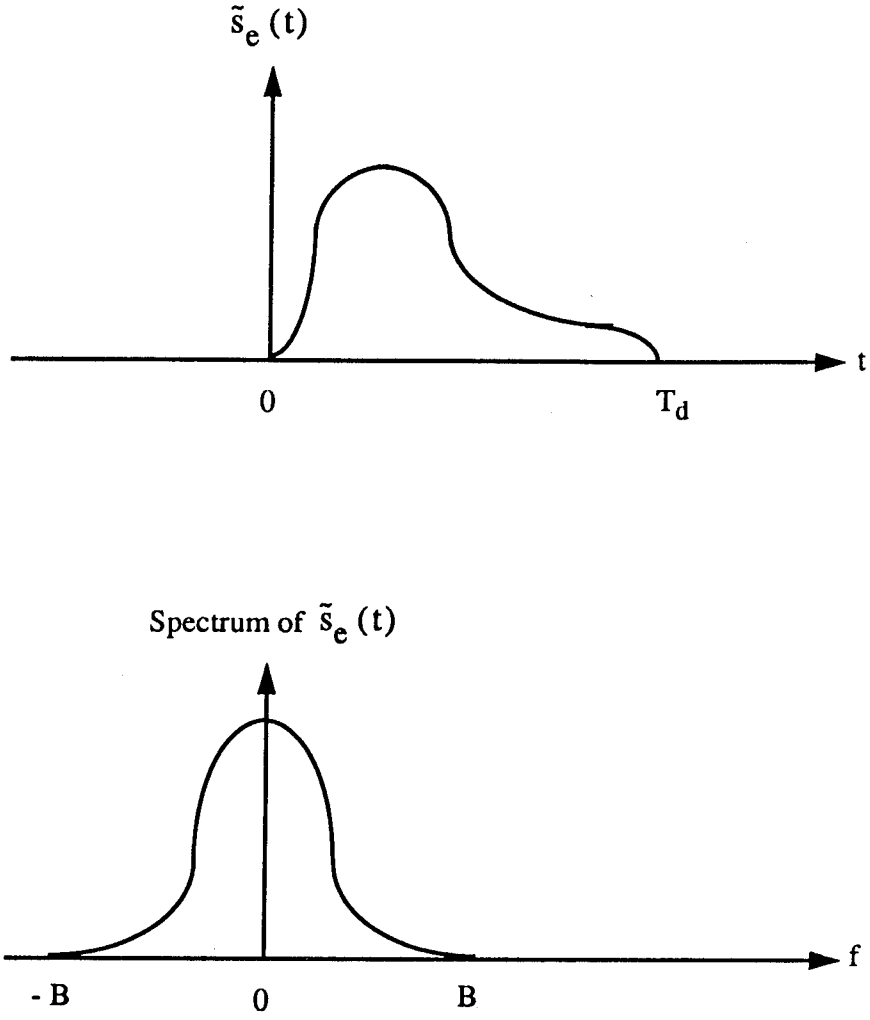

Figure 6.2 - Sketch of $\tilde{s}_e(t)$ and its spectrum.

$$\frac{1}{\lambda} \geq NT. \tag{6.12}$$

6.2 Discrete-time Discrete-frequency Ambiguity Function

The continuous time continuous frequency correlation function, whose magnitude squared is equal to the AF, is given by

$$\begin{aligned}\phi_{\tilde{f}}(\tau,f) &= \int_{-\infty}^{+\infty} \tilde{f}(t-\tau_a)\tilde{f}^*(t-\tau)e^{j2\pi(f_a-f)t}dt \\ &= \int_{-\infty}^{+\infty} \tilde{f}(t-\tau_a)e^{j2\pi f_a t}\tilde{f}^*(t-\tau)e^{-j2\pi ft}dt \end{aligned} \tag{6.13}$$

where the subscript $\tilde{f}$ denotes the fact that the time-frequency correlation is with respect to the signal $\tilde{f}(\cdot)$. Let

$$\tilde{g}(t) = \tilde{f}(t-\tau_a)e^{j2\pi f_a t}. \tag{6.14}$$

$\tilde{g}(t)$ is the desired target return at the input of the radar receiver with actual time delay τ_a and actual doppler frequency f_a. $\tilde{f}(t-\tau)e^{j2\pi ft}$ is the reference signal used by the matched filter in the receiver with reference time delay τ and reference Doppler frequency f. For convenience, the subscript H is not used in this analysis. As a function of $\tilde{g}(t)$, we can write

$$\phi_{\tilde{f}}(\tau,f) = \int_{-\infty}^{+\infty} \tilde{g}(t)\tilde{f}^*(t-\tau)e^{-j2\pi ft}dt. \tag{6.15}$$

This choice for representing $\phi_{\tilde{f}}(\cdot,\cdot)$ is meaningful in the sense that it involves the

correlation of the desired target return with the reference signal to obtain the time frequency correlation $\phi_F(\cdot,\cdot)$.

6.3 Sampling the signal in time and the signal spectrum in frequency

Now assume that discrete samples are present at the input of the receiver instead of a continuous waveform. Let the discrete samples be obtained by sampling a continuous waveform both in time and frequency. Following the same procedure as developed in the previous section, the versions of $\tilde{g}(t)$ and $\tilde{f}(t)$ that are sampled in both time and frequency are expressed as

$$\hat{\tilde{g}}_p(t) = \sum_{m=-\infty}^{+\infty} \sum_{k=-\infty}^{+\infty} \tilde{g}_e(kT)\ \delta(t-kT-\tfrac{m}{\lambda})$$

$$\hat{\tilde{f}}_p(t) = \sum_{n=-\infty}^{+\infty} \sum_{\ell=-\infty}^{+\infty} \tilde{f}_e(\ell T)\ \delta(t-\ell T-\tfrac{n}{\lambda}) \qquad (6.16)$$

where the sequences $\tilde{g}_e(kT)$ and $\tilde{f}_e(kT)$ have been limited to the intervals $[\gamma NT, (N-1)T + \gamma NT]$, γ an integer and $[0, (N-1)T]$, respectively. The time frequency correlation function involving $\hat{\tilde{g}}_p(t)$ and $\hat{\tilde{f}}_p(t)$ is given by

$$\phi_{\hat{f}_p}(\tau,f) = \int_{-\infty}^{+\infty} \hat{g}_p(t)\hat{f}_p^*(t-\tau)\, e^{-j2\pi ft}dt$$

$$= \int_{-\infty}^{+\infty} \sum_{m=-\infty}^{+\infty} \sum_{k=-\infty}^{+\infty} \tilde{g}_e(kT)\, \delta(t-kT-\tfrac{m}{\lambda})$$

$$\cdot \sum_{n=-\infty}^{+\infty} \sum_{\ell=-\infty}^{+\infty} \tilde{f}_e^*(\ell T)\, \delta(t-\tau-\ell T-\tfrac{n}{\lambda})\, e^{-j2\pi ft}dt. \qquad (6.17)$$

Let $p=k-\ell$ and $q=m-n$. Then, $\ell=k-p$ and $n=m-q$. Note that

$$\delta(t-kT-\tfrac{m}{\lambda})\, \delta(t-\tau-\ell T-\tfrac{n}{\lambda})$$

$$= \delta(t-kT-\tfrac{m}{\lambda})\, \delta(t-\tau-kT+pT-\tfrac{m}{\lambda}+\tfrac{q}{\lambda})$$

$$= \delta(t-kT-\tfrac{m}{\lambda})\, \delta([t-kT-\tfrac{m}{\lambda}]-[\tau-pT-\tfrac{q}{\lambda}]) \qquad (6.18)$$

$$= \delta(t-kT-\tfrac{m}{\lambda})\, \delta(\tau-pT-\tfrac{q}{\lambda}).$$

Therefore,

$$\phi_{\hat{f}_p}(\tau,f) = \sum_{m=-\infty}^{+\infty} \sum_{k=-\infty}^{+\infty} \cdot \sum_{q=-\infty}^{+\infty} \sum_{p=-\infty}^{+\infty} \tilde{g}_e(kT)\tilde{f}_e^*(kT-pT)$$

$$\int_{-\infty}^{+\infty} \delta(\tau-pT-\tfrac{q}{\lambda})\, \delta(t-kT-\tfrac{m}{\lambda})\, e^{-j2\pi ft}dt$$

$$= \sum_{m=-\infty}^{+\infty} \sum_{k=-\infty}^{+\infty} \sum_{q=-\infty}^{+\infty} \sum_{p=-\infty}^{+\infty} \tilde{g}_e(kT)\tilde{f}_e^*(kT-pT). \qquad (6.19)$$

$$\delta(\tau-pT-\tfrac{q}{\lambda})\, e^{-j2\pi f[kT+\frac{m}{\lambda}]}.$$

Poisson's sum formula states that

$$\sum_{m=-\infty}^{+\infty} e^{-j2\pi f\frac{m}{\lambda}} = \lambda \sum_{m=-\infty}^{+\infty} \delta(f-m\lambda). \tag{6.20}$$

Thus,

$$\phi_{\tilde{f}_p}(\tau,f) = \sum_{m=-\infty}^{+\infty}\sum_{k=-\infty}^{+\infty}\sum_{q=-\infty}^{+\infty}\sum_{p=--\infty}^{+\infty} \tilde{g}_e(kT)\,\tilde{f}_e^*(kT-pT)$$
$$\delta(\tau-pT-\tfrac{q}{\lambda})\;\lambda\;\delta(f-m\lambda)e^{-j2\pi fkT}. \tag{6.21}$$

Assume λ and T are chosen such that $\frac{1}{\lambda T} = L$ where L is an integer greater than (N-1).

Also, let $\nu = p+\frac{q}{\lambda T} = p+qL$. Note that υ is also an integer. As q ranges from $-\infty$ to $+\infty$, υ also varies between $-\infty$ and $+\infty$. Introducing the change of index, $p = \nu-\frac{q}{\lambda T}$, $\phi_{\tilde{f}_p}(\tau,f)$ can be expressed as

$$\phi_{\tilde{f}_p}(\tau,f) = \lambda \sum_{m=-\infty}^{+\infty}\sum_{k=-\infty}^{+\infty}\sum_{q=-\infty}^{+\infty}\sum_{\nu=-\infty}^{+\infty} \tilde{g}_e(kT)\,\tilde{f}_e^*(kT-\nu T+\tfrac{q}{\lambda})$$
$$\delta(\tau-\nu T)\;\delta(f-m\lambda)\;e^{-j2\pi m\lambda kT}. \tag{6.22}$$

By defining the discrete-time discrete-frequency correlation function of $\tilde{f}_p(t)$ as

$$\hat{\phi}_{\tilde{f}_p}(\nu,m)=\lambda \sum_{k=-\infty}^{+\infty}\sum_{q=-\infty}^{+\infty} \tilde{g}_e(kT)\tilde{f}_e^*(kT-\nu T+\tfrac{q}{\lambda})\;e^{-j2\pi m\lambda kT}, \tag{6.23}$$

the expression for $\phi_{\tilde{f}_p}(\tau,f)$ can be written as

$$\phi_{\hat{f}_p}(\tau,f) = \sum_{\nu=-\infty}^{+\infty} \sum_{m=-\infty}^{+\infty} \hat{\phi}_{\hat{f}_p}(\nu,m)\ \delta(\tau-\nu T)\ \delta(f-m\lambda). \tag{6.24}$$

Note that $\phi_{\hat{f}_p}(\tau,f)$ is periodic both in time and frequency.

Sampling only the signal in time

From the expression for $\hat{\tilde{g}}_p(t)$, observe that the m=0 term results in

$$\hat{\tilde{g}}_p(t)\Big|_{m=0} = \sum_{k=-\infty}^{+\infty} \tilde{g}_e(kT)\delta(t-kT) = \hat{\tilde{g}}_e(t). \tag{6.25}$$

Also, from the expression for $\hat{\tilde{f}}_p(t)$, observe that the n=0 term results in

$$\hat{\tilde{f}}_p(t)\Big|_{n=0} = \sum_{\ell=-\infty}^{+\infty} \tilde{f}_e(\ell T)\delta(t-\ell T) = \hat{\tilde{f}}_e(t). \tag{6.26}$$

Since q=m-n, m=n=0 implies q=0. Hence, when q=m=n=0,

$$\phi_{\hat{f}_p}(\tau,f)\Big|_{q=m=n=0} = \int_{-\infty}^{+\infty} \hat{\tilde{g}}_e(\tau)\ \hat{\tilde{f}}_e(t-\tau)e^{-j2\pi ft}dt \tag{6.27}$$

$$\Delta\ \phi_{\hat{f}_e}(\tau,f)\ .$$

By straight forward substitution of the expressions for $\hat{\tilde{g}}_e(t)$ and $\hat{\tilde{f}}_e(t-\tau)$, we obtain

$$\phi_{\hat{f}_e}(\tau,f) = \int_{-\infty}^{\infty} \sum_{k=-\infty}^{\infty} \tilde{g}_e(kT)\ \delta(\tau-kT) \sum_{\ell=-\infty}^{\infty} \tilde{f}_e(\ell T)\ \delta(t-\tau-\ell T)\ e^{-j2\pi ft}dt. \tag{6.28}$$

Let $\nu=k-\ell$. Then $\ell=k-\nu$. Observe that

$$\begin{aligned}\delta(t-kT)\ \delta(t-\tau-\ell T) &= \delta(t-kT)\ \delta(t-\tau-kT+\nu T)\\ &= \delta(t-kT)\ \delta[(t-kT)-(\tau-\nu T)]\\ &= \delta(t-kT)\ \delta(\tau-\nu T).\end{aligned} \tag{6.29}$$

It follows that

$$\begin{aligned}\phi_{\hat{f}_e}(\tau,f) &= \sum_{k=-\infty}^{\infty}\sum_{\nu=-\infty}^{\infty} \tilde{g}_e(kT)\ \tilde{f}_e^*(kT-\nu T)\\ &\quad \int_{-\infty}^{\infty} \delta(t-kT)\ \delta(\tau-\nu T)\ e^{-j2\pi ft}dt\\ &= \sum_{k=-\infty}^{\infty}\sum_{\nu=-\infty}^{\infty} \tilde{g}_e(kT)\ \tilde{f}_e^*(kT-\nu T)\ \delta(\tau-\nu T)\ e^{-j2\pi fkT}\ .\end{aligned} \tag{6.30}$$

Note that $\phi_{\hat{f}_e}(\tau,f)$ is sampled in the delay variable τ since the correlation function is nonzero only for $\tau = \nu T$ where ν is an integer.

Although $\phi_{\hat{f}_e}(\tau,f)$ is a continuous function of the frequency variable f, in practice the correlation function will be evaluated only at frequencies spaced λ Hertz apart. In effect, $\phi_{\hat{f}_e}(\tau,t)$ is sampled in frequency as well. Analytically this is accomplished by multiplying $\phi_{\hat{f}_e}(\tau,f)$ with

$$\mathrm{comb}_{\lambda}(f) = \lambda \sum_{m=-\infty}^{\infty} \delta(f-m\lambda). \tag{6.31}$$

This yields

$$\phi_{\hat{f}_e}(\tau,f)\ \mathrm{comb}_{\lambda}(f) = \lambda \sum_{k=-\infty}^{\infty} \sum_{\nu=-\infty}^{\infty} \sum_{m=-\infty}^{\infty} \tilde{g}_e(kT)\ \tilde{f}_e^{*}(kT-\nu T)\ e^{-j2\pi fkT}\ \delta(\tau-\nu T)\ \delta(f-m\lambda)$$

$$= \lambda \sum_{k=-\infty}^{\infty} \sum_{\nu=-\infty}^{\infty} \sum_{m=-\infty}^{\infty} \tilde{g}_e(kT)\ \tilde{f}_e^{*}(kT-\nu T)\ e^{-j2\pi m\lambda kT}\ \delta(\tau-\nu T)\ \delta(f-m\lambda)\ . \tag{6.32}$$

The discrete-time discrete-frequency correlation function is defined to be

$$\hat{\phi}_{\hat{f}_e}(\nu,m) = \lambda \sum_{k=-\infty}^{\infty} \tilde{g}_e(kT)\ \tilde{f}_e^{*}(kT-\nu T)\ e^{-j2\pi m\lambda kT}\ . \tag{6.33}$$

Then

$$\phi_{\hat{f}_e}\ \mathrm{comb}_{\lambda}(f) = \sum_{\nu=-\infty}^{\infty} \sum_{m=-\infty}^{\infty} \hat{\phi}_{\hat{f}_e}(\nu,m)\ \delta(\tau-\nu T)\ \delta(f-m\lambda)\ . \tag{6.34}$$

Recall that

$$\tilde{g}_e(kT) = \tilde{f}_e(kT-\tau_s)\ e^{j2\pi f_s kT}\ . \tag{6.35}$$

If λ is viewed as the frequency spacing in the DFT for $\hat{\tilde{f}}_e(t)$, then $\lambda = \frac{1}{NT}$.

Consequently, the discrete-time discrete-frequency correlation function for the time sampled signal $\hat{\tilde{f}}_e(t)$ becomes

$$\hat{\phi}_{\tilde{f}_e}(\nu,m) = \frac{1}{NT} \sum_{k=-\infty}^{\infty} \tilde{f}_e(kT-\tau_a)\, \tilde{f}_e^*(kT-\nu T)\, e^{-j2\pi(\frac{m}{NT}-f_a)kT} \quad . \tag{6.36}$$

This is the form we will use for the discrete-time discrete-frequency correlation function of the truncated, time sampled signal, $\tilde{f}_e(t)$. By definition, the corresponding discrete-time discrete-frequency ambiguity function is

$$\hat{\theta}_{\tilde{f}_e}(\nu,m) = |\hat{\phi}_{\tilde{f}_e}(\nu,m)|^2 \quad . \tag{6.37}$$

Thus, we have the desired expression for the time sampled signal.

7 LINK BETWEEN THE DISCRETE-TIME DISCRETE-FREQUENCY AMBIGUITY FUNCTION AND THE CONTINUOUS-TIME CONTINUOUS-FREQUENCY AMBIGUITY FUNCTION

In this chapter, we are interested in finding the relationship between the discrete-time discrete-frequency correlation function $\hat{\phi}_{\hat{f}_p}(\nu, m)$ and the continuous-time continuous-frequency correlation function $\phi_{\tilde{f}_e}(\tau, f)$.

7.1 Sampling the Signal in Time and the Signal Spectrum in Frequency

By definition, the signal $\tilde{f}_e(t)$ is nonzero only over the interval [0, (N-1)T]. The periodic signal $\tilde{f}_p(t)$ is formed by replicating $\tilde{f}_e(t)$ every $\frac{1}{\lambda}$ seconds. Specifically,

$$\tilde{f}_p(t) = \tilde{f}_e(t) * \mathrm{comb}_{\frac{1}{\lambda}}(t) \tag{7.1}$$

where

$$\mathrm{comb}_{\frac{1}{\lambda}}(t) = \sum_{\ell=-\infty}^{+\infty} \delta(t-\tfrac{\ell}{\lambda}). \tag{7.2}$$

$\hat{\tilde{f}}_p(t)$ is obtained by sampling $\tilde{f}_p(t)$ every T seconds. In particular,

$$\hat{\tilde{f}}_p(t) = \tilde{f}_p(t) \cdot \mathrm{comb}_T(t) \tag{7.3}$$

where

$$\mathrm{comb}_T(t) = \sum_{k=-\infty}^{+\infty} \delta(t-kT). \tag{7.4}$$

By definition, the time-frequency correlation function between the signals $\tilde{f}(t)$ and $\tilde{g}(t)$ is

$$\phi_{\tilde{g},\tilde{f}}(\tau,f) = \int_{-\infty}^{+\infty} \tilde{g}(t)\, \tilde{f}^{*}(t-\tau)\, e^{-j2\pi ft} dt. \tag{7.5}$$

When $\tilde{g}(t) = \tilde{f}(t-\tau_a)\, e^{j2\pi f_a t}$, $\phi_{\tilde{g},\tilde{f}}(\tau,f)$ is only a function of $\tilde{f}(t)$. Hence, we replace the subscript $\tilde{g},\tilde{f}$ by $\tilde{f}$ and write

$$\phi_{\tilde{f}}(\tau,f) = \int_{-\infty}^{+\infty} \tilde{g}(t)\, \tilde{f}^{*}(t-\tau)\, e^{-j2\pi ft} dt. \tag{7.6}$$

Consider now the time-frequency correlation function given by

$$\phi_{\tilde{f}_e}(\tau,f) = \int_{-\infty}^{+\infty} \tilde{g}_e(t)\, \tilde{f}_e^{*}(t-\tau)\, e^{-j2\pi ft} dt. \tag{7.7}$$

The following properties hold. These are derived in Appendix A.

1. $$\phi_{\tilde{f}_p}(\tau,x) = \phi_{\tilde{f}_p,\tilde{g}_p}(\tau,x) = \int_{-\infty}^{+\infty} \phi_{\tilde{f}_e,\tilde{g}_e}(\beta,x)\phi_{\mathrm{comb}_{\frac{1}{\lambda}},\mathrm{comb}_{\frac{1}{\lambda}}}(\tau-\beta,x)\, d\beta$$
$$= \int_{-\infty}^{+\infty} \phi_{\tilde{f}_e}(\beta,x)\phi_{\mathrm{comb}_{\frac{1}{\lambda}},\mathrm{comb}_{\frac{1}{\lambda}}}(\tau-\beta,x)\, d\beta \tag{7.8}$$

$$2.\quad \phi_{\hat{f}_p}(\tau,f) = \phi_{\hat{f}_p,\hat{g}_p}(\tau,f) = \int_{-\infty}^{+\infty} \phi_{\tilde{f}_p,\tilde{g}_p}(\tau,x)\phi_{comb_T,comb_T}(\tau,f-x)\,dx \tag{7.9}$$

$$= \int_{-\infty}^{+\infty} \phi_{\tilde{f}_p}(\tau,x)\phi_{comb_T,comb_T}(\tau,f-x)dx$$

where $$\tilde{g}_p(t) = \tilde{g}_e(t) * comb_{\frac{1}{\lambda}}(t) \tag{7.10}$$

and $$\hat{\tilde{g}}_p(t) = \tilde{g}_p(t)\ .\ comb_T(t). \tag{7.11}$$

We see, therefore, that

$$\phi_{\tilde{f}_p}(\tau,f) = \int_{-\infty}^{+\infty}\int \phi_{\tilde{f}_e}(\beta,x)\ \phi_{comb_{\frac{1}{\lambda}},comb_{\frac{1}{\lambda}}}(\tau-\beta,x)\ \phi_{comb_T,comb_T}(\tau,f-x)\,d\beta\,dx \tag{7.12}$$

where

$$\phi_{comb_T,comb_T}(\tau,f-x) = \int_{-\infty}^{+\infty} \sum_{k=-\infty}^{+\infty} \delta(t-kT) \sum_{\ell=-\infty}^{+\infty} \delta(t-\tau-\ell T)\ e^{-j2\pi(f-x)t}dt$$

$$= \sum_{k=-\infty}^{+\infty} \sum_{\ell=-\infty}^{+\infty} \int_{-\infty}^{+\infty} \delta(t-kT)\ \delta(t-\tau-\ell T)\ e^{-j2\pi(f-x)t}dt \tag{7.13}$$

and

$$\phi_{\mathrm{comb}_{\frac{1}{\lambda}},\mathrm{comb}_{\frac{1}{\lambda}}}(\tau-\beta,x) = \int_{-\infty}^{+\infty} \sum_{\ell=-\infty}^{+\infty} \delta(t-\tfrac{\ell}{\lambda}) \sum_{k=-\infty}^{+\infty} \delta(t-\tau+\beta-\tfrac{k}{\lambda})\, e^{-j2\pi xt} dt$$

$$= \sum_{\ell=-\infty}^{+\infty} \sum_{k=-\infty}^{+\infty} \int_{-\infty}^{+\infty} \delta(t-\tfrac{\ell}{\lambda})\, \delta[t-(\tau-\beta)-\tfrac{k}{\lambda}]\, e^{-j2\pi xt} dt. \qquad (7.14)$$

Let $m=k-\ell$. Then $\ell=k-m$ and

$$\phi_{\mathrm{comb}_T,\mathrm{comb}_T}(\tau,f-x) = \sum_{k=-\infty}^{+\infty} \sum_{m=-\infty}^{+\infty} \int_{-\infty}^{+\infty} \delta(t-kT)\, \delta(t-\tau-kT+mT)\, e^{-j2\pi(f-x)t} dt$$

$$= \sum_{k=-\infty}^{+\infty} \sum_{m=-\infty}^{+\infty} \int_{-\infty}^{+\infty} \delta(t-kT)\, \delta(\tau-mT)\, e^{-j2\pi(f-x)t} dt$$

$$= \sum_{k=-\infty}^{+\infty} \sum_{m=-\infty}^{+\infty} \delta(\tau-mT)\, e^{-j2\pi(f-x)kT}. \qquad (7.15)$$

Using the Poisson sum formula,

$$\sum_{m=-\infty}^{+\infty} \delta(\tau-mT) = \frac{1}{T} \sum_{m=-\infty}^{+\infty} e^{-j2\pi\frac{m}{T}\tau}. \qquad (7.16)$$

Therefore, the expression for $\phi_{\mathrm{comb}_T,\mathrm{comb}_T}(\cdot,\cdot)$ becomes

$$\phi_{\mathrm{comb}_T,\mathrm{comb}_T}(\tau,f-x) = \frac{1}{T} \sum_{k=-\infty}^{+\infty} \sum_{m=-\infty}^{+\infty} e^{-j2\pi(f-x)kT}\, e^{-j2\pi\frac{m}{T}\tau}. \qquad (7.17)$$

Following a similar procedure on the expression for $\phi_{\mathrm{comb}_{\frac{1}{\lambda}},\mathrm{comb}_{\frac{1}{\lambda}}}(\tau-\beta,x)$ we obtain

$$\phi_{\mathrm{comb}_{\frac{1}{\lambda}},\mathrm{comb}_{\frac{1}{\lambda}}}(\tau-\beta,x) = \lambda \sum_{\ell=-\infty}^{+\infty} \sum_{n=-\infty}^{+\infty} e^{-j2\pi x\frac{\ell}{\lambda}}\, e^{-j2\pi n\lambda(\tau-\beta)}. \qquad (7.18)$$

Substituting the simplified expressions for $\phi_{comb_{\frac{1}{\lambda}},comb_{\frac{1}{\lambda}}}(\tau-\beta,x)$ and $\phi_{comb_T,comb_T}(\tau,f-x)$

into that for $\phi_{i_p}(\tau,f)$, we get

$$\phi_{i_p}(\tau,f) = \int\int_{-\infty}^{+\infty} \phi_{i_e}(\beta,x) \cdot \frac{\lambda}{T}$$

$$\cdot \sum_{\ell=-\infty}^{+\infty} \sum_{n=-\infty}^{+\infty} e^{-j2\pi x\frac{\ell}{\lambda}} e^{-j2\pi n\lambda(\tau-\beta)}$$

$$\cdot \sum_{k=-\infty}^{+\infty} \sum_{m=-\infty}^{+\infty} e^{-j2\pi(f-x)kT} e^{-j2\pi\frac{m}{T}\tau} d\beta\, dx. \qquad (7.19)$$

From Poisson's sum formula, note that

$$\sum_{k=-\infty}^{\infty} e^{-j2\pi(f-x)kT} = \frac{1}{T} \sum_{k=-\infty}^{\infty} \delta\left(f-x-\frac{k}{T}\right) \qquad (7.20)$$

and

$$\sum_{n=-\infty}^{\infty} e^{-j2\pi(\tau-\beta)n\lambda} = \frac{1}{\lambda} \sum_{n=-\infty}^{\infty} \delta\left(\tau-\beta-\frac{n}{\lambda}\right). \qquad (7.21)$$

Hence,

$$\phi_{\tilde{f}_p}(\tau,f) = \int\int_{-\infty}^{\infty} \phi_{\tilde{f}_e}(\beta,x) \cdot \frac{\lambda}{T} \cdot \frac{1}{T} \cdot \frac{1}{\lambda} \cdot$$

$$\sum_{\ell=-\infty}^{\infty} \sum_{n=-\infty}^{\infty} e^{-j2\pi x\frac{\ell}{\lambda}} \delta(\tau-\beta-\frac{n}{\lambda}).$$

$$\sum_{k=-\infty}^{\infty} \sum_{m=-\infty}^{\infty} \delta(f-x-\frac{k}{T}) e^{-j2\pi\frac{m}{T}\tau} \, d\beta \, dx$$

$$= \frac{1}{T^2} \sum_{\ell=-\infty}^{\infty} \sum_{n=-\infty}^{\infty} \sum_{k=-\infty}^{\infty} \sum_{m=-\infty}^{\infty} e^{-j2\pi\frac{m}{T}\tau}.$$

$$\int\int_{-\infty}^{\infty} \phi_{\tilde{f}_e}(\beta,x) \, e^{-j2\pi x\frac{\ell}{\lambda}} \, \delta(\tau-\beta-\frac{n}{\lambda}) \, \delta(f-x-\frac{k}{T}) \, d\beta \, dx$$

$$= \frac{1}{T^2} \sum_{\ell=-\infty}^{\infty} \sum_{n=-\infty}^{\infty} \sum_{k=-\infty}^{\infty} \sum_{m=-\infty}^{\infty} e^{-j2\pi\frac{m}{T}\tau}$$

$$\phi_{\tilde{f}_i}(\tau-\frac{n}{\lambda},f-\frac{k}{T}) \, e^{-j2\pi(f-\frac{k}{T})\frac{\ell}{\lambda}}. \qquad (7.22)$$

Recall that λ is chosen such that $\lambda = 1/LT$, where L is an integer greater than N-1. Then

$$e^{j2\pi\frac{k}{T}\frac{\ell}{\lambda}} = e^{j2\pi\frac{k}{T}\ell LT} = 1. \qquad (7.23)$$

The expression for $\phi_{\tilde{f}_p}(\tau,f)$ is simplified further by again recognizing from Poisson's sum formula that

$$\sum_{m=-\infty}^{\infty} e^{-j2\pi\frac{m}{T}\tau} = T \sum_{m=-\infty}^{\infty} \delta(\tau-mT) \qquad (7.24)$$

and

$$\sum_{\ell=-\infty}^{\infty} e^{-j2\pi f\frac{\ell}{\lambda}} = \lambda \sum_{\ell=-\infty}^{\infty} \delta(f-\ell\lambda). \tag{7.25}$$

It follows that

$$\phi_{\hat{f}_p}(\tau,f) = \frac{1}{T^2} \cdot \lambda \cdot T \cdot \sum_{\ell=-\infty}^{\infty} \sum_{n=-\infty}^{\infty} \sum_{k=-\infty}^{\infty} \sum_{m=-\infty}^{\infty} \phi_{\tilde{f}_e}(\tau-\frac{n}{\lambda},f-\frac{k}{T})$$

$$\delta(\tau-mT)\ \delta(f-\ell\lambda)$$

$$= \frac{\lambda}{T} \sum_{\ell=-\infty}^{\infty} \sum_{n=-\infty}^{\infty} \sum_{k=-\infty}^{\infty} \sum_{m=-\infty}^{\infty} \phi_{\tilde{f}_e}(mT-\frac{n}{\lambda},\ell\lambda-\frac{k}{T})$$

$$\delta(\tau-nT)\ \delta(f-\ell\lambda)$$

$$= \frac{1}{T} \sum_{m=-\infty}^{\infty} \sum_{\ell=-\infty}^{\infty} \left\{\lambda \sum_{k=-\infty}^{\infty} \sum_{n=-\infty}^{\infty} \phi_{\tilde{f}_e}(mT-\frac{n}{\lambda},\ \ell\lambda-\frac{k}{T})\right\} \tag{7.26}$$

$$\delta(\tau-mT)\ \delta(f-\ell\lambda).$$

Let λ be the spacing between two successive frequency components of the N-point DFT for $\tilde{f}_e$. Then

$$\lambda = \frac{1}{NT}. \tag{7.27}$$

This implies that L = N. Observe that this value for L is greater than (N-1), as required to prevent aliasing in the time domain. Hence,

$$\phi_{\hat{\tilde{f}}_p}(\tau,f) = \frac{1}{T} \sum_{m=-\infty}^{\infty} \sum_{\ell=-\infty}^{\infty} \left\{ \frac{1}{NT} \sum_{k=-\infty}^{\infty} \sum_{n=-\infty}^{\infty} \phi_{\tilde{f}_e}([m-nN]T, [\ell-kN]\frac{1}{NT}) \right\}$$

$$\delta(\tau-mT)\ \delta(f-\frac{\ell}{NT}). \qquad (7.28)$$

$\phi_{\hat{\tilde{f}}_p}(\tau,f)$ can also be written as

$$\phi_{\hat{\tilde{f}}_p}(\tau,f) = \frac{1}{T} \sum_{m=-\infty}^{+\infty} \sum_{\ell=-\infty}^{+\infty} \hat{\phi}_{\hat{\tilde{f}}_p}(m,\ell)\ \delta(\tau-mT)\ \delta(f-\frac{\ell}{NT}) \qquad (7.29)$$

where

$$\hat{\phi}_{\hat{\tilde{f}}_p}(m,\ell) = \frac{1}{NT} \sum_{n=-\infty}^{+\infty} \sum_{k=-\infty}^{+\infty} \phi_{\tilde{f}_e}([m-nN]T, [\ell-kN]\frac{1}{NT}). \qquad (7.30)$$

$\hat{\phi}_{\hat{\tilde{f}}_p}(m,\ell)$, the discrete-time discrete-frequency correlation function of the discrete periodic signal $\hat{\tilde{f}}_p$, is a repetition every $\frac{1}{\lambda}$ = NT seconds in time and $\frac{1}{T}$ Hertz in frequency of the continuous-time continuous-frequency correlation function for the continuous time limited signal $\tilde{f}_e(t)$.

7.2 Sampling the Signal in Time and the Correlation Function in Frequency

Equation (7.30) expresses the relationship between the continuous-time continuous-frequency autocorrelation function $\phi_{\tilde{f}_e}(\cdot,\cdot)$ and the discrete-time discrete-frequency autocorrelation function $\hat{\phi}_{\hat{\tilde{f}}_p}(\cdot,\cdot)$. Recall that the signal $\hat{\tilde{f}}_p(t)$ is sampled in

time every T seconds while the spectrum of $\hat{\tilde{f}}_p(t)$ is sampled in frequency every λ Hertz where $\lambda = \frac{1}{NT}$.

In a similar manner, we now find the expression of the discrete-time discrete-frequency autocorrelation function $\hat{\phi}_{\hat{f}_e}(\cdot,\cdot)$ of the signal $\hat{\tilde{f}}_e(t)$ which is sampled only in time every T seconds. Consider the time-limited signal $\tilde{f}_e(t)$. $\hat{\tilde{f}}_e(t)$ is obtained by sampling $\tilde{f}_e(t)$ every T seconds. In particular,

$$\hat{\tilde{f}}_e(t) = \tilde{f}_e(t) \cdot comb_T(t) \tag{7.31}$$

where

$$comb_T(t) = \sum_{k=-\infty}^{+\infty} \delta(t-kT). \tag{7.32}$$

Using properties developed in Appendix A,

$$\phi_{\hat{f}_e}(\tau,f) = \int_{-\infty}^{+\infty} \phi_{f_e}(\tau,x)\ \phi_{comb_T,comb_T}(\tau,f-x)\ dx \tag{7.33}$$

where, as shown in the previous section,

$$\phi_{comb_T,comb_T}(\tau,f-x) = \frac{1}{T} \sum_{k=-\infty}^{+\infty} \sum_{m=-\infty}^{+\infty} e^{-j2\pi(f-x)kT} e^{-j2\pi\frac{m}{T}\tau}. \tag{7.34}$$

Substituting the expression for $\phi_{comb_T,comb_T}(\tau,f-x)$ into that for $\phi_{\tilde{f}_e}(\tau,f)$, we get

$$\phi_{\tilde{f}_e}(\tau,f) = \int_{-\infty}^{+\infty} \phi_{\tilde{f}_e}(\tau,x) \frac{1}{T} \sum_{k=-\infty}^{+\infty} \sum_{m=-\infty}^{+\infty} e^{-j2\pi(f-x)kT} e^{-j2\pi\frac{m}{T}\tau} dx. \tag{7.35}$$

From Poisson's sum formula, note that

$$\sum_{k=-\infty}^{+\infty} e^{-j2\pi(f-x)kT} = \frac{1}{T} \sum_{k=-\infty}^{+\infty} \delta(f-x-\frac{k}{T}). \tag{7.36}$$

Hence,

$$\phi_{\tilde{f}_e}(\tau,f) = \int_{-\infty}^{\infty} \phi_{\tilde{f}_e}(\tau,x) \frac{1}{T^2} \sum_{k=-\infty}^{+\infty} \sum_{m=-\infty}^{+\infty} e^{-j2\pi\frac{m}{T}\tau} \delta(f-x-\frac{k}{T}) dx$$

$$= \frac{1}{T^2} \sum_{k=-\infty}^{+\infty} \sum_{m=-\infty}^{+\infty} \phi_{\tilde{f}_e}(\tau,f-\frac{k}{T}) e^{-j2\pi\frac{m}{T}\tau}. \tag{7.37}$$

This expression can be simplified further by recognizing from Poisson's sum formula that

$$\sum_{m=-\infty}^{+\infty} e^{-j2\pi\frac{m}{T}\tau} = T \sum_{m=-\infty}^{+\infty} \delta(\tau-mT). \tag{7.38}$$

It follows that

$$\phi_{\hat{f}_e}(\tau,f) = \frac{1}{T} \sum_{k=-\infty}^{+\infty} \sum_{m=-\infty}^{+\infty} \phi_{\tilde{f}_e}(\tau, f-\frac{k}{T})\ \delta(\tau - mT)$$

$$= \frac{1}{T} \sum_{k=-\infty}^{+\infty} \sum_{m=-\infty}^{+\infty} \phi_{\tilde{f}_e}(mT, f-\frac{k}{T})\ \delta(\tau - mT). \qquad (7.39)$$

Since $\tilde{f}_e(t)$ is time limited to the interval $[0, T_d]$, $\phi_{\hat{f}_e}(\tau,f)$ is time limited in the argument τ to the interval $[\tau_a - T_d, \tau_a + T_d]$, as shown in Appendix B. Observe in the latter expression for $\phi_{\hat{f}_e}(\tau,f)$ that the argument τ takes on only the discrete values mT where m is an integer. Due to the finite time extent of $\phi_{\hat{f}_e}(\tau,f)$, m needs to range only from $\gamma-(N-1)$ to $\gamma+(N-1)$, where γ is the integer value closest to $\frac{\tau_a}{T}$, in order to cover that portion of the τ-axis for which $\phi_{\hat{f}_e}(\tau,f)$ is nonzero. Thus,

$$\phi_{\hat{f}_e}(\tau,f) = \frac{1}{T} \sum_{k=-\infty}^{\infty} \sum_{m=\gamma-(N-1)}^{n=\gamma+(N-1)} \phi_{\tilde{f}_e}(mT, f-\frac{k}{T})\ \delta(\tau - mT). \qquad (7.40)$$

Because $\hat{\tilde{f}}_e(t)$ is sampled in time every T seconds, we see that $\phi_{\hat{f}_e}(\tau,f)$ is sampled in τ every T seconds. In other words, $\phi_{\hat{f}_e}(\tau,f)$ is a discrete-time continuous-frequency autocorrelation function.

In practice, $\phi_{\hat{f}_e}(\tau,f)$ will be evaluated only at discrete points in the τ-f plane.

Consequently, we now sample $\phi_{\hat{f}_e}(\tau,f)$ in frequency. Analytically, this is accomplished by multiplying $\phi_{\hat{f}_e}(\tau,f)$ with

$$\text{comb}_K(f) = K \sum_{\ell=-\infty}^{\infty} \delta(f-\ell K). \tag{7.41}$$

This yields

$$\begin{aligned}\phi_{\hat{f}_e}(\tau,f)\ \text{comb}_K(f) &= \frac{K}{T} \sum_{k=-\infty}^{\infty} \sum_{m=\gamma-(N-1)}^{\gamma+(N-1)} \sum_{\ell=-\infty}^{\infty} \\ &\phi_{\hat{f}_e}(mT, f-\frac{k}{T})\ \delta(\tau-mT)\ \delta(f-\ell K) \\ &= \frac{K}{T} \sum_{k=-\infty}^{\infty} \sum_{m=\gamma-(N-1)}^{\gamma+(N-1)} \sum_{\ell=-\infty}^{\infty} \\ &\phi_{\hat{f}_e}(mT, \ell K-\frac{k}{T})\ \delta(\tau-mT)\ \delta(f-\ell K).\end{aligned} \tag{7.42}$$

By examination of the latter expression, the discrete-time discrete-frequency autocorrelation function of the time sampled signal $\hat{\hat{f}}_e(t)$ is defined to be

$$\hat{\phi}_{\hat{f}_e}(m,\ell) = \sum_{k=\infty}^{\infty} \phi_{\hat{f}_e}(mT, \ell K-\frac{k}{T});\ -\infty \le \ell \le \infty,\ \gamma-(N-1) \le m \le \gamma+(N-1). \tag{7.43}$$

then

$$\phi_{\hat{f}_e}(\tau,f)\ \text{comb}_K(f) = \frac{K}{T} \sum_{m=\gamma-(N-1)}^{\gamma+(N-1)} \sum_{\ell=-\infty}^{\infty} \hat{\phi}_{\hat{f}_e}(m,\ell)\ \delta(\tau-mT)\ \delta(f-\ell K). \tag{7.44}$$

Recognizing that

$$\mathrm{comb}_K(f) = K \sum_{\ell=-\infty}^{\infty} \delta(f-\ell K), \tag{7.45}$$

it follows from the above expression that

$$\phi_{\tilde{f}_e}(\tau,f) = \frac{1}{T} \sum_{m=\gamma-(N-1)}^{\gamma+(N-1)} \hat{\phi}_{\tilde{f}_e}(m,f)\ \delta(\tau-mT) \tag{7.46}$$

Note that the k=0 term of $\hat{\phi}_{\tilde{f}_e}(m,\ell)$ is given by

$$\hat{\phi}_{\tilde{f}_e}(m,\ell)\big|_{k=0} = K\ \phi_{\tilde{f}_e}(mT,\ell K);\ -\infty \le \ell \le \infty,\ \gamma-(N-1) \le m \le \gamma+(N-1). \tag{7.47}$$

Therefore, the k=0 term is nothing more than a constant times the continuous-time continuous-frequency autocorrelation function of the time limited continuous signal $\tilde{f}_e(t)$ evaluated at the points (mT, ℓK) in the τ-f plane where m and ℓ are integers such that $\gamma-(N-1) \le m \le \gamma+(N-1)$ and $-\infty \le \ell \le \infty$. Also, note that $\hat{\phi}_{\tilde{f}_e}(m,\ell)$ is the replication in frequency of $\phi_{\tilde{f}_e}(mT,\ell K)$ every $\frac{1}{T}$ Hertz. As was the case in the previous section, the DFT of N time samples spaced every T seconds results in a transform whose frequency components are spaced every $\frac{1}{NT}$ Hertz. Consequently, K is chosen such that

$$K = \frac{1}{NT}. \tag{7.48}$$

Then $\hat{\phi}_{\tilde{f}_e}(m,\ell)$ becomes

$$\hat{\phi}_{\tilde{f}_e}(m,\ell) = \frac{1}{NT} \sum_{k=-\infty}^{\infty} \phi_{\tilde{f}_e}(mT,[\ell-kN]\frac{1}{NT});\gamma-(N-1) \le m \le \gamma+(N-1). \qquad (7.49)$$

From the previous section, the discrete-time discrete-frequency autocorrelation function of the signal $\hat{\tilde{f}}_p(t)$, which was generated by sampling both $\tilde{f}_e(t)$ in time and its spectrum in frequency, was defined to be

$$\hat{\phi}_{\tilde{f}_p}(m,\ell) = \frac{1}{NT} \sum_{n=-\infty}^{\infty} \sum_{k=-\infty}^{\infty} \phi_{\tilde{f}_e}\left([m-nN]T,[\ell-kN]\frac{1}{NT}\right) . \qquad (7.50)$$

It is seen that $\hat{\phi}_{\tilde{f}_e}(m,\ell)$ can be obtained from $\hat{\phi}_{\tilde{f}_p}(m,\ell)$ by letting n=0 in the expression for $\hat{\phi}_{\tilde{f}_p}(m,\ell)$. In a similar manner, it can be shown that the discrete-time discrete-frequency autocorrelation function for $\tilde{f}_e(t)$, when only the spectrum of $\tilde{f}_e(t)$ is sampled in frequency, can be obtained from $\hat{\phi}_{\tilde{f}_p}(m,\ell)$ by letting k=0 in the expression for $\hat{\phi}_{\tilde{f}_p}(m,\ell)$,.

7.2 Aliasing considerations

It is shown in Appendix B that $\phi_{\tilde{f}_e}(\tau,f)$ has both twice the time duration of the signal $\tilde{f}_e(t)$ and twice the frequency duration of the spectrum of $\tilde{f}_e(t)$. The expression

that relates $\hat{\phi}_{\tilde{f}_e}(m,\ell)$ to $\phi_{\tilde{f}_e}(mT,[\ell-kN]\frac{1}{NT})$ shows that $\phi_{\tilde{f}_e}(mT,\frac{\ell}{NT})$ is replicated in frequency every $\frac{1}{T}$ Hertz. This is illustrated in Figure 7.1 where the spectrum of $\tilde{f}_e(t)$ is assumed to be bandlimited to the frequency interval [-B, B]. In order to avoid aliasing, it is necessary that

$$\frac{1}{T} \geq 4B. \tag{7.51}$$

Therefore, the signal $\tilde{f}_e(t)$ must be sampled in time at a rate that is no less than twice the Nyquist rate if aliasing is to be avoided between the replications of $\phi_{\tilde{f}_e}(mT,\frac{\ell}{NT})$. When aliasing is avoided, we have

$$\hat{\phi}_{\tilde{f}_e}(m,\ell) = \frac{1}{NT}\,\phi_{\tilde{f}_e}(mT,\frac{\ell}{NT}) \tag{7.52}$$

where $\gamma-(N-1) \leq m \leq \gamma+(N-1)$. From Appendix B it is apparent that the primary interval is spanned over frequency for those values of ℓ such that $\rho-(N-1) \leq \ell \leq \rho+(N-1)$ where the value of ρ is the closest integer smaller or equal to $\frac{f_s}{\Lambda} = f_s NT$. Since the discrete-time discrete-frequency ambiguity function is the magnitude squared of the discrete-time discrete-frequency time-frequency correlation function it follows that

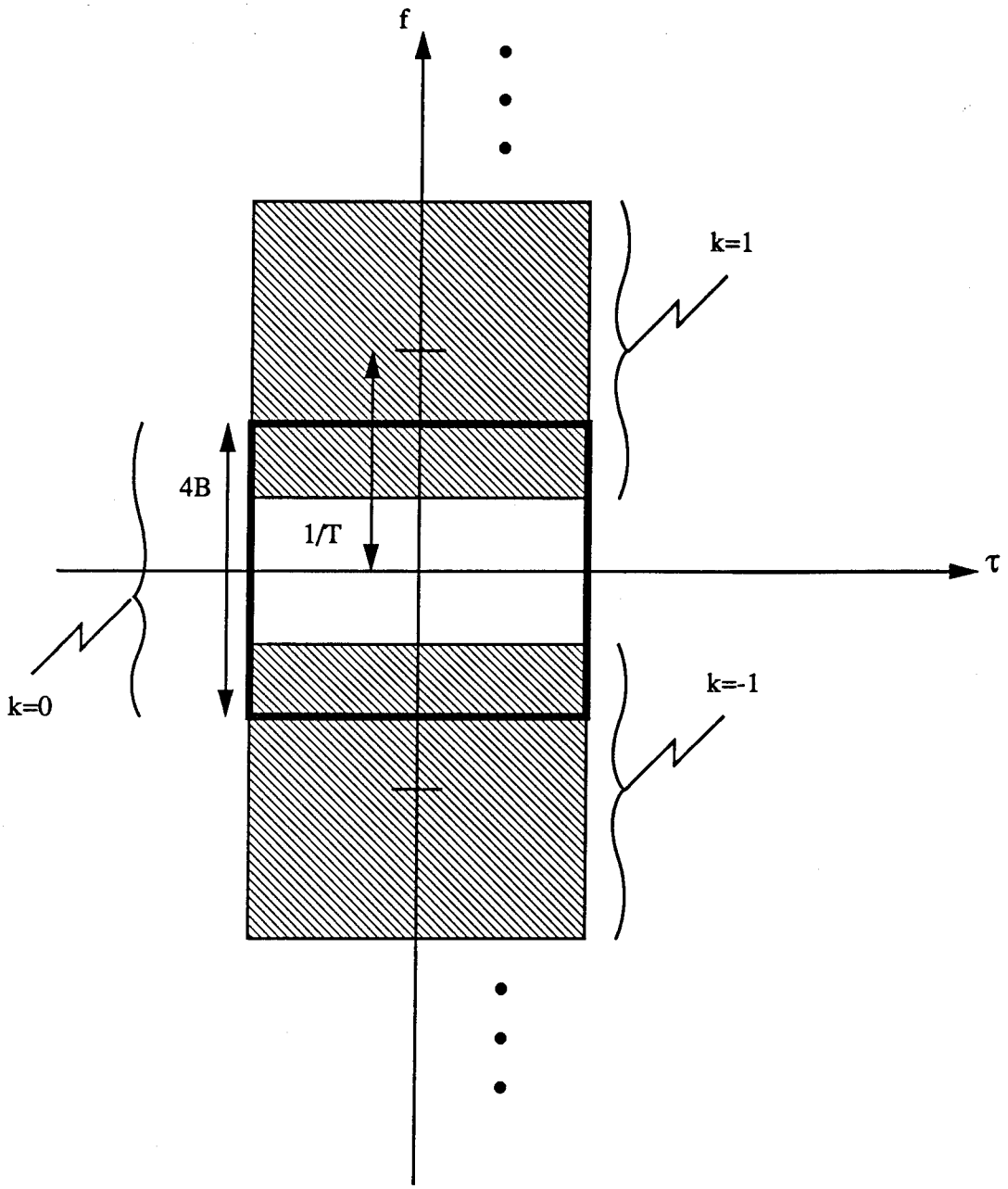

Fig. 7.1 Sketch illustrating replication in frequency of $\phi_{f_s}(mT, \frac{\ell}{NT})$

$$\hat{\Theta}_{\tilde{f}_s}(m,\ell) = |\hat{\Phi}_{\tilde{f}_s}(m,\ell)|^2 \tag{7.53}$$

is periodic in frequency with the primary interval extending for $\gamma-(N-1) \le m \le \gamma+(N-1)$ and $\rho-(N-1) \le \ell \le \rho+(N-1)$.

The effects of aliasing for the complex envelope

$$\tilde{f}(t) = \sqrt{2w}\ \frac{\sin 2\pi wt}{2\pi wt} = \sqrt{2w}\ \mathrm{sinc}(2wt) \tag{7.54}$$

are shown in Figs. 7.2(a) through (d). Because of the presence of the sinc function, $\tilde{f}(t)$ is bandlimited to a bandwidth of w Hertz. By analysis, the continuous-time continuous-frequency AF of $\tilde{f}(t)$ is

$$\Theta_{\tilde{f}}(\tau,f) = \left| \mathrm{rect}\left(\frac{f-f_a}{4w}\right) \frac{(2w-|f-f_a|)}{2w}\ \mathrm{sinc}\left[(\tau-\tau_a)(2w-|f-f_a|)\right]\right|^2 . \tag{7.55}$$

This is plotted in Fig. 7.2(a) for w=1. The discrete-time discrete-frequency AF of the sampled signal $\tilde{f}(t)$, using a sampling frequency equal to twice the Nyquist rate, is shown in Fig. 7.2(b). Note the periodicity of the AF along the frequency axis and the lack of aliasing. The AF in the primary interval of Fig. 7.2(b) is identical to the continuous-time continuous-frequency AF in Fig. 7.2(a). When the sampling rate is dropped to 1.8 and 1.5 times the Nyquist rate, noticeable aliasing occurs, as shown in Figs. 7.2(c) and (d). The aliasing becomes more severe as the sampling rate is decreased. A sampling rate less than twice the Nyquist rate can be used only if the aliasing that is introduced can be tolerated.

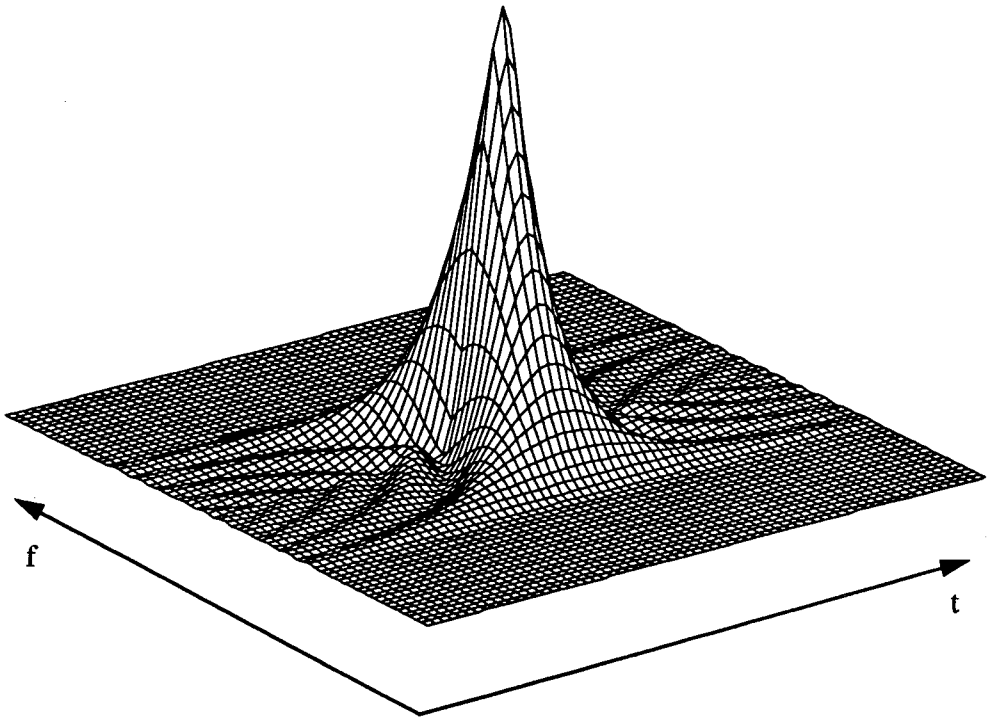

Fig. 7.2 (a) - Original continuous ambiguity function

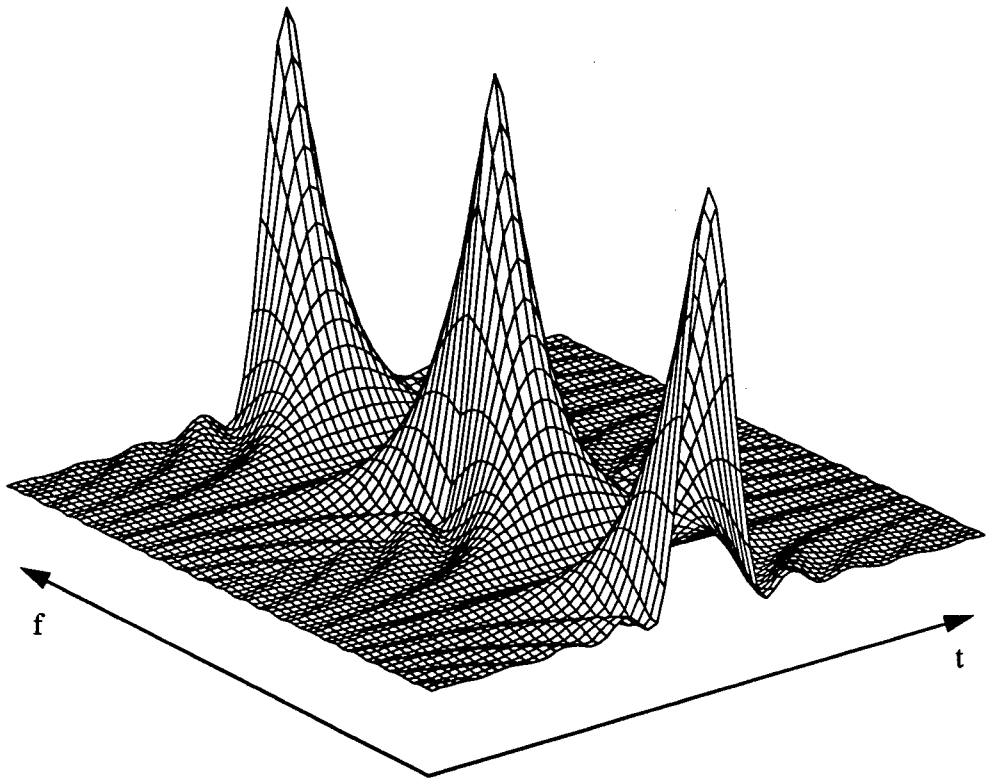

Fig. 7.2 (b) - Discrete ambiguity function: 2 Nyquist rate sampling

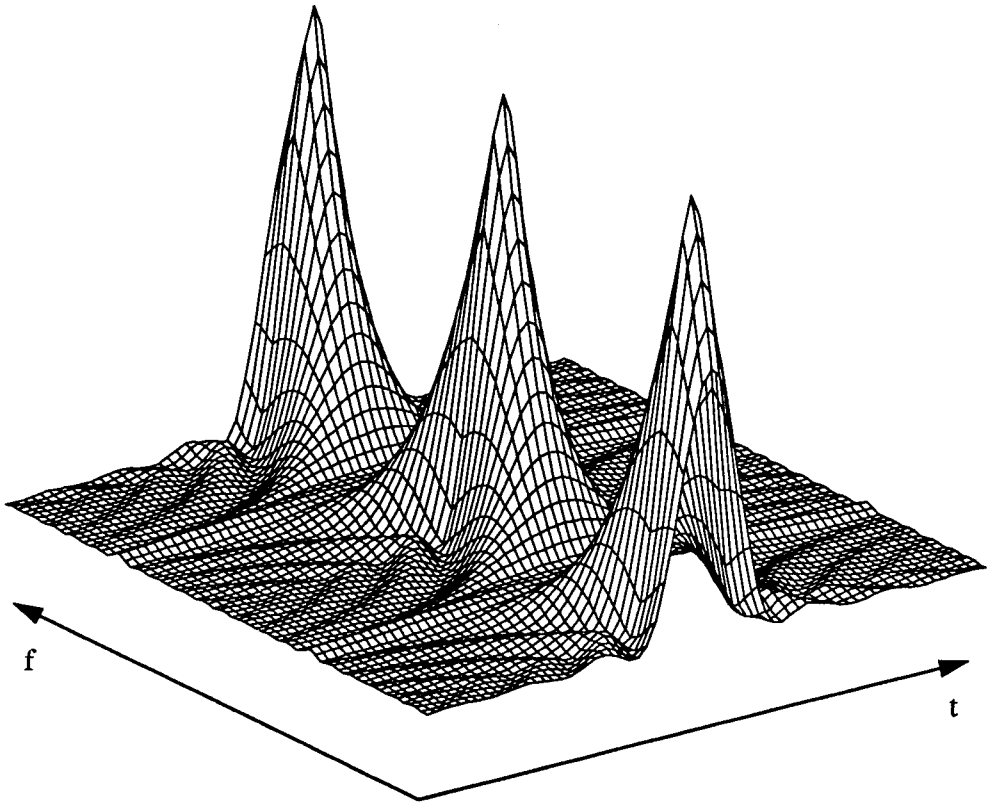

Fig. 7.2 (c) - Discrete ambiguity function: 1.8 Nyquist rate sampling

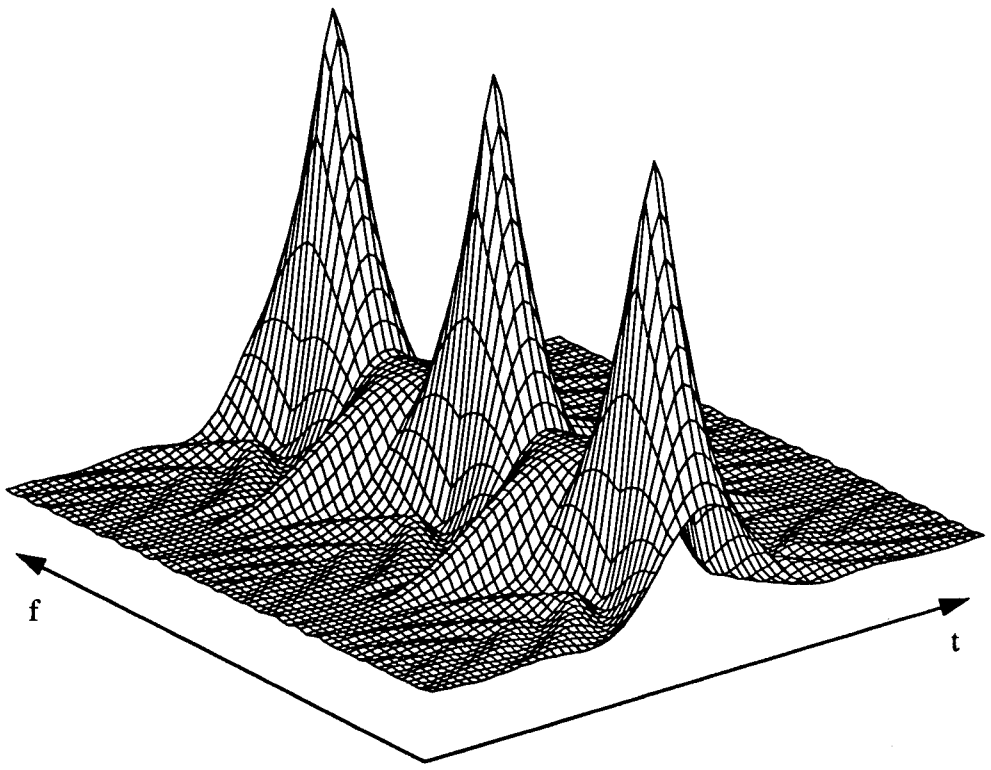

Fig. 7.2 (d) - Discrete ambiguity function: 1.5 Nyquist rate sampling

8 RECONSTRUCTION OF THE CONTINUOUS AF FROM THE DISCRETE-TIME DISCRETE-FREQUENCY AF

In this chapter we consider the reconstruction of the continuous ambiguity function when the discrete-time discrete-frequency ambiguity function is available. A number of cases are considered.

8.1 Signals Sampled in Both Time and Frequency.

Recall that $\hat{\tilde{f}}_p(t)$ is the periodic signal obtained by sampling both $\tilde{f}_e(t)$ and its spectrum in time and frequency, respectively. Define

$$\text{rect}_{\frac{1}{\lambda}}(t) = \begin{cases} 1 & 0 \le t < \frac{1}{\lambda} \\ 0 & \text{elsewhere.} \end{cases} \tag{8.1}$$

Then the sampled version of $\tilde{f}_e(t)$ (see Figure 6.1) is given by

$$\hat{\tilde{f}}_e(t) = \hat{\tilde{f}}_p(t)\ \text{rect}_{\frac{1}{\lambda}}(t)\ . \tag{8.2}$$

$\tilde{f}_e(t)$ can be recovered from $\hat{\tilde{f}}_e(t)$ by low pass filtering the latter. In particular,

$$\tilde{f}_e(t) = \hat{\tilde{f}}_e(t) * h_{LP}(t) \tag{8.3}$$

where

$$h_{LP}(t) = \text{sinc}(\frac{t}{T}). \tag{8.4}$$

It follows that

$$\tilde{f}_e(t) = \sum_{n=-\infty}^{+\infty} \hat{f}_e(nT)\ \mathrm{sinc}\left(\frac{t-nT}{T}\right) . \tag{8.5}$$

Recognizing that

$$\hat{\tilde{f}}_e(t) = \hat{\tilde{f}}_p(t)\ \mathrm{rect}_{\frac{1}{\lambda}}(t) = \hat{\tilde{f}}_p(t)\ f_2(t) \tag{8.6}$$

$$\hat{\tilde{g}}_e(t) = \hat{\tilde{g}}_p(t)\ \mathrm{rect}_{\frac{1}{\lambda}}(t-\tau_a) = \hat{\tilde{g}}_p(t)\ g_2(t) \tag{8.7}$$

and using the product property (A.2) from Appendix A, the time-frequency correlation function of $\hat{\tilde{f}}_e(t)$ can be written as

$$\begin{aligned} \phi_{\hat{\tilde{g}}_e,\hat{\tilde{f}}_e}(\beta,f) &= \int_{-\infty}^{+\infty} \phi_{\hat{\tilde{g}}_p,\hat{\tilde{f}}_p}(\beta,x)\ \ \phi_{g_2,f_2}(\beta,f-x)\ dx \\ &= \int_{-\infty}^{+\infty} \phi_{\hat{\tilde{f}}_p}(\beta,x)\ \ \phi_{g_2,f_2}(\beta,f-x)\ dx \\ &= \phi_{\hat{\tilde{f}}_e}(\beta,f) \end{aligned} \tag{8.8}$$

where $\hat{\tilde{g}}_p(t) = \hat{\tilde{f}}_p(t-\tau_a)\ e^{j2\pi f_a t}$, $f_2(t) = \mathrm{rect}_{\frac{1}{\lambda}}(t)$, and $g_2(t) = \mathrm{rect}_{\frac{1}{\lambda}}(t-\tau_a)$. With respect to $\hat{\tilde{g}}_e(t)$, notice that $\mathrm{rect}_{\frac{1}{\lambda}}(t-\tau_a)$ is nonzero for $\tau_a \le t \le \tau_a + \frac{1}{\lambda}$.

Also, recognizing that

$$\tilde{f}_e(t) = \hat{\tilde{f}}_e(t) * h_{LP}(t) = \hat{\tilde{f}}_e(t) * f_3(t) \tag{8.9}$$

$$\tilde{g}_e(t) = \hat{\tilde{g}}_e(t) * h_{LP}(t)\, e^{j2\pi f_a t} = \hat{\tilde{g}}_e(t) * g_3(t) \tag{8.10}$$

and using the convolution property (A.1) from Appendix A, the time-frequency correlation function of $\tilde{f}_e(t)$ can be expressed as

$$\begin{aligned}\phi_{\tilde{g}_e,\tilde{f}_e}(\tau,f) &= \int_{-\infty}^{\infty} \phi_{\hat{\tilde{g}}_e,\hat{\tilde{f}}_e}(\beta,f)\, \phi_{g_3,f_3}(\tau-\beta,f)\,d\beta \\ &= \int_{-\infty}^{\infty} \phi_{\hat{\tilde{f}}_e}(\beta,f)\, \phi_{g_3,f_3}(\tau-\beta,f)\,d\beta = \phi_{\tilde{f}_e}(\tau,f)\end{aligned} \tag{8.11}$$

where $\hat{\tilde{g}}_e(t) = \hat{\tilde{f}}_e(t-\tau_a)\, e^{j2\pi f_a t}$, $f_3(t) = h_{LP}(t)$, and $g_3(t) = h_{LP}(t)\, e^{j2\pi f_a t}$. $g_3(t)$ arises because, in order to pass undistorted the spectrum of $\tilde{g}_e(t)$, a rect function centered at f_a should be used to filter the spectrum of $\tilde{g}_e(t)$. This is equivalent to convolving $\hat{\tilde{g}}_e(t)$ with $h_{LP}(t)\, e^{j2\pi f_a t}$. We see, therefore, that

$$\phi_{\tilde{f}_e}(\tau,f) = \iint_{-\infty}^{+\infty} \phi_{\hat{\tilde{f}}_p}(\beta,x)\, \phi_{g_2,f_2}(\beta,f-x)\, \phi_{g_3,f_3}(\tau-\beta,f)\, d\beta\, dx \tag{8.12}$$

where

$$\phi_{g_2,f_2}(\beta,f-x) = \int_{-\infty}^{+\infty} \text{rect}\,\tfrac{1}{\lambda}(t-\tau_a)\ \text{rect}\,\tfrac{1}{\lambda}(t-\beta)\ e^{-j2\pi(f-x)t}dt\ . \qquad (8.13)$$

Fig. 8.1 shows the plots of $\text{rect}\,\frac{1}{\lambda}(t-\tau_a)$ and $\text{rect}\,\frac{1}{\lambda}(t-\beta)$. The product of the two functions is non-zero for the following cases:

<u>Case A</u> $\quad \tau_a < \beta < \tau_a + \frac{1}{\lambda}$ and t runs from β to $\tau_a + \frac{1}{\lambda}$

<u>Case B</u> $\quad \tau_a - \frac{1}{\lambda} < \beta < \tau_a$ and t runs from τ_a to $\beta + \frac{1}{\lambda}$

For Case A, $\tau_a < \beta < \tau_a + \frac{1}{\lambda}$. Then

$$\phi_{g_2,f_2}(\beta,f-x) = \int_{\beta}^{\tau_a+\frac{1}{\lambda}} e^{-j2\pi(f-x)t}\,dt$$

$$= \frac{e^{-j2\pi(f-x)t}}{-j2\pi(f-x)} \Bigg|_{\beta}^{\tau_a+\frac{1}{\lambda}}$$

$$= \frac{e^{-j2\pi(f-x)\beta} - e^{-j2\pi(f-x)(\tau_a+\frac{1}{\lambda})}}{j2\pi(f-x)}$$

$$= e^{-j2\pi(f-x)\left[\frac{\beta+\tau_a}{2}+\frac{1}{2\lambda}\right]} \frac{e^{-j2\pi(f-x)\left[(\frac{\beta-\tau_a}{2})-\frac{1}{2\lambda}\right]} - e^{+j2\pi(f-x)\left[\frac{(\beta-\tau_a)}{2}-\frac{1}{2\lambda}\right]}}{j2\pi(f-x)}\ . \qquad (8.14)$$

For Case B, $\tau_a - \frac{1}{\lambda} < \beta < \tau_a$. Then

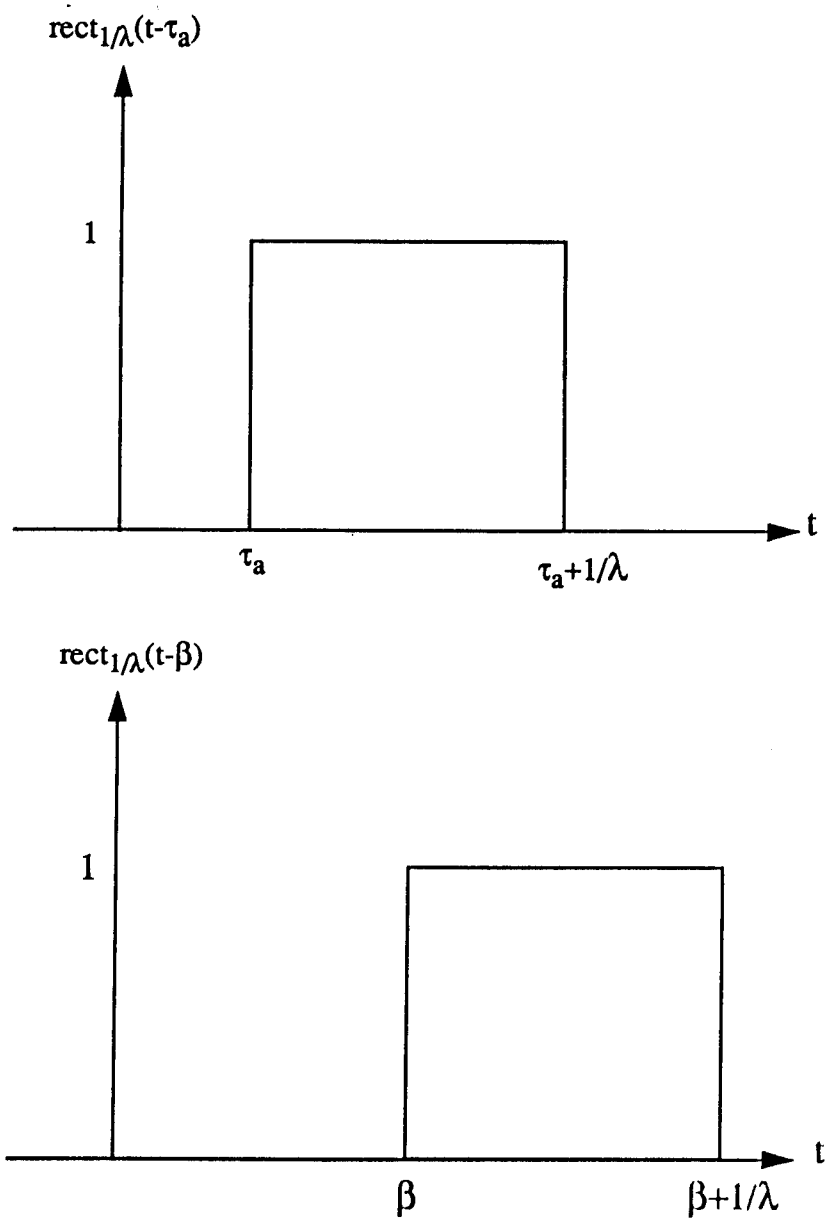

Figure 8.1 Sketches of $\text{rect}_{\frac{1}{\lambda}}(t-\tau_a)$ and $\text{rect}_{\frac{1}{\lambda}}(t-\beta)$ for arbitrary values of τ_a and β.

$$\phi_{g_2,f_2}(\beta,f-x) = \int_{\tau_a}^{\beta+\frac{1}{\lambda}} e^{-j2\pi(f-x)t}\,dt$$

$$= \frac{e^{-j2\pi(f-x)}}{-j2\pi(f-x)}\Bigg|_{\tau_a}^{\beta+\frac{1}{\lambda}}$$

$$= \frac{e^{-j2\pi(f-x)\tau_a} - e^{-j2\pi(f-x)\left(\beta+\frac{1}{\lambda}\right)}}{j2\pi(f-x)}$$

$$= e^{-j2\pi(f-x)\left[\frac{\beta+\tau_a}{2}+\frac{1}{2\lambda}\right]} \frac{e^{-j2\pi(f-x)\left[\frac{\tau_a-\beta}{2}-\frac{1}{2\lambda}\right]} - e^{+j2\pi(f-x)\left[\frac{\tau_a-\beta}{2}-\frac{1}{2\lambda}\right]}}{j2\pi(f-x)} \quad . \tag{8.15}$$

Noticing that $\beta > \tau_a$ for Case A while $\beta < \tau_a$ for Case B, the results obtained for $\phi_{g_2,f_2}(\beta,f-x)$ for both cases A and B can be combined to result in

$$\phi_{g_2,f_2}(\beta,f-x) = -\,e^{-j2\pi(f-x)\left[\frac{\beta+\tau_a}{2}+\frac{1}{2\lambda}\right]} \cdot \frac{\sin\left\{2\pi(f-x)\left[\frac{|\beta-\tau_a|}{2}-\frac{1}{2\lambda}\right]\right\}}{\pi(f-x)} \quad . \tag{8.16}$$

The expression of $\phi_{g_3,f_3}(\tau-\beta,f)$ is given by

$$\phi_{g_3,f_3}(\tau-\beta,f) = \int_{-\infty}^{+\infty} \tilde{h}_{LP}(t)\, e^{+j2\pi f_a t}\, h^*_{LP}(t-[\tau-\beta])\, e^{-j2\pi ft}\,dt. \tag{8.17}$$

It is readily shown [4] that $\phi_{g_3,f_3}(\tau-\beta,f)$ can also be expressed as

$$\phi_{g_3,f_3}(\tau-\beta,f) = \int_{-\infty}^{+\infty} \tilde{H}_{LP}(jv-jf_a)\, \tilde{H}^*_{LP}(jv-jf)\, e^{j2\pi v(\tau-\beta)}\,dv \tag{8.18}$$

where $\tilde{H}_{LP}(jv)$ is the Fourier transform of $\tilde{h}_{LP}(t)$. Since $\tilde{h}_{LP}(t)$ is the sinc function, its

Fourier transform is given by

$$\tilde{H}_{LP}(jf) = T \, \text{rect}_{\frac{1}{T}} [T(f+\tfrac{1}{(2T)})]. \tag{8.19}$$

The expression for $\phi_{g_3,f_3}(\tau-\beta,f)$ becomes, therefore,

$$\phi_{g_3,f_3}(\tau-\beta,f) = T^2 \int_{-\infty}^{+\infty} \text{rect}_{\frac{1}{T}}[T(\nu-f_a+\tfrac{1}{(2T)})] \, \text{rect}_{\frac{1}{T}}[T(\nu-f+\tfrac{t}{(2T)})] \, e^{j2\pi\nu(\tau-\beta)} \, d\nu. \tag{8.20}$$

Sketches of $\text{rect}_{\frac{1}{T}}[T(\nu-f_a+\frac{1}{(2T)})]$ and $\text{rect}_{\frac{1}{T}}[T(\nu-f+\frac{1}{(2T)})]$ are shown in Fig. 8.2. The product of these two functions is nonzero for the following cases:

<u>Case A</u> $\quad f_a < f < f_a+\frac{1}{T}$ and ν runs from $f-\frac{1}{(2T)}$ to $f_a+\frac{1}{(2T)}$

<u>Case B</u> $\quad f_a-\frac{1}{T} < f < f_a$ and ν runs from $f_a-\frac{1}{(2T)}$ to $f+\frac{1}{(2T)}$

For Case A, $f_a < f < f_a+\frac{1}{T}$. Then

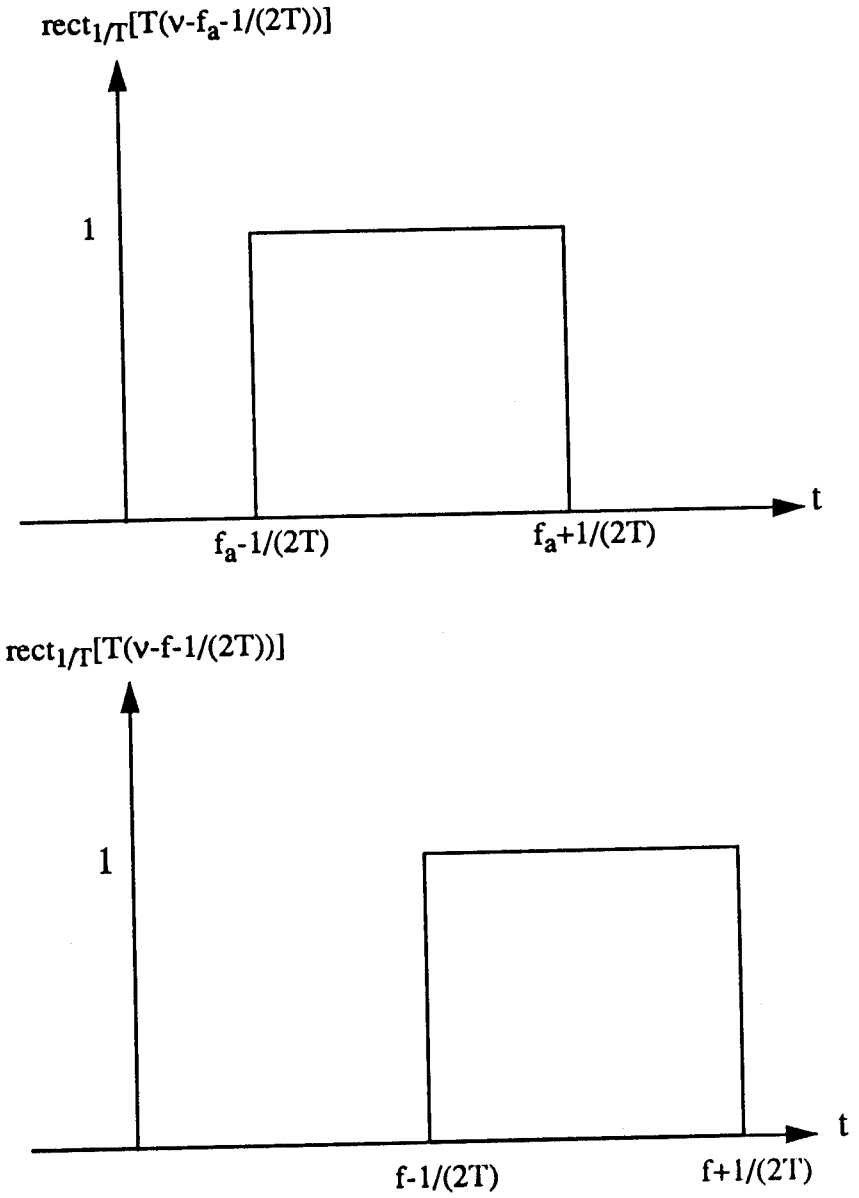

Fig 8.2 Sketches of $\text{rect}_{\frac{1}{T}}[T(\nu - f_a + \frac{1}{(2T)})]$ and $\text{rect}_{\frac{1}{T}}[T(\nu - f + \frac{1}{(2T)})]$ for arbitrary f and f_a.

$$\phi_{g_3,f_3}(\tau-\beta,f) = \int_{f-\frac{1}{(2T)}}^{f_a+\frac{1}{(2T)}} T^2\, e^{j2\pi v(\tau-\beta)}\, dv$$

$$= T^2 \left. \frac{e^{j2\pi v(\tau-\beta)}}{j2\pi(\tau-\beta)} \right|_{f-\frac{1}{(2T)}}^{f_a+\frac{1}{(2T)}}$$

$$= T^2 \frac{e^{j2\pi(f_a+\frac{1}{(2T)})(\tau-\beta)} - e^{j2\pi(f-\frac{1}{(2T)})(\tau-\beta)}}{j2\pi(\tau-\beta)}$$

$$= T^2\, e^{j2\pi(f+f_a)\frac{\tau-\beta}{2}} \cdot \frac{e^{j2\pi(f_a-f+\frac{1}{T})\frac{\tau-\beta}{2}} - e^{-j2\pi(f_a-f+\frac{1}{T})\frac{\tau-\beta}{2}}}{j2\pi(\tau-\beta)} . \qquad (8.21)$$

For Case B, $f_a - \frac{1}{T} < f < f_a$. Then

$$\phi_{g_3,f_3}(\tau-\beta,f) = \int_{f_a-\frac{1}{(2T)}}^{f+\frac{1}{(2T)}} T^2\, e^{j2\pi v(\tau-\beta)}\, dv$$

$$= T^2 \left. \frac{e^{j2\pi v(\tau-\beta)}}{j2\pi(\tau-\beta)} \right|_{f_a-\frac{1}{(2T)}}^{f+\frac{1}{(2T)}}$$

$$= T^2 \frac{e^{j2\pi(f+\frac{1}{(2T)})(\tau-\beta)} - e^{j2\pi(f_a-\frac{1}{(2T)})(\tau-\beta)}}{j2\pi(\tau-\beta)}$$

$$= T^2\, e^{j2\pi(f+f_a)\frac{\tau-\beta}{2}} \cdot \frac{e^{j2\pi(f-f_a+\frac{1}{T})\,(\frac{\tau-\beta}{2})} - e^{-j2\pi(f-f_a+\frac{1}{T})\,(\frac{\tau-\beta}{2})}}{j2\pi(\tau-\beta)} . \qquad (8.22)$$

Notice that $f > f_a$ for Case A while $f < f_a$ for Case B. The results obtained for $\phi_{g_3,f_3}(\tau-\beta,f)$ for both Case A and B can then be combined to result in

$$\phi_{g_3,f_3}(\tau-\beta,f) = -\, T^2\, e^{j2\pi(f+f_a)\frac{\tau-\beta}{2}} \frac{\sin\left\{2\pi\left[|f-f_a|-\frac{1}{T}\right]\frac{\tau-\beta}{2}\right\}}{\pi(\tau-\beta)} . \qquad (8.23)$$

Substituting the expression derived for $\phi_{g_2,f_2}(\beta,f-x)$ and $\phi_{g_3,f_3}(\tau-\beta,f)$ into that of $\phi_{\hat{f}_e}(\tau,f)$

we obtain

$$\phi_{\hat{f}_e}(\tau,f) = \int_{-\infty}^{+\infty}\int T^2\, \hat{\phi}_{\hat{f}_p}(\beta,x) \cdot \frac{\sin\left\{2\pi(f-x)\left[\frac{|\beta-\tau_a|}{2} - \frac{1}{2\lambda}\right]\right\}}{\pi(f-x)}$$

$$\frac{\sin\left\{2\pi\left[|f-f_a|-\frac{1}{T}\right]\frac{\tau-\beta}{2}\right\}}{\pi(\tau-\beta)}$$

$$e^{-j2\pi(f-x)\left[\frac{\beta+\tau_a}{2}+\frac{1}{2\lambda}\right] + j2\pi(f+f_a)\frac{\tau-\beta}{2}}\, d\beta\, dx \qquad (8.24)$$

We now replace the expression for $\hat{\phi}_{\hat{f}_p}(\beta,x)$, as derived in Section 7.1, Eq. (7.29).

Also, letting $\lambda = \frac{1}{NT}$, $\phi_{\hat{f}_e}(\tau,f)$ becomes

$$\phi_{\hat{f}_e}(\tau,f) = T^2 \int_{-\infty}^{+\infty}\int \frac{1}{T} \sum_{m=-\infty}^{+\infty} \sum_{\ell=-\infty}^{+\infty} \hat{\phi}_{\hat{f}_p}(m,\ell)\, \delta(\beta-mT)\, \delta\left(x-\frac{\ell}{NT}\right)$$

$$\frac{\sin\left\{2\pi(f-x)\left[\frac{|\beta-\tau_a|}{2} - \frac{1}{2\lambda}\right]\right\}}{\pi(f-x)}$$

$$\frac{\sin\left\{2\pi\left[|f-f_a|-\frac{1}{T}\right]\frac{\tau-\beta}{2}\right\}}{\pi(\tau-\beta)}$$

$$e^{-j2\pi(f-x)\left[\frac{\beta+\tau_a}{2}+\frac{1}{2\lambda}\right] + j2\pi(f+f_a)\frac{\tau-\beta}{2}}\, d\beta dx \qquad (8.25)$$

Carrying out the integrations, we have

$$\phi_{\tilde{f}_e}(\tau,f) = T \sum_{m=-\infty}^{+\infty} \sum_{\ell=-\infty}^{+\infty} \hat{\phi}_{\hat{f}_p}(m,\ell) \cdot \frac{\sin\left\{2\pi(f-\frac{\ell}{NT})\left[\frac{|mT-\tau_a|}{2} - \frac{NT}{2}\right]\right\}}{\pi(f-\frac{\ell}{NT})}$$

$$\frac{\sin\left\{2\pi\left[|f-f_a|-\frac{1}{T}\right]\frac{\tau-mT}{2}\right\}}{\pi(\tau-mT)}$$

$$e^{-j2\pi(f-\frac{\ell}{NT})\left[\frac{mT+\tau_a}{2}+\frac{NT}{2}\right]+j2\pi(f+f_a)\frac{\tau-mT}{2}} \quad . \tag{8.26}$$

This latter expression for $\phi_{\tilde{f}_e}(\tau,f)$ allows recovery of the continuous-time continuous-frequency correlation function of $\tilde{f}_e(t)$ from the discrete-time discrete-frequency correlation function of $\hat{f}_p(t)$. Notice that a priori knowledge of τ_a and f_a is required for the reconstruction of $\phi_{\tilde{f}_e}(\tau,f)$.

8.2 Signals Sampled Only in Time

As pointed out in Section 8.1, $\tilde{f}_e(t)$ can be recovered from $\hat{f}_e(t)$ by low pass filtering the latter. Namely,

$$\begin{aligned}\tilde{f}_e(t) &= \hat{f}_e(t) * h_{LP}(t) \\ &= \hat{f}_e(t) * \text{sinc}\left(\frac{t}{T}\right) \\ &= \sum_{n=-\infty}^{+\infty} \hat{f}_e(nT)\ \text{sinc}\left(\frac{t-nT}{T}\right) .\end{aligned} \tag{8.27}$$

Using property (A.1) of Appendix A, we can write that

$$\phi_{\hat{f}_a}(\tau,f) = \int_{-\infty}^{+\infty} \phi^{\wedge}_{\hat{f}_a}(\beta,f)\ \phi_{g_3,f_3}(\tau-\beta,f)\ d\beta \tag{8.28}$$

where $\phi_{g_3,f_3}(\tau-\beta,f)$ was derived in Section 8.1, Eq. (8.23). It is given by

$$\phi_{g_3,f_3}(\tau-\beta,f) = -T^2\, e^{j2\pi(f+f_a)\frac{\tau-\beta}{2}}\ \frac{\sin\left\{2\pi\left[|f-f_a|-\frac{1}{T}\right]\frac{\tau-\beta}{2}\right\}}{\pi(\tau-\beta)}\ . \tag{8.29}$$

Therefore,

$$\phi_{\hat{f}_a}(\tau,f) = \int_{-\infty}^{+\infty} -T^2\ \phi^{\wedge}_{\hat{f}_a}(\beta,f)\ e^{j2\pi(f+f_a)\frac{\tau-\beta}{2}}$$

$$\frac{\sin\left\{2\pi\left\{|f-f_a|-\frac{1}{T}\right]\frac{\tau-\beta}{2}\right\}}{\pi(\tau-\beta)}\ d\beta\ . \tag{8.30}$$

Recall from Section 7.2, Eq. (7.46) that

$$\phi^{\wedge}_{\hat{f}_a}(\beta,f) = \frac{1}{T} \sum_{m=\gamma-(N-1)}^{\gamma+(N-1)} \phi^{\wedge}_{\hat{f}_a}(m,f)\ \delta(\beta-mT) \tag{8.31}$$

where γ is the closest integer to τ_a/T. Substituting the expression for $\phi^{\wedge}_{\hat{f}_a}(\beta,f)$ into that of $\phi_{\hat{f}_a}(\tau,f)$, the latter becomes

$$\phi_{\tilde{f}_a}(\tau,f) = -T \int_{-\infty}^{+\infty} \sum_{m=\gamma-(N-1)}^{\gamma+(N-1)} \hat{\phi}_{\hat{f}_a}(m,f)\ \delta(\beta-mT)\ e^{j2\pi(f+f_a)\frac{\tau-\beta}{2}}$$

$$\frac{\sin\left\{2\pi\left[|f-f_a|-\frac{1}{T}\right]\frac{\tau-\beta}{2}\right\}}{\pi(\tau-\beta)}\ d\beta$$

$$= -T \sum_{m=\gamma-(N-1)}^{\gamma+(N-1)} \hat{\phi}_{\hat{f}_a}(m,f)\ e^{j2\pi(f+f_a)\frac{\tau-mT}{2}}$$

$$\frac{\sin\left\{2\pi\left[|f-f_a|-\frac{1}{T}\right]\frac{\tau-mT}{2}\right\}}{\pi(\tau-mT)}\ . \qquad (8.32)$$

This latter expression for $\phi_{\tilde{f}_a}(\tau,f)$ allows the recovery of the continuous-time continuous-frequency correlation function of $\tilde{f}_a(t)$ from the discrete-time continuous frequency correlation function of the time sampled signal $\hat{\tilde{f}}_a(t)$.

In a previous section it was shown that aliasing in the discrete-time discrete-frequency AF can be avoided by sampling $\tilde{f}_a(t)$ at a rate greater than or equal to twice the Nyquist rate. When the Doppler frequency, f_a, is known, the Nyquist rate suffices, as explained below. The Doppler shifted spectrum of $\tilde{f}_a(t)$ is sketched in Fig. 8.3 for $f_a > 0$. Since f_a is known, it is possible to shift the spectrum to the origin, as shown in Fig. 8.4, by appropriately mixing the received signal with a sinusoidal oscillator tuned to f_a. For the spectrum of Fig. 8.3 the Nyquist rate is given by

$$f_s = 2B. \qquad (8.33)$$

Samples obtained employing the Nyquist rate can be used to interpolate to any other values for $\tilde{f}_a(t)$. To avoid aliasing of the discrete-time discrete-frequency AF, recall

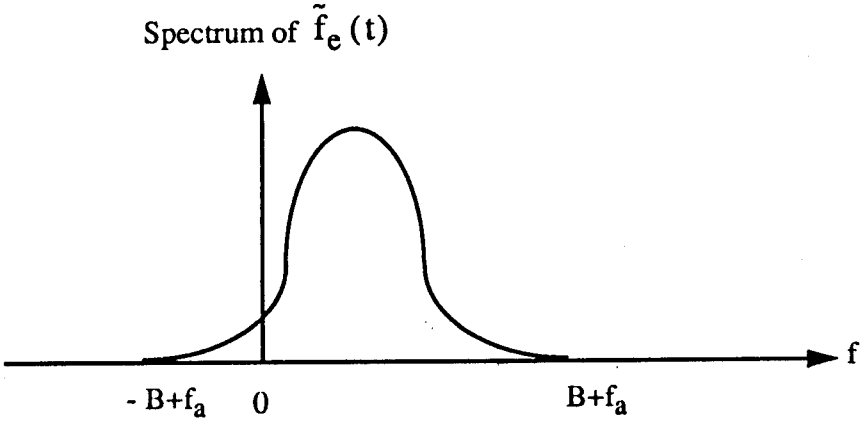

Fig. 8.3 Doppler shifted spectrum of $\tilde{f}_e(t)$ assuming $f_a > 0$.

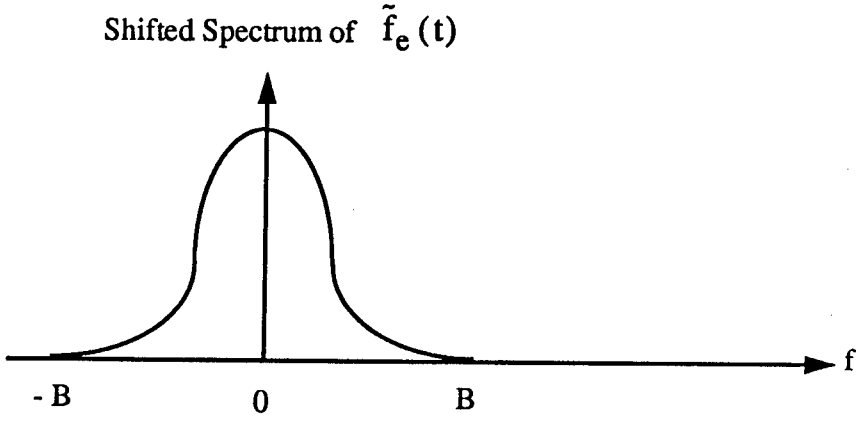

Fig. 8.4 Spectrum of Fig. 8.3 shifted to the origin

that the sampling rate should be at least as large as

$$2f_s = 4B. \tag{8.34}$$

However, using interpolation, the 4B samples per unit time can be generated from the 2B samples per unit time. Hence, if the Doppler frequency is known, aliasing can be avoided even when the sampling rate is as small as the Nyquist rate.

When the Doppler frequency, f_a, is unknown but its maximum value, $f_{a\ max}$ is known, alaising can be avoided by sampling at

$$f_s = 2(B+f_{a\ max}) \tag{8.35}$$

where$(B+f_{a\ max})$ is the largest possible frequency for the Doppler shifted spectrum of $\tilde{f}_o(t)$ This is true, because, as was done for the known Doppler case, the $2(B+f_{a\ max})$ samples per unit time can be used to generate the 4B samples per unit time required to avoid aliasing.

When the Doppler shift is completely unknown, it is guaranteed that no aliasing will occur only if the sampling rate is greater than or equal to 4B, which is twice the Nyquist rate.

9 SIGNAL REPRESENTATION FOR THE NON-COOPERATIVE CASE.

9.1 Introduction

From a signal processing perspective, non-cooperative bistatic radar differs from the cooperative case with dedicated transmitter in two major respects:

i) The transmitted signal is not designed specifically for bistatic radar applications, and

ii) A significant discrepancy can exist between the actual transmitted signal and the signal which at the receiver is assumed to have been transmitted.

The implications of (i) are a generally reduced performance compared to the cooperative case with dedicated transmitter, and the possible need for special processing which takes into account the nature of the transmitted signal - e.g., TV broadcast signals, FM broadcast signals. These issues require more extensive investigation and will not be addressed here.

The implications of (ii) are also a reduction in detection performance compared to the cooperative case with dedicated transmitter. A first step toward a thorough evaluation of this effect is a suitable signal representation for the non-cooperative case. This is considered in Section 9.2.

9.2 Signal Representation

We consider an actual transmitted signal with complex envelope as in (2.12),

$$\tilde{f}(t) = A(t)\, e^{j\Phi(t)}, \tag{9.1}$$

resulting in a received signal as in (2.22), assuming a single point target:

$$s_R(t) = \sqrt{2}\ \mathrm{Re}\left\{ \sqrt{E_t}\tilde{b}\tilde{f}(t-\tau_a)\ e^{j\omega_{Da}t}\ e^{j\omega_c t}\right\}. \tag{9.2}$$

An incorrect representation, at the receiver, of the transmitted signal can involve errors in

a) the assumed transmitted carrier frequency

b) the epoch, i.e., the exact timing of the transmitted signal

c) the complex envelope

We see from (9.2) that an error in ω_c, which will be denoted ω_ϵ, adds to or subtracts from ω_{Da}. Similarly, an error in epoch, denoted τ_ϵ, adds to or subtracts from τ_a. Specifically, suppose that the reference waveform available at the receiver is delayed by τ_ϵ compared to the actual transmitted signal, and up-shifted in carrier angular frequency by ω_ϵ, giving

$$\tilde{f}_{ref}(t) = A(t-\tau_\epsilon)\ e^{j\phi(t-\tau_\epsilon)}\ e^{j\omega_\epsilon t} = \tilde{f}(t-\tau_\epsilon)\ e^{j\omega_\epsilon t} \tag{9.3}$$

Expressing (9.2) in terms of $\tilde{f}_{ref}(t)$ as given in (9.3), we have

$$s_R(t) = \sqrt{2}\ \mathrm{Re}\left\{\sqrt{E_t}\tilde{b}\ \tilde{f}_{ref}(t+\tau_\epsilon-\tau_a)\ e^{j(\omega_{Da}-\omega_\epsilon)t}\ e^{j\omega_c t}\right\}, \tag{9.4}$$

where any complex constants are absorbed into $\tilde{b}$.

Consider now an error in the complex envelope. Let the transmitted complex envelope, as assumed at the receiver, be

$$\tilde{f}(t) + \tilde{f}_\epsilon(t) = A(t)\, e^{j\phi(t)} + A_\epsilon(t)\, e^{j\phi_\epsilon(t)}. \tag{9.5}$$

The term $\tilde{f}_\epsilon$ is assumed to be devoid of a component proportional to $\tilde{f}$; that is,

$$\int \tilde{f}(t)\, \tilde{f}_\epsilon^*(t)dt = 0.$$

Combining (9.5) with (9.3) gives for the reference waveform at the receiver

$$\tilde{f}_{ref}(t) = \left[\tilde{f}(t-\tau_\epsilon) + \tilde{f}_\epsilon(t-\tau_\epsilon)\right] e^{j\omega_\epsilon t}. \tag{9.6}$$

In terms of this reference waveform, the expression for the received signal (9.2) becomes

$$s_R(t) = \sqrt{2}\ \mathrm{Re}\left\{ \sqrt{E_t}\ \tilde{b}\left[\tilde{f}_{ref}(t+\tau_\epsilon-\tau_a) - f_\epsilon(t-\tau_a)e^{j\omega_\epsilon t}\right] e^{j(\omega_{D_a}-\omega_\epsilon)t}\ e^{j\omega_c t}\right\}. \tag{9.7}$$

Next we consider how the various errors reflected in (9.7) affect the expression for the ambiguity function. We use the symmetrical form of the ambiguity function given in (2.51),

$$\theta(\tau',\omega_D') = \left|\int_{-\infty}^{\infty} \tilde{f}(t-\tfrac{\tau'}{2})\, \tilde{f}^*(t+\tfrac{\tau'}{2})\, e^{j\omega_D' t}\, dt\right|^2, \tag{9.8}$$

where $\tau' = \tau_a - \tau_H$ and $\omega_D' = \omega_{D_a} - \omega_{D_H}$. In order to express the ambiguity function as a function of R_R and V_a, the receiver-to-target range and the target velocity component along the bistatic bisector, the substitutions derived in Chapter 4 have to be used. This is not done here in order to simplify the discussion.

Now let the received signal (9.7) get processed with hypothesized delay and

Doppler τ_H and ω_{D_H}, respectively. Thus, let

$$\tau'' = \tau_a - \tau_\epsilon - \tau_H, \text{ and } \omega_D'' = \omega_{D_a} - \omega_\epsilon - \omega_{D_H}. \tag{9.9}$$

This leads to the following expression for the ambiguity function:

$$\begin{aligned} \theta(\tau'',\omega_D'') &= \left| \int_{-\infty}^{\infty} \tilde{f}(t-\tfrac{\tau''}{2})\, \tilde{f}^*_{ref}\,(t+\tfrac{\tau''}{2})\, e^{j\omega_D''t}\, dt \right|^2 \\ &= \left| \int_{-\infty}^{\infty} \left[\tilde{f}_{ref}(t-\tfrac{\tau''}{2}) - \tilde{f}_\epsilon(t-\tfrac{\tau''}{2}-\tfrac{\tau_\epsilon}{2}) e^{j\omega_\epsilon t} \right] \tilde{f}^*_{ref}(t+\tfrac{\tau''}{2})\, e^{j\omega_D''t}\, dt \right|^2 \end{aligned} \tag{9.10}$$

The infinite limits on the integral have been carried along but may not be applicable, depending on the nature of the transmitted waveform (see the discussion leading up to (2.42)). We see that the time-frequency correlation function in this case consists of the time-frequency correlation of the reference signal, and an error term:

$$\begin{aligned} \phi(\tau'',\omega_D'') = &\int_{-\infty}^{\infty} \tilde{f}_{ref}(t-\tfrac{\tau''}{2})\, \tilde{f}^*_{ref}(t+\tfrac{\tau''}{2})\, e^{j\omega_D''t}\, dt \\ &- \int_{-\infty}^{\infty} \tilde{f}_\epsilon(t-\tfrac{\tau'}{2})\, \tilde{f}^*_{ref}(t+\tfrac{\tau''}{2})\, e^{j\omega_D't}\, dt. \end{aligned} \tag{9.11}$$

Equations (9.10) and (9.11) express the ambiguity function and time-frequency correlation function from the point of view of the receiver, that is, based on $\tilde{f}_{ref}$. An alternative formulation, in terms of the transmitted signal $\tilde{f}$, may be more useful for system design and analysis purposes. This results in the expression:

$$\theta(\tau'',\omega_D'') = \left| \int_{-\infty}^{\infty} \tilde{f}(t-\frac{\tau''}{2})\left[\tilde{f}^*(t+\frac{\tau''}{2}) + \tilde{f}_\epsilon^*(t+\frac{\tau''}{2})\right] e^{j\omega_D'' t}\, dt\right|^2 \tag{9.12}$$

$$\begin{aligned}\phi(\tau'',\omega_D'') = &\int_{-\infty}^{\infty} \tilde{f}(t-\frac{\tau''}{2})\, \tilde{f}^*(t+\frac{\tau''}{2})\, e^{j\omega_D'' t}\, dt \\ &+ \int_{-\infty}^{\infty} \tilde{f}(t-\frac{\tau''}{2})\, \tilde{f}_\epsilon^*(t+\frac{\tau''}{2})\, e^{j\omega_D'' t}\, dt.\end{aligned} \tag{9.13}$$

We observe that the time-frequency correlation function in (9.11) and in (9.13) consists of the superposition of two separate functions. Concentrating on the formulation (9.13), $\phi(\tau'',\omega_D'')$ is the sum of the ordinary time-frequency correlation of the transmitted signal, $\phi_{tr}(\tau'',\omega_D'')$, and an error term, $\phi_\epsilon(\tau'',\omega_D'')$. Both these terms incorporate the errors in epoch and in frequency, τ_ϵ and ω_ϵ. Thus, (9.13) can be written

$$\phi(\tau'',\omega_D'') = \phi_{tr}(\tau'',\omega_D'') + \phi_\epsilon(\tau'',\omega_D''). \tag{9.14}$$

The ambiguity function (9.12) then becomes

$$\begin{aligned}\theta(\tau'',\omega_D'') &= |\phi_{tr}(\tau'',\omega_D'') + \phi_\epsilon(\tau'',\omega_D'')|^2 \\ &= \theta_{tr}(\tau'',\omega_D'') + \theta_\epsilon(\tau'',\omega_D'') + 2\mathrm{Re}\ \phi_{tr}\, \phi_\epsilon\end{aligned} \tag{9.15}$$

where

$$\theta_{tr}(\tau'',\omega_D'') = \left| \int_{-\infty}^{\infty} \tilde{f}(t-\frac{\tau''}{2})\, \tilde{f}^*(t+\frac{\tau''}{2})\, e^{j\omega_D'' t} dt \right|^2,$$

$$\theta_{\epsilon}(\tau'',\omega_D'') = \left| \int_{-\infty}^{\infty} \tilde{f}(t-\frac{\tau''}{2})\, \tilde{f}_{\epsilon}^*(t+\frac{\tau''}{2})\, e^{j\omega_D'' t}\, dt \right|^2.$$

and we have the bounds

$$\begin{aligned} \theta_{tr}(\tau'',\omega_D'') + \theta_{\epsilon}(\tau'',\omega_D'') - 2\sqrt{\theta_{tr}\theta_{\epsilon}} &\le \theta(\tau'',\omega_D'') \\ &\le \theta_{tr}(\tau'',\omega_D'') + \theta_{\epsilon}(\tau'',\omega_D'') + 2\sqrt{\theta_{tr}\theta_{\epsilon}} \end{aligned} \tag{9.16}$$

Clearly, the effect of an error in complex envelope is somewhat unpredictable, and this type of error needs further study. For instance, the nature of the transmitted waveform can significantly influence the magnitude of this type of error.

9.3 Discussion

What preliminary conclusions can be drawn from the development in Sec. 9.2?

A general form of the ambiguity function for non-cooperative bistatic radar is given in (9.12), referenced to the transmitted signal $\tilde{f}$ and incorporating errors in the reference waveform used by the receiver, $\tilde{f}_{ref}$. The simplest case arises when the difference between $\tilde{f}_{ref}$ and $\tilde{f}$ is solely due to a timing error τ_{ϵ} and an error in carrier frequency, ω_{ϵ}. In that case, the term $\tilde{f}_{\epsilon}^*(t+\frac{\tau''}{2})$ within the bracket is zero, and $\theta(\tau'',\omega_D'')$ has the same shape as the ordinary ambiguity function for the signal which is radiated at the transmitter. However, the function suffers erroneous displacements

in the τ and ω_D directions by amounts τ_ϵ and $\omega_{D\epsilon}$, respectively. In (9.12) this is evidenced by the fact that the variables are τ'' and ω_D'' (as defined in (9.9)), instead of τ' and ω_D'. The manner in which these displacements in τ and ω_D affect the bistatic ambiguity function (expressed as a function of R_R and V_a) will, of course, depend on the bistatic geometry and can be analyzed using the principle of Chapter 4.

If the discrepancy between $\tilde{f}_{ref}$ and $\tilde{f}$ cannot be expressed in terms of errors in timing and/or frequency, we have an "error in the complex envelope". This case is much more complicated. The time-frequency correlation function (9.13) now has an extra term due to the error component $\tilde{f}_\epsilon$, which enters in a nonlinear manner into the ambiguity function.

Generally speaking, this case will give rise to a spreading of the ambiguity function. A detailed analysis of this case will have to consider specific transmitted waveforms, specific bistatic configurations, as well as the likelihood of various amounts of error in the complex envelope for a given type of transmitted signal.

Finally, if in addition to an error in the complex envelope there also are timing and frequency errors, then the ambiguity function with distortions just described is subjected also to the displacements in the τ and ω_D directions, as in the first case.

10 SUMMARY AND CONCLUSIONS

This investigation was primarily devoted to the ambiguity function analysis for bistatic radar systems. The major contributions of this effort are outlined below.

1. In most of the existing literature, ambiguity function is simply defined without providing any relationship with fundamental radar signal processing problems. We showed the manner in which the ambiguity function arises naturally when solving the radar signal detection problem and the associated parameter estimation problem. The derivation of ambiguity function based on the basic principles of detection and estimation theory was presented.
2. The manner in which the bistatic geometry affects the ambiguity function was derived. It was shown that delay and Doppler are no longer the appropriate arguments for plotting the ambiguity function due to the geometry and the nonlinear relationships. Illustrative examples showed the unexpected behavior of the ambiguity function plots.
3. For sampled radar signals, expressions for both continuous-time continuous-frequency and discrete-time discrete-frequency ambiguity functions were derived. Relationships between them were established. It was shown that a sampling rate of greater than or equal to twice the Nyquist rate is needed to avoid aliasing.
4. A signal model that incorporates various uncertainties in the reference signal at the receiver for the non-cooperative bistatic radar was developed.

11 REFERENCES

1. Skolnik, M.I., Introduction to Radar Systems, McGraw-Hill, New York, 1980.

2. Rihaczek, A.W., Principles of High-Resolution Radar, McGraw-Hill, New York, 1969.

3. Cook, C.E., and Bernfeld, M., Radar Signals, Academic Press, New York, 1967.

4. Van Trees, H.L., Detection, Estimation, and Modulation Theory, vol.3, Wiley, New York, 1971.

5. Jackson, M.C., "The Geometry of Bistatic Systems," IEE Proceedings, vol. 133, Part F, No. 7, pp. 604-612, December 1986.

6. Willis, N.J., Bistatic Radar, Artech House, 1991.

7. Oppenheim A.V., and Schafer R.W., Digital Signal Processing, Prentice Hall, Englewood Cliffs, NJ, 1975.

APPENDIX A

TWO PROPERTIES OF THE CORRELATION FUNCTION

In this appendix, two properties of the time-frequency correlation function needed for the analysis of the main text, are derived.

Recall that

$$\phi_{\tilde{g}_1,\tilde{f}_1}(\tau,f) = \int_{-\infty}^{+\infty} \tilde{g}_1(t)\, \tilde{f}_1^*(t-\tau)\, e^{-j2\pi ft} dt.$$

Property 1 (convolution of two time signals)

If $\tilde{f}(t) = \tilde{f}_1(t) * \tilde{f}_2(t)$ and $\tilde{g}(t) = \tilde{g}_1(t) * \tilde{g}_2(t)$, where the asterisk denotes convolution, then

$$\phi_{\tilde{g},\tilde{f}}(\tau,f) = \int_{-\infty}^{\infty} \phi_{\tilde{g}_1,\tilde{f}_1}(\lambda,f)\, \phi_{\tilde{g}_2,\tilde{f}_2}(\tau-\lambda,f)\, d\lambda. \qquad (A.1)$$

Proof

The left hand side of (A.1) can be written as

$$\phi_{\tilde{g},\tilde{f}} = \int_{-\infty}^{\infty} \left\{ \int_{-\infty}^{\infty} \tilde{g}_1(x)\, \tilde{g}_2(t-x)dx \right\} \left\{ \int_{-\infty}^{\infty} \tilde{f}_1^*(y)\, \tilde{f}_2^*(t-\tau-y)dy \right\} e^{-j2\pi ft}dt$$

$$= \iiint_{-\infty}^{\infty} \tilde{g}_1(x)\, \tilde{f}_1^*(y)\, \tilde{g}_2(t-x)\, \tilde{f}_2^*(t-\tau-y)\, e^{-j2\pi ft}dx\,dy\,dt.$$

The right hand side of (A.1) is,

$$\int_{-\infty}^{\infty} \phi_{\tilde{g}_1,\tilde{f}_1}(\lambda,f)\, \phi_{\tilde{g}_2,\tilde{f}_2}(\tau-\lambda,f)\, d\lambda = \int_{-\infty}^{\infty} \left\{ \int_{-\infty}^{\infty} \tilde{g}_1(u)\, \tilde{f}_1^*(u-\lambda)\, e^{-j2\pi fu}\, du \right\}$$

$$\left\{ \int_{-\infty}^{\infty} \tilde{g}_2(v)\, \tilde{f}_2^*(v-\tau+\lambda)\, e^{-j2\pi fv}dv \right\} d\lambda$$

$$= \iiint_{-\infty}^{\infty} \tilde{g}_1(u)\, \tilde{f}_1^*(u-\lambda)\, \tilde{g}_2(v)\, \tilde{f}_2^*(v-\tau+\lambda)\, e^{-j2\pi f(u+v)}\, du\,dv\,d\lambda.$$

In the above expression, let t=u+v so that v=t-u. The above triple integral then becomes

$$\iiint_{-\infty}^{\infty} \tilde{g}_1(u)\, \tilde{f}_1^*(\mu-\lambda)\, \tilde{g}_2(t-u)\, \tilde{f}_2^*(t-u-\tau+\lambda)\, e^{-j2\pi ft}\, du\,dt\,d\lambda.$$

Now let x=u and y=u-λ. The triple integral then reduces to

$$\iiint_{-\infty}^{\infty} \tilde{g}_1(x)\, \tilde{f}_1^*(y)\, \tilde{g}_2(t-x)\, \tilde{f}_2^*(t-\tau-y)\, e^{-j2\pi ft}dx\,dy\,dt$$

which is the same as the left hand side of the expression found previously.

Property 2 (product of two time signals)

If $\tilde{f}(t) = \tilde{f}_1(t)\,\tilde{f}_2(t)$ and $\tilde{g}(t) = \tilde{g}_1(t)\,\tilde{g}_2(t)$, then

$$\phi_{\tilde{g},\tilde{f}}(\tau,f) = \int_{-\infty}^{\infty} \phi_{\tilde{g}_1,\tilde{f}_1}(\tau,x)\,\phi_{\tilde{g}_2,\tilde{f}_2}(\tau,f-x)\,dx. \qquad (A.2)$$

Proof

By definition,

$$\phi_{\tilde{g},\tilde{f}}(\tau,f) = \int_{-\infty}^{\infty} \tilde{g}_1(t_1)\,\tilde{g}_2(t_1)\,\tilde{f}_1^*(t_1-\tau)\,\tilde{f}_2^*(t_1-\tau)\,e^{-j2\pi ft_1}\,dt_1.$$

This represents the left hand side of (A.2). Let's now expand the expression on the right hand side. We obtain

$$\int_{-\infty}^{\infty} \phi_{\tilde{g}_1,\tilde{f}_1}(\tau,x)\,\phi_{\tilde{g}_2,\tilde{f}_2}(\tau,f-x)\,dx = \int_{-\infty}^{\infty}\int_{-\infty}^{\infty} \tilde{g}_1(t_1)\,\tilde{f}_1^*(t_1-\tau)\,e^{-j2\pi xt_1}\,dt_1$$

$$\int_{-\infty}^{\infty} \tilde{g}_2(t_2)\,\tilde{f}_2^*(t_2-\tau)\,e^{-j2\pi(f-x)t_2}\,dt_2\,dx$$

$$= \int\int\int_{-\infty}^{\infty} \tilde{g}_1(t_1)\,\tilde{f}_1^*(t_1-\tau)\,\tilde{g}_2(t_2)\,\tilde{f}_2^*(t_2-\tau)\,e^{-j2\pi[x(t_1-t_2)+ft_2]}\,dt_1\,dt_2\,dx.$$

However,

$$\int_{-\infty}^{+\infty} e^{-j2\pi x(t_2-t_1)}\,dx = \delta(t_2-t_1).$$

Therefore, the right hand side of (A.2) becomes

$$\int_{-\infty}^{+\infty}\int \tilde{g}_1(t_1)\,\tilde{f}_1^*(t_1-\tau)\,\tilde{g}_2(t_2)\,\tilde{f}_2^*(t_2-\tau)\,e^{-j2\pi f t_2}\,\delta(t_2-t_1)\,dt_1\,dt_2$$

$$= \int_{-\infty}^{+\infty} \tilde{g}_1(t_1)\,\tilde{g}_2(t_1)\,\tilde{f}_1^*(t_1-\tau)\,\tilde{f}_2^*(t_1-\tau)\,e^{-j2\pi f t_1}\,dt_1$$

which is the same as the expression found for the left hand side of (A.2).

APPENDIX B

TIME AND FREQUENCY EXTENT OF THE CORRELATION FUNCTION

By definition, $\tilde{f}_e(t)$ is time limited to the interval $[0, T_d]$ where $T_d = (N-1)T$ is the time duration of $\tilde{f}_e(t)$ and N equals the number of time samples uniformly spaced by an interval T over the signal duration. Assume that $\tilde{f}_e(t)$ has a spectrum that is approximately bandlimited to the frequency interval [-B, B] where B is defined to be the signal bandwidth as shown in Fig. B-1. To avoid aliasing of the frequency spectrum, the sampling rate for $\tilde{f}_e(t)$ should be greater than or equal to the Nyquist rate. Since T denotes the sampling interval, the Nyquist principle requires that

$$\frac{1}{T} \geq 2B.$$

We now consider sampling in frequency the spectrum of $\tilde{f}_e(t)$. Uniformly sampling in frequency with a sampling interval equal to λ Hertz causes $\tilde{f}_e(t)$ to be replicated in time every $\frac{1}{\lambda}$ seconds. To avoid aliasing in time, it is necessary that

$$\frac{1}{\lambda} \geq T_d = (N-1)T+\epsilon$$

where ϵ is a small positive constant. Equivalently,

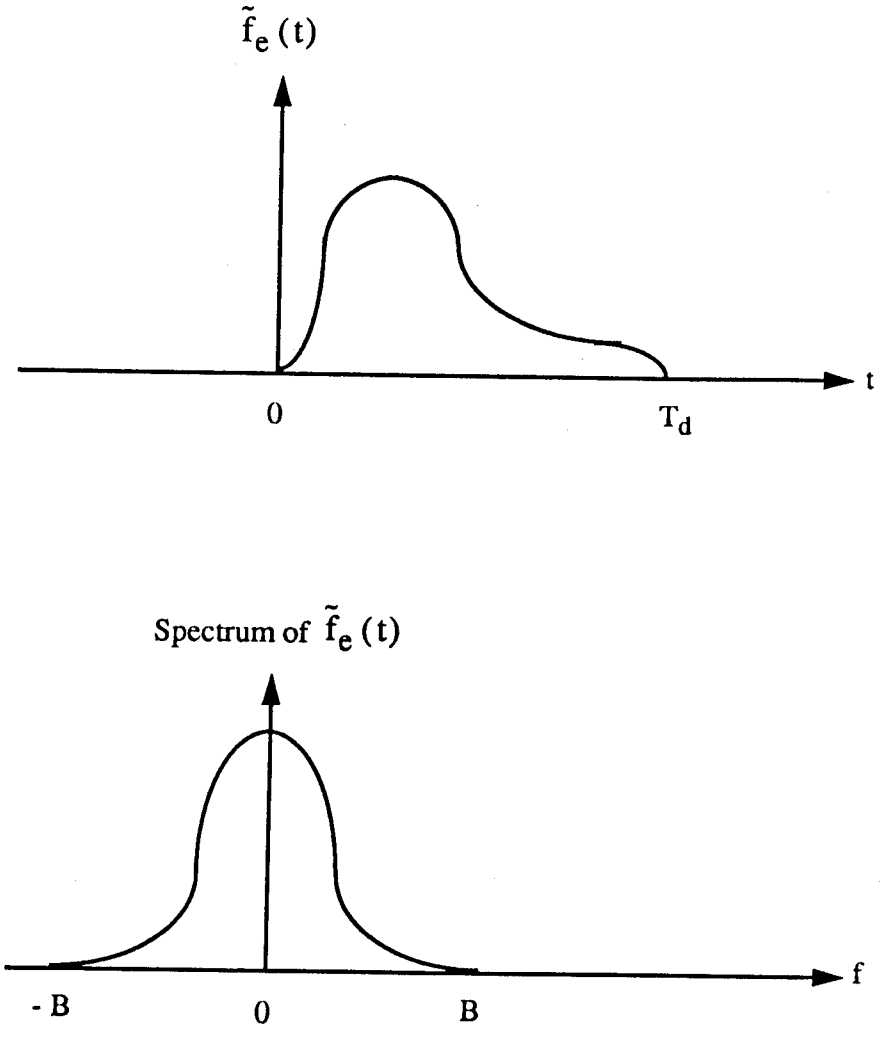

Fig. B-1 Sketch of $\tilde{f}_e(t)$ and its spectrum.

$$\frac{1}{\lambda} \geq NT.$$

Recall that the continuous-time continuous-frequency autocorrelation function of $\tilde{f}_e(t)$ is given by

$$\phi_{\tilde{f}_e}(\tau,f) = \int_{-\infty}^{\infty} \tilde{g}_e(t)\, \tilde{f}_e^*(t-\tau)\, e^{-j2\pi ft}\, dt$$

where

$$\tilde{g}_e(t) = \tilde{f}_e(t-\tau_a)\, e^{j2\pi f_a t}.$$

From Schwartz's inequality,

$$|\phi_{\tilde{f}_e}(\tau,f)| \leq \int_{-\infty}^{\infty} |\tilde{g}_e(t)|\,|\tilde{f}_e^*(t-\tau)|\, dt$$

$$= \int_{-\infty}^{\infty} |\tilde{f}_e(t-\tau_a)|\; |\tilde{f}_e(t-\tau)|\, dt.$$

Sketches of $|\tilde{f}_e(t-\tau_a)|$ and $|\tilde{f}_e(t-\tau)|$ are shown in Fig. B-2. By inspection of Fig. B-2, the integrand in the bound on $|\phi_{\tilde{f}e}(\tau,f)|$ is nonzero <u>for all t</u> only when

$$\tau_a - T_d \leq \tau \leq \tau_a + T_d.$$

Note that this is a time interval of duration $2T_d$ centered at τ_a. Because of the time-limited duration of $\tilde{f}_e(t)$, it is seen that $\phi_{\tilde{f}_e}(\tau,f)$ is also time limited with a duration equal to twice that of $\tilde{f}_e(t)$. In addition, Schwartz's inequality reveals that $\phi_{\tilde{f}_e}(\tau,f)$ has

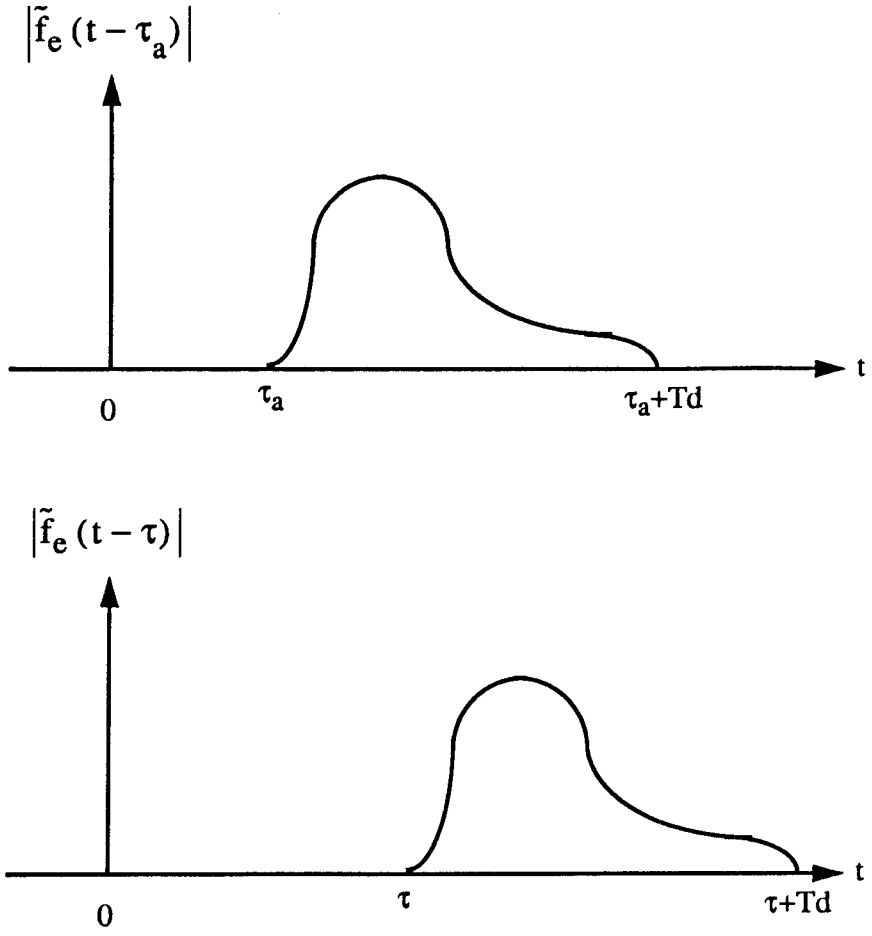

Fig. B-2 Sketches of $|\tilde{f}_e(t-\tau_a)|$ and $|\tilde{f}_e(t-\tau)|$.

its maximum value when $\tau = \tau_a$ and $f = f_a$.

Having determined the duration of $\phi_{\tilde{f}_e}(\tau,f)$ along the τ axis, we now examine its extent along the frequency axis. It is readily shown that $\phi_{\tilde{f}_e}(\tau,f)$ can also be expressed as

$$\phi_{\tilde{f}_e}(\tau,f) = \int_{-\infty}^{\infty} \tilde{G}_e(j\nu)\, \tilde{F}_e^*[j(\nu - f)]\, e^{j2\pi\nu\tau}\, d\nu$$

where $\tilde{F}_e[j\nu]$ is the Fourier transform of $\tilde{f}_e(t)$ and $\tilde{G}_e[j\nu]$ is the Fourier transform of $\tilde{g}_e(t)$ given by

$$\tilde{G}_e[j\nu] = \tilde{F}_e[j(\nu - f_a)]\, e^{-j2\pi\nu\tau_a}.$$

From Schwartz's inequality,

$$|\phi_{\tilde{f}_e}(\tau,f)| \le \int_{-\infty}^{+\infty} |\tilde{G}_e[j\nu]|\, |\tilde{F}_e^*[j(\nu - f)]|\, d\nu$$

$$= \int_{-\infty}^{+\infty} |\tilde{F}_e[j(\nu - f_a)]|\, |\tilde{F}_e[j(\nu - f)]|\, d\nu\ .$$

Sketches of $|\tilde{F}_e[j(\nu - f_a)]|$ and $|\tilde{F}_e[j(\nu - f)]|$ are shown in Fig. B-3.

By inspection of Fig. B-3, the integrand in the bound on $|\phi_{\tilde{f}_e}(\tau,f)|$ is nonzero <u>for all ν</u> only when

$$f_a - 2B \le f \le f_a + 2B.$$

Notice that this is a frequency interval of duration 4B centered at f_a. Because the

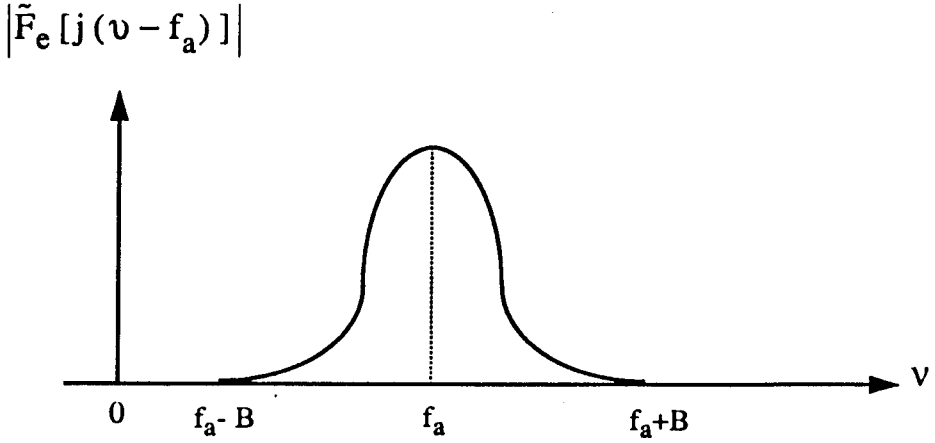

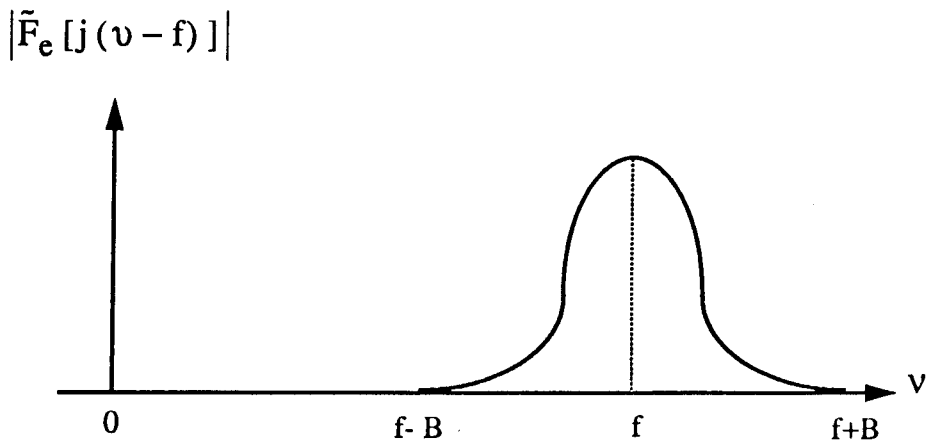

Fig. B-3 Sketches of $|\tilde{F}_e[j(\nu - f_a)]|$ and $|\tilde{F}_e[j(\nu - f)]|$.

spectrum of $\tilde{f}_e(t)$ is confined to the interval [-B,B], it is seen that $\phi_{\tilde{f}_e}(\tau,f)$ is confined to a frequency interval twice as large. As mentioned previously, Schwartz's inequality shows clearly that $\phi_{\tilde{f}_e}(\tau,f)$ has its maximum value when $\tau = \tau_a$ and $f = f_a$.

In summary, $\phi_{\tilde{f}_e}(\tau,f)$ is centered at (τ_a,f_a) and is limited both in time, with a duration equal to twice that of $\tilde{f}_e(t)$, and in frequency, with a frequency extent equal to twice that of the spectrum of $\tilde{f}_e(t)$.

*U.S. GOVERNMENT PRINTING OFFICE: 1995-610-126-50169

Rome Laboratory

Customer Satisfaction Survey

RL-TR-_____

Please complete this survey, and mail to RL/IMPS, 26 Electronic Pky, Griffiss AFB NY 13441-4514. Your assessment and feedback regarding this technical report will allow Rome Laboratory to have a vehicle to continuously improve our methods of research, publication, and customer satisfaction. Your assistance is greatly appreciated.
Thank You

_____

_____

Organization Name:_____(Optional)

Organization POC: _____(Optional)

Address:_____

1. On a scale of 1 to 5 how would you rate the technology developed under this research?

5-Extremely Useful 1-Not Useful/Wasteful

Rating_____

Please use the space below to comment on your rating. Please suggest improvements. Use the back of this sheet if necessary.

2. Do any specific areas of the report stand out as exceptional?

Yes___ No_____

If yes, please identify the area(s), and comment on what aspects make them "stand out."

3. Do any specific areas of the report stand out as inferior?

Yes___ No___

If yes, please identify the area(s), and comment on what aspects make them "stand out."

4. Please utilize the space below to comment on any other aspects of the report. Comments on both technical content and reporting format are desired.

MISSION

OF

ROME LABORATORY

Mission. The mission of Rome Laboratory is to advance the science and technologies of command, control, communications and intelligence and to transition them into systems to meet customer needs. To achieve this, Rome Lab:

a. Conducts vigorous research, development and test programs in all applicable technologies;

b. Transitions technology to current and future systems to improve operational capability, readiness, and supportability;

c. Provides a full range of technical support to Air Force Materiel Command product centers and other Air Force organizations;

d. Promotes transfer of technology to the private sector;

e. Maintains leading edge technological expertise in the areas of surveillance, communications, command and control, intelligence, reliability science, electro-magnetic technology, photonics, signal processing, and computational science.

The thrust areas of technical competence include: Surveillance, Communications, Command and Control, Intelligence, Signal Processing, Computer Science and Technology, Electromagnetic Technology, Photonics and Reliability Sciences.